Biofouling in reverse and forward osmosis membrane systems

Bucs, Szilard

DOI
10.4233/uuid:d79265ec-f4dc-415a-8e8c-2be6b683dd46

Publication date
2017

Document Version
Final published version

Citation (APA)
Bucs, S. (2017). *Biofouling in reverse and forward osmosis membrane systems*. [Dissertation (TU Delft), Delft University of Technology]. https://doi.org/10.4233/uuid:d79265ec-f4dc-415a-8e8c-2be6b683dd46

BIOFOULING IN REVERSE AND FORWARD OSMOSIS MEMBRANE SYSTEMS

SZILÁRD SÁNDOR BUCS

Cover design by: Balázs Mózes-Finta

Printed by: Ipskamp Printing, Enschede (www.ipskampprinting.nl)

Layout: Szilárd Bucs

ISBN: 978-94-028-0878-0

Biofouling in reverse and forward osmosis membrane systems

Proefschrift

ter verkrijging van de graad van doctor
aan de Technische Universiteit Delft;
op gezag van de Rector Magnificus prof. ir. Karel Ch.A.M. Luyben;
voorzitter van het College voor Promoties
in het openbaar te verdedigen op **04.12.2017 om 10:00 uur**

door

Szilárd Sándor BUCS

Chemical Engineer, University "Politehnica" of Bucharest
geboren te Târgu Mureș, Roemenië

Dit proefschrift is goedgekeurd door de promotoren:
promotor: Prof. dr. J.S. Vrouwenvelder and
co-promotor: Dr. ir. C. Picioreanu

Samenstelling promotiecommissie:

Rector Magnificus	chairman
Prof.dr. J.S. Vrouwenvelder	Delft University of Technology
Dr.ir. C. Picioreanu	Delft University of Technology
Prof.dr.ir. A.R.D. Verliefde	Ghent University
Dr. J.C. Kruithof	Wetsus
Prof.dr.ir. W.G.J. van der Meer	Delft University of Technology
Prof.dr. G.J. Witkamp	Delft University of Technology
Prof.dr.ir. M.C.M. van Loosdrecht	Delft University of Technology

Content

Summary

Global freshwater demand has significantly increased over the past century and continued growth is expected in the coming century. Since more than 97 percent of the water in the world is seawater, desalination technologies have the potential to solve the fresh water crisis. Currently, the most used desalination technology is reverse osmosis, where a semipermeable membrane is used to separate the salt from the water. The driving force of reverse osmosis desalination is hydraulic pressure, which has to be greater than the osmotic pressure of the seawater. Due to the high hydraulic pressure reverse osmosis has a high energy demand. Lately, hybrid desalination systems, e.g. indirect desalination with forward osmosis combined with low pressure reverse osmosis are getting more importance. Forward osmosis is also a membrane based process that uses the osmotic pressure difference as driving force. One of the main advantages of forward osmosis is the limited amount of external energy requirement compared to reverse osmosis. The major problem of membrane desalination process is fouling, the accumulation of unwanted material on the membrane surface, causing performance decline and increase of costs. Several types of fouling can occur in membrane processes, biofouling (microbial biofilm formation), scaling (mineral salt precipitation), organic fouling (deposition of organic macromolecules) and colloidal fouling (deposition of particulate matter). In practice biofouling is considered as the major problem in membrane systems.

The objective of this thesis was to better understand how different processes of physical, chemical and biological nature affect and lead to biofilm formation in spiral wound membrane systems. To achieve this goal, new methods had to be developed. Systematic laboratory studies on membrane biofouling require experimental conditions that are well-defined and representative for practice. However, flow rate variations affect biofilm formation, morphology, detachment and the impact of the accumulated biomass on membrane performance parameters such as feed channel pressure drop. Therefore, an automated system to enable constant flow operation and accurate monitoring of operational parameters of small-scale membrane fouling monitors has been developed and tested (*Chapter 2*). The flow in spiral wound membrane systems

is determined by the feed spacer geometry. To study hydrodynamics in spiral wound membrane systems, the micro-scale flow distribution in spacer-filled flow channels was determined with particle image velocimetry (*Chapter 3*). Two-dimensional water velocity fields were measured in a flow cell at several planes throughout the flow channel height. Three-dimensional computational fluid dynamics simulations were performed using the same geometries and flow parameters as in the experiments. The numerical results were in good agreement with the experimentally determined flow fields, thus supporting the use of model-based studies in the optimization of feed spacer geometries and operational conditions.

The influence of biodegradable organic nutrient load on biofouling was investigated at varying crossflow velocity, nutrient concentration, flow shear and feed spacer thickness (*Chapter 4*). Results showed that the organic nutrient load determined the amount of accumulated biomass. The same amount of accumulated biomass was found at constant nutrient load, irrespective of linear flow velocity, shear or feed spacer thickness. Reducing the nutrient load by pre-treatment slowed-down the biofilm formation. The impact of accumulated biomass on membrane performance can be reduced by applying a lower crossflow velocity or a thicker feed spacer.

Surface coating of membranes and feed spacers was investigated as a way to control biofilm development and biofouling impact on membrane performance (*Chapter 5*). Commercial reverse osmosis membranes were coated with hydroxyehtyl methacrylate and perfluorodecyl acrylate copolymer films of optimized chemistry and thickness. Biofouling studies with coated and uncoated membranes and feed spacers were performed. Results showed that the amphiphilic coating delayed the biofilm formation and influenced the biofilm composition (higher extracellular polymeric substance content). The coating showed strong attachment to the membrane and spacer, still being present at the end of the biofouling study. However, membrane and spacer coating alone was not sufficient to avoid or control biofilm development.

A three-dimensional mathematical model for biofouling of feed spacer channels including hydrodynamics, solute transport and biofilm formation was developed in COMSOL Multiphysics and MATLAB software (*Chapter 6*). Results of this study indicate that the feed channel pressure drop increase caused by biofilm formation can be reduced by using thicker and modified feed

spacer geometry and a lower flow rate in the feed channel. The increase of feed channel pressure drop by biomass accumulation was strongly influenced by the biofilm location: biomass on the feed spacer had a higher impact on feed channel pressure drop than the biomass accumulated on the membrane surface.

Forward osmosis (FO) is an emerging membrane technology with a range of possible water treatment applications including desalination. Wastewater recovery has been identified to be particularly suitable for practical applications of forward osmosis. However, biofouling is also a problem in forward osmosis membrane processes involving wastewater effluents. The study on the influence of feed spacer thickness on performance and biofouling development at the feed side of the forward osmosis membrane (*Chapter 7*) demonstrated that the biomass amount alone does not determine the performance decline. Importantly, it was shown that the performance decline caused by biomass accumulation in forward osmosis can be reduced by using a thicker feed spacer, as also reported in other studies for reverse osmosis spiral wound systems.

The experimental and computational evaluation of biofilm formation in forward osmosis (*Chapter 8*) processes revealed that the presence of a biofilm on the membrane significantly affects the external concentration polarization and can become the limiting factor for water permeation. Unlike in reverse osmosis systems, the same amount of biomass leads to stronger water flux decline (less water production) when the biofilm develops on the draw side of the forward osmosis membrane, compared to the biofilm formed on the feed side, due to higher concentration polarization induced by the foulant layer in the draw channel. Not only biofilm properties such as hydraulic permeability and mean thickness, but also the biofilm porosity and spatial heterogeneity must be considered when evaluating biofouling effects on the performance of membrane-based separation systems. Since biofilm formed in forward osmosis membrane systems tend to grow thicker, and more porous than in reverse osmosis, measurements obtained in forward osmosis are needed to reveal how the biofilm parameters develop in time and to supply the numerical models with realistic parameter values enabling detailed understanding of the processes. Knowledge in biofilm processes in forward osmosis may lead to more effective biofouling control strategies in both forward and reverse osmosis membrane systems.

Samenvatting

De wereldwijde vraag naar zoetwater is in de afgelopen eeuw aanzienlijk toegenomen en in de toekomst wordt een verdere toename verwacht in de behoefte naar zoetwater. Aangezien meer dan 97 procent van het water in de wereld zoutwater is, kunnen ontziltingstechnologieën de zoetwatercrisis oplossen. Momenteel is de meest gebruikte ontziltingstechnologie omgekeerde osmose, waar een semipermeabel membraan wordt gebruikt om water van zout te scheiden. De drijvende kracht van omgekeerde osmose ontzilting is de hydraulische druk die groter moet zijn dan de osmotische druk van het zeewater. Door de hoge hydraulische druk heeft omgekeerde osmose een hoge energiebehoefte. In de afgelopen tijd zijn hybride ontziltingssystemen steeds belangrijker geworden, b.v. indirecte ontzilting met forward osmose gecombineerd met lage druk omgekeerde osmose. Forward osmose is ook een membraan gebaseerd proces waarbij het osmotische drukverschil dient als drijvende kracht voor watertransport over het membraan. Een van de voornaamste voordelen van forward osmose is de lagere energiebehoefte ten opzichte van omgekeerde osmose. Het belangrijkste probleem van membraan gebaseerde ontzilting is vervuiling, accumulatie van ongewenst materiaal op het membraanoppervlak, waardoor de membraanprestaties afnemen en economische kosten van waterproductie toenemen. Verschillende soorten vervuilingen kunnen zich voordoen in membraansystemen, biofouling (microbiële biofilmvorming), scaling (minerale zoutafzetting), organische verontreiniging (afzetting van organische macromoleculen) en colloïdale vervuilingen (afzetting van deeltjes). In de praktijk is biofouling een dominant probleem.

Het doel van dit proefschrift was om beter te begrijpen hoe verschillende fysieke, chemische en biologische processen invloed hebben op biofilm-accumulatie in spiraalgewonden membraan systemen. Om dit doel te bereiken, moesten nieuwe methoden ontwikkeld worden. Systematische laboratoriumstudies aan membraan biofouling vereisen experimentele condities die goed gedefinieerd en representatief zijn voor de praktijk. Variaties in de waterstroomsnelheid in membraansystemen beïnvloeden de vorming van biofilm, morfologie, sloughing en de impact van de geaccumuleerde biomassa op membraanprestatieparameters, zoals de drukval over het feed spacer-kanaal.

Daarom is een geautomatiseerd systeem voor constante waterstroom en nauwkeurige monitoring van membraan operationele parameters voor kleine monitors ontwikkeld en getest (*hoofdstuk 2*). De waterstroomsnelheid in spiraalgewonden membraansystemen wordt bepaald door de geometrie van de feed spacer. Om hydrodynamica te bestuderen in spiraalgewonden membraansystemen, werd de waterstroomverdeling op microschaal in spacerkanalen bepaald met particle image velocimetry (*hoofdstuk 3*). Tweedimensionale watersnelheden werden gemeten in een monitor op verschillende vlakken over de hoogte. Driedimensionale computersimulaties van fluid dynamics werden uitgevoerd met dezelfde spacer geometrieën en waterstroom als in de experimenten. De numerieke resultaten waren in goede overeenstemming met de experimenteel bepaalde waterstroomkarakteristieken, die het gebruik van modelgebaseerde studies ondersteunen voor de optimalisatie van de spacer-geometrie en operationele condities.

De invloed van biologisch afbreekbare organische nutriëntbelasting - product van nutriëntconcentratie en lineare waterstroomsnelheid - op biofouling werd onderzocht bij verschillende waterstroomsnelheden, nutriëntconcentraties, shear en spacerdikte (*hoofdstuk 4*). Resultaten toonden aan dat de organische nutriëntbelasting de hoeveelheid geaccumuleerde biomassa bepaald. Dezelfde hoeveelheid geaccumuleerde biomassa werd gevonden bij constante nutriëntbelasting, ongeacht de lineaire waterstroomsnelheid, shear of spacerdikte. Het verminderen van de nutriëntbelasting door biologische waterzuivering vertraagde de biofilmaccumulatie. De invloed van geaccumuleerde biomassa op membraanprestaties kan worden verminderd door een lagere waterstroomsnelheid of gebruik van een dikkere spacer.

Coating van membranen en spacers werd onderzocht als een manier om biofouling te beheersen (*hoofdstuk 5*). Commerciële omgekeerde osmose membranen werden gecoat met dunne hydroxyehtyl methacrylaat en perfluorodecylacrylaat copolymer films. Biofouling studies werden uitgevoerd met gecoate en niet-gecoate membranen en spacers. Resultaten toonden aan dat de amphiphilic coating de biofilmvorming vertraagde en de biofilmsamenstelling beïnvloedde (hogere extracellular polymeric substance gehalte). De coating liet een sterke binding zien aan het membraan en de spacer, die nog aan het einde van de biofouling studie aanwezig was.

Membraan- en spacercoating alleen was niet voldoende om biofilmontwikkeling te voorkomen of beheersen.

Een driedimensionaal wiskundig model voor biofouling van spacerkanalen waaronder hydrodynamica, mass-transport en biofilmvorming was ontwikkeld in COMSOL Multiphysics en MATLAB software (*hoofdstuk 6*). Resultaten van deze studie geven aan dat de drukvaltoename veroorzaakt door biofilmvorming kan worden verminderd door het gebruik van dikkere en aangepaste geometrie spacers en een lagere stroomsnelheid in het spacerkanaal. De toename van de spacerkanaal drukval door geaccumuleerde biomassa werd sterk beïnvloed door de biofilmlokatie: biomassa op de spacer had een hogere invloed op de drukval dan de biomassa geaccumuleerd op het membraanoppervlak.

Forward osmose (FO) is een opkomende membraantechnologie met een scala aan mogelijke waterbehandeling toepassingen waaronder ontzilting. Waterhergebruik is geïdentificeerd als bijzonder geschikt voor praktische toepassingen van forward osmose. Biofouling is echter ook een probleem bij forward osmose membraanprocessen gevoed met effluent van afvalwaterzuiveringen. De studie van de invloed van spacerdikte op membraanperformance en biofouling-accumulatie op de voedingszijde van het forward osmose membraan (*hoofdstuk 7*) toonde aan dat de biomassahoeveelheid alleen niet bepalend was voor de afgenomen membraanperformance. De afgenomen membraanperformance als gevolg van geaccumuleerde biomassa in forward osmose kan worden beperkt door gebruik van een dikkere spacer, zoals gerapporteerd in andere studies aan omgekeerde osmose membraansystemen.

Uit de experimentele en numerieke evaluatie van biofilmvorming in forward-osmose processen (*hoofdstuk 8*) bleek dat de aanwezigheid van een biofilm op het membraan de externe concentratiepolarisatie significant beïnvloedt en de beperkende factor kan zijn voor water productie. In tegenstelling tot omgekeerde osmosesystemen, leidt dezelfde hoeveelheid biomassa in forward osmose tot een sterkere waterfluxafname (minder waterproductie) wanneer de biofilm zich ontwikkelt aan de concentraatzijde van het membraan. Dit verschil wordt veroorzaakt door de hogere concentratie polarisatie in de biofilm aan de concentraatzijde van het forward osmose membraan. In aanvulling op biofilmeigenschappen zoals hydraulische permeability en dikte, dienen ook de

biofilmporositeit en ruimtelijke heterogeniteit in overweging te worden genomen bij het evalueren van biofouling-effecten op de performance van membraan-gebaseerde scheidingssystemen. Aangezien de biofilm gevormd in forward osmose membraansystemen dikker en meer poreus zijn dan in omgekeerde osmose, zijn metingen verkregen in forward osmose nodig om te begrijpen hoe de biofilmparameters in tijd ontwikkelen en om de numerieke modellen te leveren met realistische parameterwaarden waardoor gedetailleerd inzicht kan worden verkregen in biofilmprocessen. Kennis in biofilm processen in forward osmose kan leiden tot effectievere biofouling controle strategieën in zowel forward osmose en omgekeerde osmose membraan systemen.

١

Introduction

FRESH WATER AVAILABILITY

Global freshwater use has grown over the past century from an estimated annual 580 km^3 in 1900 to 3829 km^3 in 2000, and continued increase is expected in the coming century (World Water Assessment Programme, 2012). Currently, more than two billion people live in highly water-stressed areas (Figure 1.1) (UNDP, 2006; Vörösmarty et al., 2000). Because of the uneven distribution of fresh water in time and space, the situation is likely to worsen in the future as regions expected to experience more extreme climate conditions and rapidly growing demands in water-use sectors: agriculture (crop production, livestock), domestic (municipal), and industry (energy, manufacturing) (Vörösmarty et al., 2000).

A sufficient, secure water supply is essential for meeting basic human needs and for the functioning of many sectors of the economy, making an understanding of future water demands crucial for policy makers to address the water scarcity challenge for the current and the generations to come (UNDP, 2006; WHO, 2015). The consequences of imbalances between water supply and demand are already known, and are occurring in many countries around the globe (WHO, 2015).

Since more than 97 percent of the water in the world is seawater, desalination technologies have the potential to solve the fresh water crisis. Seawater desalination is already used in many countries mainly in water scares regions such as the Middle East, but also in some countries with adequate freshwater resources (Figure 1-2).

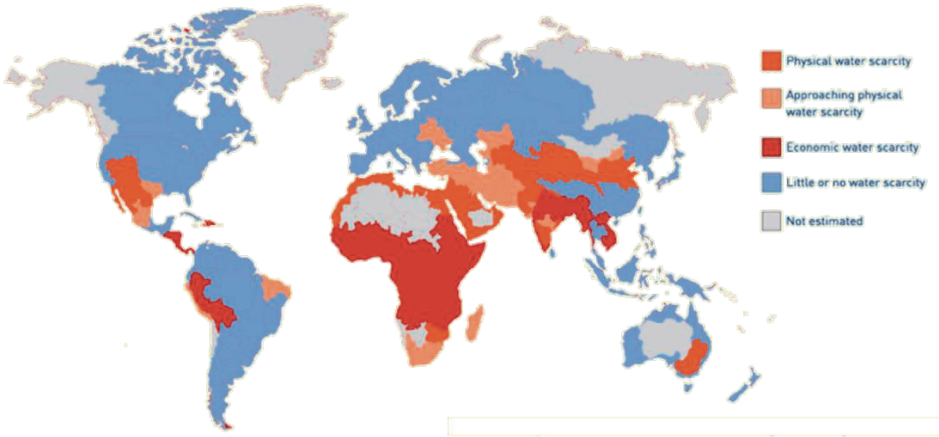

Figure 1-1: Water scarcity map (image adapted from International Water Management Institute).

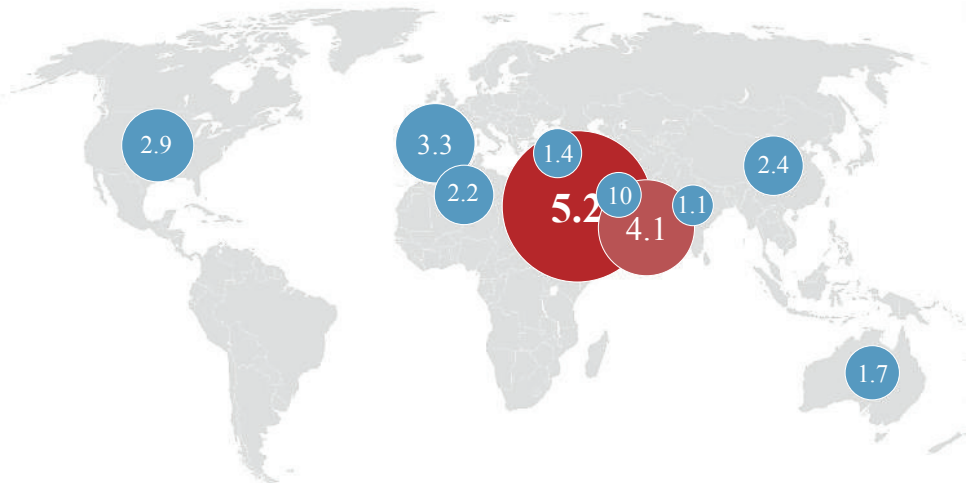

Figure 1-2: The ten largest desalination capacity by countries. The numbers represents the desalination capacity in million m^3 per day.

Desalination technologies can be separated in two major groups: thermal desalination and membrane desalination. Thermal desalination separates salt from water by evaporation and condensation, whereas in membrane desalination water diffuses through a membrane, while salts are almost completely retained.

While thermal desalination was the main desalination technology in the past, membrane based desalination technologies gained importance in the last decade, reaching 60 percent of the global desalination capacity in 2015 with a continuously increasing trend (Pankratz, 2012). This is explained by the improvement in efficiency and lower energy demand of the membrane based desalination processes. Reverse osmosis (RO) and nanofiltration (NF) currently holds the largest desalination capacity globally (Lattemann et al., 2010). Beside RO and NF there are also alternative membrane based desalination processes include electro-dialysis (ED), membrane distillation (MD) and forward osmosis (FO).

MEMBRANE BASED DESALINATION PROCESSES

Forward osmosis

Osmosis is the naturally occurring process in which water from solution passes through a semipermeable membrane to dilute a more concentrated solution. The driving force of osmotic processes is the difference in chemical potential between the solutions separated by the membrane. Practically, the difference in chemical potential is represented by a difference in concentrations.

The osmotic pressure π depends on the mole fraction of water x_W in the solution:

$$\pi = -\frac{R \times T}{V_b} \ln(x_W) \qquad 1\text{-}1$$

with molar volume of water V_b, ideal gas constant R and temperature T. In the direct osmosis, the flux of water J_W through the semipermeable membrane is proportional with the local osmotic pressure difference, $\Delta\pi$, but altered by the difference in hydraulic pressure, Δp, that may exist on the two sides of the membrane. The proportionality factor is called membrane permeability, A:

$$J_W = A(\Delta\pi - \Delta p) \qquad 1\text{-}2$$

Osmosis can be used for water treatment in a process called forward osmosis (FO). There are two main approaches for water desalination with FO, namely direct and indirect desalination (Valladares Linares et al., 2014b). The direct FO desalination concept is similar to other conventional membrane based

desalination processes (e.g. reverse osmosis, nanofiltration) in which fresh water is directly extracted from a saline water (seawater or brackish water). Direct FO desalination uses saline water as the feed solution (FS) and an osmotic reagent such as a non-volatile salt like NaCl, or a volatile salt such as ammonia–carbon dioxide solution, among others (Chekli et al., 2012), as the draw solution (DS). In this process, an additional step, a draw solution recovery process, is needed to separate the DS from the solution in the diluted DS to recover fresh water (McCutcheon et al., 2005).

In indirect desalination, typically, an impaired water source is used as "feed" solution and treated by extracting water with high salinity water as the "draw" solution. Seawater and brackish water are potential DSs for indirect desalination. The attractiveness of this process is to extract clean water from the feed using free osmotic energy, leading to partially desalinated water (diluted DS) which can be further desalinated by a subsequent low-pressure reverse osmosis (LPRO) step as part of an FO–LPRO hybrid process (Yangali-Quintanilla et al., 2011), and thus reduce the cost of the entire desalination process.

Reverse osmosis

Reverse osmosis (RO) uses the same principle of water passage through a membrane separating solutions of different concentrations, but it applies hydraulic pressure on the concentrated solution as driving force for the process. Thus, the direction of the water passing through the membrane is reversed:

$$J_W = A(\Delta p - \Delta \pi) \qquad 1\text{-}3$$

In equation 1-3 the driving force is the applied pressure Δp which now has to overcome the osmotic pressure difference $\Delta\pi$. Based on this principle, fresh water can be separated from saline water and this leads to fresh water production through desalination.

Reverse osmosis is currently the most frequently used desalination process with the aid of membranes. Reverse osmosis membranes are made of certain polymers that present semi-permeability. These membranes are able to reject nearly all colloidal or dissolved matter from aqueous solutions, resulting a more concentrated solution called "brine" and fresh water, usually referred as "permeate". The most important criterion for the RO membranes is the

rejection factor, R_m, which gives their permeability for dissolved substances. The rejection factor is defined from the ratio of concentrations in permeate, C_p, and brine, C_b:

$$R_m = 1 - \frac{C_p}{C_b} \qquad 1\text{-}4$$

Typical salt rejection coefficients for RO must be greater than 0.98 (DOW, 2014).

Besides its application in the production of drinking water, RO is also applied for the effluent treatment and separation of diverse chemical compounds from aqueous solutions in industrial applications.

Pre-treatment processes

Forward and reverse osmosis processes are used to separate solutes from water. However, raw water contains also particulate components, which must be removed before applying RO and FO, otherwise strong fouling could occur in the membrane modules. Pre-treatment of the raw water is commonly done by microfiltration (MF) or ultrafiltration (UF) membranes, in order to remove fine colloidal particles, bacteria, viruses and larger organic molecules (e.g., proteins, humic acids). Besides MF and UF, nanofiltration (NF) membranes reject molecules with a molecular weight greater than 200 g/mole, while RO and FO remove all dissolved compounds from water. Pressures applied in industrial RO plants vary between 15 bar (in brackish water desalination) and up to 80 bar in seawater desalination, while there is no hydraulic pressure applied in FO (Greenlee et al., 2009).

Membrane modules

Commercially available membrane modules include spiral wound, hollow fibre, tubular and plate-and-frame modules (Mulder, 1996). Amongst these, the hollow fibre modules and spiral wound modules are the most common, due to their high membrane area to volume ratio. The hollow fibre modules require more comprehensive pre-treatment than the spiral-wound membranes and they also tend to foul more rapidly (Butt et al., 1997). Spiral wound membrane modules ranging from RO to UF are widely used for commercial applications. The applications include desalination, water treatment, water reclamation,

treatment of industrial waste water, product treatment in the dairy industry and recovery of valuable products in the pharmaceutical industry (Mulder, 1996).

A schematic diagram of a spiral wound membrane module is shown in Figure 1-3. The major components of an spiral wound module are the membrane, the feed and permeate channels, spacers which keep the membrane leaves apart, the permeate tube and the membrane housing (Dickson et al., 1994). The feed channel spacer also enhances mass transfer near the membrane but inevitably increases pressure loss along the membrane leaf (Da Costa et al., 1994; Radu et al., 2010). Membrane sheets with the spacers in between are glued together on three sides to form a leaf and multiple leaves are rolled up around the permeate tube to create the feed and permeate channels.

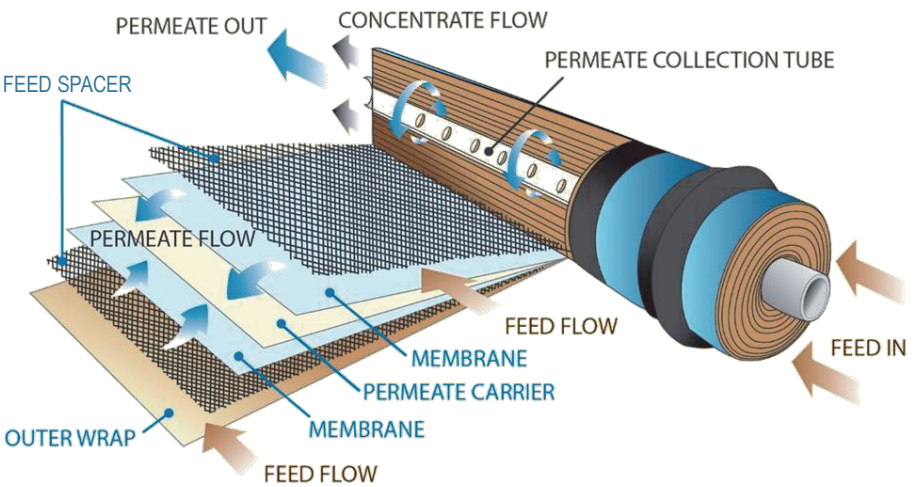

Figure 1-3: Schematic representation of a spiral wound membrane module (figure adapted from Conwed Plastics Inc.).

A pressurised module housing holds the membrane leaves in place to prevent unwinding. Usually three or more modules are connected in series in the pressure vessels (Schwinge et al., 2004a).

The geometry of a spiral wound membrane module is described by the number of membrane leaves, the length and width of each membrane leaf, and the feed and permeate channels height. The channel heights are defined by the feed and permeate spacer heights. The spacers themselves are characterised by the mesh length (distance between spacer filaments), filament diameter and orientation

of the filaments (Picioreanu et al., 2009). The feed solution flows in an axial direction parallel to the permeate tube through the feed channel. The solvent (produced fresh water) passes through the membrane and flows as permeate spirally along the curved permeate channel until it is collected in the permeate tube.

The major problems for the performance of spiral wound membrane modules are concentration polarization, organic and biofouling and high feed channel pressure loss (Schwinge et al., 2004a). The performance of the modules is affected by many factors:

- spacers geometry, which greatly affect local mixing, mass transfer and pressure loss,
- fouling propensity and cleaning ability,
- plant design and operating conditions, such as feed pre-treatment, feed concentration, feed pressure and permeate recovery.

Membrane fouling

Four major types of fouling can occurs in spiral wound membrane systems: colloidal (suspended particles such as silica), inorganic (salt precipitations such as metal hydroxides and carbonates), organic (natural organic matters such as humic acid), and biological (such as bacteria and fungi). Because the reverse osmosis and forward osmosis membranes are nonporous, the formation of a fouling layer on the membrane surface is referred to as the dominant fouling mechanism (Kang and Cao, 2012). RO membrane fouling is closely related to the interaction between the membrane surface and the foulant. Previous studies indicated that the physicochemical properties of RO membrane surface, such as hydrophilicity, roughness and electrostatic charge, and the feed spacer geometry are major factors influencing membrane fouling (Louie et al., 2011; Vrouwenvelder et al., 2009a).

Particles in colloidal size range (1 nm – 10 μm) can be present in the feed water and will deposit on the membrane surface. Colloidal particles reported to cause problems in spiral wound membrane systems include aluminium silicate clays, silica, iron and manganese oxides (Tang et al., 2011). Inorganic fouling or scaling is the formation of mineral deposits on the membrane surface. As the feed water becomes more concentrated in salt towards the end of the membrane module some salt may reach their solubility limit and form precipitate. The

most commonly reported precipitates in spiral wound membrane systems are calcium carbonate, calcium sulphate, calcium phosphate, barium sulphate and silica (Antony et al., 2011).

Several organic macromolecules like polysaccharides, humic acids and proteins may deposit at the membrane surface. In wastewater effluent used as NF/RO feed as well as in natural waters, dissolved organic matter is very likely to be present. In seawater, algal organic matter may be found as transparent exopolymer particles (Villacorte et al., 2009).

Biofouling represents the "Achilles heel" of the membrane process because microorganisms can multiply over time; even if 99.9 percent of them are removed with pre-treatment of the feed water, there are still enough microbial cells remaining which can continue to grow at the expense of biodegradable substances in the feed water (Flemming, 1997). Biofouling can be considered as a biotic form of organic fouling, while fouling caused by organic matter derived from microbial cellular debris can be considered as an abiotic form of biofouling (Flemming, 2002). Biofouling has been known as a contributing factor to more than 45 percent of all membrane fouling (Nguyen et al., 2012) and has been reported as a major problem in nanofiltration (NF) and reverse osmosis (RO) membrane filtration (Flemming, 1997; Nguyen et al., 2012). The greatest effect of biofilms on membrane systems may be attributed to the physical properties of the extracellular polymeric substance (EPS) matrix generated by the embedded microorganisms. Relevant characteristics of the EPS matrix are:

- gel-like structure with reduced efficiency of convection processes and greater importance of diffusional processes
- porosity of the gel, which controls the permeation rate of water through a biofilm
- fluid friction resistance, caused by the rough, viscoelastic properties of biofilms

Several fouling control strategies have been developed and tested in full-scale installations. Colloidal, inorganic and organic fouling can generally be controlled by pre-treatment or by dosage of chemicals (antiscalants). However, biofouling can only be delayed by pre-treatment but not eliminated. Dosage of oxidising biocides such as free chlorine is not possible due to damage of the

membrane structure. Several non-oxidising biocides were proven to be used as nutrient by the microorganism enhancing biofilm growth (Creber et al., 2010b; Vrouwenvelder et al., 2000). Current research focus on membrane surface modification, non-oxidizing biocides development and modification of the feed channel geometry and operating condition in order to eliminate or reduce the biofouling in the spiral wound membrane systems (Araújo et al., 2012b; Bertheas et al., 2009; Geraldes et al., 2003; Louie et al., 2011; Tang et al., 2009; Wang et al., 2012).

Despite the efforts on controlling fouling in spiral wound membrane systems, biofouling is still the major problem in membrane filtration processes, causing increased energy demand and unstable operation. Fundamental understanding of the biofilm formation in spiral wound membrane systems is crucial in order to develop strategies to control and keep biofouling at an acceptable level.

SCOPE AND OUTLINE OF THE THESIS

The objective of this thesis was to better understand the biofouling mechanisms in spiral wound reverse osmosis and forward osmosis membrane systems using experimental and mathematical approaches.

The thesis is structured in three themes: (i) method development, (ii) impact of nutrients, materials and operating conditions on biofilm developments in reverse osmosis spiral wound membrane systems and (iii) biofouling in forward osmosis membrane systems.

Systematic laboratory studies on membrane biofouling require experimental conditions that are well defined and representative for practice. Hydrodynamics and flow rate variations affect biofilm formation, morphology, and detachment and impacts on membrane performance parameters such as feed channel pressure drop. The objective of this study was to develop a system to provide an accurately measured, stable water flow through the MFSs, enabling to study biofouling in spiral wound membrane systems systematically, under well-controlled and defined conditions (***Chapter 2***). The impact of different spacer geometries on the water flow pattern is not easily measurable experimentally due to the inherently small length-scales involved. Alternatively, advances in numerical performance have led to computational fluid dynamics (CFD) techniques being the primary means to understand the fluid flow in spacer-

filled channels. Therefore, the micro-scale flow patterns in a feed spacer-filled channel under conditions representative for current practical applications (i.e., similar linear flow velocity and channel dimensions) using particle image velocimetry (PIV) was experimentally evaluated, and compared with three-dimensional numerical simulations (***Chapter 3***).

The second theme of the thesis is focusing on the biofilm development in spiral wound membrane systems under various conditions. The influence of biodegradable organic nutrient load on biofouling, addressing the feed channel pressure drop increase (operational parameter) and biofilm development was determined in ***Chapter 4***. ***Chapter 5*** evaluated the impact of the membrane and feed spacer surface modification on biofilm formation and biofouling control in membrane systems. The study presented in ***Chapter 6*** evaluated the biofilm development under various operational conditions and the impact of biomass location by numerical simulations.

High energy demand for current pressure drive desalination technologies has limited its use in several regions. One of the main advantages of forward osmosis (FO) is the limited amount of external energy requirement. For desalination applications of FO, there are two possible approaches, *direct* and *indirect* desalination. In *direct* FO desalination processes fresh water is directly extracted from seawater or brackish water by using the high salinity water as feed solution and an osmotic reagent as draw solution. In *indirect* FO desalination, the high salinity water is used as draw solution and an impaired water such as secondary wastewater effluent is used as of feed solution. The attractiveness of *indirect* FO desalination beside the low-cost draw solution (seawater or brackish water) relies on the diluted draw solution (diluted seawater) which can be used as feed water in a subsequent desalination process like reverse osmosis, thus reducing the cost of the entire desalination process. The last theme (***Chapter 7*** and ***8***) focuses on biofouling and its effect on forward osmosis membrane systems. The influence of feed spacer, biofilm properties, location and surface coverage was analysed experimentally and by numerical simulations.

The thesis is structured as a paper dissertation, i.e. it consists of a number of scientific articles, except for the introduction chapter. Some repetitions are consequently unavoidable in individual chapters. Small adaptations have been made to improve the chapters.

٢

Experimental Setup for Stable Flow Conditions in Membrane Biofouling Studies

Abstract

Systematic laboratory studies on membrane biofouling require experimental conditions that are well defined and representative for practice. Hydrodynamics and flow rate variations affect biofilm formation, morphology, and detachment and impacts on membrane performance parameters such as feed channel pressure drop. There is a suite of available monitors to study biofouling, but systems to operate monitors have not been well designed to achieve an accurate, constant water flow required for a reliable determination of biomass accumulation and feed channel pressure drop increase. Studies were done with membrane fouling simulators operated in parallel with manual and automated flow control, with and without dosage of a biodegradable substrate to the feed water to enhance biofouling rate. High flow rate variations were observed for the manual water flow system (up to ≈9%) compared to the automatic flow control system (<1%). The flow rate variation in the manual system was strongly increased by biofilm accumulation, while the automatic system maintained an accurate and constant water flow in the monitor. The flow rate influences the biofilm accumulation and the impact of accumulated biofilm on membrane performance. The effect of the same amount of accumulated biomass on the pressure drop increase was related to the linear flow velocity. Stable and accurate feed water flow rates are essential for biofouling studies in well-defined conditions in membrane systems.

Published as:

Szilard S. Bucs, Nadia Farhat, Amber Siddiqui, Rodrigo Valladares Linares, Andrea I. Radu, Joop C. Kruithof, Johannes S. Vrouwenvelder (2015) Development of a setup to enable stable and accurate flow conditions for membrane biofouling studies. *Desalination and Water Treatment*, **57**: 12893-12901.

INTRODUCTION

Biofouling, the unwanted deposition and growth of biofilms (Flemming, 2002), is a problem encountered in most membrane installations in the water industry (Peña et al., 2012). Extensive pre-treatment and/or chemical dosage to feed water can prevent particulate fouling or scaling, however, biofouling remains a major problem, especially in spiral wound membrane systems (Baker and Dudley, 1998; Flemming et al., 1997; Schneider et al., 2005; Shannon et al., 2008; Tasaka et al., 1994; van Loosdrecht et al., 2012; Vrouwenvelder et al., 2008b). Biofilm growth in membrane systems and the impact on membrane performance is affected by several interrelated factors, such as the availability of biodegradable nutrients, hydrodynamics (Bucs et al., 2014b; Radu et al., 2012; Vrouwenvelder et al., 2009b; Ying et al., 2013), feed spacer design, and surface material (Kang and Cao, 2012), and it is not directly related to parameters measured in the feed water such as total organic carbon (TOC) concentration and bacterial cell number (Vrouwenvelder et al., 2008b). Therefore, there is a need for systematic, controlled laboratory studies with a well-designed membrane biofouling monitor system, representative for full-scale applications. Many monitors have been developed to study biofilm growth (Bakke et al., 2001; Blanco et al., 2011; Boorsma et al., 2011; Cloete and Maluleke, 2005; Donlan et al., 2004). Most monitors were designed to simulate biofouling in heat exchangers, cooling towers, and water distribution networks (Zhang et al., 2011; Zinn et al., 1999), and were not representative for biofouling in membrane systems. Although the mentioned applications share the same problem, biofilm development and the impact on performance might be entirely different. For example, a biofilm monitor developed to study the biofouling growth in a water distribution network will not be representative for biofouling development in membrane filtration installations. Fouling in membrane-based water treatment installations causes an increase in normalized pressure drop over the feed channel and/or reduction in normalized flux and/or increase in salt passage (Ridgeway and Foundation, 2003). In order to enable improved plant performance, monitor studies should be carried out to get a better understanding of the biofilm development process, in order to formulate more suitable control strategies. A membrane biofouling monitor system is defined as a device, where water-containing nutrients passes through a flow cell, containing a membrane and a feed spacer to which micro-organisms attach and grow to form a biofilm. Operational data can be obtained from the monitor

like pressure drop increase, water flux, and feed water flow rate, and allows visual observation of fouling development. For a representative application, the monitor should resemble the spiral wound membrane element, in terms of materials and hydrodynamic conditions: the flow distribution should be uniform, and the pressure drop should be similar to spiral wound elements and should have the same feed water composition. The relationship between linear flow velocity and pressure drop for the monitor should be representative of the spiral wound membrane element. Currently, monitors containing membranes and feed spacers, differing in terms of size and operation mode are available to study the biofilm development in spiral wound membrane systems (Vrouwenvelder et al., 2007a, 2007b, 2006). Many of these monitors have shown to be suitable for biofouling studies in membrane filtration systems, but require close attention during operation (Dreszer et al., 2014a; Nguyen et al., 2012). The driving force in applied membrane fouling simulator (MFS) setups to generate flow through the MFS is the drinking water distribution network pressure. The flow rate is controlled manually by a valve installed at the outflow side of the flow cell. During the experiments, the flow rate is measured manually, and the valve is adjusted to keep a constant flow rate. When fouling occurs, flow adjustments have to be more frequently done, making these monitor setups difficult to operate. Therefore, there is a need for a system to enable constant flow operation and accurate monitoring of operational parameters of small-scale membrane monitors. Such a system should provide a constant feed flow under biofilm accumulation conditions in the monitor and accurate measure of the pressure drop across the flow channel (Table 2.1).

Table 2.1: Inventory of the required features, current status and the developed system for operation of membrane fouling simulators.

	required features of the system	current status	developed system
1.	stable, constant water flow	manual reading and frequent manual adjustments	automated system with flow sensor and continuous automatic adjustments
2.	adjustable feed pressure for permeate production	depending on the feed water pressure (1 – 4 bar)	the system can be operated between 0 – 17 bar
3.	accurate measurements and readings of operation parameters	manual reading with high time frames	automated adjustable reading frequency from 1 second up to 24 hours
4.	easy and flexible operation	need for feed pressure and operation parameter readings	operates without feed pressure and can be manipulated remotely
5.	compatibility with current flow cells to study fouling in spiral wound systems	compatible only with low pressure cell, without permeate production	compatible with current flow cells

The objective of this study was to develop a system to provide an accurately measured, stable water flow through the MFSs, enabling to study biofouling in spiral wound membrane systems systematically, under well-controlled and defined conditions.

MATERIALS AND METHODS

Description of the developed biofilm monitor setup

The biofilm monitor setup was equipped with a water pump, pressure dampener, thermometer, flow meter, flow cell, differential pressure transmitter, and a back-pressure valve to enable unit pressurization (Figure 2-1). All sensors and the feed water pump were connected to a central computer (TAC Vista Server). The server logged all data received from the sensors and also regulated the feed water transport pump. The water flow through the flow cell was provided by a pump (metering diaphragm pump, Hydra-Cell G20, Wanner Engineering, USA). To eliminate pulsation in the water flow, a pressure dampener was installed right at the outlet of the pump. The pump can be connected directly to a water distribution network or a break (equalization) tank. According to the manufacturer's specifications, the maximum water flow rate of the pump is 230 $L \cdot h^{-1}$ at a pressure of 17 bar.

A paddle wheel flow sensor (Flow X3, Italy) was installed on the outlet tube of the pump after the pressure dampener. The flow sensor was connected to the server, and the flow was monitored continuously. A pre-set flow rate was maintained by increasing or slowing down the rotation speed of the water pump according to the flow sensor signal by the server. Thus, a constant flow rate can be maintained automatically, even when fouling causes a pressure drop increase in the flow cell.

Dosage of chemicals was provided by a diaphragm metering pump (Stepdos 08, KNF Lab, Germany) which can operate at low flow rates (0.08–80 $mL \cdot min^{-1}$). A ceramic differential pressure sensor (Endress + Hauser PMD70, Germany) was connected to the flow cell inlet and outlet. The pressure drop over the flow cell was measured hourly and logged on the server. The unit can be operated with different flow cells up to a pressure of 17 bar, allowing the study of biofilm formation in filtration systems at different pressures, flow rates, and with or

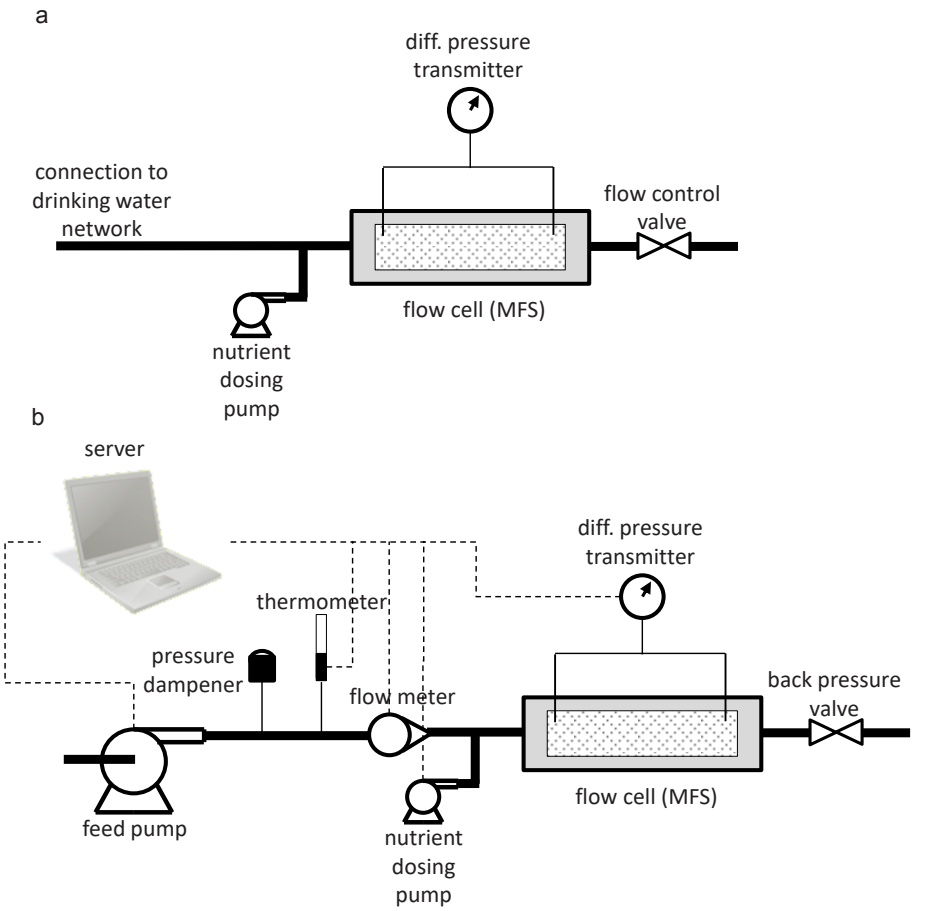

Figure 2-1: Schematic representation of the system for membrane fouling simulator operation, (a) with manual flow control and the (b) developed setup with automatic flow control and data logging system.

without permeate production. On the flow cell outlet, a back pressure valve was installed to control the working pressure of the MFS unit.

System validation

The MFS (Vrouwenvelder et al., 2007b) was used in this developed setup to validate the system. Commercially available reverse osmosis (RO) membrane sheets and 31 mil (787 µm) thick feed spacers were used. To create representative hydrodynamics in the flow cell, the flow rate was set at 16 $L \cdot h^{-1}$, resulting in a linear flow velocity of 0.163 $m \cdot s^{-1}$. Tap water was used as the feed for the units. A solution of sodium acetate, sodium nitrate, and sodium

Table 2.2: Experimental conditions for the studies to evaluate the suitability of the developed system for biofouling studies with constant water flow.

Description	Aspect studied	Nutrient dosage	Results
manual flow control reference system	flow accuracy, stability and pressure drop	with and without	Figure 2-2
automatic flow control system (developed)	flow-rate accuracy	without	Figure 2-3
	flow accuracy, stability and pressure drop	with and without	Figure 2-4
comparison manual and automatic flow control in biofilm formation studies	pressure drop and biofilm accumulation	with and without	Figure 2-5

dihydrogen orthophosphate in a mass ratio C:N:P of 100:20:10, respectively, was employed with a C concentration in the feed water of 400 µg·L-1.

Evaluation of the fouling material

After eight days of operation and a significant pressure drop increase over the unit with substrate dosage, the flow cells were opened, and the membrane and feed spacer were analysed. Adenosine triphosphate (ATP) and TOC were measured to quantify the accumulated biomass. Energy-dispersive X-ray (EDX) measurements were carried out to determine inorganic deposition and screen for biofilm accumulation on the membrane surface.

RESULTS

A system was developed to provide an accurate and stable water flow to MFSs. Comparison studies were performed with the manual flow control system (used in earlier MFS studies) and the developed automatic flow control system to assess (i) feed water flow rate stability, (ii) feed channel pressure drop, and (iii) biofilm accumulation. Studies were done with and without dosage of biodegradable organic nutrients to the MFS feed water to enhance biofilm formation. A summary of the studies is shown in Table 2.2.

Evaluation of manually controlled reference system

Earlier investigations with the manually controlled flow system have shown varying water flow rates in time passing through the monitors, especially, when significant biofilm accumulation on the feed spacer and membrane sheets in the monitor occurred. Delayed correction of the flow rate affected the pressure drop over the monitor. To quantify the variation of flow rate and its impact on pressure drop development, parallel studies were done using (i) a monitor

without nutrient dosage and (ii) a monitor with nutrient dosage. The water flow rate and pressure drop were monitored in time. The flow rate for the monitor without nutrient dosage showed variations up to ±3 percent of the set feed flow rate (16 $L \cdot h^{-1}$ and 0.16 $m \cdot s^{-1}$) during the research period (Figure 2-2a), while the pressure drop over the monitor was relatively constant with time (Figure 2-2b). For the MFS with nutrient dosage, during the first four days of the study, the flow rate showed variations up to ±3 percent and a relative constant pressure drop. After four days, higher flow rate variations up to ±9 percent (Figure 2-2a) were found corresponding to stronger pressure drop variations (Figure 2-2b). In other words, the manual flow control system was influenced by the impact of biofilm formation, resulting in significant variations in terms of flow rate and corresponding pressure drop (up to ± 9 percent). Systematic biofouling studies under well-controlled conditions require a more accurate and stable water flow. Therefore, an automatic flow control system was developed.

Evaluation of the automatic flow control system

The developed automatic system for feed water flow control was evaluated on the (i) accuracy of the flow rate, (ii) flow stability, and (iii) pressure drop development with and without nutrient dosage.

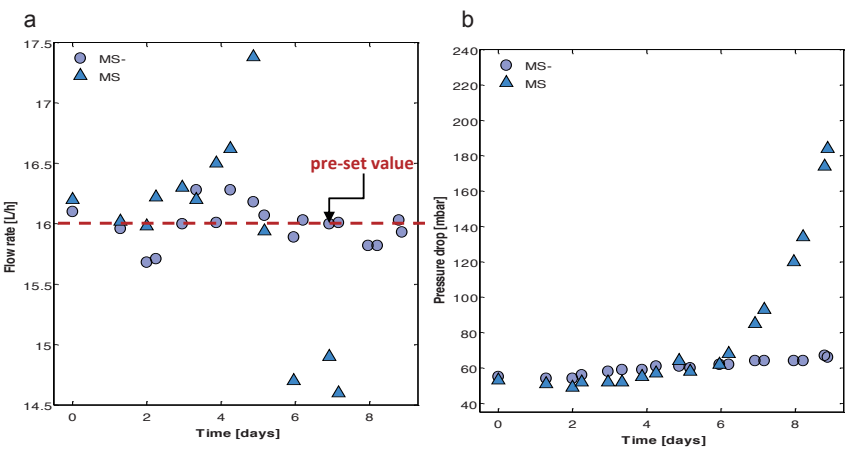

Figure 2-2: Feed water flow-rate (a) and pressure drop in time (b) over the MFS systems with manual flow control and fed with water without (MS-) and with supplemented (MS) biodegradable nutrient.

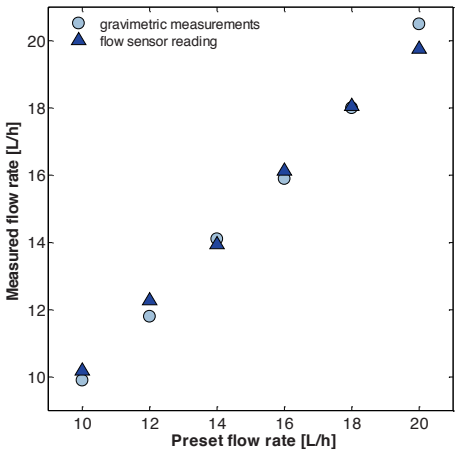

Figure 2-3: Correlation between pre-set and measured flow-rate of the developed automated system for the range 10 to 20 $L \cdot h^{-1}$.

Flow rate accuracy

The accuracy of the automatic water flow control system was determined by comparison of set point and gravimetrically measured flow rates for the range 10 – 20 $L \cdot h^{-1}$ (equal to a linear velocity of 0.10 – 0.20 $m \cdot s^{-1}$). Gravimetric flow measurements were carried out to validate the accuracy of the automatic system.

The set point and gravimetrically measured flow rates showed a linear relationship for the range of 10 – 18 $L \cdot h^{-1}$ (Figure 2-3). Less than one percent flow deviation was observed. A good correlation was found between the automatic system set flow and the gravimetrically measured flow rates. The automatic system was shown to be suitable to provide and maintain an accurate flow rate without biofilm accumulation.

Flow stability during biofilm development

The automatic system for MFS operation was evaluated by operating monitors in parallel (i) without and (ii) with nutrient dosage to the monitor feed water. The flow rate and pressure drop were monitored in time. Irrespective of nutrient dosage to the automatic system, flow rate variations smaller than one percent were observed during the whole research period (Figure 2-4a). In time, (i) without nutrient dosage the pressure drop over the monitor was constant (Figure 2-4b), while (ii) with nutrient dosage the pressure drop increased sharply. During the research period, the automatic system enabled an accurate, stable water flow with variations smaller than one percent of the set flow rate.

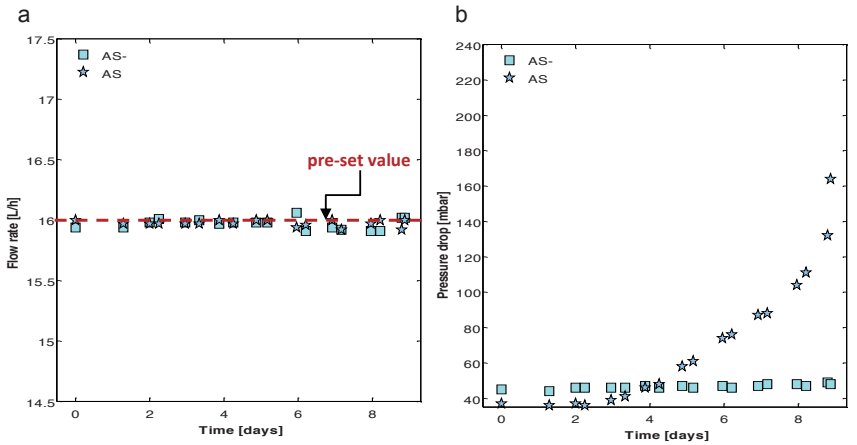

Figure 2-4: Feed water flow-rate (a) and pressure drop in time (b) over the MFS systems with automatic flow control fed with water without (AS-) and with dosed (AS) biodegradable nutrient.

Manual and automatic flow control in biofilm formation studies

To determine the influence of both manual and automatic flow regulation on pressure drop development and biofilm accumulation, monitor studies were performed. Two manually regulated monitors, and two automatically regulated monitors were run in parallel with and without nutrient dosage.

With nutrient dosage, the pressure drop increased for both the manual and automatic system (Figure 2-5a). At the end of the eight-day research period, the pressure drop increase was lower for the manual system compared to the automatic system (Figure 2-5b), while the same amount of accumulated biomass (ATP and TOC) was found for both the systems (Figure 2-5c,d). SEM–EDX measurements of the feed spacer and membrane surface from the monitors showed the (i) absence of inorganic deposition in all systems and (ii) presence of biofouling in the systems fed with nutrient dosage. The flow rate variations of the manual system caused a significantly lower pressure drop than the automatic system with the more accurate flow control. The automatic flow control system provided an accurate and constant feed flow rate to the flow cell irrespective of fouling accumulation.

DISCUSSION

The main objective of this study was to develop a system which can provide a constant water flow to the MFSs, enabling biofouling studies in MFS units

under well-defined conditions. The developed automatic system was compared with a manually flow controlled system used in previous studies (Araújo et al., 2012a; Creber et al., 2010b; Miller et al., 2012; Vrouwenvelder et al., 2009b). For these two systems, water flow rate variations, and its impact on pressure drop increase with and without biomass accumulation were compared (Figure 2-2, Figure 2-4, Figure 2-5). Much lower flow variations were observed for the automatic water flow system (<1%) compared to the manual system (up to ~ 9%).

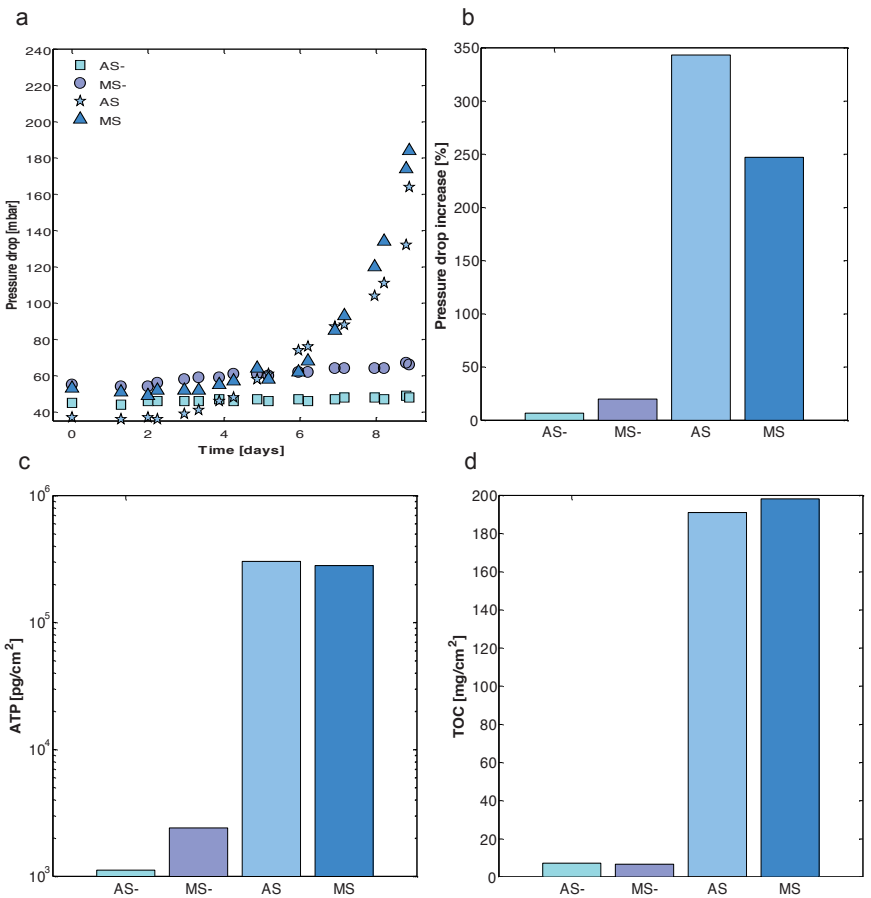

Figure 2-5: Pressure drop in time (a) and pressure drop increase (b), and accumulated biomass in ATP and TOC (c, d) for manually and automatic controlled setups. Manual flow control without substrate (MS-) and with dosed substrate (MS). Automatic flow control without substrate (AS-) and with dosed substrate (AS). In all cases the initial pressure drop was lower for the automatic setups.

It was shown that fluctuations in feed water flow rate directly impacts the measured performance indicators (i.e. pressure drop). Therefore, an automatic water flow control system is essential for systematic biofouling studies in MFSs.

Importance of accurate and stable feed flow

A suite of monitors has been developed to study the biofilm formation and related performance decline (biofouling) in membrane systems for water treatment (Flemming, 2003). For representative biofouling studies, the MFS units are designed to have similar hydrodynamics as in spiral wound membrane modules. Although the developed MFSs are suitable for biofouling studies, the way in which the monitors are operated may impact the results. Hydrodynamic conditions affect biofilm formation and morphology in spiral wound membrane systems (Vrouwenvelder et al., 2010b, 2009b); at lower flow rates: (i) the same amount of accumulated biomass has a lower impact on membrane performance and (ii) biofilm accumulation is slower, while at high flow rates biofilm accumulation is more rapid and a different biofilm morphology is observed. The water flow rate and thus, water flow rate variations have an impact on the biofilm accumulation rate and morphology and changes in flow rate may lead to biomass detachment. The impact of accumulated biomass on the feed channel pressure drop depends on the linear flow velocity (Vrouwenvelder et al., 2011b, 2009b). Clearly, constant and accurate water flow is very important. The developed automatic system enabled a constant flow rate with variations smaller than one percent throughout the experimental studies, while for the manual system variations were found up to three percent without biofilm formation and up to nine percent with biofilm formation. The manual system biofilm formation strongly influenced the flow rate. Membrane performance is evaluated by feed channel pressure drop increase and/or permeate flux decline. Both membrane performance parameters are affected by the water flow rate. Our study illustrates that a sensitive, accurate water flow monitoring is required for an accurate determination of the impact of fouling accumulation on membrane performance parameters. In summary, stable and accurate feed water flow rates are needed for controlled membrane biofouling studies using monitors. The developed automatic setup for monitor operation is suitable to maintain an accurate constant water flow rate enabling reliable pressure drop measurements.

Evaluation of earlier research done with manual flow control

Earlier membrane biofouling studies with monitors used a manual flow control system involving a combined flow control with back pressure valve which was located after the monitor (Figure 2-1a). The flow control system had a spring and membrane regulating the water flow to a certain extent. The manual water flow system showed the same accumulated amount of biofilm as the automatic flow system after the nine-day study, in which the feed channel pressure drop over the monitors showed a clear difference in pressure drop increase (Figure 2-5). The same bio- film accumulation illustrates that the results of the earlier membrane biofouling studies using MFSs with manual flow control are still valid. However, systematic well-controlled studies on biofouling require a stable water flow.

CONCLUSIONS

An automatic system for constant and automatic flow control of feed water to MFSs was developed and evaluated. Results were compared with a manual flow control system, previously used for membrane biofouling studies. Based on the results, the following conclusions can be made:

- Stable and accurate feed water flow rates are needed for controlled membrane biofouling studies: this was achieved by the automatic setup.
- Correct pressure drop measurements requires an accurate constant water flow rate.
- The developed automatic system for monitor operation is suitable to maintain an accurate constant water flow rate, enabling accurate pressure drop measurements and more stable biofilm growth.

۳

Hydrodynamic Characterization of Spacer-Filled Channels

Abstract

Micro-scale flow distribution in spacer-filled flow channels of spiral-wound membrane modules was determined with a particle image velocimetry system (PIV), aiming to elucidate the flow behaviour in spacer-filled flow channels. Two-dimensional water velocity fields were measured in a flow cell (representing the feed spacer-filled flow channel of a spiral wound reverse osmosis membrane module without permeate production) at several planes throughout the channel height. At linear flow velocities (volumetric flow rate per cross-section of the flow channel considering the channel porosity, also described as crossflow velocities) used in practice (0.074 and 0.163 $m \cdot s^{-1}$) the recorded flow was laminar with only slight unsteadiness in the upper velocity limit. At higher linear flow velocity (0.3 $m \cdot s^{-1}$) the flow was observed to be unsteady and with recirculation zones. Measurements made at different locations in the flow cell exhibited very similar flow patterns within all feed spacer mesh elements, thus revealing the same hydrodynamic conditions along the length of the flow channel. Three-dimensional (3-D) computational fluid dynamics simulations were performed using the same geometries and flow parameters as the experiments, based on steady laminar flow assumption. The numerical results were in good agreement (0.85-0.95 Bray-Curtis similarity) with the measured flow fields at linear velocities of 0.074 and 0.163 $m \cdot s^{-1}$, thus supporting the use of model-based studies in the optimization of feed spacer geometries and operational conditions of spiral wound membrane systems.

Published as:

Szilard S. Bucs, Rodrigo Valladares Linares, Jeremy O. Marston, Andrea I. Radu, Johannes S.Vrouwenvelder, Cristian Picioreanu (2015) Experimental and numerical characterization of the water flow in spacer-filled channels of spiral-wound membranes. *Water Research* **87**: 299–310.

INTRODUCTION

Membrane filtration processes for seawater desalination and wastewater reuse are becoming increasingly important. In a spiral-wound membrane module, most commonly used in these water treatment processes, the membrane sheets are rolled around an inner tube. To keep the membrane leaf's apart a relatively thin spacer net is inserted. The feed spacer promotes flow instabilities to enhance mass transfer and reduce concentration polarization (Fimbres-Weihs et al., 2006; Gao et al., 2013). However, aside from a beneficial impact, the feed spacer also contributes to pressure drop increase along the flow channel. Furthermore, a major drawback in membrane technology is fouling, i.e. accumulation of unwanted material on the membrane and spacer surface (Antony et al., 2011; Baker and Dudley, 1998; Flemming, 2002; Ridgway et al., 1983; Salvador Cob et al., 2012). Micro-sized particles, colloids, organic macromolecules can deposit and microbial cells can grow and form biofilms on the membrane and spacer surfaces and decrease the filtration performance (Flemming, 1997; Tang et al., 2011; Yiantsios and Karabelas, 2003). Baker and Dudley (1998) reported that initial deposition of fouling occurred on the feed spacer filaments and on the membrane alongside the spacer and, with time, intruded upon the remaining free membrane area.

It was shown that fouling accumulation can be controlled to some degree by suitable hydrodynamic conditions (Sablani et al., 2001). Moreover, the same amount of accumulated fouling material can have a different impact on performance, depending on the hydrodynamic conditions (Araújo et al., 2012a; Bucs et al., 2014a; Valladares Linares et al., 2014a; Vrouwenvelder et al., 2011a). Feed spacer geometry and operational conditions (e.g., flow velocity, transmembrane pressure, etc.) have a profound influence on the flow pattern and foulant deposition in spacer-filled channels (Radu et al., 2014; Vrouwenvelder et al., 2009). To design new spacers with the least pressure drop, minimal fouling propensity, and maximum mass transfer, it is therefore important to both be able to determine experimentally and to numerically calculate the hydrodynamics (i.e., velocity and pressure profiles, shear at the walls, etc.) in these flow channels.

The impact of different spacer geometries on the flow pattern is not easily measurable experimentally due to the inherently small length-scales involved.

Alternatively, advances in numerical performance have led to computational fluid dynamics (CFD) techniques being the primary means to understand the fluid flow in spacer-filled channels. Some studies have simulated fluid flow and mass transfer in simplified two-dimensional setups (Schwinge et al., 2002; Radu et al., 2010). However, in recent years, three-dimensional (3-D) numerical models are becoming increasingly accessible, developed mainly with an emphasis on the effect of feed spacer on hydrodynamics and mass transfer in feed spacer channels (Koutsou et al., 2007; 2009; Saeed et al., 2012). Simplified cylindrical shapes have been used for representation of spacer filaments in most of the numerical studies. However, microscopic observations of the feed spacer revealed that the spacers used in commercially available spiral-wound membrane modules have more irregular geometry, with filaments varying in thickness (Fimbres-Weihs and Wiley, 2010; Picioreanu et al., 2009; Vrouwenvelder et al., 2010c). Simulations by Picioreanu et al. (2009) showed that the feed channel pressure drop for a simplified spacer with cylindrical filaments is significantly different from more realistic spacer geometry with variations in filament thickness. The importance of realistic spacer geometries in numerical studies was also revealed by a recent experimental and numerical study on particle deposition in spacer channels at various feed spacer orientations (Radu et al., 2014).

In contrast with the abundance of numerical studies, only a few experimental investigations were carried out to directly visualize and characterize the flow patterns in feed spacer-filled channels. This may be partly due to the geometrical complexity and small dimensions of the flow channels (thereby the need for microscopic techniques), but also due to the high temporal resolution required (i.e., very fast flows require use of fast cameras).

Nuclear magnetic resonance (NMR) or magnetic resonance imaging (MRI) has been used to locally resolve (in 3-D) the velocity and shear stress distribution in tube reactors containing biofilms (Manz et al., 2003; Wagner et al., 2010). In spacer-filled channels with and without biofilm, NMR was used to visualize and measure two-dimensional velocity profiles (Vrouwenvelder et al., 2010c). Formation of preferential flow patterns was observed as biofouling evolved in time. However, as a limitation of the method used, the flow cell was operated with 10 times lower linear flow velocity than normally used in practice, and the measured velocity had to be averaged over the flow channel height.

Doppler optical coherence tomography (DOCT) was also used to measure and visualize the local velocity profile in a spacer-filled channel (Gao et al., 2013). The DOCT could reveal the flow profile normal to the main flow direction at different sections along the flow channel. Furthermore, the development of eddies were observed next to the spacer filaments.

Particle image velocimetry (PIV) was used to characterize the flow next to the membrane surface at different linear flow velocities by Gimmelshtein and Semiat (2005) and Willems et al. (2010). Gimmelshtein and Semiat (2005) found laminar flow at commonly used linear flow velocities (0.06–0.17 $m \cdot s^{-1}$), with (expectedly) increasing mixing intensity at higher linear flow velocities. The measured flow fields were in good agreement with the two-dimensional numerical simulations developed by the authors (Gimmelshtein and Semiat, 2005). Willems et al. (2010) used PIV techniques to achieve a quantitative description of the two-phase flow in spacer-filled channel. Although the temporal resolution was low, the study showed how the flow direction changed along the channel height and also evaluated the impact of bubbly flow on local velocity. PIV techniques were also applied to investigate the flow patterns in flow channels using modified saw-tooth spacer geometries (Liu et al., 2015). However, the flow channel thickness (4 mm) in these experiments was much higher than in reverse osmosis/nanofiltration systems applied in practice.

In summary, all of these experimental methods have some limitations in terms of the flow channel thicknesses used, the applied linear flow velocity, the spatial or temporal resolution. As such, the objectives of this study were: (i) to evaluate the micro-scale flow patterns in a feed spacer-filled channel under conditions representative for current practical applications (i.e., similar linear flow velocity and channel dimensions) using a PIV system, and (ii) to compare the measured flow fields with three-dimensional numerical simulations.

MATERIALS AND METHODS

Experimental

Micro-scale fluid flow patterns in spacer-filled channels were experimentally investigated by particle image velocimetry (PIV).

Flow cell. For PIV measurements, a fully transparent flow cell was constructed from two high quality glass slides (2.5 cm width and 7.5 cm length, VWR International, West Chester, PA) (Figure 3-1). Commercially available non-woven Toray feed spacer with 31 mil (0.787 mm) thickness was inserted between the glass slides. The height of the flow cell was adjusted to fit the feed spacer thickness and to avoid bypass flow below or above the spacer, then the whole ensemble was glued with epoxy resin on the sides. Water connectors were fabricated from nylon tubing with 4 mm (for inlet) and 6 mm (for outlet) inner diameter (Figure 3-1).

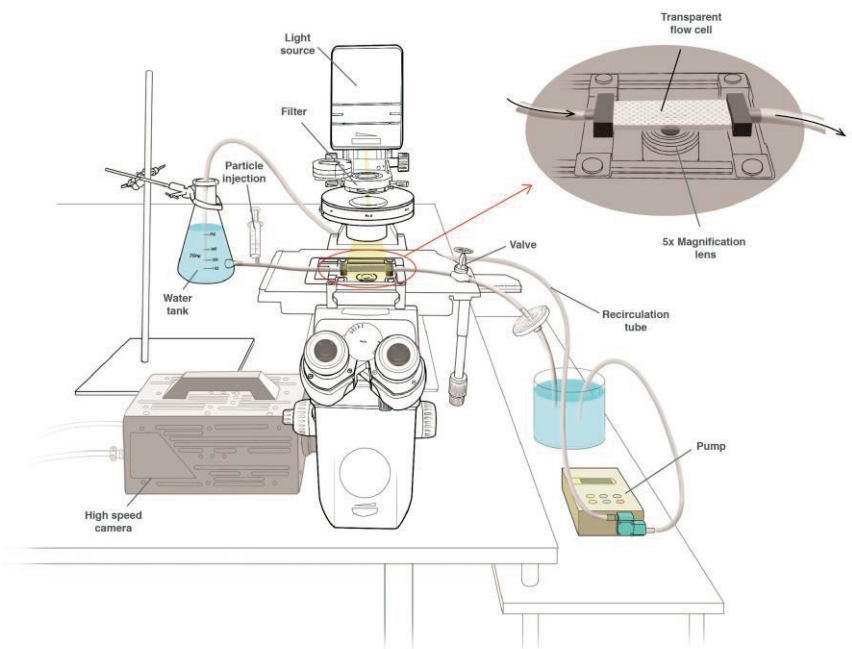

Figure 3-1: Experimental setup used for water flow measurements and visualization, using particle image velocimetry (PIV). The experimental setup consisted of an elevated water tank, a transparent flow cell with a feed spacer, a particle injection point, a microscope and a high speed camera.

In order to keep the flow cell transparent, no membrane sheets were inserted into the flow channel and the flow cell was operated without permeate production. The impact of permeation on the cross flow velocity in our lab scale flow cell (7.5 cm long) is negligible since the permeate velocity (typically in the order of 10 μm·s^{-1}, (Radu et al., 2010) is four orders of magnitude lower than the linear flow velocity of the feed water (in the order of 10 cm·s^{-1}). Even without permeation, the presence of a membrane sheet instead of glass wall would not visibly influence the flow pattern, because the average roughness of an RO membrane is in the order of 50 nm (Ishigami et al., 2012), three orders of magnitude lower than our depth of field for flow visualization in *z* direction.

To eliminate pulsations generated by pumps, hydrostatic pressure was used instead to drive the water flow through the flow cell. A 3 L reservoir was placed about 1 m above the flow cell and connected to the flow cell inlet. The flow rate was adjusted with a valve connected to the flow cell outlet. To maintain constant flow-rate the water level was kept constant in the reservoir by recirculating the water (Figure 3-1). The Reynolds number was calculated according to Schock and Miquel (1987), equation 3-1.

$$\mathrm{Re} = \frac{u_m \cdot d_h \cdot \rho}{\eta} \qquad 3\text{-}1$$

with u_m being the imposed linear (i.e. average) flow velocity. ρ and η are the water density and viscosity at 20°C (998 kg·m^{-3} and 0.001 Pa·s, respectively), and d_h is the hydraulic diameter (≈1 mm), calculated from the total volume between the glass slides, V_{Tot}, the spacer volume, V_{Sp}, and the wetted surface A_{w} (equation 3-2) including feed spacer and both glass slides (Schock and Miquel, 1987).

$$d_h = \frac{4(V_{Tot} - V_{Sp})}{A_w} \qquad 3\text{-}2$$

The flow rate was measured gravimetrically at the outlet. Measurements were performed at three linear inflow velocities: u_m=0.163 m·s^{-1} (Re=160), 0.074 m·s^{-1} (Re=70) and 0.294 m·s^{-1} (Re=300).

Particles. For flow visualization, silver coated hollow glass beads of 10 μm diameter (neutrally buoyant, ρ_p=1.05 g·cm^{-3}, ±5% size distribution) were

injected into the inlet tubing of the flow cell during the measurements (P/N 10089, TSI Incorporated, Shoreview, MN). A volume of 10 mL suspension of particles (≈0.5 mg·L^{-1} concentration) was injected right before the PIV measurements were made. Seeding density was kept above eight particles for an imaged area of 32 pixels × 32 pixels. A 5 μm pore size filter was mounted to the outflow tube to prevent recirculation and eventual deposition of the injected particles.

Visualization. For typical PIV measurements a laser strobe is used as light source with a cylindrical lens to limit the illuminated region to the area of interest. To use conventional PIV setup for visualizing the flow in a spacer-filled channel at different heights the laser beam should have been placed perpendicular to the camera, thus allowing illumination of the flow channel at various heights (z direction). The dimension of the flow channel and the presence of the feed spacer limited the possibility of using conventional PIV. For the presented measurements a modified PIV setup was used which allowed capturing the flow pattern at various heights within the spacer-filled channel. Particles were visualized using an inverted microscope (Axio Imager, Zeiss Microscopy GmbH, Germany) in combination with a high-speed camera (Fastcam SA5, Photron Inc. San Diego, CA) and a 5× objective lens with 0.13 numerical aperture (NA). To narrow the depth of field (DOF), a 550 nm filter (BP 550/25, 537-563 nm) was placed in front of the light source, so that a 42 to 44 μm focal depth was achieved, equation 3-3.

$$DOF = \frac{\lambda \cdot n}{NA^2} \qquad 3\text{-}3$$

where λ = 0.550 μm is the light wavelength and n = 1.33 is the refractive index of water.

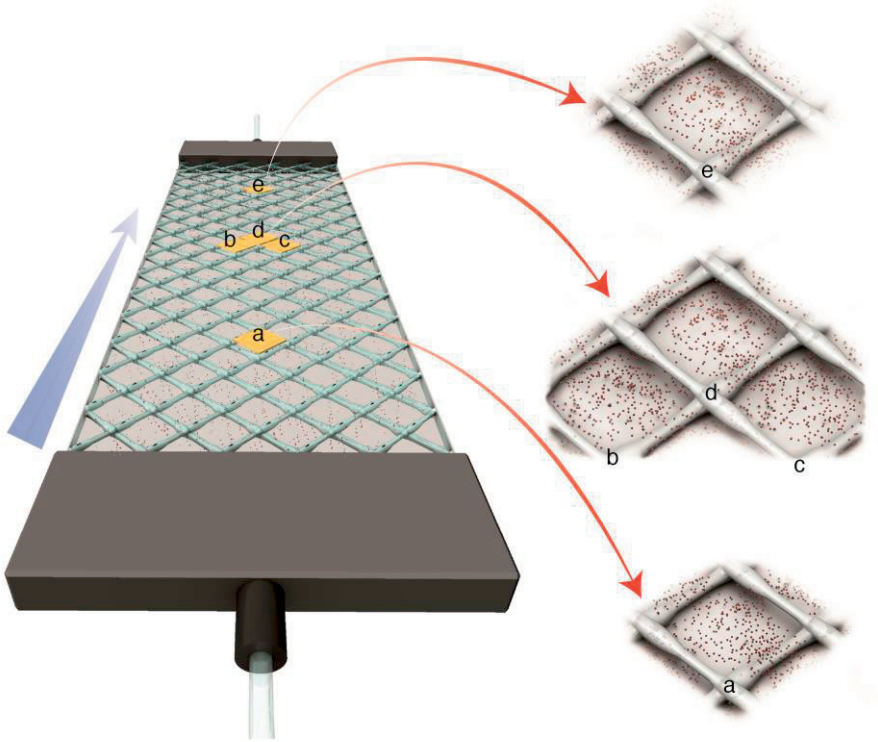

Figure 3-2: Schematic representation of the flow cell and the five feed spacer elements (a to e) used to assess the water flow reproducibility at different locations in the flow cell.

The camera was set to capture 7000 frames per second (fps) with an exposure time of 1/30,000 s, sufficient to eliminate particle motion blur. The obtained image size was 1024×1024 pixels. For each measurement 100 consecutive frames were processed. The angle of view and DOF allowed capturing an area of approximately one feed spacer mesh element (approximately 4 mm × 4 mm) from the flow cell (Figure 3-2). To obtain a complete overview of the flow pattern in the channel, measurements were repeated at different feed spacer mesh elements (x and y direction) and at different positions along the channel height (z direction), for each experimental condition.

Calculation and visualization of velocity fields. The captured video clips were analyzed by a commercially available PIV software (DaVis, LaVision GmbH, Goettingen, Germany), using a sequential frame cross correlation method. For quantitative analysis the software was calibrated based on the pixel size (4 μm × 4 μm) on the captured video clips, which was the same for all PIV

measurements. The analyses performed on the video data were the calculation of velocity fields and streamlines. The same velocity field calculation procedure was repeated for different z positions (i.e., at maximum 18 different heights in the flow channel). The measured vector fields were visualized and statistically analyzed by custom-written routines in MATLAB (MATLAB 2014b, MathWorks, Natick, MA, www.mathworks.com). 100 PIV measurements (i.e., image frames over 0.14 milliseconds (ms)) were taken at each position and averaged in time to minimize the loss of tracked particles.

Numerical model

Experimental measurements were compared with results from three-dimensional CFD calculations. The model geometry (4.38×4.38×0.787 mm^3) included one feed spacer mesh element (Figure 3-3), with a realistic representation of the spacer geometry constructed with curved surfaces based on Scanning Electron Microscopy images (similar to the procedure from Radu et al., 2014). The hydrodynamic calculations assumed stationary flow of incompressible fluid in laminar flow conditions, according to the Navier-Stokes and continuity equations 3-4:

$$\begin{aligned} \rho(\mathbf{u}\cdot\nabla)\mathbf{u} + \nabla p &= \nabla\cdot(\eta\nabla\mathbf{u}) \\ \nabla\cdot\mathbf{u} &= 0 \end{aligned} \qquad 3\text{-}4$$

where $\mathbf{u} = (u_x, u_y, u_z)$ is the vector of local liquid velocity, p is the pressure, ρ and η are the density and dynamic viscosity of water (20ºC). Similar to the approach used in Radu et al. (2014), periodic flow conditions were set between the inlet and outlet, as well as between the lateral boundaries (Figure 3-3b), implying identical flow velocity fields on pairs of boundaries (in with out and left with right). This approximates the flow profile corresponding to a spacer element situated within an array, sufficiently far from the flow cell walls not to experience entrance/exit or wall effects (Radu et al., 2014). The flow was driven by a pressure difference imposed between inlet and outlet, calculated from an additional constraint such that the desired linear flow velocity u_m is obtained. The water flow was calculated without permeate production, therefore no-slip boundary conditions were set to the top, bottom and spacer surfaces. The steady laminar flow equations were solved in COMSOL Multiphysics (v4.4, Comsol Inc., Burlington, MA) with finite element methods, on a tetrahedral mesh with maximum size of 50 μm.

Calculation and visualization of velocity fields. The flow fields calculated with COMSOL were averaged over intervals of Δz = 40 µm before comparing simulation results with the PIV measurements. This averaging procedure was necessary because the measurements were recorded with a depth of field of approx. 40 µm. Therefore, the *x*-*y* velocity fields presented at a certain *z* coordinate should be understood as averages between *z*±20 µm (Figure 3-3a). The flow fields were plotted using a Python script with Matplotlib graphic library (Hunter, 2007), showing streamlines, velocity magnitude and flow direction.

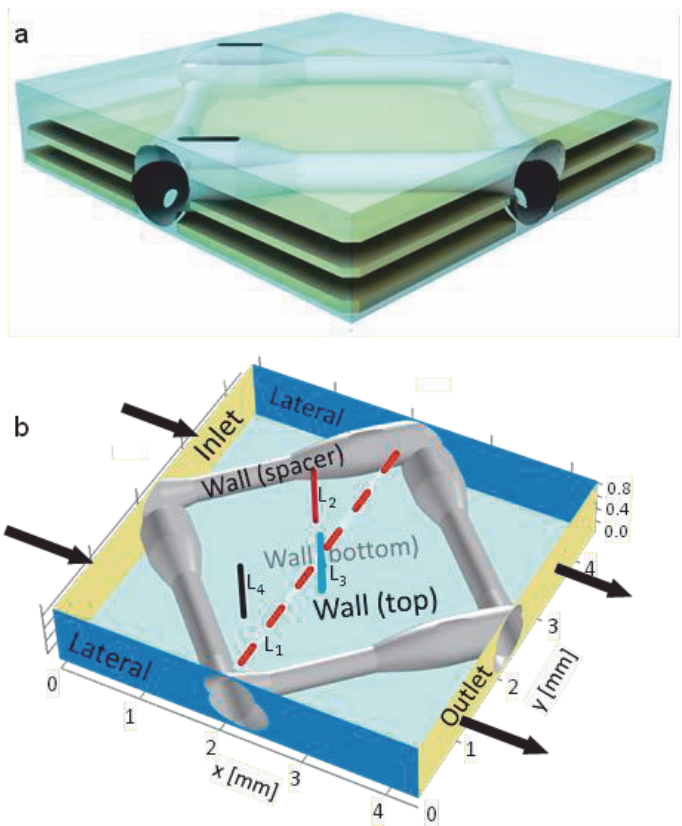

Figure 3-3: a) Positions of *x*-*y* slices (*x* coordinate corresponds to the main flow direction and *y* coordinate is normal to the main flow direction) taken for comparing measured and calculated vector fields at different heights in the flow channel (*z*=200, 400 and 650 µm). The three slices have a thickness of 40 µm each. b) The computational domain for hydrodynamic simulations includes one spacer element, with spacer resembling the geometry used in practise and positions of cut lines for comparing measured (PIV) and calculated flow velocity as shown in Figure 3-9. Line L_1 is in the *x*-*y* plane at *x*=2 mm, L_2-L_4 are in the *y*-*z* planes at (*x*, *y*) = (1.48, 3.12), (2.06, 2.22) and (1.48, 1.45) mm, respectively.

Statistic similarity. The Bray-Curtis similarity was used to analyse the differences between measured and model-calculated 2-D velocity magnitude distributions, as well as the similarity between PIV measurements at different locations, and between velocity fields averaged over different time intervals. The Bray-Curtis dissimilarity or 'distance', d_{BC}, between two sets of data a and b, each containing n points to be compared, is a normalization method defined as (Krebs, 1999):

$$d_{BC} = \sum_{k=1}^{n}(a_k - b_k) \Big/ \sum_{k=1}^{n}(a_k + b_k) \qquad 3\text{-}5$$

The similarity between the sets a and b was then defined as

$$S_{BC} = 1 - d_{BC} \qquad 3\text{-}6$$

Since all velocity magnitudes are positive, the similarity S_{BC} is always between 0 and 1, with maximum value of 1 for perfectly similar velocity fields.

RESULTS

In this study the water flow patterns were investigated in spacer-filled channels using PIV in a flow cell and 3-D CFD techniques under various conditions: (i) varying location along the length and width of the channel, (ii) different measured time frames, and (iii) varying linear flow velocities.

Flow pattern change over channel height

The PIV measurements allowed the determination of flow velocity patterns in x-y planes, at different heights z in the channel, an example of which is presented in Figure 3-4. These planar velocity fields clearly show how the flow direction changes over the channel height, with two specific zones becoming apparent. Near the bottom (between z=0 and 300 μm) and near the top walls (between z = 550 and 800 μm) the flow direction mostly follows the nearby located spacer fibre orientation, i.e., at 45 degrees with respect to the main flow direction (Figure 3-4). Thus, there is a 90 degrees change in the flow direction from bottom to top, so that in the middle of the channel (z = 350 to 500 μm) a convergence region develops, with the liquid following the main flow direction (left to right in x direction). Because the real spacer geometry includes various positions of filament thinning, the velocity magnitude changes creating zones

with fast and slow flow, which are not symmetric against the middle/centre plane at z = 400 μm. The maximum measured flow velocity within this experiment was 0.45 m·s^{-1} at $z \approx 300$ μm for the used average flow velocity of 0.163 m·s^{-1}.

Spatial reproducibility

To test the method reproducibility and the flow uniformity over the spacer-filled channel, the velocity distribution was measured at five locations (x, y) in the flow cell, as indicated in Figure 3-2.

Table 3.1: Spatial reproducibility of measured flow field at five locations in the flow cell (*a* to *e)*, at three different heights in the flow channel z = 200, 400 and 650 μm.

	Bray – Curtis similarity (S_{BC})				
position* / height in the channel	a	b	c	d	e
z=200 μm	0.97	0.98	0.96	0.98	0.97
z=400 μm	0.95	0.94	0.94	0.96	0.95
z=650 μm	0.96	0.98	0.97	0.98	0.97

*see Figure 3-2

The flow patterns were similar at all measured locations, represented in Table 3.1 at three heights in the channel. The 2-D flow magnitude distribution at each location was compared by the Bray-Curtis similarity S_{BC} with the average over the five locations. The flow measured at the five locations proved to be very similar, with S_{BC} slightly better for the slices taken near the flow channel bottom and top (S_{BC} = 0.96-0.98) than for the middle slices (S_{BC} = 0.94-0.96), indicating that a measurement taken at any spacer cell could be considered representative of the entire flow channel. The rest of the measurements in this study were therefore done in the feed spacer mesh element *d*, located as shown in Figure 3-2.

Steady and unsteady flow - effect of different flow velocities

In order to study the effect of water velocity on the flow regime, measurements were done at three linear velocities: a reference velocity of 0.163 m·s^{-1}, which is commonly used in practical operation (Vrouwenvelder et al., 2009), a lower velocity of 0.074 m·s^{-1} and a higher velocity of 0.294 m·s^{-1}. These correspond to Reynolds numbers 160, 70 and 300, respectively. The velocity magnitude for 100 consecutive measurements in time (all at the same point x=2 mm, y=2 mm) is plotted in Figure 3-5 for the three Re numbers. As the Re number increases,

larger fluctuations of measured velocity can be observed. At Re=70 the flow is shown to be stable in time and it can be considered steady. At Re=300 fluctuations between 20-50% of the linear flow velocity were recorded, which clearly indicate an unsteady flow regime. The flow at Re=160 (as used in practice) shows only a mildly unsteady behaviour with fluctuations of 10% from average velocity. Most flow fluctuations seemed to occur near the top and bottom walls of the spacer-filled flow channel in the regions with the highest local flow velocities.

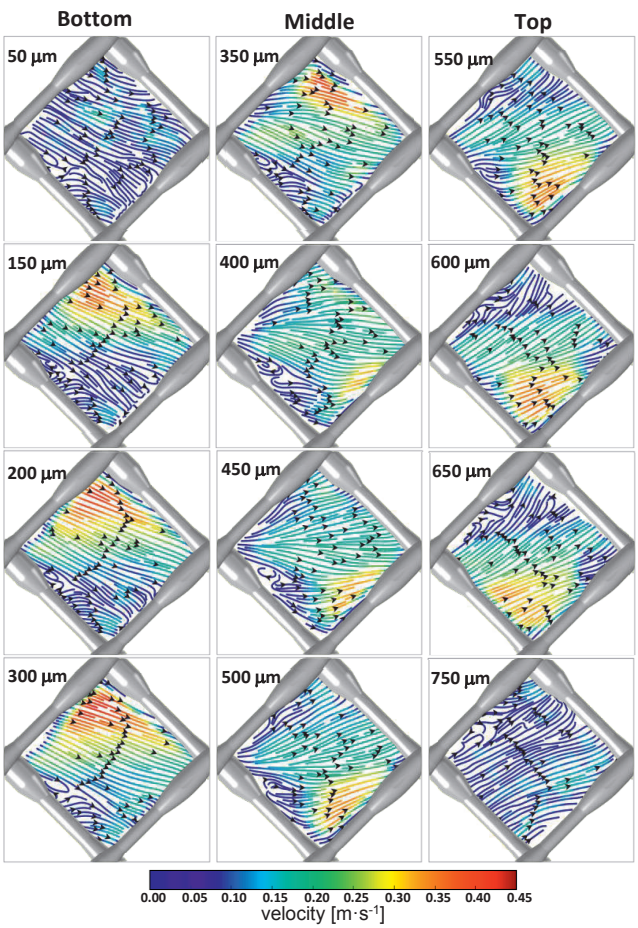

Figure 3-4: Measured flow pattern in *x-y* slices at different heights in the flow channel (*z* direction, the heights should be interpreted as the middle of the region where the measurements were taken, e.g. 50 µm represents the region between 30 and 70 µm in the channel) showing streamlines and flow direction (black arrows). The flow velocity magnitude is represented by the colour scale of a streamline. The main flow direction with an average flow velocity of 0.163 m·s^{-1} (Re=160) was rom left to right.

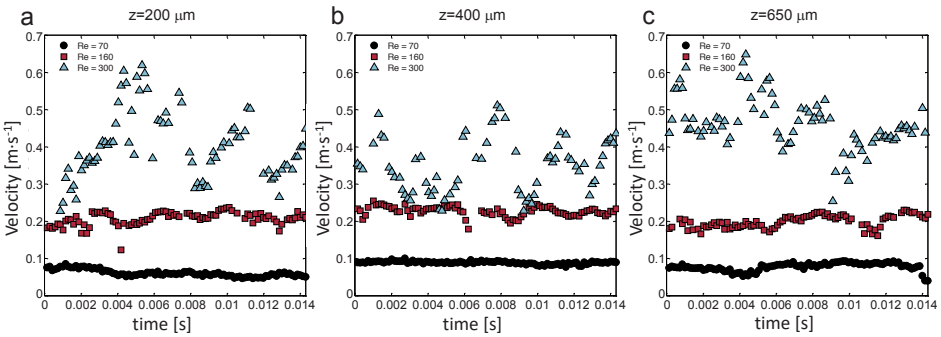

Figure 3-5: Measured local velocity magnitude over time at three flow velocities (corresponding to Re=70, 160 and 300), in the middle of a feed spacer element (x=2 mm, y=2 mm) at different heights in the flow channel: a) z=200 μm, b) z=400 μm and c) z=650 μm. While the flow is mostly steady at Re=70, it changes to unsteady (large velocity fluctuations) at Re=300. The flow at Re=160 is only slightly unsteady.

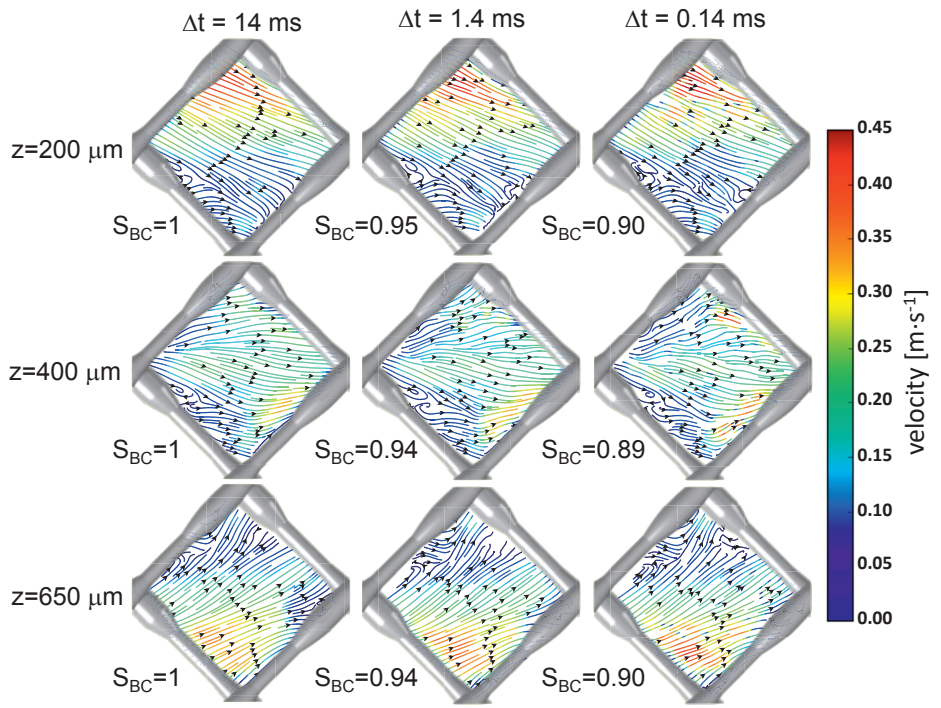

Figure 3-6: Time-dependence of the measured flow field at different heights in the channel z = 200, 400 and 650 μm. 2-D distributions of the flow velocity are shown averaged over periods of 0.14 ms, 1.4 ms and 14 ms. The Bray-Curtis similarity (S_{BC}) was calculated relative to the largest imaging time scale (Δt = 14 ms). The main flow direction with an average flow velocity of 0.163 m·s^{-1} (Re=160) was from left to right. Streamlines and colour scale are as in Figure 3-4.

To quantitatively assess the error associated with time-averaging, the velocity field at Re=160 was averaged over three time intervals Δt: 0.14 ms (2 frames or 1 measurement), 1.4 ms (10 measurements) and 14 ms (100 measurements), shown in Figure 3-6. The Bray-Curtis similarity was then calculated relative to the largest time scale (Δt =14 ms), showing a 94% similarity for the velocity field averaged over 1.4 ms and 90% similarity for 1 measurement (0.14 ms).

The time averaged measured velocity distributions at three Re at different heights in the channel is presented in Figure 3-7. Similar flow regions as for the Re = 160 can also be observed for Re=70 and 300: high and mostly one-directional velocities near the top and bottom walls and a flow convergence region with slower flow in the middle of the channel, where the flow changes direction. For Re=300, however, eddies (recirculation zones) were observed in the lower region of the channel (Figure 3-7, z = 200 μm, Re = 300). The maximum measured flow velocities were 0.20, 0.45 and 0.64 $m \cdot s^{-1}$ at Re = 70, 160 and 300, respectively.

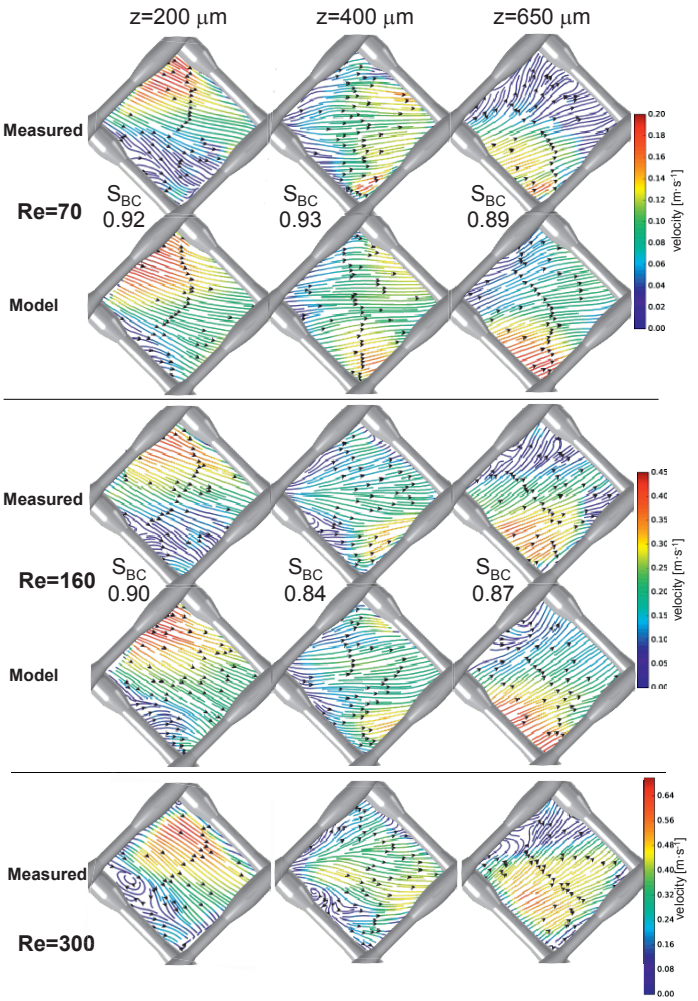

Figure 3-7: Comparison between measured and calculated flow fields at Re=70 (top), Re=160 (middle) and Re=300 (bottom), at three channel heights z = 200, 400 and 650 μm. Streamlines show as colour scale the flow velocity magnitude. S_{BC} numbers represent the calculated similarity indices (Bray-Curtis) between measured and calculated 2-D velocity distributions.

The nonlinear increase of the measured maximum velocity with the increase of Re indicates a change in the flow regime from laminar to transitional or turbulent at Re = 300 (where at a linear increase the maximum velocity would have been 0.82 instead of the observed 0.64 $m \cdot s^{-1}$).

Measurements compared with CFD model

Flow fields determined with PIV at Re = 70, 160 and 300 were compared with those resulted from fluid dynamics calculations, using steady laminar

incompressible Navier-Stokes equations. An example of computed flow represented by streamlines clearly shows the two main flow directions near the top and bottom membrane surfaces (Figure 3-8a). Velocity components u_x, u_y and u_z at three heights in the channel are presented in Figure 3-8b for a CFD simulation at Re = 160. The dominant velocity component is in the x direction (u_x between 0-0.4 $m \cdot s^{-1}$), whilst the u_y component is more important close to the top and bottom walls, with ranges between -0.3 and 0.3 $m \cdot s^{-1}$ and near-zero values in the middle of the channel (at z = 400 μm) where the flow changes direction. The vertical velocity component, u_z, has the largest values mostly close to the spacer fibres (between -0.2 and 0.2 $m \cdot s^{-1}$), in the regions where the flow passes from one feed spacer mesh element to another.

Comparisons between measured and calculated x-y velocity projections, $\sqrt{u_x^2 + u_y^2}$ in different planes z are presented in Figure 3-7. The Bray-Curtis similarity between measured and calculated velocity distributions are good overall (S_{BC}>0.84). It appears that the model predicts better the velocity distributions at lower Re, where the laminar flow was shown to be steady (Figure 3-5). However, at Re = 160, where slight velocity fluctuations were measured, the model assuming steady laminar flow still compares favourably to the experimental data (Figure 3-7). At Re = 300, the steady laminar assumption does not hold anymore and the measurements cannot be compared with steady flow calculations. The measured maximum velocity (0.64 $m \cdot s^{-1}$) was ~30% less than the velocity calculated with steady laminar flow (0.82 $m \cdot s^{-1}$).

Measured velocity profiles can also be compared with numerical model results along cut lines in the z direction, as shown in Figure 3-3b. This comparison between measured and modelled flow data along a 1-D profile enables further (and more direct) evaluation of model accuracy.

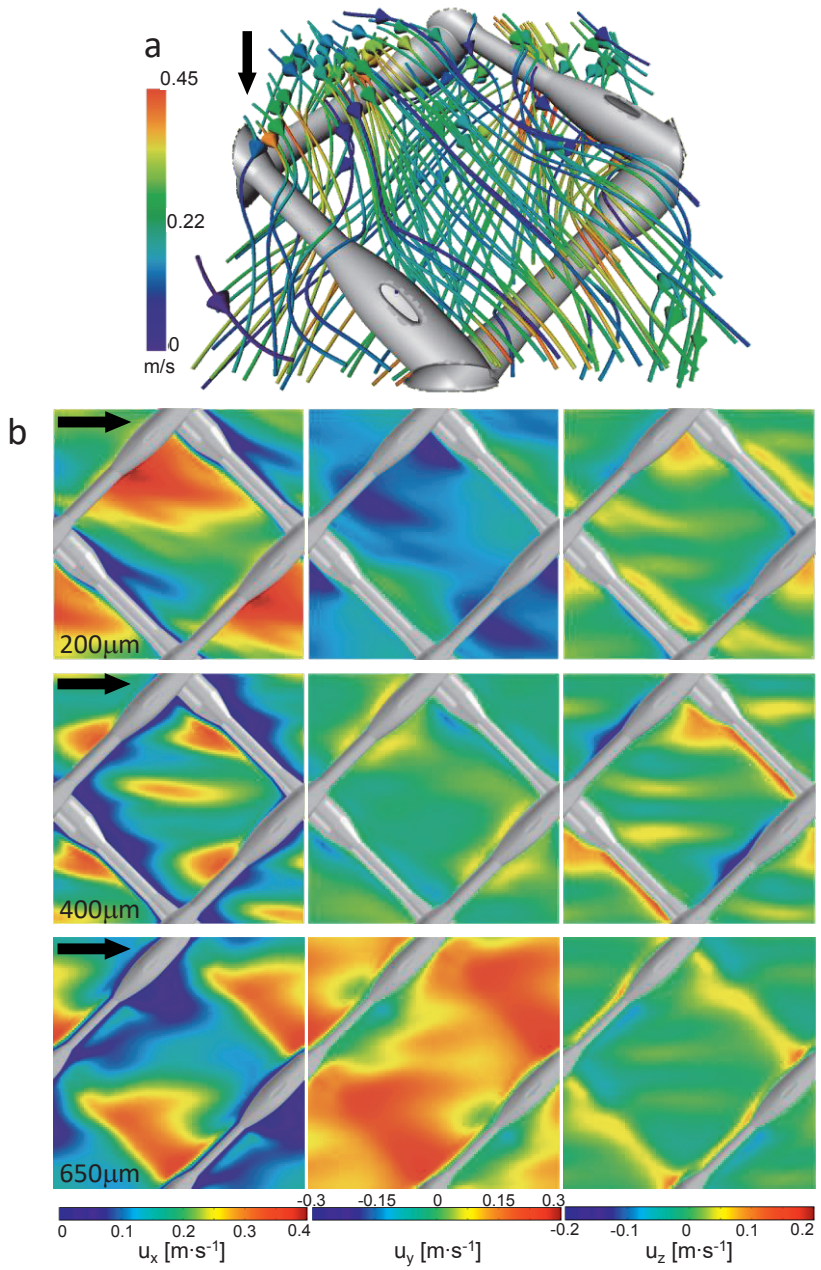

Figure 3-8: (a) Streamlines of simulated flow in a feed spacer element (flow direction from top to bottom). Colours show the velocity magnitude from 0 m·s^{-1} (blue) to 0.45 m·s^{-1} (orange). (b) Computed distribution of velocity components u_x, u_y and u_z at two heights in the flow channel (200, 400 and 650 µm). The CFD simulation was made at Re=160, assuming steady laminar flow (direction from left to right).

For example, calculated velocities on a line across the main flow direction in the middle of a feed spacer mesh element, shown in Figure 3-9a, exhibit good agreement with the measurements. Several steps and maxima can be observed in the measured velocity profiles near the bottom (z = 200 μm) and top (z = 650 μm) walls, which are also revealed by the simulations. Also, the velocity magnitude is correctly calculated, with a steep change from 0 m·s^{-1} next to the spacer to a maximum of 0.4 m·s^{-1} on the opposite side. In the middle section (z = 400 μm) the velocity changes within a narrower interval, showing 3-4 peaks. The discrepancies in terms of local velocity peaks between the simulations and the experimental measurements can most likely be attributed to the simplified spacer geometry adopted in the model (the model geometry was constructed with parametric surfaces to approximate the SEM measurements). Measurements of the x-y projected velocities at different heights z in the channel, shown in Figure 3-9b, are more difficult to perform and with less resolution. Along line L_3 in the middle of the feed spacer mesh element two velocity peaks can be observed on the measured and calculated velocity profiles.

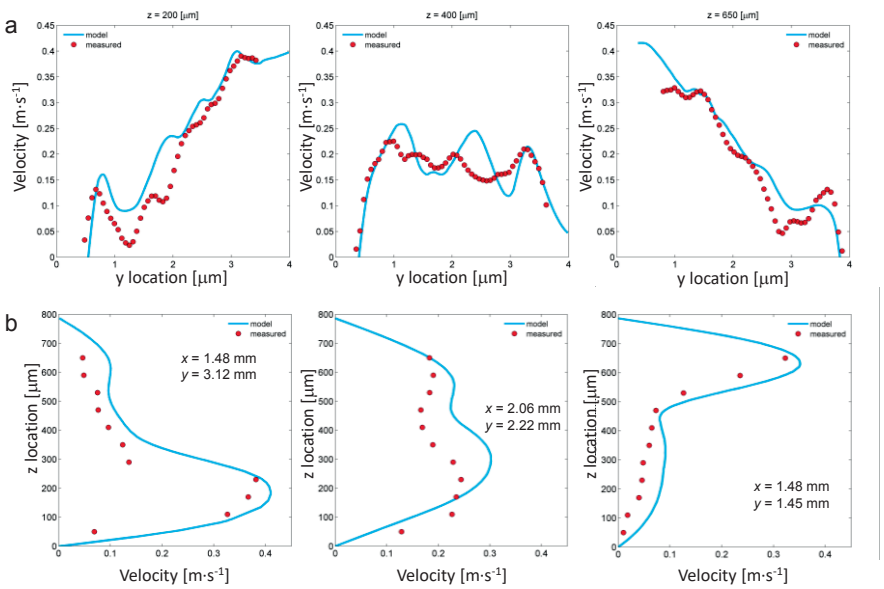

Figure 3-9: Comparison between measured (circle symbols) and calculated (lines) flow velocity magnitude along a line perpendicular to the main flow direction (a) line L_1 in the x-y plane at $x \approx$ 2 mm and different channel heights (z=200, 400 and 650 μm), and (b) lines L_2, L_3, L_4 in the y-z plane at different x and y positions (see Figure 3-3 for positions of L_1-L_4). The CFD simulation was made at Re=160, assuming steady laminar flow.

DISCUSSION

In this study water flow in a spacer-filled channel under hydrodynamic conditions used in practice was evaluated. PIV measurements at different locations along the spacer-filled channel of the flow cell at varying heights revealed steady and laminar flow conditions at linear flow velocities commonly used in practice (u_m = 0.05-0.2 m·s^{-1}), where also the 3-D CFD simulations were in good agreement with the measured data.

Flow regimes

An important result of this study is that the possibility of laminar and steady flow in the velocity range used in practice (u_m = 0.07-0.2 m·s^{-1}) was confirmed. The flow appears to be laminar with only slight unsteadiness in the upper velocity limit. Although a velocity of 0.2 m·s^{-1} can be achieved in the lead module of a membrane plant, as permeate is produced along the modules, the velocity drops towards the end and it can reach 0.07 m·s^{-1} (Malek et al., 1996). Higher velocities, where the flow was observed to be unsteady (e.g., 0.3 m·s^{-1}), are not commonly used in practice for spiral wound reverse osmosis or nanofiltration modules, as these would result in large axial pressure drops. However, the presence of laminar flow in our experimental conditions should be cautiously interpreted, because in these flow-cell measurements a constant inlet velocity was achieved. It is still possible that in practice the unsteady flow starts to develop at lower velocities if the inlet flow rate is not very well controlled and fluctuates.

A previous study on PIV measurements for Re up to 4000 (Gimmelshtein and Semiat, 2005) reported laminar flow up to Re = 1200 with small fluctuations using feed spacer with a thickness of 800 μm (≈ 31 mil). These results are in contrast with the findings of the current study, where for Re > 200 unsteady transient flow was measured. However, one should note that the equation used to calculate Re in Gimmelshtein and Semiat (2005) was based on the channel height and did not include any correction to account for the spacer presence.

$$\mathrm{Re} = \frac{2 \cdot u \cdot h \cdot \rho}{\eta} \qquad 3\text{-}7$$

where u is the magnitude of local liquid velocity, ρ and η are the density and dynamic viscosity of water and h is the channel height.

Based on the equation used in Gimmelshtein and Semiat (2005), the Re at linear flow velocities used in this study are 110, 256 and 463. Mojab et al. (2010) evaluated experimentally and with a numerical model flow characteristics for a spacer geometry scaled-up by a factor 10 compared to the commonly used spacer thickness for Re ranging from 100 to 1000 and reported that transition from steady to unsteady flow occurred above Re=250.

Flow field measurements using Doppler OCT indicated the presence of swirling flows next to the spacer filaments in the vertical (*y*-*z*) plane at a linear flow velocity of 0.03 $m \cdot s^{-1}$ (Gao et al., 2013). It was expected to capture the impact of the swirling flows (in the *y*-*z* plane) on the flow captured with PIV in *x*-*y* planes, taking in consideration that the Doppler OCT measurements were performed at a much lower linear flow velocity than the PIV measurements, however, no eddies or disturbed flow were found until an inflow velocity of ~0.3 $m \cdot s^{-1}$. These differences might point to the need for an improved interpretation of Doppler OCT images, as also suggested by Gao et al., (2013).

The water flow velocities over the spacer-filled channel height were measured in this study with a much higher spatial resolution (Δz = 40 μm, Figure 3-4 and Figure 3-9b) than in a previous report of spacer-filled channels for membrane filtration processes (Δz = 300-600 μm in Willems et al., 2010). This allowed capturing the gradual change in flow direction over the flow channel height (*z* direction). Focusing on only one feed spacer mesh element provided a more accurate *x*-*y* resolution than in other studies, revealing more details of the flow structure and the existence of small recirculation zones behind the spacers at Re=160 (Figure 3-4), and even larger recirculation zones at Re=300 (Figure 3-7).

Repeated measurements in different feed spacer mesh elements along the flow cell showed that the flow pattern is very similar at all monitored locations. Similar results were obtained in particle deposition experiments (Radu et al., 2014). This indicates that flow observations performed in small flow cells are representative, at least for clean (i.e., not fouled) modules.

Solute transfer

Understanding the detailed (micro-scale) flow dynamics is relevant for understanding solute transport (e.g., salts) and for the design of feed spacers

that promote the best mixing possible with the least energy input. Our results clearly demonstrate the existence of faster flow near the top and bottom membrane surfaces and a slower flow in the middle of the flow channel. The fast flow will result in better solute transfer near the membranes, where the concentration polarization layer forms. However, the existence of recirculation zones at the linear velocities used in practice seems to be limited. Moreover, the slow laminar flow in the last module (at the end of the pressure vessel with the lowest velocity) would favour salt precipitation and scaling. Knowledge of the detailed flow features could allow further investigations of mass transfer coefficients in the feed channel, using the constant wall concentration approach as suggested in Koutsou et al. (2009) and Fimbres-Weihs and Wiley (2010).

CFD model

A key result of this study is the good agreement between the PIV measured and the computed water flow fields. It reveals that the steady laminar flow assumption in the CFD simulations allows a good description of the actual flow in the spacer-filled channel. Furthermore, the obtained results also imply that for clean flow channels the computational domain can be reduced to one feed spacer mesh element with periodic boundary conditions for hydrodynamic calculations, if permeation flux contribution to velocity change is negligible. This approach gives confidence in pursuing model-based studies for designing other feed spacer geometries with reduced pressure drop and fouling, while still providing good solute transfer. Flow pattern has been shown (Radu et al., 2014) to be of crucial importance in the deposition and development of foulant layers, both for scaling and for biofouling.

The velocity field resulted from numerical simulations is sensitive to the accuracy (or realism) of used feed spacer geometry, which influences the comparison with experimental measurements. It is therefore imperative that the 3-D spacer geometry is represented in the model as closely as possible to the real shape of spacers used in practice. This has been pointed out also by other numerical and experimental studies (Picioreanu et al., 2009; Radu et al., 2014). In future studies we will use directly the solid geometries reconstructed from computerized tomography (CT) scans.

Further studies

The focal depth on the channel height (z) was set here with approximation within 40 μm. A narrower focal depth would allow taking more optical slices, thus more resolution over the channel height. For this, other lenses with higher numerical aperture and other light sources with lower wavelength (e.g., UV light) could be used.

Tomographic PIV would allow for capture of the flow velocity component in the z-direction (Elsinga et al., 2006; Casey et al., 2013). However, for such a narrow flow channel it would be very difficult to set up cameras to measure the flow from a lateral view. Especially, the presence of an opaque feed spacer will not allow the lateral observation of the flow channel.

For further model validation, other spacer geometries and spacer orientation should be tested. It is of interest to evaluate the impact of fouling on the local velocity field, since the water flow may become unsteady at lower linear flow velocities in the presence of fouling. It should also be tested whether the methods could be applied for forward osmosis (FO) and pressure-retarded osmosis (PRO) flow channels.

CONCLUSIONS

A particle image velocimetry (PIV) method was implemented to measure detailed water flow fields in a flow-cell simulating at small scale conditions encountered in the feed spacer-filled flow channels of spiral-wound membrane modules. Narrow focal depth allowed optical sectioning at multiple (maximum 18) levels along the channel height of this lab-scale spacer-filled flow channel.

At linear velocities between u = 0.07-0.2 $m \cdot s^{-1}$ (as used in practice) the measured flow appears to be laminar with only slight unsteadiness in the upper velocity limit. At higher velocities (0.3 $m \cdot s^{-1}$) the flow was observed to be unsteady with appearance of local recirculation zones.

Measurements taken at different locations in the flow cell (in several feed spacer mesh elements) showed very similar water flow patterns (S_{BC} = 0.94-0.98), indicating the same hydrodynamic conditions along and across a small flow channel without permeate production.

Computational fluid dynamics simulations based on steady laminar flow assumption were in good agreement with the measured flow fields (lowest S_{BC} = 0.84). This supports the use of model-based studies in the optimization of spacer geometries and operational conditions.

٤

Impact of Organic Nutrient Load on Biofouling Rate

Abstract

The influence of organic nutrient load on biomass accumulation (biofouling) and pressure drop development in membrane filtration systems was investigated. Nutrient load is the product of nutrient concentration and linear flow velocity. Biofouling e excessive growth of microbial biomass in membrane systems e hampers membrane performance. The influence of biodegradable organic nutrient load on biofouling was investigated at varying (i) crossflow velocity, (ii) nutrient concentration, (iii) shear, and (iv) feed spacer thickness. Experimental studies were performed with membrane fouling simulators (MFSs) containing a reverse osmosis (RO) membrane and a 31 mil thick feed spacer, commonly applied in practice in RO and nanofiltration (NF) spiral-wound membrane modules. Numerical modelling studies were done with identical feed spacer geometry differing in thickness (28, 31 and 34 mil). Additionally, experiments were done applying a forward osmosis (FO) membrane with varying spacer thickness (28, 31 and 34 mil), addressing the permeate flux decline and biofilm development. Assessed were the development of feed channel pressure drop (MFS studies), permeate flux (FO studies) and accumulated biomass amount measured by adenosine triphosphate (ATP) and total organic carbon (TOC). Our studies showed that the organic nutrient load determined the accumulated amount of biomass. The same amount of accumulated biomass was found at constant nutrient load irrespective of linear flow velocity, shear, and/or feed spacer thickness. The impact of the same amount of accumulated biomass on feed channel pressure drop and permeate flux was influenced by membrane process design and operational conditions. Reducing the nutrient load by pre-treatment slowed-down the biofilm formation. The impact of accumulated biomass on membrane performance was reduced by applying a lower crossflow velocity and/or a thicker and/or a modified geometry feed spacer. The results indicate that cleanings can be delayed but are unavoidable

Published as:

Szilard S. Bucs, Rodrigo Valladares Linares, Mark C.M. van Loosdrecht, Joop C. Kruithof, Johannes S. Vrouwenvelder (2014) Impact of organic nutrient load on biomass accumulation, feed channel pressure drop increase and permeate flux decline in membrane systems. *Water Research* **67**: 227–42.

INTRODUCTION

By membrane filtration processes like nanofiltration (NF) and reverse osmosis (RO) high quality water is produced from all types of water sources including seawater and sewage. Because the global demand for fresh water is growing, application of these membrane technologies is increasing strongly. One of the most serious operational problems of NF and RO is biofouling - excessive growth of biomass - affecting the performance of these membrane systems. Biofouling influences the (i) amount and quality of the produced fresh water, (ii) reliability of water production and (iii) cost (Shannon et al., 2008). Numerous authors have described biofouling problems in membrane installation (Baker and Dudley, 1998; Ridgway et al., 1983; Schneider et al., 2005; Tasaka et al., 1994; Vrouwenvelder et al., 2008b). Recently, the study of membrane biofouling has intensified (Al Ashhab et al., 2014; Ben-Sasson et al., 2014; Habimana et al., 2014; Khan et al., 2014; Shannon et al., 2008; Sim et al., 2013; Ying et al., 2013), showing that biofouling is still considered as an important problem in practice.

Biofilm growth is defined as biofouling when the growth of microorganisms, typically as a biofilm, becomes substantial enough to cause an unacceptable decline of membrane performance (Vrouwenvelder et al., 2008b). The normalized pressure drop increase and/or the flux decline of membrane installations are considered to be an operational problem when they exceed 10 – 15 percent of the start-up values. Deviations larger than 10 – 15 percent require corrective actions to improve membrane performance and to avoid restricted guarantees by the manufacturers of membrane elements (DOW, 2014; GE Water, 2009; Hydranautics, 2001, see Supplementary material).

In spiral-wound membrane modules, two types of pressure drop can be distinguished: the feed channel pressure drop (FCP), the pressure drop between feed and concentrate lines and the transmembrane pressure drop (TMP), the differential pressure between feed and permeate lines. When the TMP is increased, i.e. by biofouling, the permeate flux is declined. The feed pressure must be increased to maintain the same water production.

Concentration polarization may have a strong impact on membrane performance (Chong et al., 2008a, 2008b, Herzberg and Elimelech, 2007a, 2007b). Concentration polarization can influence biofilm formation in several

ways. Concentration polarization of salts may restrict biofilm development while concentration polarization of biodegradable nutrients may enhance biofilm development. The presence of a biofilm also contributes to concentration polarization and enhances osmotic pressure (Chong et al., 2008a; Herzberg and Elimelech, 2007a, 2007b, Radu et al., 2011, 2010).

Biofouling in spiral-wound NF and RO membranes has been studied with monitors, test rigs, pilot and full scale installations for extensively pre-treated water (Vrouwenvelder et al., 2009a). The membrane fouling simulator (MFS), the monitor used in this study has shown to be representative for spiral-wound RO and NF membrane modules (Vrouwenvelder et al., 2007a, 2007b, 2006). The same development of FCP increase and biofilm formation was observed in membrane elements in the same position of an NF installation, operated with or without permeate production. Mass transfer calculations supported the observations that the permeate flux is not playing a significant role in the nutrient supply to the fouling layer. Test-rig and full-scale studies with different types of fresh feed water showed that biofilm concentrations of membrane modules correlated very well with FCP-increase (Vrouwenvelder et al., 2009a). Moreover, in systems suffering from biofouling cleaning cycles are governed by the pressure drop over the feed channel. Therefore, in both spiral-wound NF and RO systems biofouling is predominantly a feed spacer problem (Vrouwenvelder et al., 2009a, 2009b).

Feed spacers are important for membrane performance and play an important part in biofouling of membrane systems. Feed spacers, commonly applied in water treatment practice, consist of polypropylene and have a similar geometry (with spacer strands at a 90 position and a porosity of ~0.85). A 31 mil (1 mil = 0.0254 mm) thick feed spacer is most commonly used in spiral wound NF and RO modules for water treatment in The Netherlands. Baker et al. (1995) reported that initial deposits of fouling accumulated alongside the membrane feed channel spacer and with time these deposits encroached upon the remaining free membrane area. Van Paassen et al. (1998) observed an exponential increase of the feed channel pressure drop caused by biomass build up onto the feed spacer of the membrane modules, caused by chemical dosage to the feed water. Tran et al. (2007) found that the vicinity of the feed spacer strands was most affected by fouling. Strategies to reduce feed spacer biofouling have been addressed, e.g. intermittent air/water flushing

(Cornelissen et al., 2007) and applying thick feed spacers (Bartels et al., 2008; K Majamaa et al., 2009).

The shear is increased by increasing the linear flow velocity. A compact smooth biofilm is formed at high shear force, while a thick, fluffy biofilm is produced at low shear force (Beun et al., 2002; Peyton, 1996; Tijhuis et al., 1996; Van Loosdrecht et al., 1995; Wasche et al., 2002). In spiral-wound membrane systems, the shear force has an impact on the pressure drop increase and biomass accumulation (Vrouwenvelder et al., 2010a). In membrane based water treatment practice, spiral-wound membrane modules are placed in pressure vessels. A pressure vessel contains up to eight membrane elements in series. Each membrane element produces water causing a gradient in water velocity and related shear over the pressure vessel length. Most biofouling was observed in the membrane element at the feed side of the installation, the location with the highest crossflow velocity, shear and nutrient concentration (Carnahan et al., 1995; Vrouwenvelder et al., 2008b). A short period of a much higher shear caused by e.g. a reverse flush may remove biofilm from spiral wound membrane elements (Vrouwenvelder et al., 2010a). The removal of biomass from the membrane module may be enhanced by applying spacers with modified thickness and/or geometry. The effect of shear force on biofouling is a function of the linear flow velocity, but varying the velocity also changes the nutrient load, the product of nutrient concentration and linear flow velocity.

The nutrient load, nutrient concentration and hydrodynamics (linear flow velocity) affect biofilm formation. The thickness, structure, stability and density of the biofilm are influenced by nutrient load and hydrodynamic shear stress/ flow regime (Kwok et al., 1998; Melo and Bott, 1997; Pereira et al., 2002; Peyton, 1996; Van Loosdrecht et al., 1995; Vrouwenvelder et al., 2010b; Wasche et al., 2002; Wijeyekoon et al., 2004). The effect of nutrient load on biofouling of membranes systems has not been reported. It is important to study the effect of shear on biofouling at constant nutrient load by applying both single phase flow (water) and two phase flow (water with air sparging: bubble flow).

No conclusive studies have been found on the impact of biodegradable organic nutrient load on biofouling in NF and RO membrane systems. In the Scopus database of December 2013, the number of publications satisfying the search

criteria ‘‘nutrient load’’ (including “substrate load”, “organic load” and “carbon load”) and “biofouling” (including “biofilm”, “growth” and “biomass”) in the article title, abstract and keywords amounted 19: Most papers found with the search criteria “nutrient or substrate load” address eutrophication and N and P load. A few papers found with “carbon and organic load” predominantly address (novel) wastewater treatment system performance. Sun and Leiknes (2012) studied nitrogen removal and membrane performance with a two-stage biofilm membrane bioreactor (MBR). They reported that the membrane fouling rate increased with increasing influent organic load. Sun and Leiknes (2012) used as feed water three dilution ratios of raw wastewater and tap water, thereby varying parameters such as suspended solids, (organic and inorganic) nutrient load and nutrient concentration. Therefore, the impact of biodegradable organic nutrient load on biofouling was not studied exclusively.

For spiral-wound RO and NF membrane systems, three papers including some data on the role of nutrient load on biofilm development have been published recently (Vrouwenvelder et al., 2010a, 2009b; Ying et al., 2013). Ying et al. (2013) concluded in their study on the effect of shear rate on biofouling that in RO membrane systems biofilm formation was dominated by the organic loading rate rather than the shear force. They compared low shear (at high loading) and high shear (at low and high loading) by varying crossflow velocity and total organic carbon concentration in one set of experiments. In their study a varying shear rate at a constant high TOC concentration (10 $mg \cdot L^{-1}$) produced similar biomass amounts (Ying et al., 2013). The impact of the nutrient load on biofouling was not the key message of these papers. The reported data did not allow a conclusive evaluation of the role of the organic nutrient load on biomass accumulation under several process conditions. The effect of nutrient load should be distinguished from the role of e.g. nutrient concentration, crossflow velocity, shear and feed spacer thickness.

Phosphate limitation can reduce biofilm growth (Lehtola et al., 2004; Miettinen et al., 1997), even in the presence of high concentrations of organic nutrients (Vrouwenvelder et al., 2010a), but such a biofouling control strategy would require a very extensive phosphate removal. The concentration of biodegradable organic nutrients in the feed water is an important issue for biofilm growth in membrane systems, and is therefore a frequently pursued

approach for biofouling control (e.g. by pre-treatment reducing the biodegradable organic nutrient concentration of the water). Therefore, the focus of this study was the organic nutrient load.

The objective of this study was to determine the influence of biodegradable organic nutrient load on biofouling, addressing the feed channel pressure drop increase, permeate flux decline (operational parameter) and biofilm development. Experimental studies were performed with monitors containing a feed spacer at variable and constant nutrient load. Numerical modelling studies were performed at constant nutrient load with identical feed spacer geometries differing in thickness. Additionally, experiments were done applying a forward osmosis (FO) membrane with varying spacer thickness (28, 31 and 34 mil), addressing permeate flux decline and biofilm development. The feed spacers had a similar geometry as applied in practice in spiral-wound NF and RO membrane systems. The results were used to evaluate the impact of organic nutrient load on biofouling and to discuss a potentially effective strategy for biofouling control.

To the authors knowledge this is the first conclusive study on the impact of the biodegradable organic nutrient load on biofilm accumulation in spiral-wound NF and RO and flat sheet FO membrane systems, addressing the impact of nutrient concentration, crossflow velocity, shear, and feed spacer thickness.

MATERIALS AND METHODS

Applied systems

MFS monitor, experimental set-up, membrane and spacers

In all practical experiments, a steel membrane fouling simulator (MFS) with external dimensions of 0.07 m × 0.30 m × 0.04 m was used (Vrouwenvelder et al., 2008b). Coupons of feed spacer, membrane and product spacer can be placed in the MFS resulting in the same spatial dimensions as in spiral wound membrane elements. Identical MFSs were operated simultaneously in parallel, Figure 4-1. The development of fouling was monitored by measuring the pressure drop increase over the feed spacer channel of the MFS and by analysis of sheets of membrane and spacer taken from the monitor for ATP and TOC. In addition, visual observations were made using the MFS sight window prior to membrane and spacer sampling. During operation, the MFS window was

covered with a light-tight lid to prevent growth of phototrophic organisms. The installation consisted of two pressure reducing valves, manometer, dosing point (for dosage of nutrient), MFS and flow controller (Graf von der Schulenburg et al., 2009; Vrouwenvelder et al., 2007a, 2007b). The MFSs were operated at a pressure of 1.20 bar to avoid degassing. Unless mentioned otherwise, the feed water flow was 16 $L \cdot h^{-1}$ equal to a linear flow velocity of 0.16 $m \cdot s^{-1}$, representative for practice (Vrouwenvelder et al., 2009b).

The feed spacer used is a 31 mil (787 μm) thick propylene diamond-shaped feed spacer, with spacer strands in a 90 position and a porosity of ~0.85, most commonly used in spiral wound NF and RO modules for water treatment in The Netherlands.

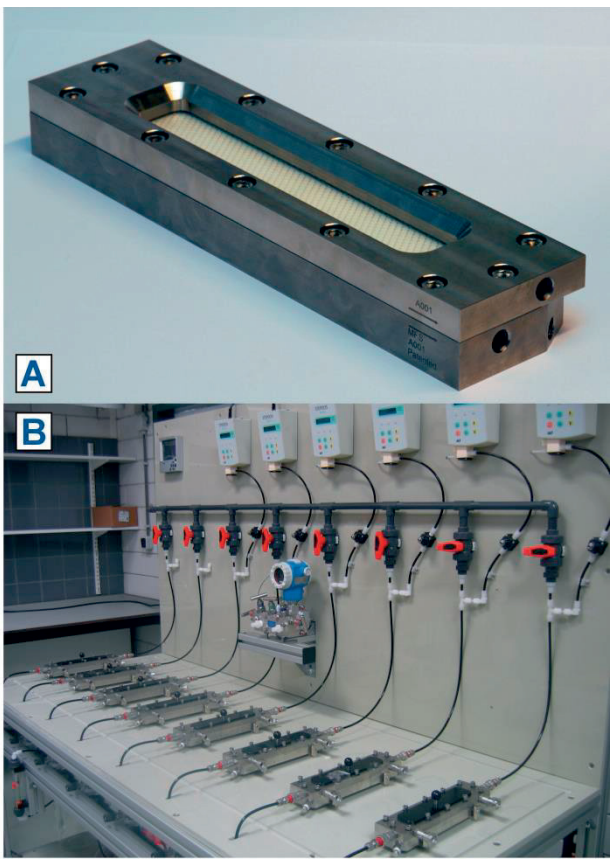

Figure 4-1: Membrane Fouling Simulator (MFS) and standard set-up to operate 8 MFS units in parallel (Vrouwenvelder et al., 2006, 2007a, b).

The feed spacers used in the experimental and simulated in the numerical modelling studies had the same spatial orientation, diamond (i.e., 45 rotated against the main flow direction) as in spiral wound membrane modules. In other words, the feed spacer was placed in a 45 flow contact angle in both the monitors and the numerical model studies, similar to membrane modules applied for water treatment. In the MFS research membranes and spacer sheets were taken from virgin spiral-wound membrane elements. New, unused feed and product spacers and RO membranes were used.

Forward osmosis

The forward osmosis (FO) membranes used in this study were made of cellulose triacetate embedded in a polyester mesh support provided by Hydration Technology Innovations (HTI, Scottsdale, AZ, USA).

The FO membrane cell was a custom-made cross-flow cell made of poly(methyl methacrylate) (PMMA), designed to fit a 20 cm^2 sized membrane sheet. All experiments were performed with the active layer of the membrane facing the FO feed solution, leaving the membrane support side in contact with the draw solution. The layout of the FO system is described by Valladares Linares et al. (2014).

Two DOW diamond-shaped spacers of 28 and 31 mil (1 mil = 0.0254 mm) thickness (Dow-Filmtec, Midland, MI, USA) used in commercial spiral wound RO modules, and one modified FO spacer produced by HTI with a thickness of 46 mil (HTI, Scottsdale, AZ, USA), were used for the experiments.

A municipal secondary wastewater effluent was used for 20 h to condition the FO system with bacteria. Subsequently, the system was fed with sterile synthetic wastewater for 5 filtration cycles (Valladares Linares et al., 2013).

The following procedure was used to grow a biofilm on the membrane feed side surface: i) inoculation for 20 h with municipal secondary wastewater effluent, and ii) five-cycle experiment with recirculation of synthetic wastewater effluent as feed solution and clean four percent NaCl as draw solution; each cycle recovered 30 percent of the initial feed solution volume (300 mL), after which both feed and draw solution were replaced. The same autopsy methods were used as described for the RO experiments.

Feed water and nutrient dosage

Drinking water prepared from anaerobic groundwater (subsequently treated by aeration, rapid sand filtration, deacidification, softening and rapid sand filtration at treatment plant Spannenburg in The Netherlands) is distributed without applying primary chemical disinfection or post disinfection causing a disinfectant residual. For all membrane fouling simulator (MFS) experiments this drinking water was used as the feed water source. Microscopic investigation showed a total bacterial cell number of 3 × 105 cells mL^{-1} in the feed water. These bacterial cell numbers (cells cm^{-2}) were determined with epifluorescence microscopy using acridine orange as fluorochrome, applying a slightly adapted method to eliminate fading (ASTM, 1993; Hobbie et al., 1977). All fluorescing bacterial cells were counted. The number of colony forming units (CFU) on R_2A media (Reasoner's 2 agar, Reasoner and Geldreich, 1985) was 2 × 103 CFU mL^{-1} after 10 days incubation at 25℃.

The nutrient solution dosed to enhance biofilm growth was composed of sodium acetate, sodium nitrate and sodium dihydrogen orthophosphate in a mass ratio C:N:P of 100:20:10, employed at different concentrations (Araújo et al., 2012b; Creber et al., 2010a, 2010b; Miller et al., 2012; Vrouwenvelder et al., 2009a). All chemicals were purchased in analytical grade from Boom B.V. (Meppel, The Netherlands) and were dissolved in deionized water. The pH value of the nutrient solution was set at 11 by adding sodium hydroxide, in order to restrict bacterial growth in the nutrient container. Fresh nutrient solutions were prepared every four days. From a nutrient container of 5 L, a concentrated nutrient solution was dosed into the feed water prior to the MFS at a flow rate of 0.03 $L{\cdot}h^{-1}$. A constant dosing was maintained using a peristaltic pump (Masterflex, Cole Palmer, Vernon Hills, USA). The dosage of the nutrient solution was checked periodically by measuring the weight of the nutrient container. The dosing flow rate of the nutrient solution (0.03 $L{\cdot}h^{-1}$) to the monitor feed water was low compared to the feed water flow rate (16.0 $L{\cdot}h^{-1}$, the reference feed flow). Therefore, the high pH value of the nutrient solution had no effect on the pH of the feed water of 7.8.

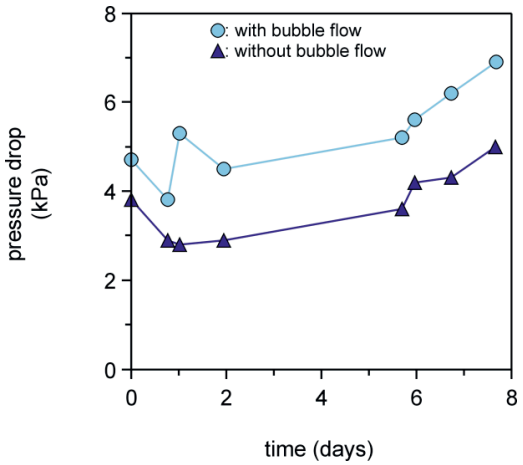

Figure 4-2: Pressure drop in time over the monitor with and without air supply to feed water containing substrate. Without air supply means that air supply was shortly interrupted for pressure drop measurements only (Vrouwenvelder et al., 2010a).

Bubble flow studies

Bubble flow studies were performed to vary shear at constant nutrient load and crossflow. In the bubble flow experiments, the MFSs were installed in a vertical position and operated in parallel. Compressed air at a pressure of 1.5 bar was fed into the feed water of the MFS between the nutrient dosing point and the MFS. The air supply tube contained a diaphragm pressure relief valve (KNF flodos diaphragm valve, Type: FDV 30 KPZ) to prevent back flow of water into the air system. A mass flow controller (5850TR, Brooks Instruments, The Netherlands) was used to regulate the air supply. Pressure drop measurements were performed in the monitors supplied with air during the experiment under two conditions: (i) continuous air supply and (ii) intermittent air supply. The pressure drop measurement during continuous bubble flow resulted in a higher pressure drop (15 mbar) compared to the pressure drop measured during temporarily interrupted air supply, Figure 4-2. The air supply caused the same pressure drop increase in the monitors supplied with and without nutrient.

Evaluation of pressure drop

Pressure drop measurements were performed with a pressure difference transmitter (Endress & Hauser, type Deltabar S: PMD70-AAA7FKYAAA). The calibrated measuring range was 0 – 5 bar (Vrouwenvelder et al., 2009c). The pressure drop transmitter was combined with a valve system developed to

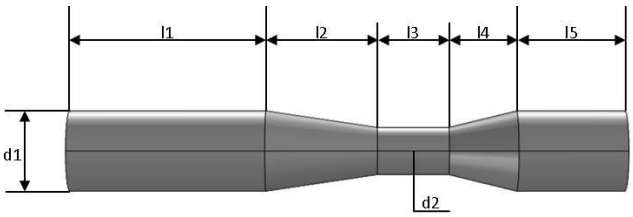

Figure 4-3: Reconstituted feed spacer filament with measured characteristic dimensions, d1 – d2 represents the filament thickness and l1 – l5 the length of the specific section along the filament (Bucs et al., 2014a).

enable measurement and logging the pressure drop over several monitors simultaneously.

Evaluation of biomass concentration

All studies were done with parallel MFS or FO operation. For each study membrane and spacer coupons from the MFSs or FO cells were autopsied after the same operation time, directly after operation was ended.

The same sampling methods and analyses were performed for all studies. Analysis performed on stacked membrane and spacer sheets were total active biomass (ATP) and TOC. Details of the methods have been described elsewhere (Vrouwenvelder et al., 2008b). ATP and TOC were selected as parameters to quantify biomass accumulation. ATP is applied to determine the concentration of active biomass. The TOC concentration is applied to determine the total organic amount of the biomass. The selection of the biomass parameters ATP and TOC was based on earlier studies by Vrouwenvelder et al. (2008) and has been applied in several studies (Araújo et al., 2012b; Beyer et al., 2014; Valladares Linares et al., 2014a). In some earlier studies, after cleaning a strong membrane performance decline caused by the accumulated material with a low ATP value and high TOC value was observed. The additionally performed total direct cell count analyses (Hobbie et al., 1977) and scanning electron microscopy (SEM – EDX) confirmed that biomass was still present and further analysis of membrane operational data showed that cleaning inactivated the biomass but did not remove it from the membrane (explaining the low ATP and high TOC values). Therefore, the combination of ATP and TOC analysis was applied for biomass quantification.

To characterize the accumulated fouling material, sections of membrane and feed spacers were taken from the MFSs. The sections (4 cm^2) were placed in a capped tube in 20 mL filled with sterile water. To determine the amount of biomass, the tubes with the membrane sections were placed in an ultrasonic cleaning bath (Bransonic, model 5510E-DTH, output 135 W, 42 kHz). Low energy sonic treatment (2 min) followed by mixing on a vortex (few seconds) was repeated three times. When the liquid was visually not homogeneous or when all biomass was not removed from the materials, additional time-interval treatments were applied with a sonifier (sample kept on ice) until the liquid was homogenous. Next, volumes of water collected from the tubes were used to determine biomass parameters, e.g. ATP. The same treatment was applied with ultrapure water for TOC analysis.

Numerical modelling

A three-dimensional (3-D) numerical model was developed to study the impact of nutrient load, biomass accumulation and feed spacer thickness on feed channel pressure drop in RO membrane systems. The model is based on the work of Picioreanu et al. (2009). Comsol Multiphysics (COMSOL 4.3a, Comsol Inc., Burlington, MA, www.comsol.com) was used for fluid dynamics and mass transport coupled with a Matlab (MATLAB 2011a, MathWorks, Natick, MA, www.mathworks.com) code for biomass attachment and growth. Geometry of a 31 mil thick feed spacer used in commercially available RO membrane modules was examined under a stereomicroscope (Leica M205 FA, Leica Microsystems) and recreated in Comsol Multiphysics. Specific dimensions of the spacer filaments were determined using Qwin Pro 3.1.0 software, Figure 4-3. The recreated 31 mil spacer geometry was proportionally scaled down/up to 28 mil and 34 mil (711 and 863 μm) thickness. The computational domain consists of five spacer units in diamond configuration (i.e., 45 rotated against the main flow direction). Although the standard size of the industrial membrane modules is 40 in. (~1 m) length with 8 in. (~0.2 m) diameter with a 40 m^2 membrane area the size of the computational domain used in this study is in the range of 105 m^2 (Figure 4.4). Using a 3-D numerical model for fluid flow and biomass accumulation (attachment and growth) for such a large scale requires a massive computational power. However the repetitive spacer geometry enables to simulate processes like fluid flow, mass transport and biomass formation on a much smaller scale.

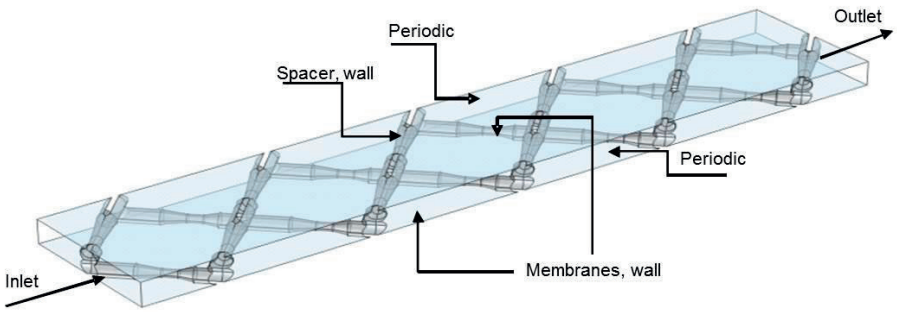

Figure 4.4: 3D representation of the computational domain with recreated feed spacer geometry and boundary conditions for the numerical simulations. The flow channel thickness corresponds with the spacer thickness (28, 31 and 34 mil for the presented simulations, 1 mil equals 25.4 mm). At the filament cross sections the spacer geometry presses against the top and bottom boundary (membrane), representing the spacer imprints into the membrane often observed during autopsies (based on Bucs et al., 2014).

Therefore, the flow channel in the numerical model was constructed in such a way that the two membrane planes cut 5 μm from the spacer top and bottom (Fimbres-Weihs and Wiley, 2007). In all numerically modelled cases, the calculated Re was lower than 200, therefore, the Navier Stokes equation was used to model the laminar, incompressible and stationary flow.

Biomass growth is a function of the local nutrient concentration (Monod, 1941). The nutrient concentration field in the numerical model was calculated from a convection – diffusion – reaction equation. In the model, the nutrient is transported by convection in the bulk liquid and by diffusion in the biomass. Biomass growth rate was calculated using simple Monod kinetics coupled with nutrient consumption rate. Biofilm formation in the computational domain consisted of two processes: biomass attachment and growth. Biomass detachment was not included in the model. Biomass was allowed to attach randomly to the membrane and spacer surface. For simulations of biomass growth the cellular automata model was used (Picioreanu et al., 2009). Boundary conditions for fluid flow and mass transport, biomass formation and model solution was set as described by Bucs et al. (2014a).

Study summary

A summary of the studies is shown in Table 4.1. Results of each study can be found in the section noted.

RESULTS

In this study the impact of the organic nutrient load on reverse osmosis (RO) and nanofiltration (NF) biofouling characterized by the development of feed channel pressure drop (FCP) and biomass concentration were investigated. The effect of (i) linear flow velocity (Figure 4-6), (ii) nutrient removal by pre-treatment (Figure 4-7), (iii) constant nutrient load at varying crossflow velocity (Figure 4-8), and shear (Figure 4-9) was assessed. Experiments performed with membrane fouling simulators (MFSs) and numerical modelling were applied to establish the effect of spacer thickness (Figure 4-10). An additional study was done with forward osmosis (FO) membranes to determine the effect of nutrient load at three spacer thicknesses (28, 31 and 34 mil, Figure 4-11).

Table 4.1: Overview of experimental studies on the impact of nutrient load on biomass accumulation in spiral-wound NF and RO, and FO membrane systems.

study	flow rate	crossflow velocity	air feed flow	nutrient concentration	nutrient load	spacer thickness
	$L \cdot h^{-1}$	$m \cdot s^{-1}$	$L \cdot h^{-1}$	$mg \cdot L^{-1}$	$mg \cdot m^{-2} \cdot s^{-1}$	mil
Varying nutrient load						
Effect of linear flow velocity at constant nutrient concentration	4.0	0.041	0	0.20	022	31
	8.0	0.082	0	0.20	0.11	31
	16.0	0.163	0	0.20	0.56	31
	24.0	0.245	0	0.20	0	31
Effect of pre-treatment: varying nutrient concentration	16.0	0.163	0	0.40	0.22	31
	16.0	0.163	0	0.20	0.11	31
	16.0	0.163	0	0.10	0.56	31
	16.0	0.163	0	0	0	31
Constant nutrient load						
Effect of crossflow velocity at constant nutrient load	4.0	0.041	0	0.40	0.56	31
	8.0	0.082	0	0.20	0.56	31
	16.0	0.163	0	0.10	0.56	31
	24.0	0.245	0	0.66	0.56	31
Effect of shear at constant nutrient load						
-S	16.0	0.163	0	0	0	31
+S	16.0	0.163	0	0.20	0.11	31
bubble flow +S	16.0	0.163	~100	0.20	0.11	31
bubble flow -S	16.0	0.163	~100	0	0	31
-S	20.0	0.200	0	0	0	31
+S	20.0	0.200	0	0.30	0.21	31
bubble flow +S	20.0	0.200	~36	0.30	0.21	31
Effect of spacer thickness at constant nutrient load	16.0	0.178	0	16.4	47.1	28
	16.0	0.163	0	16.4	47.1	31
	16.0	0.153	0	16.4	47.1	34
Forward osmosis: Effect of spacer thickness at constant nutrient load	7.2	0.141	0	115	115	28
	7.2	0.120	0	115	115	31
	7.2	0.086	0	115	115	46

To relate pressure drop increase with accumulated fouling material in the experimental studies, autopsies were performed on membranes sheets and spacers taken from the monitors.

Varying nutrient load

Effect of the linear flow velocity at constant nutrient concentration
Can biofouling be reduced by varying an operational parameter like the linear flow velocity, maintaining a constant feed water quality? To study the effect of the linear flow velocity, four monitors were operated with the same nutrient concentration (acetate carbon: 200 $mg \cdot L^{-1}$) in the feed water at different linear flow velocities (0.041, 0.082, 0.163 and 0.245 $m \cdot s^{-1}$). At the start of the experiment, the initial pressure drop was a function of the linear flow velocity, with the highest initial pressure drop at the highest linear flow velocity (Figure 4-4A). In time, the pressure drop over the monitors increased as a function of the linear flow velocity (Figure 4-4A, B). The accumulated biomass (ATP) in the monitors (determined at the end of the study) was related to the pressure drop increase, although the relationship was not linear (Figure 4-4A, C). Clearly, increasing the linear flow velocity was not reducing biofouling.

Effect of pre-treatment: varying nutrient concentration
In e.g. drinking water production, water treatment steps like slow sand filtration and activated carbon filtration reduce the microbial growth potential of the water. Can pre-treatment of water reduce biofouling in membrane installations?

To study the effect of the nutrient concentration on biofouling, four monitors were operated in a parallel study at a constant linear water flow velocity (0.163 $m \cdot s^{-1}$) fed with water containing different concentrations of a biodegradable compound (acetate carbon: 100, 200 and 400 $mg \cdot L^{-1}$) together with a blank solution without acetate addition.

With a higher nutrient concentration in the feed water a faster and larger pressure drop increase was observed over the monitors (Figure 4-5A). During the 14-day study, the pressure drop over the monitor fed with a blank solution remained constant, while the pressure drop increased when a nutrient was present (Figure 4-5B). At the end of the research period, the monitors were opened for analysis of the accumulated material on the membrane and feed spacer. The biomass load (ATP and TOC) increased with the acetate concentration in the feed water of the MFS (Figure 4-5C, D).

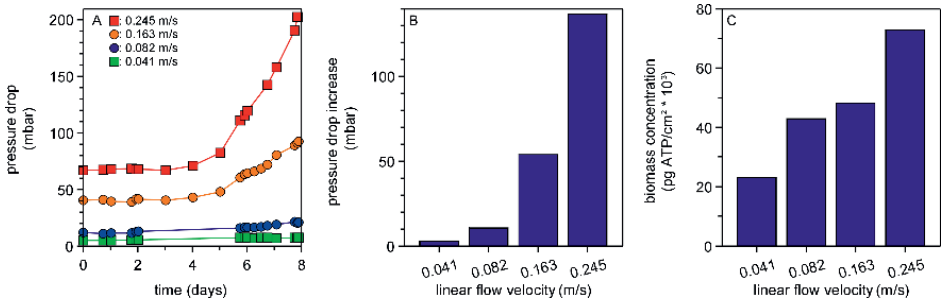

Figure 4-4: Pressure drop in time (A), pressure drop increase (B) and amount of accumulated biomass on the membrane and feed spacer in the monitor (C) after 8 days operation with different linear flow velocities and with the same concentration of biodegradable organic nutrient (200 μgC·L^{-1}) in the feed water. A higher linear velocity increased nutrient loading, pressure drop, pressure drop increase and biofilm accumulation (Araújo et al., 2012a).

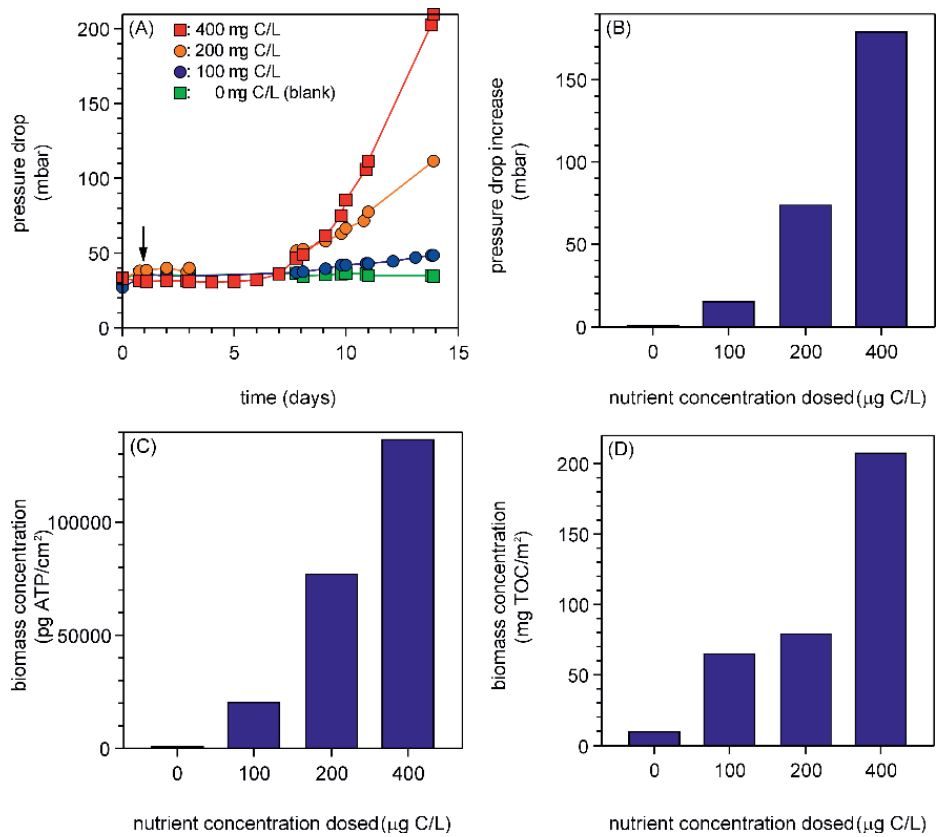

Figure 4-5: Pressure drop in time (A), pressure drop increase (B) and amount of accumulated biomass on the membrane and spacer in the monitor (C and D) after 14 days of operation without nutrient dosage and with dosage of different organic nutrient concentrations. The figure illustrates that pre-treatment removing nutrient reduced the biofouling rate (Vrouwenvelder et al., 2009a).

The TOC and ATP data showed the same trend. With lowering the nutrient concentration in the feed water decreased both the pressure drop and biomass load (Figure 4-5B-D). Visual observations showed that less material was present in the monitors supplied with lower nutrient concentrations, supporting the pressure drop results and biomass measurements.

Clearly, lowering the organic nutrient concentration reduced biofouling.

Constant nutrient load

The studies on the effect of linear flow velocity (Figure 4-4) and nutrient concentration (Figure 4-5) were performed with variable organic nutrient loads ($mg \cdot m^{-2} \cdot s^{-1}$, see Table 4.1). Differences in loading rate of biodegradable compounds may affect biofouling. The effect of varying (i) linear flow velocity, (ii) shear, and (iii) spacer thickness was studied at the same nutrient load (Table 4.1).

Effect of crossflow velocity at constant nutrient load
Comparative monitor studies were performed at constant nutrient load by varying both the linear flow velocity and feed water nutrient concentration (Table 4.1).

The pressure drop increased during the 11-day experiment (Figure 4-6A). The pressure drop increased with linear velocity (Figure 4-6B), but the accumulated amount of biomass determined in the monitors at the end of the running time was constant (Figure 4-6C, D).

The experiments showed that biomass accumulation was nutrient load related in the applied velocity and nutrient concentration range.

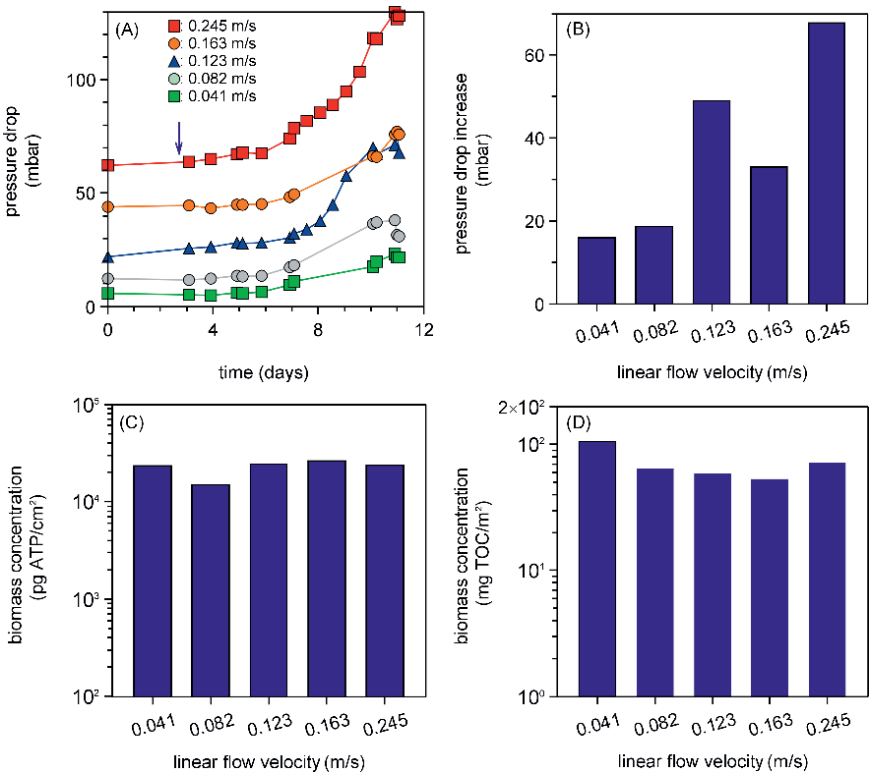

Figure 4-6: Pressure drop in time (A), pressure drop increase (B) and amount of accumulated biomass on the membrane and spacer in the monitor (C and D) after 11 days of operation at varying crossflow velocity at constant organic nutrient load. The amount of accumulated biomass was constant but the pressure drop increase was a function of the linear flow velocity (Vrouwenvelder et al., 2009b).

In monitors supplied with the same nutrient load, the amount of accumulated biomass was constant while the pressure drop increase was a function of the linear flow velocity (Figure 4-6B-D). Lowering the linear flow velocity reduced the impact of the same amount of accumulated biomass on membrane performance at constant nutrient load.

Effect of shear at constant nutrient load

To evaluate the influence of shear (single and two phase flow) on biofouling development, comparative studies with monitors were performed with constant nutrient load, nutrient concentration and fluid velocity (Figure 4-7). For the two phase flow, water sparked with air was applied (bubble flow), while for the single phase flow only water was used. “Bubble flow” caused a stronger local

gradient in shear than without “bubble flow”, maintaining the same nutrient load and fluid velocity.

Monitors without nutrient dosage without bubble flow (-S) and with bubble flow (bubble flow -S) were operated under the same conditions as the monitors with nutrient feed without bubble flow (+S) and with bubble flow (bubble flow +S). As expected, the pressure drop in the blank monitors without nutrient with and without bubble flow (-S bubble flow and -S) remained constant (Figure 4-7A, B). The pressure drop increased in the monitors supplied with nutrient (+S) with water flow only, while the pressure drop remained low in the monitors supplied with nutrient and bubble flow (bubble flow +S). At the end of the running time, the monitors were opened for analysis of the accumulated material. On the feed spacer and membrane taken from the monitors with nutrient addition without bubble flow (+S) and with bubble flow (bubble flow +S), the same, high concentration of biomass (ATP, TOC) was observed, while the monitors without nutrient dosage without bubble flow (-S) and with bubble flow (bubble flow -S) had low biomass concentrations (Figure 4-7C,D). Contrary to the pressure drop increase, the amount of biomass was not influenced by the flow regime. In other words: nutrient dosage with and without bubble flow caused the same biomass concentrations while the pressure drop increase differed strongly (Figure 4-7). Bubble flow +S caused a more compact and smooth biofilm, explaining the lower pressure drop increase

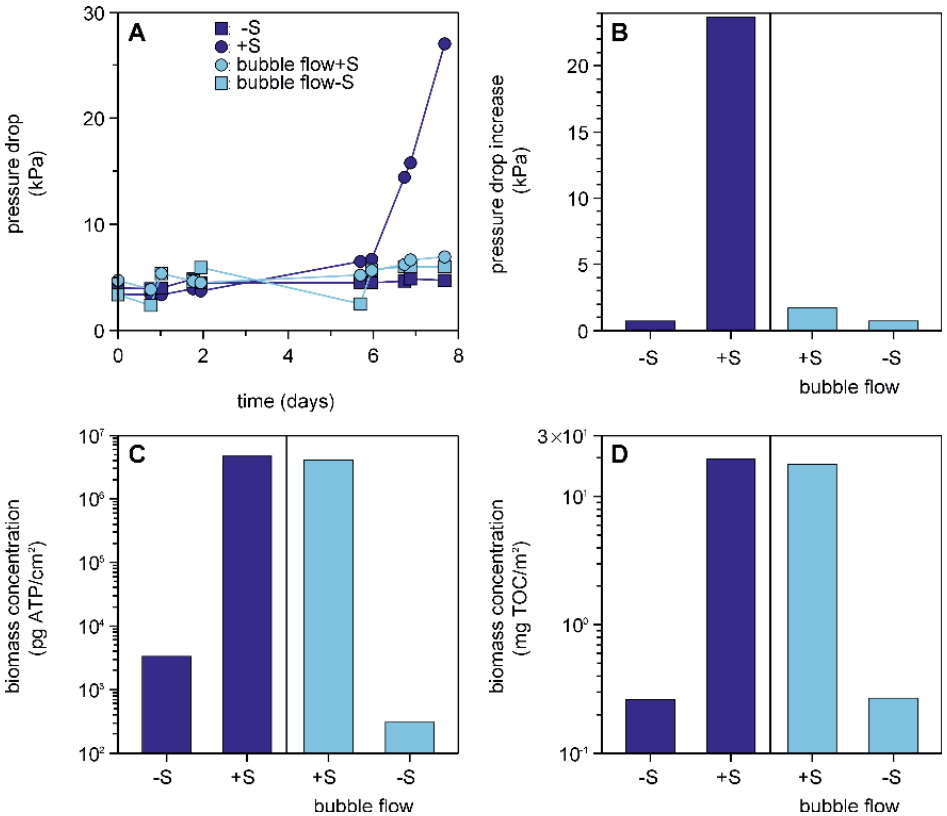

Figure 4-7: Pressure drop in time (A), pressure drop increase (B) and amount of accumulated biomass on the membrane and spacer (C and D) after 7.8 day monitor operation. The monitors were operated without nutrient dosage and with dosage of a biodegradable organic nutrient (0.20 $mgC \cdot L^{-1}$) to the feed water of the monitor without and with bubble flow to vary shear. -S = without bubble flow without nutrient dosage; +S = without bubble flow with nutrient; bubble flow +S = bubble flow with nutrient; bubble flow -S = bubble flow without nutrient dosage (Vrouwenvelder et al., 2010b).

compared to the same biomass amount developed without bubble flow +S, where the biofilm was more voluminous and fluffy.

A second study performed with the same set-up (Table 4.1) confirmed these results. A high pressure drop increase was observed for the monitor with nutrient dosage without bubble flow (+S) while the pressure drop increase was low for the monitor with nutrient and bubble flow (bubble flow +S). The biomass concentrations had the same order of magnitude.

High shear resulted in a more compact and less filamentous biofilm structure than low shear, causing a much lower pressure drop increase (Vrouwenvelder

et al., 2010b). However, the biofilm grown under low shear conditions was more easy to remove during water flushing compared to a biofilm grown under high shear (Vrouwenvelder et al., 2010b).

Clearly, the organic nutrient load determined the amount of biomass accumulation, while the shear determined the biofilm morphology and cohesion strength (Vrouwenvelder et al., 2010b). Biofouling caused by a low shear biofilm may be easier to control than high cohesion strength biofilm caused by high shear.

Effect of spacer thickness at constant nutrient load

Reducing the nutrient load is the generally accepted way to restrict the amount of accumulated biomass and to slow down the biofouling rate. Can the impact of accumulated biomass on membrane performance also be reduced by the use of modified feed spacers? Several reports have indicated that the use of thicker feed spacers caused lower pressure drops (Araújo et al., 2012a, 2012b; Bartels et al., 2008; K Majamaa et al., 2009). Earlier studies showed that numerical modelling well predicts both biofilm formation and membrane performance in spiral-wound membrane systems (Bucs et al., 2014a; Picioreanu et al., 2009).

A feed spacer geometry as applied in practice in spiral-wound NF and RO membrane modules was reconstituted in a numerical 3D model (Picioreanu et al., 2009) and scaled proportionally to the required thickness. In this study, for three spacer thicknesses (28, 31 and 34 mil) the development of pressure drop and biomass growth was modelled.

At the start of the study no biofilm presence was predicted. The pressure drop over the clean spacer channel was lower with increasing spacer thickness. In time, the modelled pressure drop increased for all spacer thicknesses. The lowest pressure drop increase was predicted for the thickest spacer (Figure 4-8B) while the same amount of biomass accumulated in the flow channel for all cases (Figure 4-8C). Biomass attached randomly on the membrane and spacer surface for all simulated spacer thicknesses (28, 31 and 34 mil). Microbial growth was governed by the local nutrient concentration. At the end of the simulations, the spatial distribution of the biomass was similar for all spacer thicknesses. A thicker feed spacer with the same geometry causes a lower pressure drop by e.g. modified hydrodynamics.

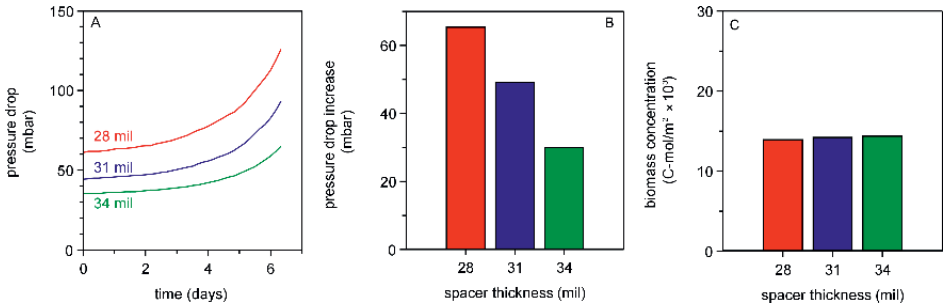

Figure 4-8: Numerical modelling experiment: Pressure drop in time (A), pressure drop increase (B) and amount of accumulated biomass on the membrane and spacer (C) after 6.5 day at constant organic nutrient load with identical geometry feed spacers varying in thicknesses: 28, 31 and 34 mil (based on Bucs et al., 2014).

A thicker feed spacer was predicted to cause a lower impact of accumulated biomass on the pressure drop than a thinner feed spacer with an identical geometry. So, the use of a thicker feed spacer may be an approach to reduce the effect of biofouling on membrane performance.

Forward osmosis: effect of spacer thickness at constant nutrient load

In an experimental study on forward osmosis (FO) the influence of feed spacers differing in thickness (28, 31 and 46 mil) was determined on biomass accumulation and permeate flux development at constant nutrient load.

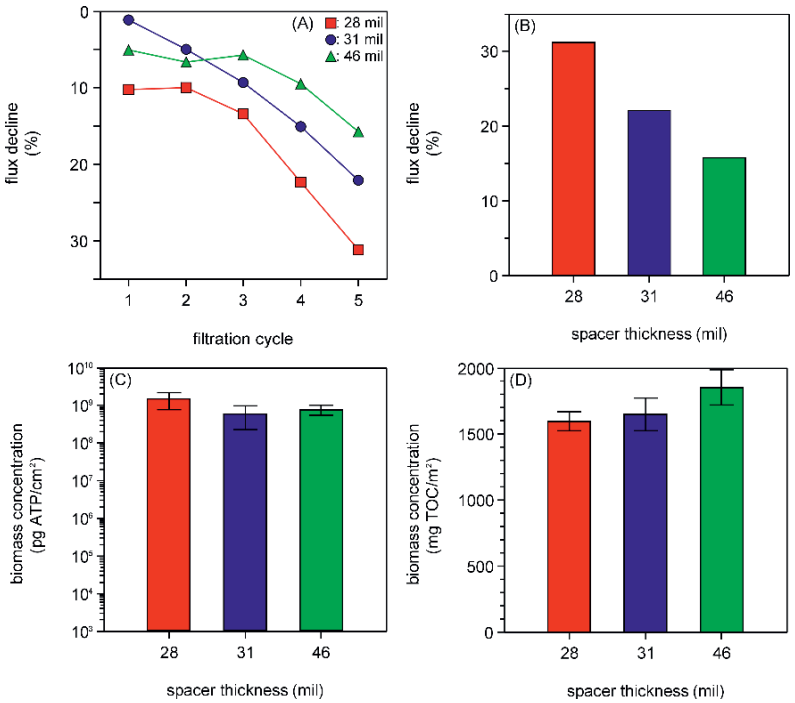

Figure 4-9: Forward osmosis study. Permeate flux decline in time (A), flux decline in % (B) and amount of accumulated biomass on the membrane and spacer (C and D) after 5 filtration cycles at constant organic nutrient load with feed spacers varying in thicknesses: 28, 31 and 34 mil (based on Valladares Linares et al., 2014).

The same initial flux of ~8 $L \cdot m^{-2} \cdot h^{-1}$ was used for 28, 31 and 46 mil thick feed spacers. In the filtration cycle, the flux declined for all spacer thicknesses (Figure 4-9A). The lowest flux decline was observed for the thickest spacer (Figure 4-9A, B) while the same amount of biomass was accumulated in the flow channel for all spacer thicknesses (Figure 4-9C, D).

The results of the forward osmosis study are in agreement with the results of the RO monitor studies: The nutrient load determined the amount of accumulated biomass while the use of a thicker feed spacer in forward osmosis membranes reduced the effect of the same amount of biomass on the permeate flux decline.

DISCUSSION

The objective of this study was to determine the influence of the organic nutrient load on biofouling of membrane systems. With constant nutrient load

the same amount of accumulated biomass was found at varying (i) crossflow velocity (Figure 4-6), (ii) shear (Figure 4-7), and (iii) feed spacer thickness (Figure 4-8 and Figure 4-9). Consequently, the nutrient load determined the amount of biomass accumulation (Figure 4-10). The nutrient load can be reduced by pre-treatment (Figure 4-5), slowing-down the rate of biomass accumulation. For the same amount of accumulated biomass, the increase of feed channel pressure drop was highest for the thinnest feed spacer and/or the highest linear flow velocity. Therefore, the impact of biofouling on membrane performance can be reduced by using a thicker feed spacer (Figure 4-8) and/or a lower linear velocity (Figure 4-6).

Biofilm accumulation dominated by organic nutrient load

Nutrient load is the product of nutrient concentration and linear flow velocity. Therefore, assessment of the effect of nutrient load on biofouling requires unravelling the individual contributions of nutrient concentration and crossflow velocity. All studies at constant nutrient load but different crossflow velocity, shear and spacer thickness consistently showed formation of the same amount of accumulated biomass (Dreszer et al., 2014b; Valladares Linares et al., 2014a; Vrouwenvelder et al., 2010a, 2009b; Ying et al., 2013). Therefore, nutrient load is the key parameter for biofilm formation, but the impact on membrane performance is depending on design (e.g. geometry) and operational aspects (e.g. crossflow velocity) of the membrane system.

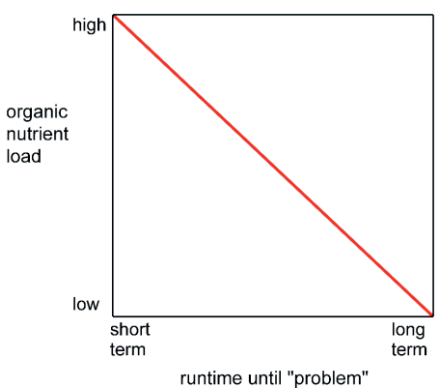

Figure 4-10: Schematic relationship between the biodegradable organic nutrient load of the feed water and of a runtime RO/NF membrane system until a biofouling problem: 10 – 15% performance reduction. A high nutrient load causes a short runtime while a low nutrient load results in a long runtime.

In literature, no conclusive studies have been found describing the impact of biodegradable organic nutrient load on biofouling in NF and RO membrane systems at various conditions (crossflow velocity, substrate concentration, shear and feed spacer thickness). For spiral-wound RO and NF membrane systems, three papers containing data on parts of the role of nutrient load on biofilm development have been published recently (Vrouwenvelder et al., 2010a, 2009b; Ying et al., 2013). In their study on the effect of shear rate on biofouling Ying et al. (2013) concluded that in RO membrane systems biofilm formation was dominated by the organic loading rate rather than the shear force. They compared low shear (at high loading) and high shear (at low and high loading) by varying crossflow velocity and total organic carbon concentration. The results presented in this paper on the effect of shear are in agreement with Ying et al. (2013). Our study addressed the role of nutrient load, linear flow velocity, nutrient concentration, shear and spacer thickness. Part of the results of earlier studies by Vrouwenvelder et al. (2010a, 2009b) have been integrated in this study to address in detail the impact of organic nutrient load on biofouling.

Strategies to reduce the nutrient load in membrane systems are applying biological pre-treatment of the feed water (e.g. by activated carbon and slow sand filtration) and/or applying lower crossflow velocities in the membrane installation (Figure 4-4). However, lower crossflow velocities may enhance concentration polarization (Chong et al., 2008a; Herzberg and Elimelech, 2007a; A. I. Radu et al., 2012), thereby reducing the amount of water production.

Reducing the impact of accumulated biomass by thicker spacer use

Pilot and full scale studies with spiral-wound membrane elements containing feed spacers with a varying thickness showed that the use of thicker spacers caused an initially lower FCP and a smaller FCP increase during biofouling (Bartels et al., 2008; Majamaa et al., 2012). Majamaa et al. (2012) studied the impact of the feed spacer thickness (22, 28, 34 and 46 mil) on the initial FCP and the response to fouling in a controlled side-by-side comparison with spiral wound RO membrane modules at pilot and full scale. Pilot scale experiments with in-parallel operated modules showed that thicker spacers caused an initially lower FCP and smaller FCP increase during operation (Majamaa et al., 2012). Full scale RO experiments with 8 inch diameter modules (28 and 34 mil

spacer thickness) in two side-by-side seven element pressure vessels showed that the vessel with a thicker spacer had a lower initial FCP and a reduced FCP increase rate over a 16 months operation period m(Majamaa et al., 2012). Bartels et al. (2008) reported full-scale studies with spiral wound RO membrane modules subsequently operated with 28, 31 and 34 mil feed spacers. Membrane elements were produced with thicker feed spacers maintaining the same membrane surface area (Bartels et al., 2008), due to e.g. better membrane module manufacturing and thinner glue lines. For membrane modules differing in feed spacer thickness no information was found on the ratio between total membrane surface area and feed water volume in the membrane module. Bartels (2008) reported for each of the 28, 31 and 34 mil spacer membrane batches the same permeate flow and recovery. As a result, the feed flow was the same as well. The results clearly showed that a thicker feed spacer caused a lower initial FCP and a lower FCP increase than a thinner feed spacer (Bartels et al., 2008).

Araujo et al. (2012a) reported that similar amounts of biomass were accumulated during parallel monitor experiments with different spacer thicknesses at constant nutrient load, while the lowest feed channel pressure increase was observed for the thickest spacer. Bucs et al. (2014a) predicted the same trend (lower impact biomass applying a thicker spacer) by numerical modelling. The feed spacer thickness studies by Majamaa et al. (Majamaa et al., 2012), Bartels et al. (2008), Araujo et al. (2012a) and Bucs et al. (2014a) are consistent with the results of feed spacer studies presented in this paper. Thicker spacers than currently applied in practice may be a feasible strategy to reduce the impact of biofouling on membrane performance.

Biofouling control

Cleanings for biofouling control seem unavoidable. With a high biodegradable organic nutrient load the membrane runtime until performance decline will be short compared to the performance decline for a low organic nutrient load while the runtime between cleanings will be shorter (Figure 4-10); but eventually always a biofouling layer builds up, even when only minute amounts of nutrients are present.

An effective strategy to control biofouling may consist of:

- delaying the build-up of biofouling by pre-treatment removing biodegradable nutrients to a large extent (Flemming et al., 1997; Vrouwenvelder et al., 2008) and dosing selected chemicals with a low nutrient content such as acids and antiscalants to membrane installations feed water (Vrouwenvelder et al., 2000).
- reducing the impact of accumulated biofilm on membrane performance applying a thicker and/or a modified geometry feed spacer (Bartels et al., 2008; Majamaa et al., 2012), and
- removing the biofilm from membrane elements (cleaning) as a last resort (Table 4.2). Clearly, there is no escape of cleaning in the long run, even with the best organic nutrient removal by pre-treatment and thicker/ modified spacer use.

Current chemical cleaning strategies are not effective to restore the original membrane performance (Creber et al., 2010a, 2010b). Chemical cleanings are effective to inactivate a significant amount of biomass, but have no or limited effect on biomass removal from the spiral-wound membrane elements (Bereschenko et al., 2011; Creber et al., 2010a, 2010b; Vrouwenvelder and Van Der Kooij, 2001).

Table 4.2: Scenario for potentially effective biofouling control of NF and RO membrane systems, consisting of three aspects.

Step	Process
1	Retarding biofilm build up by pre-treatment reducing the water biodegradable organic nutrient concentration
2	Reducing biofilm impact on membrane performance by modified membrane installation operation and design (e.g. modified spacer and hydraulics)
3	Removing biofilm through a cleaning strategy

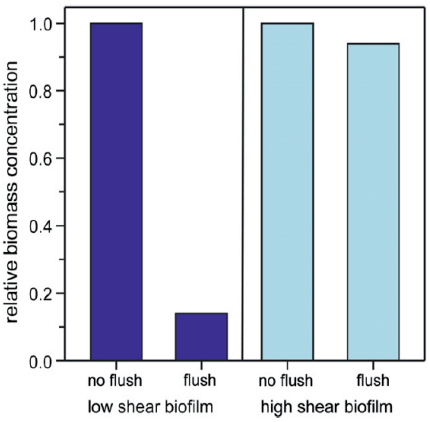

Figure 4-11: Effect of flushing (at 0.42 m s^{-1}) on biofouling developed at low and high linear flow velocity (0.06 and 0.3 m s^{-1}), indicating that a low shear biofilm is easier removed that a high shear biofilm. From Vrouwenvelder et al., 2010a.

Effective biofilm removal may be possible with modified geometry spacers (facilitating removal of detached biomass from the membrane element) and advanced cleaning strategies (e.g. intermittent air/water flush, Cornelissen et al., (2007); biofilm cohesion strength engineering, Vrouwenvelder et al., (2010b); (Figure 4-11) and feed-concentrate flow direction reversal (Vrouwenvelder et al., 2011b). Cleaning at an earlier stage may be more effective than at a later stage (Creber et al., 2010a, 2010b), suggesting that preventive cleanings may have merit to control biofouling. There is a need to develop cleaning strategies removing the fouling from the membrane elements.

CONCLUSIONS

The study on the influence of the biodegradable organic nutrient load on biofouling development in nanofiltration, reverse osmosis and forward osmosis membrane systems led to the following conclusions:

- The nutrient load determined the amount of accumulated biomass.
- The amount of accumulated biomass on the membrane and spacer was independent of the applied shear.
- Retarding the rate of biofilm formation required a lower nutrient load.
- Reducing the effect of accumulated biomass on membrane performance was achieved by a lower crossflow velocity and thicker feed spacer use.

- Cleanings for biofouling control could be delayed but were unavoidable.

An integrated approach for biofouling control was discussed, involving the combination of (i) retarding biofilm build-up by pre-treatment lowering the nutrient load, (ii) reducing the impact of accumulated biomass on performance by e.g. thicker/modified spacers and lower crossflow velocities and (iii) removing the biomass from modules applying an advanced strategy.

٥

Surface Coatings for Biofouling Control

Abstract

Surface coating of membranes and feed spacers may be important to control biofilm development and biofouling impact on membrane performance of spiral-wound reverse osmosis (RO) and nanofiltration (NF) systems. The objective of this study was to investigate the impact of an amphiphilic copolymer coating on biofilm formation and biofouling control. The coating was composed of both hydrophilic and hydrophobic monomers hydroxyehtyl methacrylate (HEMA) and perfluorodecyl acrylate (PFDA) respectively. Commercial RO membranes were coated with HEMA-PFDA copolymer films of optimized chemistry and thickness. Biofouling studies with coated and uncoated membranes and feed spacers were performed using membrane fouling simulators (MFSs) operated in parallel, fed with water containing nutrients. The pressure drop development in time was monitored and after eight days the MFSs were opened and the accumulated biofilm on the membrane and spacer sheets was quantified and characterized. The presence of the membrane coating was determined using X-ray photoelectron spectroscopy (XPS) and Fourier transform infrared spectroscopy (FTIR). Results showed that the amphiphilic coating (i) delayed the biofilm formation, (ii) influenced the biofilm composition (higher EPS content), and (iii) was still present on the membrane at the end of the biofouling study, showing that the coating was strongly attached to the membrane and spacer surface. Evaluation of the impact of anti-biofouling coatings should include (i) long-term biofilm studies using e.g. MFSs and (ii) coating presence testing before and after the fouling studies. Using coated membranes and spacers in combination with advanced cleaning strategies may be a potential suitable way to control biofouling.

Published as

Szilárd S. Bucs, Rodrigo Valladares Linares, Nadia Farhat, Asif Matin, Zafarullah Khan, Mark C.M. van Loosdrecht, Rong Yang, Minghui Wang, Karen K. Gleason, Joop C. Kruithof, Johannes S. Vrouwenvelder (2017) Coating of reverse osmosis membranes with amphiphilic copolymers for biofouling control, *Desalination and Water Treatment*, **68**: 1-11

INTRODUCTION

The use of membrane filtration processes like nanofiltration (NF) or reverse osmosis (RO) for water desalination and reuse has a great potential to meet the growing demand for fresh water. One of the major drawbacks of membrane filtration is fouling, accumulation of unwanted material (particles, inorganics, organics and biomass) on the membrane surface. Membrane fouling causes the reduction of product water quantity and quality while increasing the operational costs. The most predominant fouling type is biofouling, excessive deposition and growth of biomass on the membrane surface causing an unacceptable performance decline (Flemming, 1997; Matin et al., 2011a; Shannon et al., 2008; van Loosdrecht et al., 2012; Vrouwenvelder et al., 2008b).

Many research efforts have been carried out to reduce biofouling in membrane systems with focus on improvement of (i) pre-treatment, (ii) membrane module design and (iii) membrane surface modification. It was shown that the physicochemical properties (surface charge, roughness, hydrophilicity) of the membrane surface have impact on membrane fouling (Louie et al., 2006). It is generally accepted that hydrophilic membranes are more resistant to fouling (Kang and Cao, 2012). Surface charge and membrane roughness are important factors influencing membrane fouling. Deposition of foulant is less likely on neutral or close to neutral charged membrane surfaces (Kang and Cao, 2012; Kim and Lee, 2006). Surface morphology has a significant role on membrane fouling, because foulant are more likely to be entrained by rougher topologies than by smoother membrane surfaces (Louie et al., 2006; Sagle et al., 2009).

Membrane coating is frequently used for surface modification of conventional RO membranes. Membrane coating has been proposed to avoid or reduce membrane fouling in RO systems. Many studies showed that compared to uncoated membranes, less fouling was observed when membranes surfaces had a hydrophilic coating (Araújo et al., 2012b; Matin et al., 2014b; Tang et al., 2009; Venault et al., 2014; Yi et al., 2010; Zhao et al., 2007).

Amphiphilic copolymer coatings have been used to reduce protein and bacterial adhesion to the membrane surface. Asatekin et al. (Asatekin et al., 2009) developed nanofiltration membranes with a selective, comb-like amphiphilic copolymer layer. The developed membranes showed a high fouling resistance against bovine serum albumin (BSA) proteins during dead-end filtration

experiments (Asatekin et al., 2009). Bacterial adhesion to membranes coated with amphiphilic copolymers and the reversibility were tested using atomic force microscopy (AFM). Furthermore, the fouling resistance of the coated membrane was tested in short-term static bacterial adhesion tests as well as in long-term cross-flow filtration cells studies. Results showed no bacterial adhesion during the static test and reversible bacterial adhesion to the coated membrane in the cross-flow filtration studies (Adout et al., 2010). Baxamusa et al. (Baxamusa and Gleason, 2009) used amphiphilic copolymers (containing hydrophilic and hydrophobic groups) to reduce protein adsorption to membrane surfaces. Static protein adsorption experiments showed that less proteins adsorbed to the membranes coated with copolymers than for the membrane coated with either of the two homopolymers (Baxamusa and Gleason, 2009), suggesting that membrane coatings with amphiphilic copolymers could significantly reduce biofouling of membrane filtration systems.

The objective of this study was to investigate the impact of a surface coating by amphiphilic copolymers on biofilm formation and biofouling control in membrane systems. The coating was composed of hydrophilic hydroxyethyl methacrylate and hydrophobic perfluorodecyl acrylate. The membranes were characterized, and the presence of the amphiphilic coating was inspected before and after the biofouling studies by X-ray photoelectron spectroscopy (XPS) and Fourier transform infrared spectroscopy (FTIR) (Amadei et al., 2014; Yang et al., 2014). To evaluate the potential of the amphiphilic coating on biofilm formation and biofilm control (i) static, short-term bacterial adhesion and (ii) long-term biofouling studies were performed using membrane fouling simulators (MFSs).

MATERIAL AND METHODS

Amphiphilic membrane coating procedure

The two monomers, perfluorodecyl acrylate (PFA) and hydroxyethyl methacrylate (HEM) were heated in separate crucibles to 80 °C and 70 °C respectively while the initiator, *tert*-butyl peroxide was kept at room temperature. The relative flow rates of the monomer gases and the initiator were adjusted to obtain a content of 40% PFA in the copolymer. The commercial RO membrane samples were stored at 30 °C.

The copolymerization took place directly onto the active layer of the membrane and resulted in the formation of the copolymer film with a target thickness of around 20 nm. Film growth was monitored *in situ* by laser interferometry with the laser focused on a single point on a silicon wafer placed adjacent to the membrane sample. The film deposition was terminated once the laser interferometry indicated attainment of the desired thickness on the silicon wafer (Matin et al., 2014a).

Membrane characterization

The coated and uncoated membranes were characterized before and after the long-term biofouling studies to confirm the presence/absence of the coating.

The zeta potential was determined by a SurPASS Complete surface analyzer (Anton Paar Inc, USA) at a pH range from 3 to 10. Atomic force microscopy (AFM) was used to quantify membrane roughness (N9417S 7500 Atomic Force Microscope, Keysight Technologies, Inc., CA, USA).

X-ray photoelectron spectroscopy (XPS) analysis was used to confirm the presence of the copolymer film on the modified membranes. The analyses were conducted on an Axis Ultra DLD system under ultra-high vacuum conditions (1.6×10^{-12} bar). The surface scan was performed in the binding energy range 0–1000 eV with a resolution of 1 eV. High-resolution scans of C 1 s, F 1 s and O 1 s were conducted under similar conditions with 0.05 eV steps, pass energy 20 eV (Yang et al., 2014).

Fourier transformed infrared spectroscopy (FTIR) spectra were obtained using a Nicolet 8700 FTIR spectrometer coupled to a germanium crystal operated at 45° using OMNIC 6.2 software (Thermo Electron Corp., Hampton, NH). Two replicates of each membrane sample were measured, and five readings were taken from different points. Each spectrum represents an average of 16 scans collected in the range 600 to 4000 cm^{-1} at a resolution of 1 cm^{-1} (Amadei et al., 2014).

Short-term bacterial adhesion

For the bacterial adhesion tests, a non-pathogenic strain of *Escherichia coli* was used. The bacterial strains were tagged with a plasmid coding for green fluorescent protein to allow live cell detection with fluorescent microscopy.

The *E. coli* cells were incubated and harvested during the mid-exponential growth phase in Trypton (TT) media at 37 °C. *E. coli* K12 wild-type strain MG 1655 was grown overnight in nutrient broth at 37 °C. The bacterial solution was transferred to narrow test tubes. Membrane coupons, with dimensions of approximately 1 cm^2, were cut from the flat sheets and placed in 10 mL cell suspension. The tubes were then placed in an incubator at a temperature of 37 °C for four hours. The individual tubes were gently shaken hourly to ensure complete exposure of the membrane surface to the bacterial suspension. The membrane coupons were then rinsed gently for a few seconds with a bacteria-free broth media to remove weakly bound cells. After the exposure to bacteria, the specimens were dried either in vacuum for a couple of hours or with dry nitrogen for a few minutes. Membrane coupons were then inspected under a fluorescent microscope, and six images were taken across the membrane surface.

Long-term biofouling experiments

For the long-term biofouling experiments, the membrane fouling simulator (MFS) with external dimensions of 0.07 m × 0.20 m × 0.04 m was used (Vrouwenvelder et al., 2006). The MFS has been found a suitable tool for prediction and characterisation of membrane fouling (Dreszer et al., 2014b; Vrouwenvelder et al., 2009a; West et al., 2015). Membrane sheets were cut from an unused commercial RO membrane, TFC-HR, manufactured by Koch Membrane Systems (USA). For all studies a 34 mil (864 μm) thick feed spacer was used, resulting in a flow channel porosity of ≈ 0.85. Membrane and feed spacer coupons were placed in the MFS resulting in the same special dimensions as in spiral wound membrane systems. MFSs were operated parallel, and the development of the fouling was monitored by measuring the pressure drop over the MFSs in time. At the end of the study, the MFSs were opened, and the sheets of spacer and membrane were analysed for fouling amount and presence of coating.

The MFSs were fed with tap water, and the flow rate was set to 16 $L \cdot h^{-1}$ equal to a linear flow velocity of 0.16 $m \cdot s^{-1}$, representative for practice (Picioreanu et al., 2009). The flow rate was automatically kept constant for sensitive and accurate pressure drop measurements (Szilárd S. Bucs et al., 2015; Vrouwenvelder et al., 2009c). To enhance biofilm growth a solution of sodium acetate, sodium nitrate, and sodium dihydrogen orthophosphate in a mass ratio

C: N:P of 100:20:10, respectively, was employed increasing the C concentration in the MFS feed water with 400 $\mu g \cdot L^{-1}$. The typical C:N:P ratio in biomass is ≈ 100:20:4.3 an excess of phosphorous was dosed to ensure that phosphate limitation did not restrict biofilm formation in the MFSs (Vrouwenvelder et al., 2010a).

Evaluation of the biomass concentration

Adenosine triphosphate (ATP) was selected as parameters to quantify biomass accumulation. ATP is applied to determine the concentration of active biomass. The selection of the biomass parameters ATP was based on earlier studies (Bucs et al., 2014b; Vrouwenvelder et al., 2009d). ATP measurements were performed using an ATP analyser (Advanced Luminometer, Celsis, Belgium).

Visual inspection

Confocal Laser Scanning Microscopy (CLSM), (LSM710 upright confocal microscope, Zeiss, Germany) was used to identify and characterize biofouling on the membrane surface after the experiments. The samples were stained with the following dyes based on methods described in the literature (Chen et al., 2006; Valladares Linares et al., 2014a). For total bacterial cells 4′,6-Diamidino-2-Phenylindole (DAPI) dye (emission wavelength of 358 nm; excitation wavelength of 461 nm) was used. Fluorescein Isothiocyanate (FITC) (emission wavelength of 480 nm; excitation wavelength of 520 nm) was applied to stain the amine-reactive compound-like proteins and amino sugars, and Calcofluor White (emission wavelength of 433 nm; excitation wavelength of 355 nm) to stain β-D-glucopyranose polysaccharides. After each of these three staining stages, the sample was washed twice with phosphate-buffered saline (PBS) pH 7 to remove excess stain, and a wipe was used to remove excess dye. The fouling on the membrane surface was analysed by Scanning Electron Microscopy (SEM-EDX, Magellan, FEI). The samples were freeze dried for environmental SEM.

Biofilm composition: bacterial cells, polysaccharides and proteins

CLSM images were further analysed using ISA3D software (Beyenal et al., 2004), to quantify the differences in biofilms composition.

RESULTS

In this study, the impact of the coating of a membrane and spacer by amphiphilic copolymers on biofilm formation and biofouling control in reverse osmosis systems was investigated, applying short and long-term biofouling studies with coated and uncoated membrane sheets. The presence of the coating on the membrane was evaluated before and after the biofouling studies.

Membrane characterization

Zeta potential measurements confirmed the presence of the coating on the membrane surface prior to the biofouling studies. In the range of pH 5 up to 10 the coated membrane showed a less negative surface charge compared to the uncoated membrane (Figure 5-1a). X-ray photoelectron microscopy indicated the presence of fluorine functional groups on the coated membrane surface confirming the presence of the perfluorodecyl acrylate (Figure 5-1b).

Membrane surface roughness was evaluated by AFM. The coated membrane had a lower surface roughness than the uncoated membrane. The lower surface roughness can be explained by the presence of coating, filling the “valleys” of the membrane, reducing the membrane surface overall roughness by ≈ 60 percent (Figure 5-2). All measurements confirmed the presence of the coating on the coated membrane sheets. Overall, the coated membrane had a less negative surface charge and a lower surface roughness compared to the uncoated commercially available reverse osmosis membrane, while fluorine was detected on the coated membrane surface.

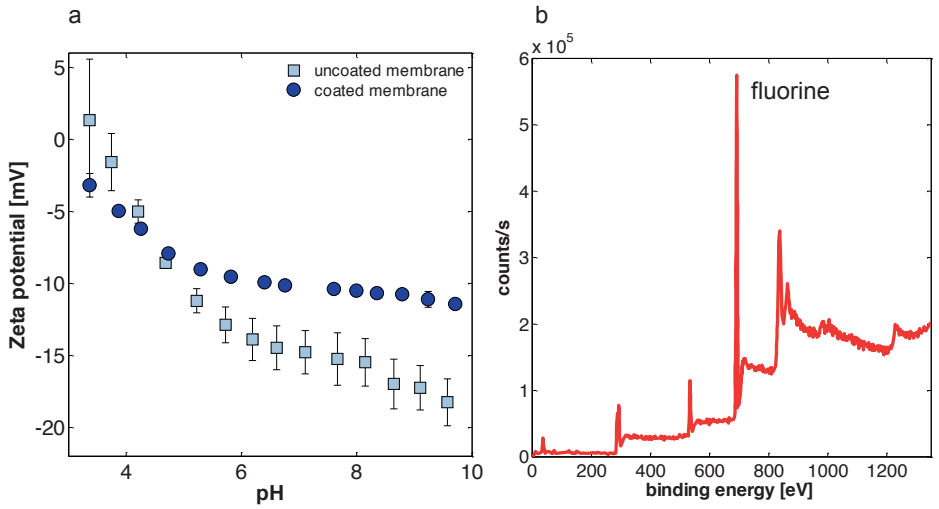

Figure 5-1: Zeta potential (a) at different pH for the un-coated and coated membranes and X-ray photoelectron spectroscopy (XPS) (b) for the coated clean, unused membrane. The XPS peak at 700 [eV] binding energy corresponds to the fluorine functional group present in the coating, indicating the presence of the coating on the coated membrane.

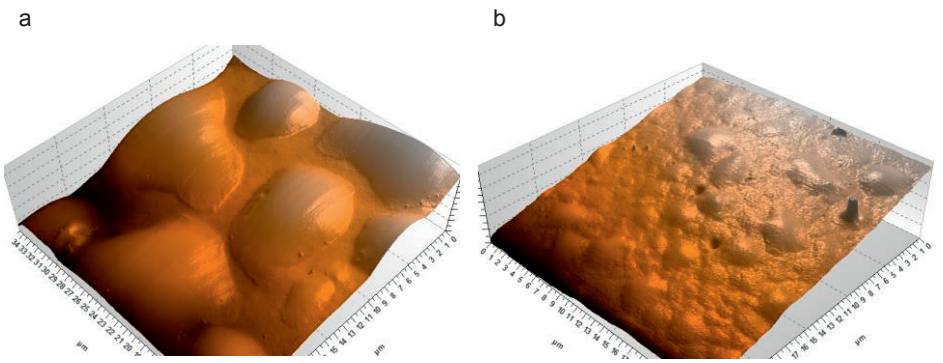

Figure 5-2: Surface roughness of the (a) un-coated and (b) coated membranes measured by atomic force microscope (AFM). A lower surface roughness was observed for the coated membrane.

Short-term bacterial adhesion tests

The antifouling properties of the coated membrane were evaluated by short-term static bacterial adhesion experiments. Coupons of coated and uncoated membranes were exposed to fluorescent *E. coli* suspensions. After four hours incubation, the coupons were rinsed to remove loosely attached bacterial cells and the membrane surface was characterized by both fluorescent microscopy

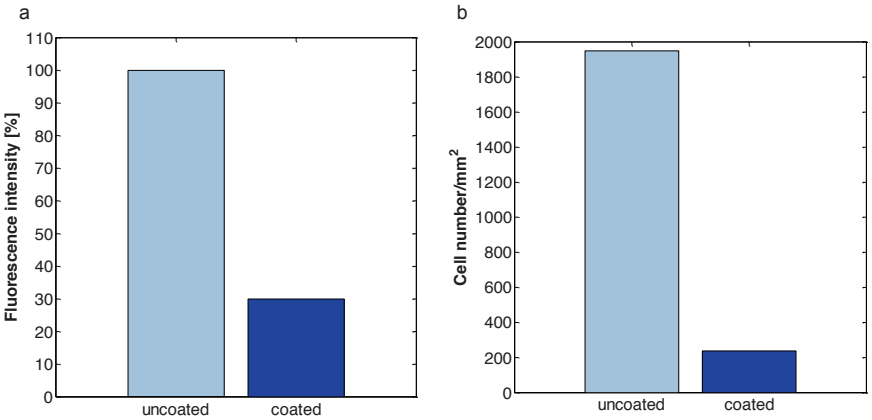

Figure 5-3: Normalized fluorescence intensity (a) and attached bacterial cell number (b) for the uncoated and coated membranes after four hour in contact with a suspension of *Escherichia coli* cells (OD600 = 0.8).

and SEM images. The high fluorescence intensity on the surface of the uncoated membrane corresponds to an abundance of attached bacterial cells (Figure 5-3a). The same trend was shown by bacterial cell counts based on SEM images (Figure 5-3b).

Long-term biofouling studies

Long-term biofouling studies were performed to evaluate the impact of membrane coating on biofouling development. The MFS units were run in parallel at similar operational conditions. To enhance the biofilm development water supplemented with biodegradable nutrients was dosed to the MFS unit with uncoated and coated materials. As control, MFS units were operated without nutrient dosage containing coated and uncoated feed spacer and membrane sheets.

Pressure drop development and biomass accumulation
During the experimental period, feed channel pressure drop was monitored as an indicator of biofilm development.

The control monitors without nutrient dosage showed no pressure drop increase during the eight-day study and no significant accumulation of biomass for the coated and uncoated membrane (Figure 5-4).

For the monitors with nutrient dosage the feed channel pressure drop strongly increased after the third day of the study, indicating biofilm development

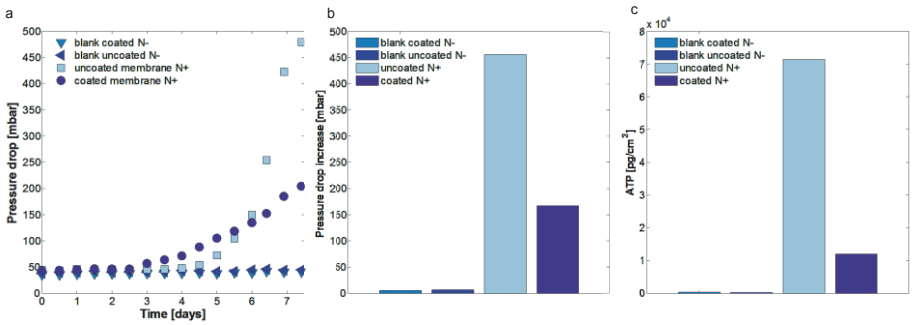

Figure 5-4: Feed channel pressure drop (a) in time and (b) pressure drop increase due to biomass accumulation, and (c) amount of accumulated biomass at the end of the experimental period. The monitors containing the uncoated and coated membrane were fed with water containing biodegradable nutrient (N+) while the blanks had no nutrient dosage (N-).

(Figure 5-4a). The coated membrane showed a lower pressure drop increase (Figure 5-4b) and lower biomass accumulation (Figure 5-4c) at the end of the eight-day monitor study compared to the monitor operated with the uncoated membrane.

Biomass characterization

Results from SEM imaging of the biofilm after the experimental period are shown in Figure 5-5. For the control membranes without nutrient dosage (uncoated and coated) no biofilm was observed on the membrane surfaces (Figure 5-5a).

With nutrient dosage, the presence of biofilm on the membrane surface was confirmed on both the uncoated and coated membrane. Less bacterial cells and more EPS were found on the SEM images for the biofilm formed on the coated membrane surface compared to the biofilm formed on the uncoated membrane (Figure 5-5b, c). Colours (bacterial cells – green, EPS – blue) were applied in the SEM images to emphasize bacterial cells and EPS.

Confocal Laser Scanning Microscopy (CLSM) images obtained for the fouled membrane surfaces are in agreement with the SEM observations. The biofilm formed on the coated membrane contained more EPS (polysaccharides and proteins) and lower bacterial cells than the biofilm formed on the uncoated membrane (Figure 5-6). CLSM images showed that the biofilm on the coated membrane was ≈ 50 percent thinner than the biofilm formed on the uncoated membrane.

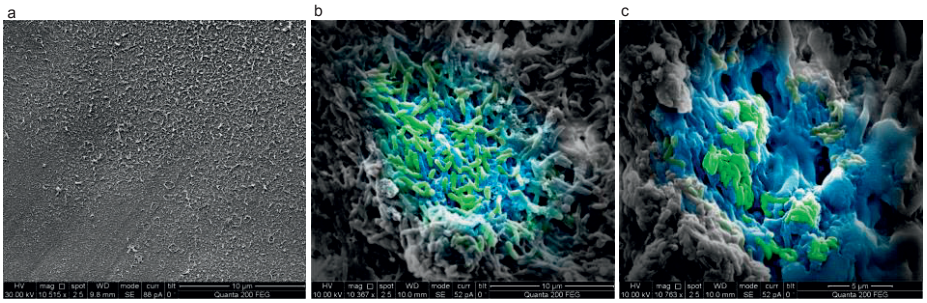

Figure 5-5: Scanning electron microscopy (SEM) images of the (a) blank, (b) uncoated and (c) coated membrane at the end of the 8 day monitor experiment. No biofilm was observed on the blank membrane (no nutrient dosage). Bacterial cells (green) and extracellular polymeric substances (EPS, blue) were detected for the biofilm formed on the uncoated and coated membrane with nutrient dosage. The colors were applied to emphasize the bacterial cells and EPS.

Further analyses of the CLSM images with ISA3D software were carried out to assess the biovolume of the bacterial cells, polysaccharides and proteins (Beyenal et al., 2004).

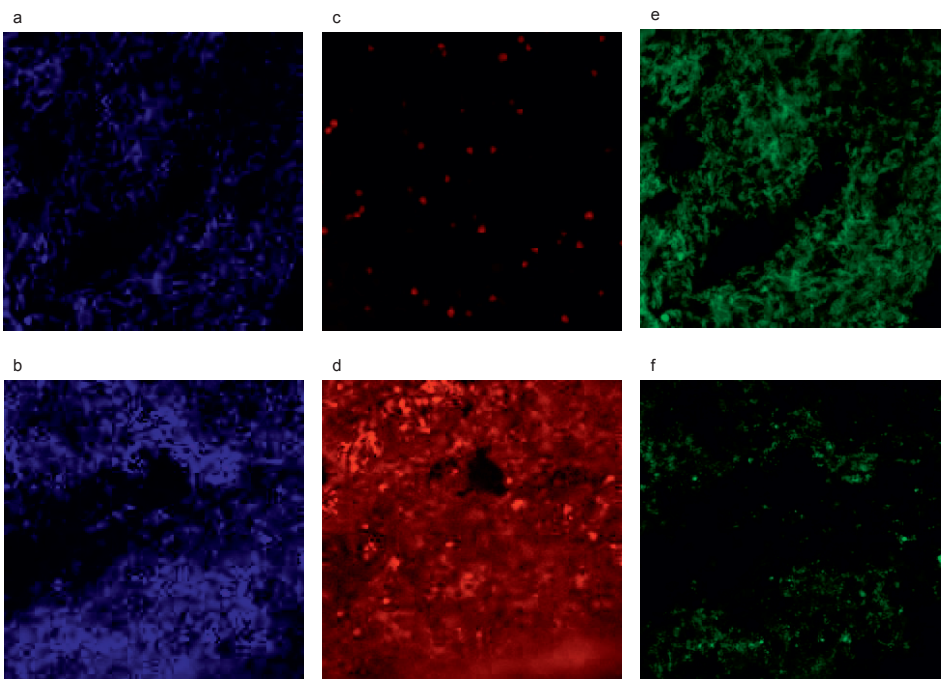

Figure 5-6: Confocal laser scanning microscopy (CLSM) images of biofilms formed on the uncoated (top row) and coated (bottom row) membrane. The images show (a, b) the polysaccharides in blue color, (c, d) the proteins with red in the biofilm matrix and (e, f) shows the bacterial cells in green color. The images were taken after 8 days of monitor operation.

These calculations confirmed less bacterial cells for the coated membrane, but more EPS material compared to the uncoated membrane. The composition of the EPS significantly differed: more proteins and less polysaccharides were found on the coated membrane surface (Figure 5-7).

Biofilm characterization methods confirmed the presence of the biofilm on both coated and uncoated membranes with nutrient dosage. Significant differences were found in the biofilms formed on the coated and uncoated membranes in terms of thickness and composition.

Stability of the applied coating

To determine the stability of the coating on the membrane, a comparison was made between (i) the coated unused membrane (clean), (ii) the coated membrane after eight days crossflow operation with biofilm development in the MFS (biofouling), (iii) and the fouled membrane after cleaning by sonication.

A unique characteristic for the coating, fluorine was found on the clean, biofouled and cleaned membrane (FTIR: Figure 5-8a, b, fluorine peaks at 1240 cm^{-1} and 1205 cm^{-1}) and on the biofouled membrane (XPS: Figure 5-9b), indicating the coating was still present on the coated membrane after crossflow operation with biofilm development and after subsequent harsh sonifier cleaning.

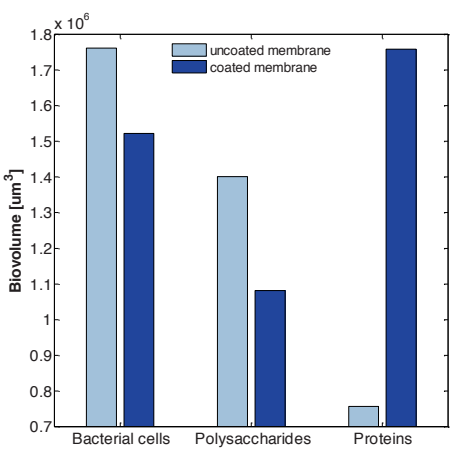

Figure 5-7: Impact of membrane coating on biofilm composition. The biofilm formed on the uncoated membrane contained more bacterial cells and polysaccharides than the biofilm formed on the coated membrane. Significant differences were observed in the protein composition of the biofilms formed on the coated and uncoated membrane.

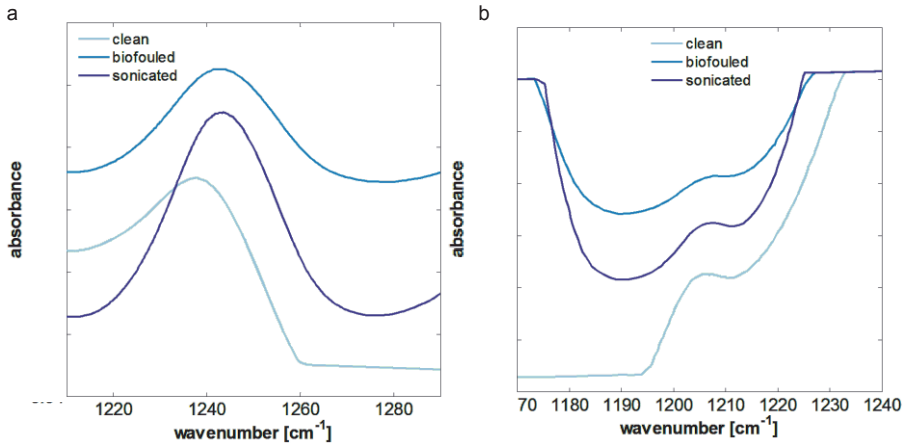

Figure 5-8: Fourier transformed infrared spectroscopy (FTIR) spectra of coated membrane before the study (coated), at the study end (biofouled) and at the end of the study after removing the biofouling layer (cleaned). Fluorine peaks (a) at 1240 cm^{-1} and (b) at 1205 cm^{-1} were found on all three samples of the coated membranes.

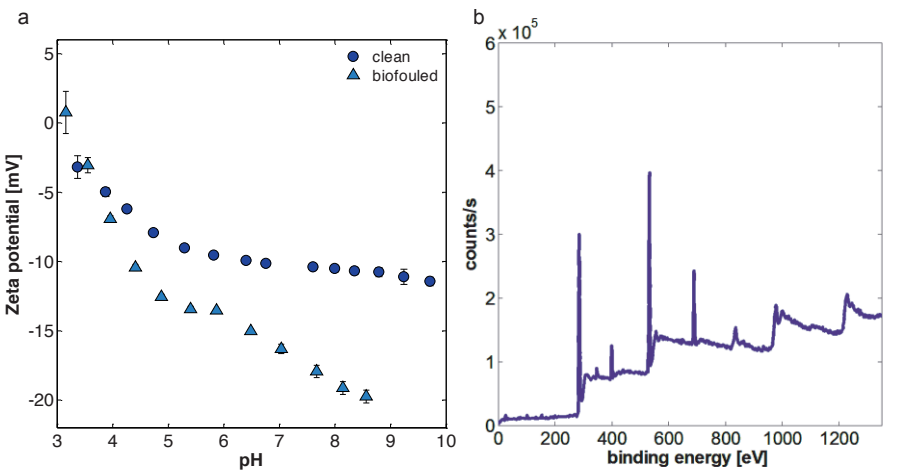

Figure 5-9: Zeta potential (a) at different pH values for the coated membranes before and after the biofouling experiment and XPS (b) for the coated membrane after the biofouling experiment. The XPS peak at 700 [eV] binding energy corresponds to the fluorine functional group present in the coating on the membrane.

The biofouled coated membrane after removal of the biofilm by sonication had a lower zeta potential profile compared to the clean (unused) coated membrane (Figure 5-9). The amphiphilic copolymer coating was well attached to the membrane and stable (as determined by two independent analytical methods) after the MFS studies.

DISCUSSION

The objectives of this study were to evaluate (i) the impact of an amphiphilic coating on biofouling control, and (ii) the stability of the membrane coating. In MFS studies the coated membrane showed a lower pressure drop increase and less biomass accumulation compared to the MFS operated with the uncoated membrane (Figure 5-3).

The developed biofilms were different in composition: the biofilm formed on the coated membrane contained more EPS (polysaccharides and proteins) and less bacterial cells (Figure 5-5 - Figure 5-7). The results showed that the coating was strongly attached to the membrane surface and was still present after the eight-days biofouling experiment (Figure 5-8, Figure 5-9). The outcome of this study shows that biofouling can be restricted, but not avoided by the tested amphiphilic membrane coating.

Impact of the coating on membrane properties

Membrane coatings are applied to eliminate or reduce membrane fouling by changing surface properties (Kang and Cao, 2012). In general, the presence of a coating increases the membrane thickness and resistance leading to a clean water flux reduction (Kang and Cao, 2012; Louie et al., 2011). Earlier studies showed that the applied amphiphilic coating has a limited impact on the permeate flux only (Matin et al., 2011b).

Need for long-term biofilm studies

In many investigations, short-term (2-6 h) static protein or bacterial cell adhesion tests were performed (Adout et al., 2010; Miller et al., 2012; Park et al., 2006; Yi et al., 2010). In some other cases short-term (2-24 h) cross-flow or dead end filtration tests were used to evaluate the impact of the coating on fouling accumulation (Asatekin et al., 2009; Madaeni and Ghaemi, 2007; Sagle et al., 2009; Wang et al., 2012; Zhao et al., 2013).

Short-term studies provide insight into initial protein or bacterial cell attachment to the membrane surface, but do not predict biofilm development (Asatekin et al., 2009; Matin et al., 2014a; Miller et al., 2012). Short-term batch tests investigating bacterial adhesion to membranes were not predictive for the fouling behaviour of membrane systems. Therefore, long-term MFS studies

were needed. Miller et al., (Miller et al., 2012) showed that long-term biofouling studies are representative for practice, while short-term protein and bacterial adhesion tests were not, which is in agreement with the findings of this study. To evaluate the anti-fouling potential of a modified membrane and/or feed spacer long-term biofilm studies has to be done, under representative conditions for practice (Louie et al., 2011, 2006; Miller et al., 2012; Vrouwenvelder et al., 2006). For now eight days studies were performed to evaluate the impact of coating on biofilm development. In practice biofilm development usually is a slow process, suggested is to do longer-term studies under well controlled conditions.

Impact of the coating on the biofouling rate

The microorganisms in biofilms live in a self-produced matrix of hydrated extracellular polymeric substances (EPS) (Flemming and Wingender, 2010). EPS consists mainly of polysaccharides and proteins, providing the mechanical stability of biofilms, and mediate their adhesion to surfaces (Flemming and Wingender, 2010). Bacterial cell-membrane surface interaction is important in the early stage of biofilm development (O'Toole et al., 2000; Palmer and White, 1997). Surface properties such as roughness, charge and free energy impacts bacterial cell attachment (Quirynen and Bollen, 1995; Sagle et al., 2009). Extracellular proteins play an important role in bacterial attachment, while polysaccharides are produced mainly in mature biofilms (O'Toole et al., 2000; Wolfaardt et al., 1994). Under stress, bacterial cells in biofilms produce more proteins than polysaccharides (Flemming and Wingender, 2010; Stewart and Franklin, 2008). Zhang et al., (Zhang et al., 2014) reported that long-term nano-silver exposure did not change the membrane fouling rate although the EPS concentration increased significantly, indicating that stress conditions affect EPS production.

Membrane surface modification by the amphiphilic coating resulted in a smoother surface with a lower surface charge causing slower biofilm development (Figure 5-4). The start of the pressure drop increase (caused by biofilm development) was not delayed by the coating. The slower biofilm development on the coating may be explained by less bacterial cell attachment, more cell detachment or both. In other words, less cells accumulated on the coated membrane and the stress resulting from the coated surface caused higher protein production by the biofilm, which is in agreement with literature

(Flemming and Wingender, 2010; O'Toole et al., 2000; Quirynen and Bollen, 1995; Sagle et al., 2009; Stewart and Franklin, 2008; Wolfaardt et al., 1994; Zhang et al., 2014).

Coating stability

Few studies using coated membranes to control fouling reported on the coating stability (Brzozowska et al., 2011; Louie et al., 2006; Ronen et al., 2015). Brzozowska et al. (Brzozowska et al., 2011) observed a weak attachment of polymer brushes to the membrane surface. The coating layer was easily removed by lateral forces (Brzozowska et al., 2011). Experiments with silver nanoparticle coated feed spacers showed silver leaching during a fouling study using a flow cell (Yang et al., 2009). Similar results were found with silver coated membranes (unpublished data). In contrary, Louie et al. (2011) reported the presence of a polyether-polyamide block copolymer coating on the membrane surface at the end of a 106 days fouling experiment.

The effectiveness of a coating to control fouling can be evaluated by the (i) fouling accumulation and performance decline and by the (ii) presence of the coating at the end of the study. Application of a coating for fouling control is only feasible when the coating is still present after long filter runs.

The long-term presence of a coating is hardly reported. Two recently published papers reported the presence of the coating after fouling studies (Brzozowska et al., 2011; Ronen et al., 2015). Out of the 30 most cited papers on membrane coating for biofouling control using the Scopus database on 2 November 2015, only one paper reported after a long-term fouling study the presence of coating on the membrane (Louie et al., 2011). Long-term lab scale studies are a first step to show the feasibility of membrane coating.

In practice, reverse osmosis membrane modules are used for much longer periods than the long-term lab scale studies. Coating stability may become critical when chemical cleaning is applied to prevent or control fouling. It is recommended to report results of studies with coatings that were not effective to prevent, reduce or delay fouling development in membrane systems. When results of studies with coatings that do not effect fouling development are not published, then other research groups could do similar studies.

Future studies

Coatings are applied with the aim to prevent, delay or control membrane fouling. The change in membrane surface properties like enhanced hydrophilicity, neutral or close to neutral surface charge and smoother membrane surface may delay, but not prevent biofouling (Kang and Cao, 2012). Membrane coating influences the biofilm composition and morphology. The same amount of biomass differing in composition and/or morphology may have a different impact on membrane performance decline. In other words, although biofilm formation is not prevented by the coating, it can significantly impact the performance decline. Studies with coated and uncoated membranes on biofouling should include determination of the biofilm composition, density and morphology and the impact thereof on membrane performance. The biofilm density (compactness) and morphology can be studied with e.g. optical coherence tomography (Dreszer et al., 2014b; Valladares Linares et al., 2015).

Membrane coating can affect the membrane cleanability. A change in biofilm composition can result in a loosely attached biofilm that can be removed by e.g. hydraulic cleaning. Moreover, changes in biofilm composition can enhance diffusion of chemicals into the biofilm during chemical cleanings.

The impact of membrane coating should be evaluated not only in terms of biofouling, but also (i) how the formed biofilm composition and morphology are affected (Vrouwenvelder et al., 2010b), and (ii) on membrane cleanability (Cornelissen et al., 2007; Creber et al., 2010b).

In summary, fouling cannot be prevented by membrane surface modification only, but in combination with other measures such as novel feed spacer geometries in spiral wound modules, operational conditions, plant design and advanced cleaning strategies can significantly improve membrane operation for desalination and water reuse.

CONCLUSIONS

Studies were done with an amphiphilic coated and uncoated reverse osmosis membrane and feed spacer involving (i) long-term biofouling studies using membrane fouling simulators and (ii) assessment of the coating presence and characteristics before and after biofouling studies including cleaning by sonification. The coated and uncoated membranes were compared based on

pressure drop development, accumulated biomass amount and composition, and membrane characteristics. Based on the results, it can be concluded that:

- amphiphilic copolymer coating
    - delayed biofilm formation,
    - did restrict, but not prevent biofilm formation,
    - influenced the biofilm composition,
    - was present on the membrane and spacer before and after the biofouling study, and after sonification treatment, indicating the coating was strongly attached to the membrane and spacer until the end of the biofouling study.
- biofouling studies using membrane fouling simulators were found to be good predictors of biofouling while short-term surface adhesion tests were not.

Studies addressing advanced cleaning strategies of membrane systems should consider to determine the impact of coated membranes and spacers on cleaning effectiveness: coated materials may be easier to clean. The assessment of the presence/absence of a membrane coating after fouling experiments should be included in the studies.

٧

Numerical Study of Feed Spacer Geometry Effects on Biofouling

Abstract

Feed spacers and hydrodynamics have been found relevant for the impact of biofouling on performance in reverse osmosis (RO) and nanofiltration (NF) membrane systems. The objectives of this study on biofouling development were to determine the impact of (i) linear flow velocity and bacterial cell load, (ii) biomass location and (iii) various feed spacer geometries as applied in practice as well as a modified geometry spacer. A three-dimensional mathematical model for biofouling of feed spacer channels including hydrodynamics, solute mass transport and biofilm formation was developed in COMSOL Multiphysics and MATLAB software. Results of this study indicate that the feed channel pressure drop increase caused by biofilm formation can be reduced by using thicker and/or modified feed spacer geometry and/or a lower flow rate in the feed channel. The increase of feed channel pressure drop by biomass accumulation is shown to be strongly influenced by the location of biomass. Results of numerical simulations are in satisfactory agreement with experimental data, indicating that this micro-scale mechanistic model is representative for practice. The developed model can help to understand better the biofouling process of spiral-wound RO and NF membrane systems and to develop strategies to reduce and control biofouling.

Published as:

Szilárd S. Bucs, Andrea I. Radu, Vasile Lavric, Johannes S. Vrouwenvelder, Cristian Picioreanu (2014) Effect of different commercial feed spacers on biofouling of reverse osmosis membrane systems: A numerical study. Desalination **343**: 26–37.

INTRODUCTION

Membrane filtration processes like reverse osmosis (RO) and nanofiltration (NF) have become increasingly important for high quality drinking water production in recent years. The major problem of this technology is biofouling — excessive growth of biomass leading to reduction of produced water quantity and quality, while increasing the operational costs.

Feed spacers are essential parts of the spiral-wound NF and RO modules that keep membranes apart to form the flow channel and to promote mixing of the fluid. Baker et al. (1995) reported that initial deposits of fouling were found to accumulate alongside the membrane feed channel spacer and with time these deposits encroached upon the remaining free membrane area. Van Paasen et al. (1998) observed an exponential increase of the feed channel pressure drop caused by biofouling build up onto the feed spacer of the membrane modules. This biofouling proved to be related with chemicals dosed to the feed water. Tran et al. (2007) found that the vicinity of the feed spacer strands was most affected by fouling. Strategies to reduce feed spacer biofouling have been addressed, e.g. periodic air/water flushing (Cornelissen et al., 2007) and applying thick feed spacers (Majamaa et al., 2010). Vrouwenvelder et al. (2009a) showed that for fresh water the feed spacer biofouling is much more important than membrane biofouling for feed channel pressure drop increase and thus for overall performance decline. In summary, feed spacers are important for membrane performance and play a key role in biofouling of membrane systems. Therefore, a better understating of the impact of feed spacers on biofouling is of primary importance for an improved design of the spiral-wound membrane modules.

According to Li et al. (2002), feed spacers can be characterized by four parameters: (i) the distance between spacer filaments, (ii) the angle between spacer filaments, (iii) the flow attack angle and (iv) the total spacer thickness. Sablani et al. (2002) studied experimentally the influence of three feed spacers varying in thickness 20, 28 and 46 mil (1 mil = 25.4 μm; i.e., a 28 mil spacer = 711 μm thick) on concentration polarization. They found a decrease in flux with decreasing spacer thickness, but the highest permeate flow was obtained for the intermediate spacer thickness. Recently, Araujo et al. (2012a) studied experimentally the effect of different spacer thickness on biofouling. Their

findings showed that with the increase of spacer thickness there is a decrease of the feed channel pressure drop due to biofouling.

Computational fluid dynamics (CFD) has become a widely used tool in studying the hydrodynamic behaviour of NF and RO membrane systems (Fimbres-Weihs and Wiley, 2010). Many studies using CFD focused on the effect of feed channel spacer on fluid flow and mass transfer with different type of spacers (Fimbres-Weihs and Wiley, 2007; Geraldes et al., 2002; Koutsou et al., 2007; Saeed et al., 2012; Shakaib et al., 2007). Simplified, cylindrical shapes were used for representation of spacer filaments in most of the numerical studies on the effect of feed spacer geometry on mass transfer and fluid flow. Stereomicroscopic observations of the feed spacer revealed that the spacers used in commercially available spiral-wound membrane modules have more complicated geometry, with filaments varying in thickness and thinning (Vrouwenvelder et al., 2008a). Picioreanu et al. (2009) found by numerical simulations that the feed channel pressure drop for a simplified spacer with cylindrical filaments is significantly different from a more realistic spacer geometry with filament thinnings. Although the effect of feed spacer geometry has been extensively studied, it is still not clear how spacers affect biofouling and the performance parameters.

In this study we examined with a numerical model the impact on feed channel pressure drop of: (i) liquid flow velocity and bacterial cell load; (ii) biomass location on the spacer and/or membrane surfaces and (iii) various feed spacer geometries (28, 31, 34 and 46 mil thick) as applied in commercially available spiral-wound reverse osmosis modules and a modified geometry having a 31 mil thick spacer. To the authors knowledge this is the first paper using a three-dimensional mathematical model on biofouling evaluating several realistic geometries (commercially available) feed spacers as used in full-scale spiral wound membrane modules.

MODEL DESCRIPTION

A three-dimensional numerical model was developed to study the impact of feed spacer geometry on the biofouling of feed channels of spiral-wound membrane modules. The model is based on the work of Picioreanu et al. (2009), implemented here in more efficient computer code coupling COMSOL Multiphysics solvers (COMSOL 4.3a, Comsol Inc., Burlington, MA,

www.comsol.com) for fluid dynamics and solute transport with MATLAB (MATLAB 2011a, MathWorks, Natick, MA, www.mathworks.com) code for biofilm formation.

Spacer geometry

Geometries corresponding to four commercially available feed spacers used in full-scale spiral-wound RO modules were characterized using a calibrated stereomicroscope (Leica M205 FA), followed by measurements using Qwin Pro 3.1.0 software, and then reconstructed in the COMSOL Multiphysics environment. The studied spacers differ in thickness, porosity and their filament shapes. For each filament, several characteristic dimensions were considered, according to Figure 6-1A. Every spacer is constructed from two perpendicular layers of filaments (Figure 6-2B), and the filaments from each layer have a unique shape. The spacer filaments differ mainly in their diameter, with several specific regions identified for all filaments determining a characteristic shape, as shown in Figure 6-1A. The dimensions and the flow channel porosity for each spacer type are presented in Table 6.1. Additionally, a hypothetical 31 mil thick modified spacer geometry was created to study the effect on feed channel porosity of spacers having the same thickness but different filament dimensions.

The spacer geometries used in commercially available RO and NF modules have standard thicknesses, but they can be provided by different manufacturers and produced by different technologies, which may lead to diverse spacer geometries.

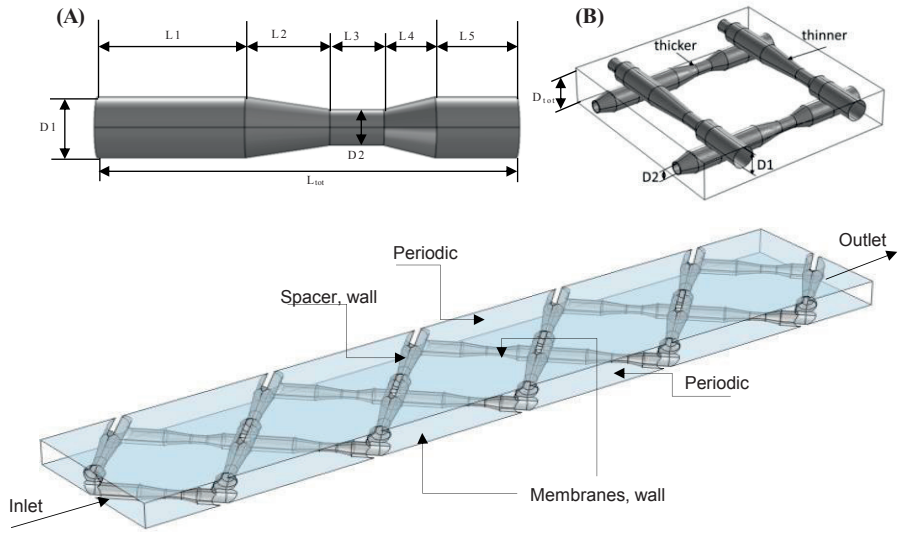

Figure 6-1: Model feed spacer geometry and computational domain. (A) General representation of spacer filaments with measured characteristic dimensions (see Table 6.1); (B) Reconstructed geometry of a representative feed spacer unit varying in filament thickness, as applied in practice in spiral-wound modules for water treatment; (C) Computational domain and boundary conditions.

These spacers vary especially with respect to the spacer unit length L_{tot} and the flow channel porosity (Table 6.1). All studied commercial feed spacers are displayed in Figure 6-2.

Computational domain

The standard size of the industrial spiral-wound RO and NF module is a length of 40 in. (~1 m) and a diameter of 8 in. (~0.2 m) with a total membrane surface area of ~40 m^2. A numerically accurate three dimensional model of flow and biofilm formation in such a large area is virtually impossible within current computational limits. Still, because of the repetitive unit spacer geometry, the essential flow and biofilm formation patterns can be captured within a smaller scale computational domain. The size of the computational domain used in this study is in the range of 10^{-5} m^2. The exact length, width and height of the computational domain differs with the spacer geometry. In all cases, five spacer units in diamond configuration (i.e., 45° rotated against the main flow direction) were placed in the computational domain (Figure 6-1). This is the current compromise between the necessary calculation time and model realism.

Table 6.1: Dimensions of different types of feed spacers used in this study, according to Fig. 1. For each spacer type, the filament dimensions (in μm) for the two layers of filaments are presented in columns: (A) thinner filament and (B) thicker filament.

Spacer thickness (mil)		28 mil		31 mil		31 mil modified		34 mil		46 mil	
		A	B	A	B	A	B	A	B	A	B
Dimensions (μm)	L1	862	877	983	299	400	400	234	281	364	171
	L2	595	740	557	132	100	100	389	535	346	420
	L3	767	595	358	417	1780	1780	500	92	561	713
	L4	178	252	340	1036	100	100	696	878	526	518
	L5	386	324	542	896	400	400	566	599	614	589
	D1	354	449	447	446	446	446	422	445	563	544
	D2	221	289	263	272	263	263	223	223	315	274
	L_{tot}	2788	2788	2780	2780	2780	2780	2385	2385	2411	2411
	D_{tot}	711		787		787		863		1168	
	channel porosity	0.90		0.89		0.92		0.88		0.88	

The computational domain consisted of feed channel volume available for flow and resulted from subtracting the spacer volume from a box bounded by membranes, inlet, outlet and lateral surfaces (Figure 6-1). An imprint of the feed channel spacer on the membranes can be observed during autopsies of spiral-wound RO modules, which suggests that the spacer filaments are actually pressing into the membranes on a sizeable contact area.

Therefore, the flow channel was constructed so that the two membrane planes cut 5 μm from the spacer top and bottom (Fimbres-Weihs and Wiley, 2007). In addition to more realistic model geometry, this construction also avoids very sharp angles in contact areas, which usually lead to computational difficulties and many unnecessarily small mesh elements.

Liquid flow, substrate transport and biofilm formation

Processes influencing biofouling may occur at very different time scales. Therefore, while the slow biofilm formation was evaluated in dynamic conditions (i.e., in time), the fast hydrodynamics and soluble substrate transport were considered stationary at each time step during biofilm development. More details regarding the time scale separation in biofilm models can be found in (Picioreanu et al., 2000).

Liquid flow

It was shown by Fimbres-Weihs and Wiley (2010) that the water flow in feed channels with spacers is laminar up to a Reynolds number (Re) of 200 for

spacers with 45° orientation of filaments, but becomes unsteady for Re between 200 and 300. Re numbers were computed according to Schock and Miquel (1987). For all geometries Re was less than 200, therefore the Navier–Stokes equations were used to model the laminar, incompressible and stationary flow which was assumed during the whole simulation process:

$$\rho(\mathrm{u}\cdot\nabla)\mathrm{u}+\nabla p=\nabla\cdot(\eta\nabla\mathrm{u})$$
$$\nabla\cdot\mathrm{u}=0 \qquad 6\text{-}1$$

with **u** = (u_x, u_y, u_z) the flow velocity vector, p the pressure, ρ the density and η the dynamic viscosity of water. The boundary conditions were set according to Figure 6-1. Fully developed laminar flow was assumed at the inlet $x = 0$, with the average fluid velocity u_{in}. On the outlet boundary at $x = L_X$, zero pressure (arbitrarily chosen as reference value) and no viscous stress conditions were imposed. The top and bottom membrane surfaces ($z = 0$ and $z = L_Z$), as well as the whole spacer surface were no-slip walls (**u** = 0). On the lateral boundaries ($y = 0$ and $y = L_Y$) periodic conditions were applied, as frequently used in simulations for geometries with a repeating pattern (Koutsou et al., 2007).

Substrate transport and reaction

Biomass grows in spiral-wound membrane modules as function of local concentrations of biodegradable substrates. The concentration field, C_S, of a single soluble substrate assumed here limiting for biomass growth was calculated from a convection–diffusion–reaction equation:

$$D_S\nabla^2 C_S-\mathrm{u}\nabla C_S+r_S=0 \qquad 6\text{-}2$$

with diffusion coefficient of substrate D_S. The substrate is transported by convection and diffusion in the bulk liquid and only by diffusion in the biofilm. The specific growth rate of the microorganisms (μ) was computed according to the simple Monod kinetics:

$$\mu=\mu_M\frac{C_S}{K_S+C_S} \qquad 6\text{-}3$$

where μ_M is the maximum specific growth rate of the microorganisms, K_S is the Monod half-saturation coefficient and C_S is the local biodegradable substrate concentration in the biofilm. Monod-type microbial growth rates are commonly applied for biofilm growth (Suidan et al., 1987; Wanner et al., 2006; Wanner

and Gujer, 1986). The biomass growth rate r_X was linear with respect to C_X (biomass concentration in the biofilm):

$$r_X = \mu \cdot C_X \qquad 6\text{-}4$$

The substrate consumption rate by biomass, r_S, was calculated neglecting the maintenance:

$$r_S = Y_S \cdot r_X \qquad 6\text{-}5$$

where Y_S is the yield coefficient (mol substrate consumed per C-mol biomass formed). A constant inlet concentration $C_{S,in}$ was assumed at $x = 0$, while the outlet ($x = L_X$) was a zero-diffusion boundary. Periodic conditions were set for the lateral boundaries at $y = 0$ and $y = L_Y$. The membranes and spacer surfaces were set as impermeable walls.

Biofilm formation

The biofilm development in the feed channel was governed in this model by two processes, microbial attachment and growth. Biomass detachment also plays a role in biofilm development, but mainly at late stages of biofouling development (i.e., thick biofilms). Effects of biofilm detachment on biofouling will therefore be addressed in follow up studies. Biomass was allowed to attach

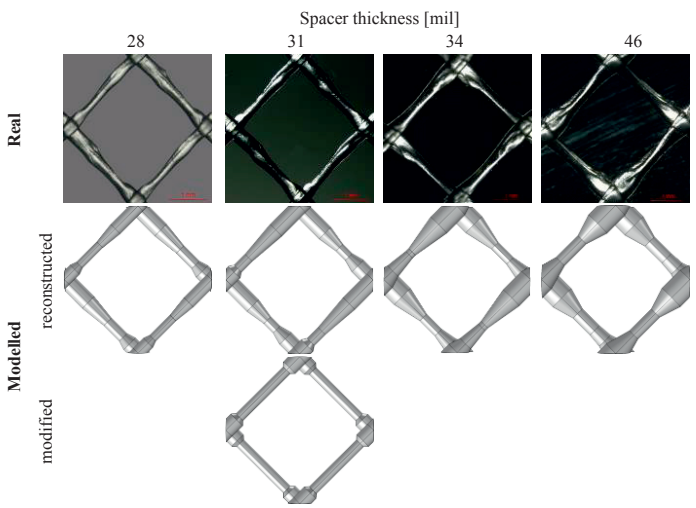

Figure 6-2: Geometries of different commercially available feed spacers: top row — microscopic images of spacers as applied in practice, bottom row — re-created and modified model geometries. One representative element is shown for each type of spacer

to randomly chosen places in the computational domain. Three different attachment modes were studied: (i) only on the spacer surface, (ii) only on the membrane surface and (iii) on both spacer and membrane surfaces. The cellular automata (CA) biofilm model developed in (Picioreanu et al., 1998a, 1998b) and modified as in (Picioreanu et al., 2009) was used to simulate the biofilm growth in a spiral-wound membrane system. The biomass growth is calculated in each volume element by a Monod equation linked to the substrate consumption rate:

$$\frac{dC_X}{dt} = r_X \qquad 6\text{-}6$$

In every volume element of a 3-d grid a maximum biomass concentration was set to C_{Xmax}. Once the maximum biomass concentration for a grid element is exceeded, the biomass amount is divided in two parts. One part will remain in place, while the second part will be repositioned in space according to the CA algorithm as explained in (Picioreanu et al., 1998a, 1998b).

Model solution

The model solution algorithm follows the procedure described in detail in (Picioreanu et al., 2009). After the model geometry was created, the biofilm development was followed iteratively in discrete time steps of size Δt = 4 h. The liquid flow and substrate distributions reach their steady state fast enough (~seconds) compared to the chosen Δt (~hours) to be considered stationary for each time interval of biofilm development. After updating the biomass distribution one time step, equations 6-1 and 6-2 are used again, for calculating the new stationary flow and concentration fields.

Table 6.2: Model parameters.

Parameter	Symbol	Value	Unit	Source
Maximum biomass concentration in a grid element	C_{Xmax}	1400	$mol \cdot m^{-3}$	(Picioreanu et al., 2009)
Biomass maximum specific growth rate	μ_m	1.25×10^{-5}	s^{-1}	chosen
Substrate half-saturation coefficient	K_S	0.05	$mol \cdot m^{-3}$	chosen
Substrate concentration in the inlet	$C_{S,in}$	0.4	$mol \cdot m^{-3}$	chosen
Yield of substrate consumed per C-mol biomass	Y_S	1	$mol \cdot (Cmol)^{-1}$	corresponding to acetate
Diffusion coefficient of substrate	D_S	1×10^{-9}	$m^2 \cdot s^{-1}$	small solute in water
Liquid density	ρ	1000	$kg \cdot m^{-3}$	water
Liquid viscosity	η	0.001	$Pa \cdot s$	water

For the calculations of liquid flow and mass transport of the soluble substrate a tetrahedral mesh was built with maximum element size of 90 μm. This resulted for 31 mil thick feed spacer geometries in a total of more than 1,300,000 mesh elements. The calculated substrate concentration field was then used in the biomass growth, followed by biomass spreading and attachment of new biomass. The main algorithm was implemented in a MATLAB script split into several steps:

- **A** define model parameters (Table 6.2), create the model geometry, computational domain and build equations in COMSOL (Figure 6-3A)
- **B** create the finite element mesh for flow and mass transport calculations in COMSOL (Figure 6-3B)
- **C** solve the laminar flow equation 6-1 in COMSOL for the flow velocity u and pressure p (Figure 6-3C)
- **D** solve substrate transport-reaction equation 6-2 for concentration C_S (Figure 6-3D)
- **E** evaluate biomass growth from equation 6-4 to get a new C_X; transport biomass by the CA method; attach new biomass (Figure 6-3E). After this biomass update the time is incremented with Δt and the algorithm flow returns to step C.

RESULTS

The model was used to investigate the effect of linear flow velocity, bacterial cell load, biomass attachment location, and different commercially available and modified feed spacer geometries on biofouling and feed channel pressure drop evolution. All simulated cases are listed in Table 6.3

Effect of linear flow velocity

The linear flow velocity varies along the length of a membrane filtration installation, consisting of several membrane elements installed in series. Also, a variation of linear flow velocities has been reported in the lead membrane elements in practice, from 0.07 to about 0.2 $m \cdot s^{-1}$ (Vrouwenvelder et al., 2009b).

Numerical simulations were run with different linear flow velocities and compared with experimental data (feed channel pressure drop, pressure drop increase) obtained in similar conditions by Vrouwenvelder et al. (2009b) in experimental studies with membrane fouling simulators (MFS).

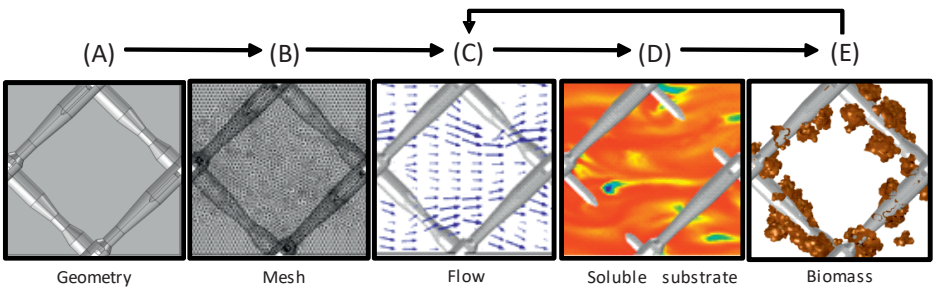

Figure 6-3: Graphical representation of the model algorithm. The arrows indicate the sequence of algorithm steps, with a loop between steps (C) and (E). (A) sets model parameters and geometry in MATLAB and COMSOL; (B) creates the 3-d tetrahedral mesh and 3-d rectangular biomass grid; (C) calculates fluid flow (blue arrows: local flow velocity in a slice at half the flow channel height); (D) calculates substrate concentration (colour scale: solute distribution in a slice at half the flow channel height; blue: minimum; red: maximum); and (E) biomass attachment and growth (brown volume: biomass). In all the top-view figures of the 3-d model system the spacer filaments are shown in grey

Table 6.3: Variable model parameters in different simulations.

	Spacer thickness [mil]	[μm]	r_{att}[1] [Cmol·m^{-2}·h^{-1}]	u_{in}[2] [m·s^{-1}]	Q[3] [L·h^{-1}]	**Attachment location**
Effect of linear flow velocity	31	787	1.08×10^{-2}	0.163 0.082 0.041	16.0 8.0 4.0	membrane + spacer
Effect of bacterial cell load	31	787	1.08×10^{-2} 5.4×10^{-3} 2.7×10^{-3}	0.163 0.082 0.041	16.0 8.0 4.0	membrane + spacer
Effect of attachment location	31	787	1.08×10^{-2}	0.163	16.0	membrane spacer membrane + spacer
Effect of spacer shape and channel porosity	31 31 modified	787	1.08×10^{-2}	0.163	16.0	membrane + spacer
Effect of spacer thickness as applied in practice - at constant flow rate	28 31 34 46	711 787 863 1168	1.08×10^{-2}	0.178 0.163 0.153 0.115	16.0	membrane + spacer
- at constant linear velocity	28 31 34 46	711 787 863 1168	1.08×10^{-2}	0.163	14.6 16.0 16.9 22.6	membrane + spacer

[1] biomass attachment rate; [2] average flow velocity in inlet; [3] liquid volumetric flow rate (as experiments from Araújo et al., (2012a))

For this set of simulations the 31 mil (787 μm) thick feed spacer geometry was used at different linear flow velocities of uin = 0.163 m·s−1 (corresponding to hydrodynamic conditions frequently encountered in industry), 0.082 m·s−1 and 0.041 m·s−1 , the other model parameters being set as listed in Table 6.2 and Table 6.3.

The initial pressure drop in absence of fouling (Figure 6-4A, day 0) showed a small difference (<10%) between the simulation and experimental initial pressure drop. This difference may be due to e.g. the variations in thickness and geometry of the spacer used in the experiments, but also to assumptions in the model calculations.

In time, the development of pressure drop caused by biofilm accumulation resulted in a similar trend for both model simulations and experimental studies. Small dissimilarities between the calculated and measured data are observed. The amount of accumulated biomass was the same at the end of the simulation studies (day 6), since the same biomass attachment rate was used for all simulations and no detachment was considered. With increasing linear flow

velocity the effect of the accumulated fouling material (biomass) on pressure drop increased (Figure 6-4B).

These results show that by applying a lower linear velocity the impact of the fouling material on performance can be significantly reduced.

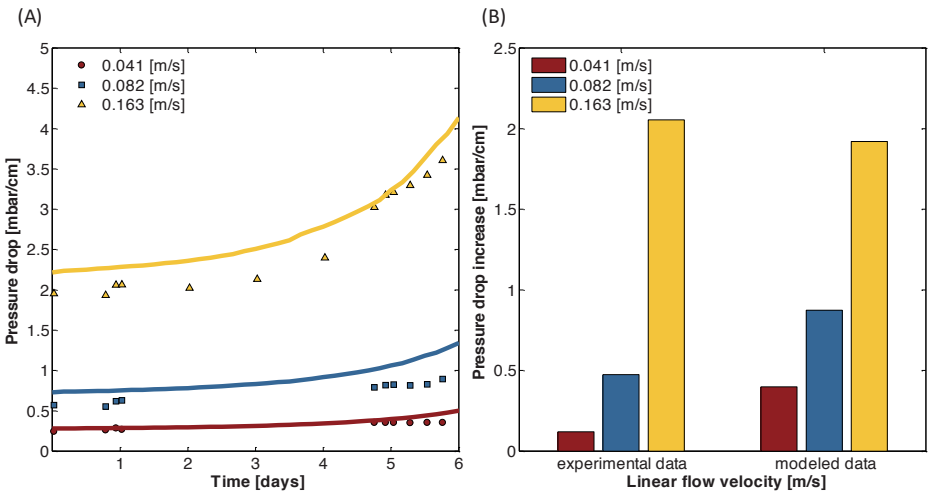

Figure 6-4: Calculated and experimentally determined data at different linear flow velocities, for the 31 mil (787 µm) thick feed spacer. (A) Pressure drop in time during the biofouling process (lines — calculated data, symbols — measured data); (B) pressure drop increase at day 6 relative to the initial pressure drop.

In summary, the biofouling model describes existing experimental observations for pressure drop and pressure drop increase well. However, in reality the linear velocity has more complex implications in terms of substrate load, bacterial transport and deposition rates, as well as biomass detachment rates. All of these factors impact the amount of accumulated biomass and, consequently, the feed channel pressure drop.

Effect of bacterial cell load

The biofouling onset may also be affected by the bacterial cell load (i.e., cell concentration multiplied by linear flow velocity) in the feed channel. It is expected that when increasing the liquid flow rate, more microorganisms would pass through the channel per unit time (Paris et al., 2007), therefore more cell attachment could take place due to the higher cell supply and higher shear rate. Eventually, a maximum deposition rate exists function of wall shear rate (Margalit et al., 2013). Because the decreased deposition efficiency at high

shear rates relates to detachment rates, not included in our model, this effect has to be systematically checked in future studies. For investigating the effect of cell load on performance decline, the 31 mil (787 µm) thick feed spacer was used in numerical simulations at different flow and cell attachment rates (Table 6.3). Three cases were studied when the transported amount of biomass varied with flow rate: the cell attachment rate was reduced proportionally with the reduction in flow rate. Comparing the results obtained at different linear flow velocities and constant attachment rate (see Table 6.3, effect of linear velocity: i.e., constant cell load) with those at flow-linked attachment rate (see Table 6.3, effect of cell load: i.e., variable cell load) reveals that at lower linear fluid velocities the impact of accumulated biomass is lower. Possibly because of differences in hydrodynamics and less biomass attachment in the flow channel (Figure 6-5). Similar results were obtained experimentally by Vrouwenvelder et al. (2009b): with variable flow rate different amounts of biomass were found during membrane autopsy. However, there can be three causes for this observation: a higher substrate transfer rate leading to more biomass growth, more cell attachment due to more biomass transported and deposited and a combination of more growth and more attachment. These results suggest that the impact of biofouling in spiral-wound membrane modules may be delayed by reducing the linear fluid velocity.

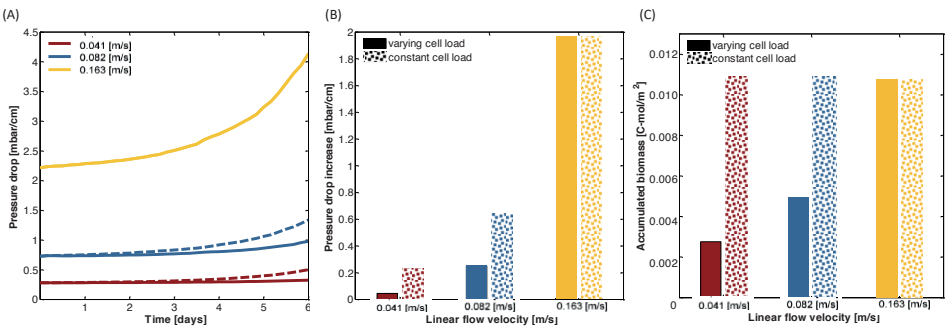

Figure 6-5: Comparing the impact of linear fluid velocity and cell load on feed channel pressure drop. (A) Pressure drop in time (connected line varying cell load, dashed line for continuous cell load), (B) pressure drop increase due to biomass accumulation (day 6), and (C) accumulated biomass concentration at different linear flow velocities (day 6)

However, in practice, applying lower linear flow velocities leads to an increase of the concentration polarization and to lower shear stress at the membrane surface, potentially affecting other types of fouling (e.g., scaling, colloidal) that may occur during RO operation.

Biomass location

Biofilm formation begins with bacterial transport followed by cell adhesion. When cells become firmly attached to the support surface, growth into micro-colonies takes place, finally leading to a mature biofilm (Pang et al., 2005). The adhesion of microorganisms in the NF and RO membrane systems depends on the hydrodynamics (Stoodley et al., 1998) and on the surface properties (hydrophobicity, surface charge, etc.) (Kang and Choi, 2005). The preferential places where cells attach in the initial phase of biofilm formation in NF and RO membranes are still unclear, but there are indications (Duddridge et al., 1982) that biofilm formation may be linked to the value of local shear stress induced by the liquid flow. It was reported that biofilm formation is not avoided by high shear stress conditions. On the contrary, biomass developed under high shear was found to be more compact and harder to remove. This is also confirmed by industrial RO membrane module autopsies, for example, Tran et al. (2007) found thicker biofilm layer underneath or in the vicinity of feed spacer. On the other hand, other studies indicate that biofilm formation begins mainly in places behind the spacer filament crossings (Picioreanu et al., 2009; Vrouwenvelder et al., 2010b, 2009a), where the shear stress level is relatively low.

With the numerical model of biofouling the consequences of biomass attachment at different locations on the development of the feed channel pressure drop were investigated. Three different scenarios are presented here, all with the same biomass attachment rate (Table 6.2): (i) attachment only to the membrane surface; (ii) random attachment to both membrane and spacer surface and (iii) attachment only to the spacer surface.

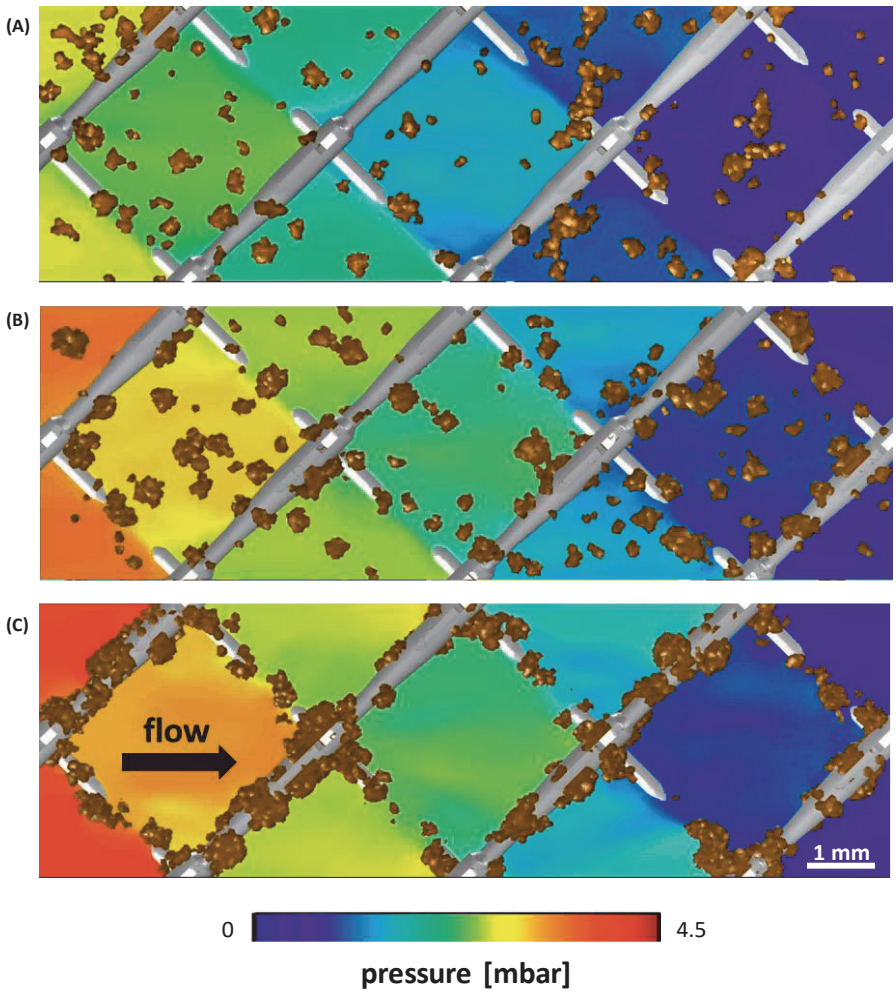

Figure 6-6: Liquid pressure and biofilm developed in the feed channel for different biomass attachment scenarios (day 6): (A) biomass attachment only on the membrane surface, (B) biomass attachment randomly on both membrane and spacer, (C) biomass attachment only on the feed spacer. The grown biomass is shown in brown and feed spacer in grey. The same amount of biomass developed in all three cases. The colour scale indicates the pressure in the plane situated at half the channel height, z = 394 μm. The arrow indicates the flow direction

Simulations were run with the same linear flow velocity and inlet substrate concentration, using the 31 mil (787 μm) thick spacer geometry presented in Figure 6-2. In the absence of biomass (at t = 0), the highest pressure drop occurs as the fluid passes between the spacer filaments and membrane sheets (Picioreanu et al., 2009). The numerical results indicate that the accumulated

biomass has a different influence on the feed channel pressure drop when attached to the spacer surface than when attached to the membrane.

The highest impact of the accumulated biomass on the feed channel pressure drop is observed when the biomass attached only to the feed spacer filaments (Figure 6-6). Presence of biomass on the spacer surface results in narrower flow channels increasing thus the local fluid velocity (Figure 6-7) which leads to higher pressure drop (compare the pressure fields in Figure 6-6C – biomass on spacer only – , with those in Figure 6-6A and B). The smallest pressure drop difference was observed when biomass attachment was only allowed on the membranes (Figure 6-8A).

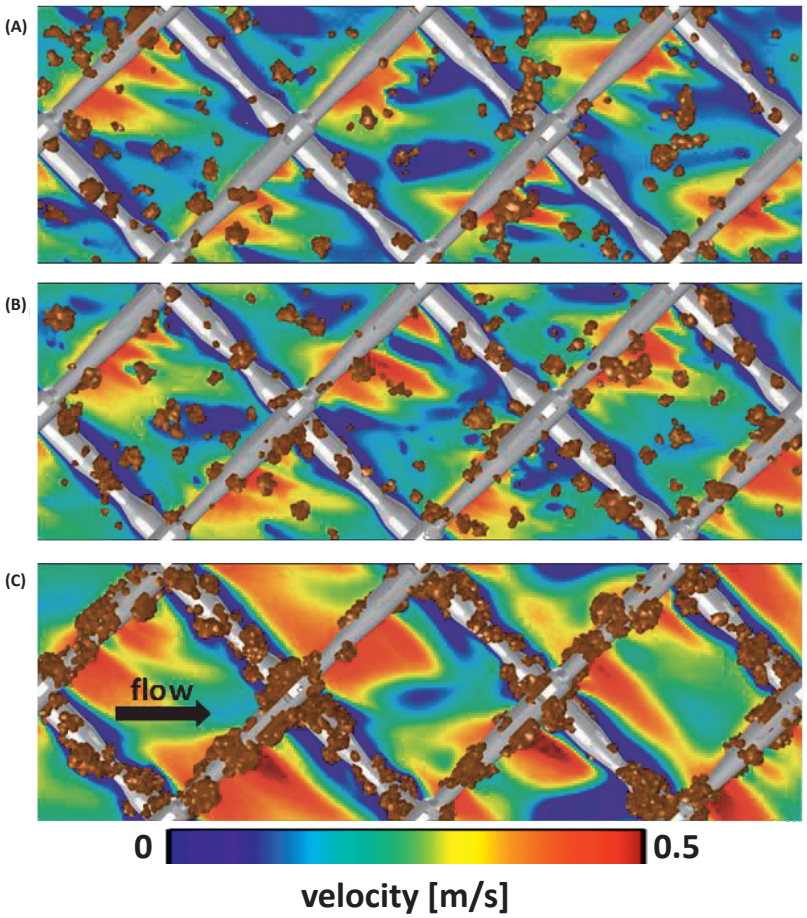

Figure 6-7: Fluid velocity and biofilm developed in the feed channel for different biomass attachment scenarios (day 6). (A) Biomass attachment only on the membrane surface, (B) biomass attachment randomly on both membrane and spacer, (C) biomass attachment only on the feed spacer. The grown biomass is shown in brown (day 6) and feed spacer in grey. The same amount of biomass developed in all three cases. The colour scale indicates the magnitude of fluid flow velocity in the plane situated at z = 197 μm. The arrow indicates the flow direction.

Because the amount of accumulated biomass was similar in all three cases (Figure 6-8C), it can be concluded that there are sensitive locations in the feed spacer channel (especially in the middle of spacer fibres) where even a small amount of biomass could lead to high performance decline.

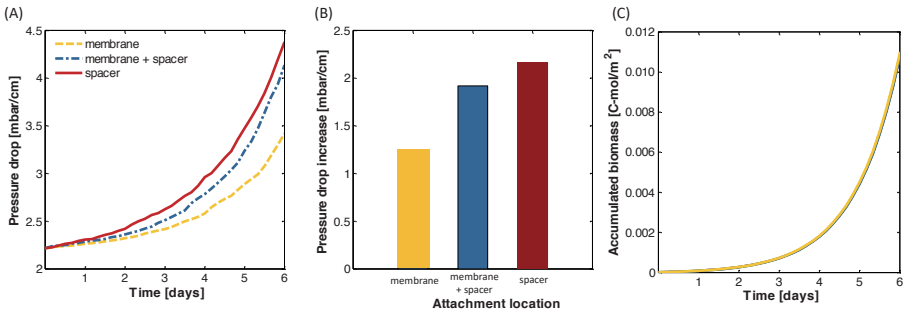

Figure 6-8: Effect of biomass attachment location on the development of feed channel pressure drop due to biofilm formation. (A) Pressure drop development in time; (B) pressure drop increase relative to the clean channel (day 6); (C) accumulated biomass in the feed channel. The biomass attachment was randomly allowed (i) only on the feed spacer filaments (red line), (ii) both on the membrane and spacer surface (blue line), and (iii) only on membrane (yellow line).

Spacer geometry

Various feed spacer geometries can be found in commercially available NF and RO membrane modules. The main roles of spacers are to provide an open channel for the flowing feed water and to promote mixing (i.e., intensify mass transfer and reduce concentration polarization (Tran et al., 2007)). The disadvantages of using feed spacers include the increase of feed channel pressure drop (an added resistance to flow) and the enhanced biofouling potential (Rukapan et al., 2012; Tran et al., 2007; Vrouwenvelder et al., 2009a). Feed spacers are most often characterized by the manufacturers just by their thickness. Nevertheless, it was shown that the distance, the angle between crossing filaments and the filament orientation are also important for performance (Guillen and Hoek, 2009; Koutsou et al., 2009; Koutsou and Karabelas, 2010; Subramani and Hoek, 2008).

The main differences of spiral-wound membrane modules are due to the installed membrane type and feed spacers geometry. This paper studies the effect of four different commercially available and one hypothetical feed spacer geometry on the feed channel pressure drop and pressure drop increase due to accumulation of biomass. The spacer geometries used in the industrial modules which are subject of this study differ in their thickness and filaments shape. The simulation conditions, such as biomass attachment rate, substrate inlet concentration and fluid linear flow velocity, were kept constant in all the cases.

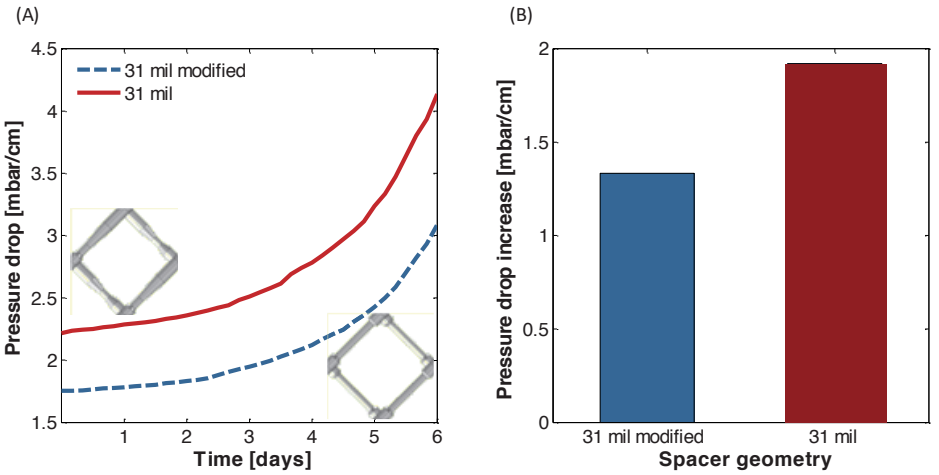

Figure 6-9: Pressure drop for two feed spacer geometries with the same thickness and same accumulated biomass amount, but differing in channel porosity. (A) Pressure drop in time; (B) pressure drop increase with biomass relative to the clean channel (day 6). Simulations were performed with a 31 mil thick feed spacer as applied in commercially available spiral-wound modules (connected line) and a 31 mil spacer modified for thinner fibres (dashed line).

Spacer shape and channel porosity

The modified spacer geometry does not represent an ideal feed spacer geometry, but rather a simple hypothetical construct used to investigate the effect of a different filament shape with the same thickness on performance decline. The numerical simulations clearly show how the feed spacer resistance to flow can be reduced by increasing channel porosity. Small changes in channel porosity (from 89% for commercial spacer to 92% for the modified spacer) led to significantly lower initial pressure drop (~20% lower) and less pressure drop increase in time in the presence of the same amount of biomass (Figure 6-9). The feed channel spacer has a narrow area of contact with membrane sheets at the cross section of the filaments. The same thickness at the filament crossings and reduced filament thickness elsewhere, result in a higher feed channel spacer porosity and consequently in a lower pressure drop increase.

These results suggest that beside the spacer thickness (giving channel height), spacer mesh size (distance between filament cross sections) and the fluid flow attack angle, the filament shape (especially its thickness and thickness variation) is also important for feed channel pressure drop and the impact of biomass on pressure drop increase.

Spacer thickness

Industrial RO and NF membrane modules are available with feed spacers differing in thickness. We studied the effect on feed channel pressure drop of four different geometries corresponding to feed spacers used in commercially available spiral-wound RO/NF modules. The studied spacers displayed in Figure 6-2 differed in thickness (28, 31, 34 and 46 mil), porosity and filament shape, and their spatial dimensions are listed in Table 6.1. Two sets of simulations were run: (i) with constant flow rate, 16 $L \cdot h^{-1}$ (i.e., different linear flow velocities for different spacer thickness) and (ii) constant linear flow velocity 0.163 $m \cdot s^{-1}$ (corresponding to various flow rates).

In case of constant flow rate the linear liquid velocity becomes a function of the spacer thickness, with the highest fluid velocity achieved for the narrower 28 mil (711 μm) spacer geometry. As expected, the highest initial pressure drop was found for the thinnest spacer geometry. Both initial pressure drop and pressure drop increase due to biofilm formation show a decreasing trend with increasing feed spacer thickness, as shown in Figure 6-10A, B. The initial pressure drop is caused only by the presence of feed spacer, while the pressure drop increase is due to biomass accumulation. Because the amount of accumulated biomass was similar for each type of spacer (~$7.1 \cdot 10^{-3}$ $Cmol \cdot m^{-2}$ after 6 days), due to identical attachment rate and substrate concentration in all cases (with neglecting biomass detachment, which could have also played a role), it was found that the feed channel pressure drop increase is less affected by biofouling when using thicker spacer.

In the second scenario, a constant linear flow velocity was applied at 0.163 $m \cdot s^{-1}$. This resulted in varying flow rates because of different channel thicknesses. Similar trend as for the simulations at constant flow rate were observed. Highest pressure drop was found with the thinnest (28 mil) and the lowest with the thickest (46 mil) feed spacer (Figure 6-10C, D). However, the initial pressure drop is lower for the case where constant linear flow velocity was applied than for the case with constant flow rate. The difference in pressure drop increase for different spacer thicknesses is similar for the two scenarios, but the change between the different thick spacer geometries is smaller for the second scenario. Results for both cases (constant linear flow velocity and constant flow rate) are in good agreement with the experimental data reported in (Araújo et al., 2012a).

DISCUSSION

The objectives of the numerical studies on biofouling development in spiral-wound NF and RO systems were to determine the influence of (i) liquid flow velocity and cell load, (ii) biomass location on the feed spacer and membrane surfaces, and (iii) various feed spacer geometries (28, 31, 34 and 46 mil thick) as applied in practice as well as a modified geometry 31 mil feed spacer. The computer simulations were in agreement with existing experimental data on the effect of liquid flow velocity (Figure 6-4) on feed channel pressure drop and pressure drop increase caused by biofilm formation, indicating that the model describes experimental data well. Biomass attachment on the feed spacer had the highest impact on pressure drop increase compared to attachment to the membrane only and both the membrane and spacer (Figure 6-6, Figure 6-8 and Figure 6-8). Comparison of an in practice applied 31 mil feed spacer with a modified 31 mil spacer geometry showed that the shape of spacer filaments influences the pressure drop and the pressure drop increase caused by biofilm accumulation (Figure 6-9). A thicker feed spacer resulted in: reduced initial pressure drop and decreased effect of accumulated biomass on pressure drop increase (Figure 6-10).

Numerical model evaluation

The numerical biofouling model describes existing experimental observations well. Compared to earlier numerical biofouling models, a more detailed geometry for the feed spacer was used (Figure 6-1, Figure 6-2). Also, the numerical model developed by Picioreanu et al. (2009) has been implemented successfully in a more efficient computer code coupling COMSOL Multiphysics solvers (COMSOL 4.3a, Comsol Inc., Burlington, MA, www.comsol.com) for fluid dynamics and solute transport with MATLAB (MATLAB 2011a, MathWorks, Natick, MA, www.mathworks. com) code for biofilm formation.

Possible future implementations into the model can be biodegradable substrate limitation and biomass detachment. The amount of accumulated biomass in an NF and RO membrane module mostly depends on the available biodegradable substrate concentration and hydrodynamics (Vrouwenvelder et al., 2009b). Although formally taken into account, the substrate limitation was not very effective due to the chosen combination of C_S and K_S and, as a result, the

biomass grew unlimited. If the biomass growth was substrate-limited, then in certain conditions the permeate flux may also have an effect on the biomass growth rate by providing more substrate near the membrane (Radu et al., 2012). Biofilm detachment was absent in the model. The biofilm was allowed to develop inside the computational domain without taking in consideration the shearing effect of hydrodynamics. These aspects will be taken into account in the future model versions.

How significantly these model limitations affect the main conclusions reached in this study remains to be evaluated in future investigations.

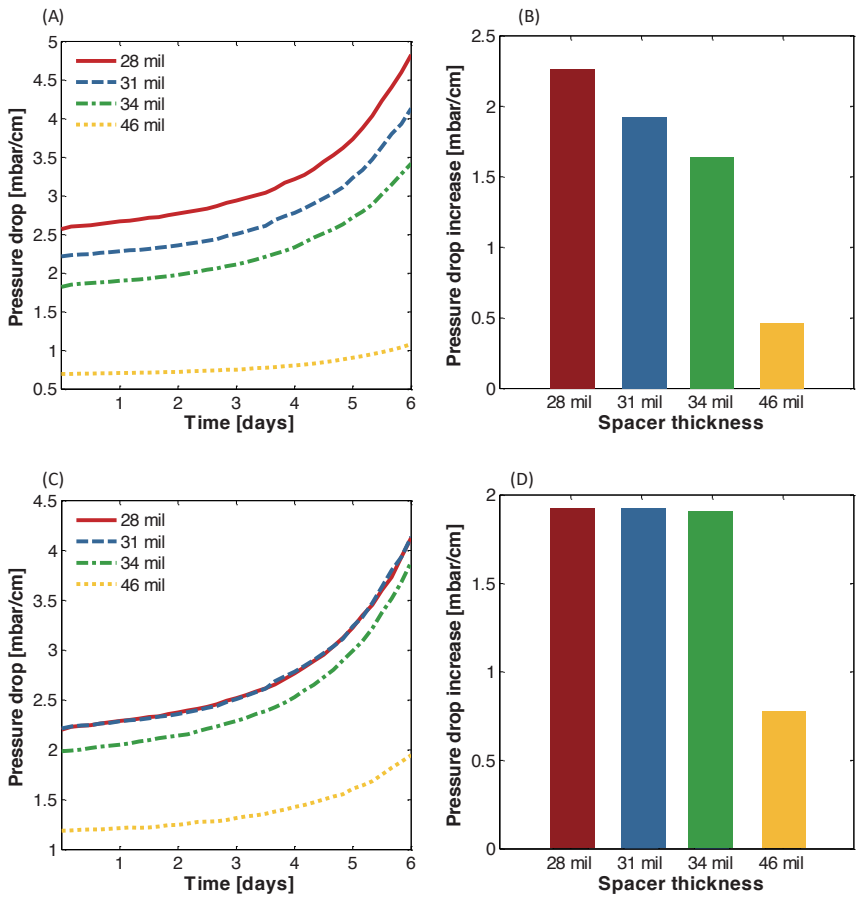

Figure 6-10: Changes in feed channel pressure drop for different feed spacer thicknesses and geometries (28, 31, 34 and 46 mil thick feed spacers) as applied in commercially available membrane modules. (A, C) Pressure drop in time, (B, D) pressure drop increase relative to the clean channel (day 0). Results at: (A, B) constant flow rate (16 $L \cdot h^{-1}$); (C, D) constant linear flow velocity (0.163 $m \cdot s^{-1}$).

However, the match between model results and experiments from Araujo et al. (2012a) suggests that the model already accounted for the main processes affecting the biofouling process.

Importance of feed spacer for biofouling

One of the factors with strong impact on the operational costs of spiral-wound RO and NF membrane water desalination plants is the pressure drop increase along the modules. The feed channel pressure drop is a result of frictional forces when the fluid flows through the module. The initial pressure drop in an RO module when the feed channel is clean (i.e., no fouling material has accumulated on membranes or spacer) is mainly the result of the feed spacer resistance, which depends on the spacer geometry. It was suggested that by decreasing the linear flow velocity the initial pressure drop can be reduced (Vrouwenvelder et al., 2010b). However, by reducing the liquid flow velocity the residence time of the solute increases, which can raise the risk for salt precipitation.

The proposed numerical model indicates that with increasing spacer thickness the effect of biofouling on feed channel pressure drop is decreasing. It was found that with reduced flow rate the amount of accumulated biomass may be lower, which is supported by the experimental findings of Vrouwenvelder et al. (2009b). However, Ahmad et al. (2005) showed in experimental studies that lowering the feed flow velocity results in an increase of concentration polarization. They also studied the effect of different feed spacer geometries on pressure drop and minimization of concentration polarization, recommending cylindrical spacer filaments at higher fluid velocities, but suggesting alternative spacer filaments at lower flow velocities. Mo and Ng (2010) have demonstrated experimentally the importance of feed spacers in reducing the effect of concentration polarization and fouling but also showed that the presence of the feed spacer creates additional resistance on the permeate flux due to the reduction in effective membrane surface area. Therefore, optimizing a spacer for minimal biofouling in practice needs to account also for the complex interactions between fluid dynamics and mass transport. In other words, a spacer and operating conditions that promote less biomass growth and thus less feed channel pressure drop may adversely affect other performance indicators.

Spiral-wound membrane elements can be produced with thicker feed spacers while maintaining the same membrane surface area (Bartels et al., 2008), indicating that using thicker feed spacers should not significantly increase the investment costs for a membrane plant. Results of Bartels et al. (2008) clearly showed that a thicker feed spacer had a lower initial feed channel pressure drop and, more importantly, a lower feed channel pressure drop increase than a thinner feed spacer. For example, in a membrane module a newly designed 34 mil feed spacer had a 16 percent lower pressure drop than the standard feed spacer of the same thickness. As a result, energy can be saved by using these modules and channel plugging due to biofouling will not rapidly occur. Moreover, the modules with thicker spacer may be more easily cleaned (Araújo et al., 2012a; Bartels et al., 2008; Creber et al., 2010b). In full-scale installations, long term studies were performed with thicker feed spacers at a significantly lower linear flow velocity (Bartels et al., 2008; K. Majamaa et al., 2009) showing that the lower linear flow velocities can be applied in practice without operational problems related to scaling due to higher concentration polarization. In addition, less biofouling was observed, needing thus a lower cleaning frequency. After cleaning, performances close to the initial values were achieved.

The development of effective biofouling control strategies in spiral-wound NF and RO systems most-likely requires detailed insight in the fouling processes obtained under representative conditions, which can be provided by a tuned combination of numerical modelling with experimental studies. Studies on biofouling control without biocides could include the balancing of feed spacer design, hydrodynamics and concentration polarization.

CONCLUSIONS

The model results emphasise the key importance of feed spacers on the biomass accumulation and performance of NF and RO membrane modules. Numerical simulations indicated that (i) at lower linear flow velocities, the pressure drop increase could be less pronounced because less biomass could accumulate, (ii) biomass on the spacer filaments leads to a higher feed channel pressure drop increase than when developing on the membranes, (iii) the relative feed channel pressure drop increase due to biomass accumulation is much higher at smaller channel porosities and (iv) at same feed flow rate

thicker spacers promote a lower pressure drop increase when overgrown with biomass.

Once the model is extended with biomass detachment, flow influenced biomass attachment and with permeation, this mechanistic approach could help to better predict the biofouling process of RO and NF membrane systems and, eventually, to develop and evaluate novel strategies and optimized spacer geometries to reduce and control biofouling.

۷

Impact of Spacer Thickness on Biofouling in Forward Osmosis

Abstract

Forward osmosis (FO) indirect desalination systems integrate wastewater recovery with seawater desalination. Niche applications for FO systems have been reported recently, due to the demonstrated advantages compared to conventional high-pressure membrane processes such as nanofiltration (NF) and reverse osmosis (RO). Among them, wastewater recovery has been identified to be particularly suitable for practical applications. However, biofouling in FO membranes has rarely been studied in applications involving wastewater effluents. Feed spacers separating the membrane sheets in cross-flow systems play an important role in biofilm formation. The objective of this study was to determine the influence of feed spacer thickness (28, 31 and 46 mil) on biofouling development and membrane performance in a FO system, using identical cross-flow cells in parallel studies. Flux development, biomass accumulation, fouling localization and composition were determined and analysed. For all spacer thicknesses, operated at the same feed flow and the same run time, the same amount of biomass was found, while the flux reduction decreased with thicker spacers. These observations are in good agreement with biofouling studies for RO systems, considering the key differences between FO and RO. Our findings contradict previous cross-flow studies on particulate/colloidal fouling, where higher cross-flow velocities improved system performance. Thicker spacers reduced the impact of biofouling on FO membrane flux.

Published as:

Rodrigo Valladares Linares, Szilárd S. Bucs, Zhenyu Li, Muhannad Abu-Ghdeeb, Gary Amy, Johannes S. Vrouwenvelder (2014) Impact of spacer thickness on biofouling in forward osmosis. *Water Research* **57**: 223 – 233

Szilard Bucs has contributed to the study design and organization, samples analysis by SEM, CLSM, ATP analyses and data interpretation. The manuscript has been written by Rodrigo Valladares Linares.

INTRODUCTION

Osmosis is a natural low energy water transport process not exploited by the drinking water and wastewater industry. The use of forward osmosis (FO) to reclaim water from wastewater is known in applications for oil/gas well drilling wastewater, landfill leachate treatment and water recycling in space missions (Cath et al. 2005, Adham et al. 2007, Holloway et al. 2007, Hickenbottom et al. 2013), which are all recent technologies with only a few years of existence. More recently, the use of osmosis to reclaim treated municipal wastewater has been demonstrated in bench-scale experiments (Valladares Linares et al. 2013a, Werner et al. 2013), where wastewater recovery is integrated with seawater desalination (designated as *indirect* FO desalination). Osmotic membrane bioreactors have been studied as well (Achilli et al. 2009). FO is a process that increases water reuse at a lower energy consumption compared to high-energy membrane processes (i.e. reverse osmosis (RO) and nanofiltration (NF)), and therefore, a cost reduction may be feasible (Yangali-Quintanilla et al. 2011).

When microorganisms are present in a membrane system, biofilm formation is inevitable due to the availability of nutrients in the water flow (Flemming et al. 1997). Biofilm formation is the accumulation of microorganisms, including extracellular polymeric substances (EPS) produced by microorganisms, on a surface due to either deposition and/or growth. When biofilm formation causes an unacceptable operational problem such as pressure drop increase, flux reduction and/or salt passage increase, it is called biofouling (Characklis and Marshall 1990).

All membrane filtration processes suffer from fouling, so the membrane elements have to be cleaned and eventually replaced. Biofouling has been identified as one of the major problems in spiral wound nanofiltration and reverse osmosis membrane operation (Winters and Isquith 1979, Paul 1991, Tasaka et al. 1994, Flemming et al. 1997, Khedr 2000, Saeed et al. 2000, Vrouwenvelder et al. 2008, van Loosdrecht et al. 2012). Feed spacers, separating the membrane sheets in cross-flow systems, are essential for membrane performance and play an important role in biofouling (Vrouwenvelder et al. 2009a).

Biofouling assessment in FO membrane studies is very limited in applications involving wastewater effluents. A study by Yoon et al. (2013) investigated

biofouling in the FO process compared to the RO process. The extent of biofouling, demonstrated by the permeate flux decline, was less severe in the FO process than the RO process. Zou et al. (2013) studied the use of feed spacers in forward osmosis systems when using microalgae as a foulant, showing that spacer use not only improved the initial FO flux, but also reduced membrane fouling propensity.

The objective of this study is to determine the influence of feed spacer thickness (28, 31 and 46 mil) on membrane performance and biofouling development in a cross-flow FO system. Experiments consisted of consecutive 5 filtration cycles using similar water flow conditions in parallel systems with different feed spacers. To the authors knowledge this is the first study on the impact of spacer thickness and biofouling in cross-flow FO systems.

MATERIALS AND METHODS

Membrane, spacers and cell configuration

The FO membranes used in this study were provided by Hydration Technology Innovations (HTI, Scottsdale, AZ), made of cellulose triacetate embedded in a polyester mesh support. The FO membrane has a thickness of 30 to 50 μm and a structural parameter S of 595 μm, defined as the ratio of the support layer thickness (Ts) and the tortuosity (τ) over the porosity (ε) of the membrane ($S = Ts\ \tau/\varepsilon$). A regular thin film composite (TFC) NF/RO membrane has a higher S value (S = 2155 μm), which translates into a lower water flux through the RO membrane compared to the FO membrane using the osmotic power difference as the driving force (Lee et al. 2010a, Yip et al. 2010).

The membrane cell was a custom-made cross-flow cell made of poly (methyl methacrylate) (PMMA), designed to fit a 20 cm^2 sized membrane sheet. All of the experiments were performed with the active layer (AL) of the membrane facing the FO feed solution (FS), leaving the support side in contact with the draw solution (DS). This configuration has been proven to be the most effective in preventing FO membrane fouling (Cornelissen et al. 2008, Mi and Elimelech 2008, Wang et al. 2010). Both feed and draw solution side were operated under a negligible hydraulic pressure (<0.01 bar).

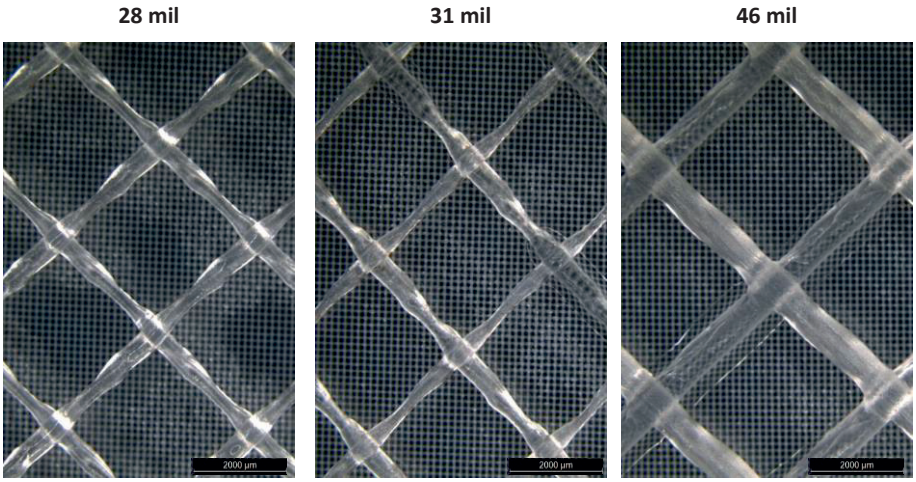

Figure 7-1: Different spacer thicknesses (28, 31 and 46 mil; 1 mil = 0.025 mm) on forward osmosis (FO) membrane. The small grid shown inside the FO membrane is the embedded polyester mesh support. All figures have the same scale.

Three spacers of different thickness were used to grow the biofilm (Figure 7-1). Two DOW diamond-shaped spacers of 28 and 31 mil (1 mil = 0.025 mm) thickness (Dow-Filmtec, Midland, MI) used in commercial spiral wound RO modules, and one modified FO spacer produced by HTI with a thickness of 46 mil (HTI, Scottsdale, AZ), used in commercially available modified FO spiral wound modules. Table 7.1 lists details concerning feed flow and characteristics for each spacer, used on both the feed and draw solution side of the membrane.

All experiments were performed with a similar nutrient load for biomass growth, which implies the use of the same feed flow and processing the same amount of water for all of the studied spacer geometries, resulting in the use of different cross-flow velocities. When biofilm grows at the same nutrient load, the effect of spacer thickness can be assessed and results compared.

Table 7.1: Feed spacers and flow conditions used in the FO cross-flow channel.

Spacer type (both sides#)	Spacer thickness (mm)	Flow rate ($L \cdot h^{-1}$)	Linear flow velocity ($m \cdot s^{-1}$)
28 mil Dow	0.711	7.2	0.141
31 mil Dow	0.787	7.2	0.120
46 mil HTI	1.168	7.2	0.086

the same feed spacer was used on both sides of the FO membrane. The study focus was on the fouling at the membrane feed side.

Water sources

Two water types were used directly, one after each other. Firstly, a municipal secondary wastewater effluent was used for 20 hours to condition the FO system with bacteria. Subsequently, the system was fed with synthetic municipal water (not containing bacteria) for 5 filtration cycles.

A municipal secondary wastewater effluent was collected from Al-Ruwais wastewater treatment plant in the city of Jeddah, Saudi Arabia. The chemical oxygen demand (COD) was 25 $mg \cdot L^{-1}$, the total organic carbon (TOC) concentration was 4.84 $mg \cdot L^{-1}$, the pH was 7.1, the conductivity was 2.33 $mS \cdot cm^{-1}$ and the osmotic pressure was 0.38 bar. The total suspended solids (TSS) and volatile suspended solids (VSS) of the effluent were 2.25 and 2.15 $mg \cdot L^{-1}$, respectively. The ATP concentration of the effluent was 215 $pg \cdot mL^{-1}$, which corresponds to a bacterial cell concentration of approximately 10^7 $cells \cdot mL^{-1}$.

For the subsequent 5 FO filtration cycles, the feed solution was a synthetic municipal wastewater already used in previous FO experiments (Valladares Linares et al. 2013a), described in Table 7.2. All the chemicals were purchased from Sigma Aldrich (Munich, Germany) and had a purity grade higher than 99.5%. The COD of the synthetic wastewater was 360 $mg \cdot L^{-1}$ before the FO process, with a TOC of 115 $mg \cdot L^{-1}$ and a pH of 5.66. For the draw solution, 4% sodium chloride (NaCl) was used to simulate Red Sea water, with a conductivity of 55 $mS \cdot cm^{-1}$ and pH of 5.74. All solutions were prepared with deionized (DI) ultra-pure water.

Table 7.2: Synthetic municipal wastewater constituents.

Compound	Concentration ($mg \cdot L^{-1}$)
Urea	91.74
NH_4Cl	12.75
Sodium acetate	79.37
Peptone	17.41
$MgHPO_4.3H_2O$	29.02
KH_2PO_4	23.40
$FeSO_4.7H_2O$	5.80
Starch	122.00
Skimmed milk power	116.19
Yeast extract	52.24
$Cr(NO_3)_3.9H_2O$	0.77
$CuCl_2.2H_2O$	0.54
$MnSO_4.H_2O$	0.11
$NiSO_4.6H_2O$	0.34
$PbCl_2$	0.10
$ZnCl_2$	0.21

Biofilm formation

The following procedure was used to grow a biofilm on the membrane feed side surface: *i*) inoculation for 20 h with municipal secondary wastewater effluent, and *ii*) 5-cycle experiment with recirculation of synthetic wastewater effluent as FS and clean 4% NaCl as DS; each cycle recovered 30% of the initial FS volume (300 mL) from the feed water, after which both FS and DS were replaced with fresh solutions.

Based on results from (Li et al. 2012) on the minor effect (difference of less than 2%) of cross-flow velocity on reverse solute flux by CTA FO membranes for velocities in the range of 0.04 to 0.16 $m \cdot s^{-1}$ (this study uses cross-flow velocities that range from 0.08 to 0.14 $m \cdot s^{-1}$), biomass growth was achieved under similar reverse draw solute flux conditions, and thus, results can be compared in terms of the effect of feed spacer thickness.

After the 5 cycles the FO cell was opened and the membrane along with the stacked spacer of the feed side were conserved for an autopsy. For TOC analysis, DI ultra-pure water was used to dilute the samples. Before using the imaging and elemental characterization techniques, membrane samples were kept hydrated and sealed at 4˚C.

To remove organic matter and disinfect the system, the following cleaning procedure, adapted from Herzberg and Elimelech (2007), was used before starting a new experiment: *i*) recirculation of 0.5% sodium hypochlorite for 2 h, *ii*) recirculation of 5 mM EDTA at pH 11 for 30 min, *iii*) recirculation of 2 mM

SDS at pH 11 for 30 min, and *iv*) sterilizing the unit by recirculation of 95% ethanol for 10 min. In-between each cleaning agent and at the end, the system was rinsed with DI ultra-pure water for 10 min.

Analytical methods

A Shimadzu TOC-V CPH total organic carbon analyser (Japan) was used to determine the organic carbon present on the membrane and feed spacer surface. The membrane and spacer were taken from the system, placed in a tube containing 20 mL of DI ultra-pure water and subsequently treated in an ultrasonic bath 3 times for 2 minutes. The obtained homogeneous solution was analysed for TOC.

A Celsis Advance Luminometer (Belgium) was used to measure the amount of Adenine 5´ Triphosphate (ATP) on membrane (and spacer) samples. The tubes with the samples of the fouling material from the membrane sections with a total area of approximately 4 cm^2, diluted in 50 mL sterile water, were placed in an ultrasonic cleaning bath (Bransonic Model 5510, 40 KHz, USA) for 2 minutes, and then mixed on a vortex mixer (Fisher Scientific, 230 V, USA) for 10 seconds at speed 7. This operation was repeated three times. Active biomass was determined in duplicate by measuring the ATP concentration from 50 µL samples, and then related to the area of membrane and spacer.

A stereomicroscope (Leica M205 FA, Leica Microsystems, Wetzlar, Germany) was used to obtain optical images from the FO membrane and spacer before and directly after the fouling experiments.

Confocal Laser Scanning Microscopy (CLSM) (LSM710 upright confocal microscope, Zeiss, Germany) was used to identify and characterize biofouling on the membrane surface after the experiments. The samples were stained with the following dyes based on methods described in the literature (Chen et al. 2006, Lee et al. 2010b): *i*) 4',6-Diamidino-2-Phenylindole (DAPI) dye (emission wavelength of 358 nm; excitation wavelength of 461 nm) was used to stain DNA to identify total bacterial cells (incubation in dark room for 20 min), *ii*) Fluorescein Isothiocyanate (FITC) (emission wavelength of 480 nm; excitation wavelength of 520 nm) was applied to stain the amine-reactive compound-like proteins and amino sugars (incubation time of 60 min); a 0.1 M sodium bicarbonate buffer was used to retain the amine groups so the dying was effective, and *iii*) Calcofluor White (emission wavelength of 433 nm;

excitation wavelength of 355 nm) was used to stain β-D-glucopyranose polysaccharides (incubation time of 1 min). After each of these three staining stages, the sample was washed twice by phosphate-buffered saline (PBS) pH 7 to remove excess stain and a wipe was used to remove excess dye or buffer remaining.

The fouling on the membrane surface was analysed by Scanning Electron Microscopy Energy Dispersive X-ray Apparatus (SEM-EDX, Magellan, FEI). The samples were freeze dried for environmental SEM.

An overview of the experimental studies and conditions is shown in Table 7.3.

Table 7.3: Overview of the forward osmosis studies performed with different spacer thicknesses.

Study	Feed spacer thickness (mil)*	Parameter evaluated / equipment used	Section
Effect of spacer thickness			
on performance	28, 31, 46	flux	3.2
on biomass accumulation	28, 31, 46	ATP and TOC	3.3
on fouling localization	28, 31, 46	stereomicroscope	3.4
on fouling composition	28, 31, 46	CLSM and SEM-EDX	3.5

*1 mil = 0.025 mm.

RESULTS

The development of performance (flux) and fouling amount, spatial localization and composition were investigated in cross flow FO cells with three feed spacers differing in thickness (28, 31 and 46 mil). To relate the flux decline with accumulated fouling material, autopsies were performed on the feed side membrane and spacer sheets.

Reproducibility

To show the reproducibility of results obtained with the proposed system, a parallel study was performed in two FO cells with the same conditions (i.e. spacer thickness, cross flow velocity, nutrient load) to grow biofilm, and flux decline was recorded. Results are shown on Figure 7-2.

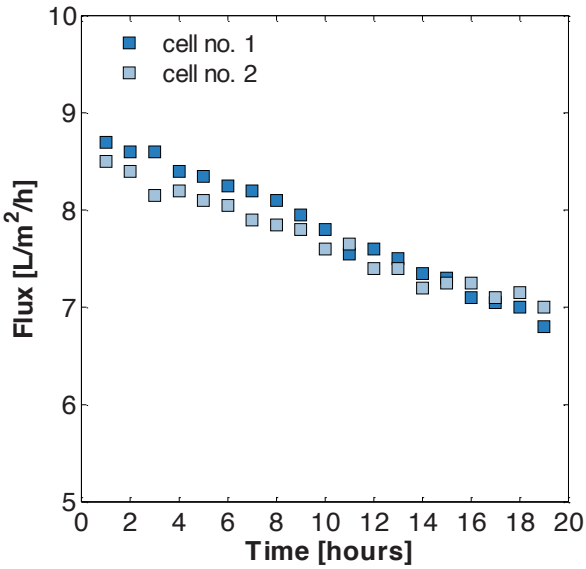

Figure 7-2: Flux ($L \cdot m^{-2} \cdot h^{-1}$) patterns over time for FO process ran in parallel cells with the same conditions for biofilm growth: spacer thickness (31 mil), cross flow velocity (0.12 $m \cdot s^{-1}$), feed water TOC of 115 $mg \cdot L^{-1}$.

Based on Figure 7-2, the results presented in the following sections can be considered representative for biofilm growth using the FO cells.

Effect of spacer thickness on performance

The FO flux patterns using the 28, 31 and 46 mil spacers are shown in Figure 7-3A-C, respectively for 5 filtration cycles. The reduction of water flux through the membrane is due to two processes: i) loss of osmotic pressure difference resulting from the simultaneous process of concentration of the FS and the dilution of DS, ii) fouling and biofilm formation on the membrane and spacer surface. However, when a new cycle is started, and the FS and DS are replaced, restoring the osmotic pressure difference, and thus the driving force for the FO process, the effect on the reduction of the flux compared to the previous cycle is only due the effect of the biofilm layer.

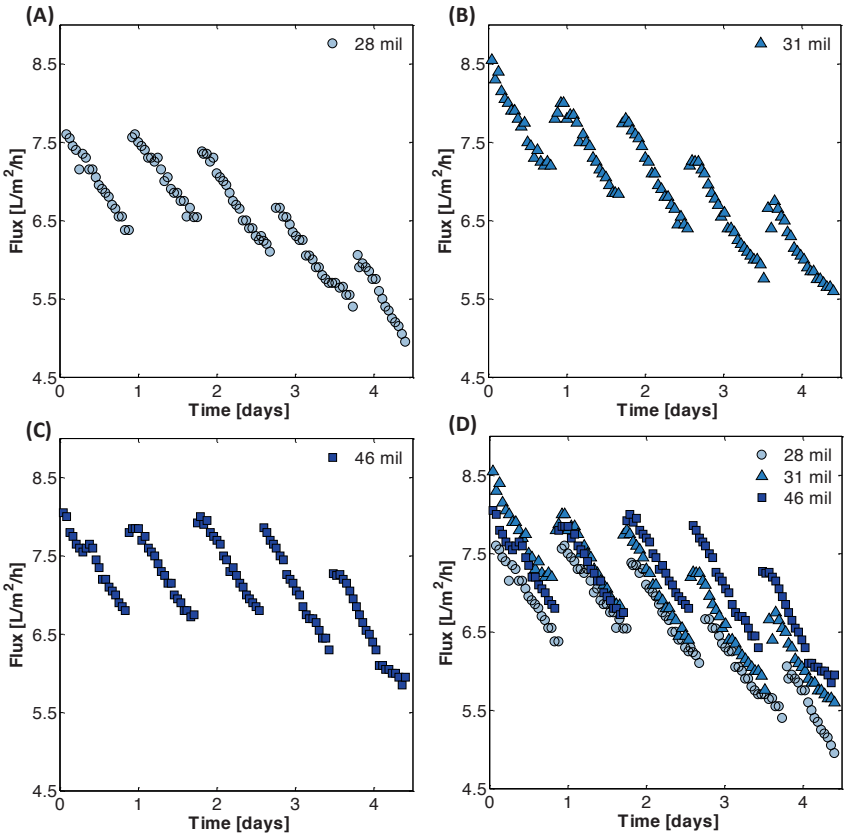

Figure 7-3: Flux ($L \cdot m^{-2} \cdot h^{-1}$) patterns over time for FO process with different spacer thicknesses (A) 28 mil, (B) 31 mil, (C) 46 mil and (D) combined graph. Each FO filtration cycle recovers 30% from feed solution to draw solution, after which both feed and draw solutions are replaced.

Results show that the 46 mil feed spacer has the best performance. With the 28 mil spacer, flux is rapidly reduced by the biofilm growth. Figure 7-3D compares the fluxes for the three different spacer thicknesses. The thickest spacer (46 mil) clearly outperforms the thinner spacers.

Flux decline calculations show that a lower flux decline can be obtained by the 46 mil thick spacer (Figure 7-4). The 28 mil spacer has the lowest performance of all spacer thicknesses throughout the experiment. The exponential curves denote the attachment and growth of a biofilm layer.

When comparing flux decline curves of the 31 mil and 46 mil feed spacers in Figure 7-4, a shadow effect (the membrane area pressed under the spacer shape has limited water permeability (Kim and Elimelech 2012)) can be observed.

With the thickest spacer the lowest (≈15%) flux decline was achieved. In terms of initial flux decline (cycle 1), the shadow effect may be lower for the 28 mil spacer compared to the 31 mil spacer, but the water mixing effect is reduced when the spacer thickness decreases, increasing concentration polarization. Consequently, a lower initial flux is expected. In the case of 46 mil spacer, the shadow effect is more significant than the mixing effect. Thus, the 46 mil spacer shows a lower initial flux compared to the 31 mil spacer.

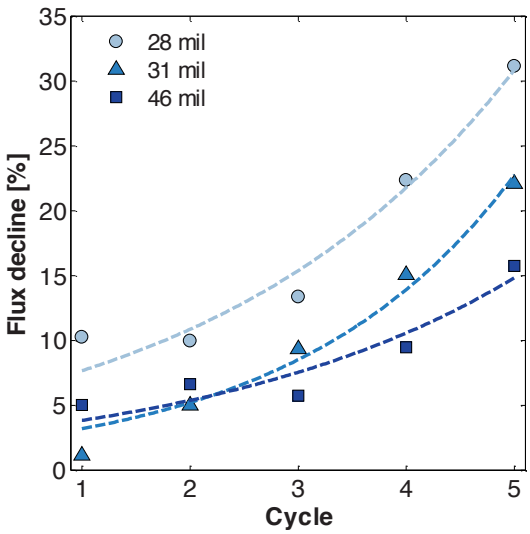

Figure 7-4: Flux decline (%) development for each filtration cycle for different spacer thicknesses (28, 31 and 46 mil); dashed lines show the exponential fit for the flux decline due to membrane surface fouling.

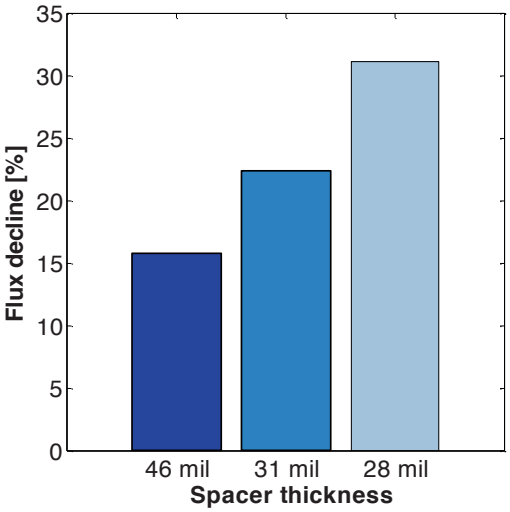

Figure 7-5: Flux decline (%) after the fifth filtration cycle for three different spacer thicknesses. The thickest spacer has the lowest flux decline, and thus, gives the best performance.

Figure 7-5 compares the flux decline for the last filtration cycle for the 3 different spacer thicknesses. Running the system with the 28 mil spacer for 5 cycles translates into a flux decline of more than 30%; if the system is run at a lower cross-flow velocity (keeping the same flow rate) using a 46 mil spacer, flux decline is significantly reduced. A thicker spacer performs better for biofouling control.

Effect of spacer thickness on biomass accumulation

After running 5 filtration cycles, recovering 30% of the water in each cycle from the feed solution to the draw solution, for each spacer thickness, the biomass concentration on a measured area of the membrane surface (including the spacer section) in contact with the FS (active layer) was calculated.

ATP values (Figure 7-6A) were found to be between 10^8 and 10^9 pg·cm^{-2}. Figure 7-6B shows the results for TOC concentration, which range from 0.15 to 0.18 mg·cm^{-2}. Spacer thickness had no significant impact on the amount of accumulated bacteria and organic matter including extracellular polymeric substances (EPS) on the membrane surface and the corresponding feed spacer for the same FO operation time.

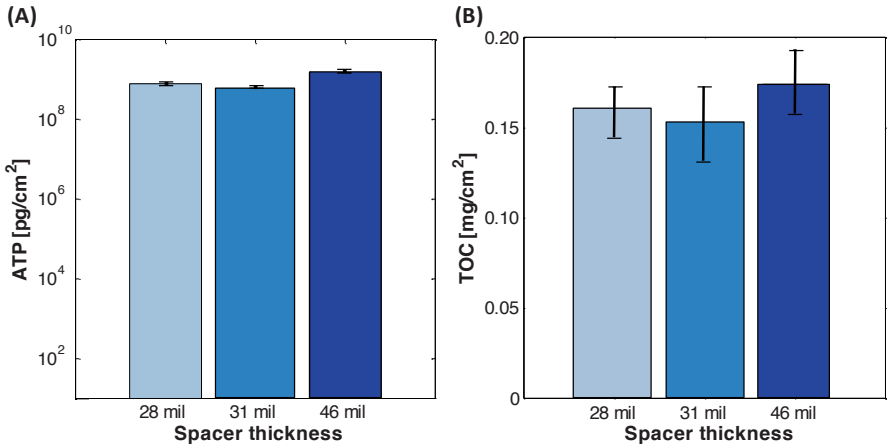

Figure 7-6: Biomass concentrations ATP (in pg ATP·cm^{-2}, A) and TOC (in mg·cm^{-2}, B) on the membrane and spacer in the flow cell operated at the same feed flow (7.2 L·h^{-1}) after 5 filtration cycles for different spacer thicknesses.

Effect of spacer thickness on fouling localization

Optical stereomicroscopy images of a fouled section of membrane and spacer show the difference in spatial distribution of biofouling for the three spacer thicknesses (Figure 7-7). Although the biomass concentration showed no significant difference between the three feed spacers, the location of the biofilm changes varied with the thickness of the spacer used.

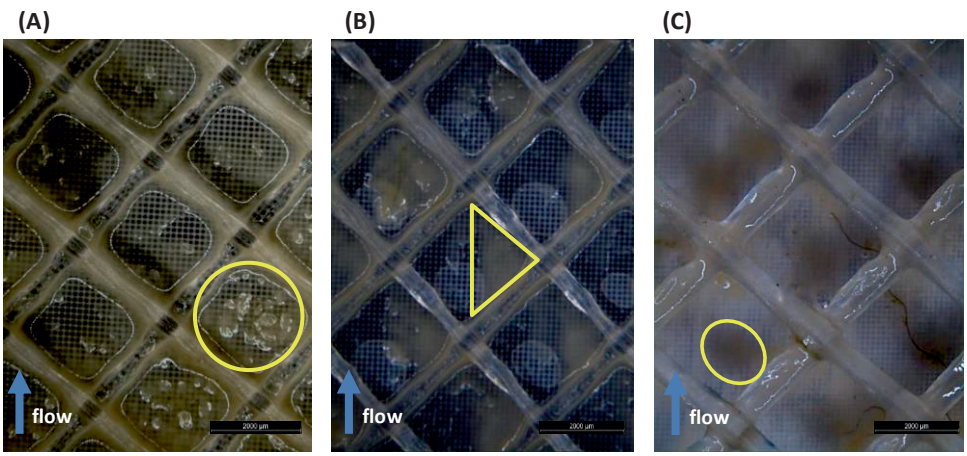

Figure 7-7: Varying localization patterns of fouling material (indicated within yellow marked areas) for different spacer thicknesses (A) 28 mil, (B) 31 mil and (C) 46 mil after 5 filtration cycles at constant flow rate (7.2 L·h^{-1}). Images were taken directly after the membrane and the spacer were removed from the FO cell and placed under a stereomicroscope. The white lines are light reflections.

For the 28 mil spacer, both membrane and spacer filaments are covered by a thick biofilm (Figure 7-7A). For the 31 mil and 46 mil feed spacers, some membrane areas and spacer filaments are not covered by the biofilm (Figure 7-7B and Figure 7-7C). The consequence of using different feed spacer thicknesses with the same feed flow is that the cross-flow velocity varies in the FO flow channel (Table 7.1). Apparently, growth of biofilm occurs in a less compact structure when a low cross-flow velocity is used (46 mil spacer) compared to a higher flow velocity (28 mil spacer). Spacer thickness and cross-flow velocity have an impact on the localization of the biofilm on the membrane surface and feed spacer filaments.

Effect of spacer thickness on fouling composition

Results from CLSM imaging of the biofilm after the FO process are shown in Figure 7-8. Presence of bacteria on the membrane surface was confirmed for all spacer thicknesses. As example the 28 mil spacer data is shown in Figure 7-8A and Figure 7-8B, where the blue spots represent stained bacterial cells with a DNA target dye (DAPI). Figure 7-8B shows the EPS (matrix of polysaccharides (purple) and proteins (green)), and bacteria (blue) on the fouling layer. Bacterial cells shown in Figure 7-8, together with operational performance decline, confirm biofouling occurrence.

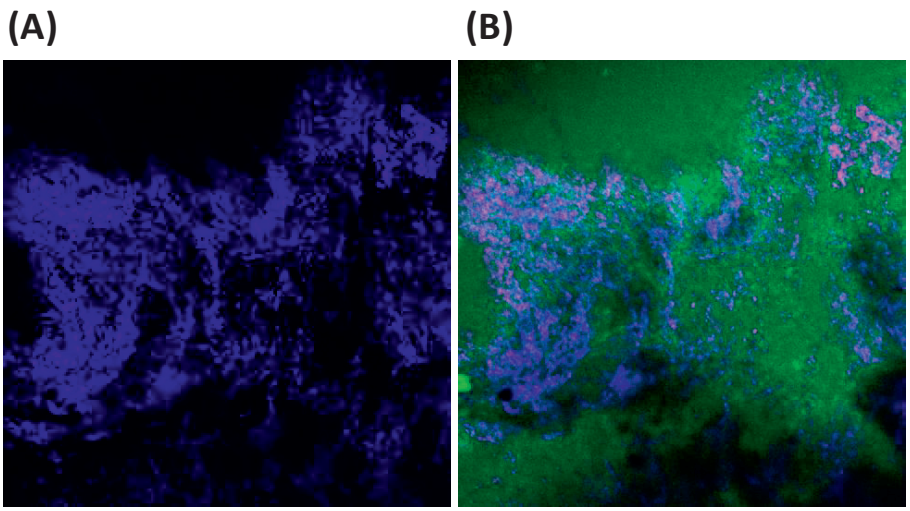

Figure 7-8: CLSM images indicating presence of (A) bacterial cells (blue) and (B) accumulation of polysaccharides (purple), proteins (green) and bacterial cells (blue) attached to the membrane surface (feed side) (425 μm^2) after 5 FO filtration cycles. The presented 28 mil spacer data is representative for all spacer thicknesses.

SEM images obtained from the fouled membrane surface for all spacer thicknesses do show similar structures resembling bacteria, EPS and some salt crystals. Figure 7-9 illustrates SEM images of a fouled membrane (using a 28 mil feed spacer) at different magnifications after 5 filtration cycles. Bacterial cells can be identified in combination with organic deposits and sodium chloride crystals, most probably coming from the DS side due to reverse draw solute flow.

An EDX analysis on the membrane surface (after the filtration experiment) for the different spacer thicknesses is shown in Table 7.4. The surface of the fouled membrane has a different composition than the virgin membrane due to the presence of EPS and some inorganic deposits, shown as an increase in the amount of sodium and chloride ions (Table 7.4). Deposited material composition showed no significant difference among the three spacer thicknesses used. Apparently, based on the few elements detected (Table 7.4) only biofouling and limited sodium chloride scaling occurred.

Table 7.4: Elemental composition (energy dispersive x-ray analysis) of the fouled surface of an FO membrane (feed side) using the 28, 31 and 46 mil feed spacers.

Element	Virgin membrane	28 mil	31 mil	46 mil
		[Wt%]		
C	71.31	52.90	44.09	50.41
O	15.50	19.68	16.89	13.84
Na	3.58	3.47	5.63	4.50
Cl	-	2.71	5.83	6.80

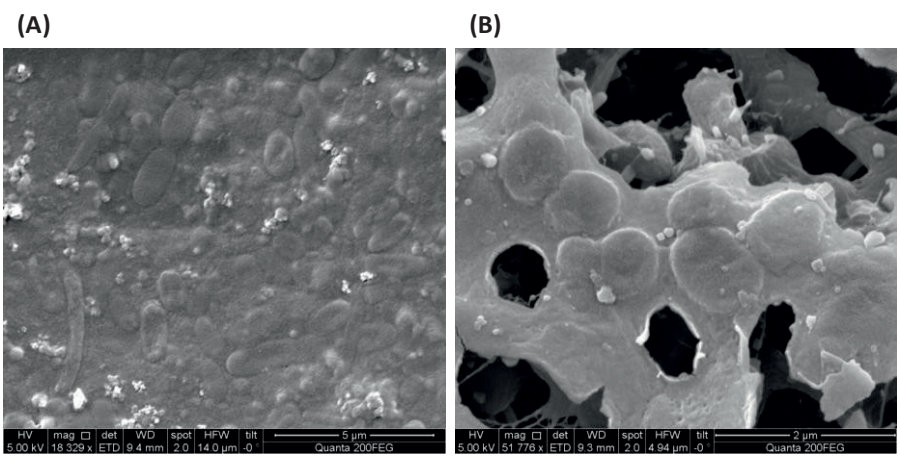

Figure 7-9: SEM images of the accumulated material (at magnification 18,000x (A) and 52,000x (B)) on the FO membrane feed side showing structures resembling bacteria, EPS material and salt crystals. The presented 28 mil spacer data is representative for all spacer thicknesses.

DISCUSSION

The objective of the study was to determine the influence of feed spacer thickness on FO performance and biofouling development and their potential for biofouling control. For all spacer thicknesses (28, 31 and 46 mil), operated at the same feed flow and the same run time, the same amount of biomass was found (Figure 7-6), while the flux reduction decreased with thicker spacers (Figure 7-4 and Figure 7-5). The thicker spacer reduced the impact of biofilm on FO membrane performance.

A previous study showed that there is limited impact on biofilm formation with and without permeate production in RO modules (Vrouwenvelder et al. 2009a). Inventories of full scale installations performance have shown that the feed channel pressure drop increase is the major problem in practice (Vrouwenvelder et al. 2008). Lab-scale studies to investigate biofilm formation in RO most often are performed without flux permeation; therefore, the parameter used to determine the impact of accumulated biomass is feed channel pressure drop. FO studies in any condition have to be performed with permeate flux. The most sensitive parameter to fouling in FO systems is permeate flux. Considering the relation for ATP/TOC shown in previous RO experiments (biofouling) compared to the relation obtained in this study (further discussed), a meaningful comparison between the two systems (RO and FO) can be made when relating the most sensitive parameter on each process: feed channel pressure drop for RO and permeate flux decline for FO.

Thickest spacer provides the best performance

The use of a thick spacer (46 mil) translates into a better performance of the FO filtration process due to the reduced effect of biofouling. A lower flux decline is achieved when the system is run at a low linear flow velocity (use of a thick spacer). Spacer thickness influences the spatial localization of biofilm in FO. Flux patterns change and due to the less compact biofilm formed, a slower flux decline was obtained when the 46 mil spacer was used. Araújo et al. (2012a, 2012b) obtained similar results for RO experiments, reporting that similar amounts of biomass accumulated during the experiment for different spacer thicknesses, but a lower feed channel pressure increase was observed when the thickest spacer was used. Bucs et al. (2013) found the same trend (lower impact

biomass at thicker spacer) using numerical modelling. Thick spacers were demonstrated to be a feasible control strategy for biofouling.

The shadow effect (limited water permeability under spacer area) for thick spacers shows a smaller influence in FO than in other osmotic membrane processes that require hydraulic pressure (i.e. pressure retarded osmosis) (Kim and Elimelech 2012). Loose biofouling structures obtained with a thick spacer (46 mil) showed a higher positive impact (improved performance) on reducing flux decline than the negative effect (reduced performance) of the shadow effect. Results show that biofouling in FO is better controlled with thick spacers, limiting the shadow effect due to the lack of hydraulic pressure.

When no spacer is used with different types of fouling in FO membrane systems, an opposite effect for a low cross-flow velocity was reported. Lee et al. (2010a) established that when three different initial cross-flow velocities (0.171, 0.256, and 0.342 $m \cdot s^{-1}$) were employed in FO fouling filtration, the flux curve for the lowest cross-flow velocity showed the highest flux decline, whilst at the highest cross-flow velocity, almost no flux decline was observed. FO feed spacers play an important role in biofouling control.

The consequence of using different feed spacer thicknesses in the FO flow channel with the same feed flow is that the cross-flow velocity varies (Table 7.1). Spacer thickness and cross-flow velocity both impacted the (i) localization of the biofilm on the membrane surface and feed spacer filaments and the (ii) effect of accumulated biomass on membrane performance. For FO, at low linear velocity the impact of biomass on flux decline is reduced, which is in agreement with results of studies on spiral wound nanofiltration and reverse osmosis systems (Vrouwenvelder et al. 2009b, Vrouwenvelder et al. 2010, Ying et al. 2013).

FO and RO show similar biofouling patterns

FO and RO systems differ from each other in several aspects: i) membrane water flux (up to 10 times higher for RO compared to FO), ii) driving force (applied hydraulic pressure versus osmotic pressure difference), iii) biofouling potential in both sides of the membrane for FO systems, and iv) existence of a reverse draw solute flux in FO processes. The effect of biofouling on the FO system performance in relation with different feed spacer thicknesses (different cross-flow velocities) is similar to reported data for RO processes.

Vrouwenvelder et al. (2009b) stated that the impact of biomass on the pressure drop increase will be lower when a low cross-flow velocity is used in the membrane system, inferring that the thickest spacer shows the best performance, and even suggesting modified spacer use as an approach to control biofouling. The 46 mil spacer used in FO filtration (lowest cross-flow velocity) controls biofouling and reduces the impact on flux decline.

This study on FO is in good agreement with results of earlier studies on RO systems concerning the impact of spacer thickness on biomass accumulation and impact of biomass on performance. Previous studies by Vrouwenvelder et al. (2010) reported that the same biomass concentrations showed different effects on pressure drop for RO. The same trend is observed in FO filtration, where similar amounts of biomass (ATP and TOC) do not determine performance decline.

The ATP concentrations found for the RO experiments (10^4 - 10^5 pg·cm^{-2}) (Vrouwenvelder et al. 2009b) are significantly lower compared to the results obtained in FO study (10^8 - 10^5 pg·cm^{-2}) (this manuscript), which indicates a higher bacterial concentration of the fouling layer for the FO process (biofouling). Although the FO experiment was performed with a high TOC feed solution (115 mg·L^{-1}), the TOC values for the FO experiments (0.15 - 0.18 mg·cm^{-2}) are only one order of magnitude larger than the results reported for RO membranes (0.01 mg·cm^{-2}). The relation ATP/TOC is higher for the FO tests (6.6×10^2 - 5.5×10^3) than for the RO tests (1.0×10^0), suggesting that a higher bacterial presence/growth on the membrane occurred during the FO tests. Moreover, a previous study on biofouling in FO processes (Yoon et al. 2013) found that the dominant factor when accounting the effect of biofouling on flux decline is the resistance of bacterial cells and not the resistance due to exopolymeric substances (EPS), mainly composed of biopolymers and protein-like substances, which are common substances found in organic fouling. Therefore, organic fouling induced by the feed solution composition cannot be considered as a critical factor in terms of its effect on flux decline; biofouling is clearly the predominant form of fouling in FO experiments performed in this study. As far as the authors' knowledge, similarities on biofouling patterns for FO and RO have not been reported before

Effect of biofilm on flux decline

Water flux through the FO membrane was affected adversely by biofilm growth. The effects of biofilm formation on membrane flux decline in the FO process can be explained by two mechanisms: (i) cake-layer formation, which includes both the resistance of bacterial cells and the resistance of the EPS (the latter being significantly lower than the former), and (ii) concentration polarization, which is expected due to the use of different spacer thicknesses and cross flow. Both cake-layer formation and concentration polarization are influenced by the spacer geometry.

The lowest flux decline after 5 days was achieved with the thickest spacer, which shows the most significant concentration polarization due to the lowest cross flow velocity (negative impact on flux). However, due to the structure of biofouling layer on the thickest spacer, a considerable lower impact on flux decline is observed compared to thinner spacers.

Future studies

This study focused on biofouling on the feed side of the FO membrane when a wastewater effluent is used as feed water. Nevertheless, the seawater biofouling potential on the draw solution side may present new insights into FO indirect desalination. Special attention should be given to the transport of small molecular weight carbon and nitrogen compounds from the FS to the DS, which may act as substrate for bacteria to grow and represent a problem for long-term operation of this type of system.

Modelling can be a useful tool to predict and prevent biofouling in FO membranes. Along with this, future studies should focus on the use of modified spacers and novel cleaning strategies, which may be in agreement with cleaning protocols already developed for FO membranes (Valladares Linares et al. 2013b), to mitigate biofouling in FO indirect desalination systems.

CONCLUSIONS

Evaluation of the study on the influence of feed spacer thickness (28, 31 and 46 mil) on performance and biofouling development on the feed side of forward osmosis membranes led to the following conclusions:

- The biomass amount alone does not determine the flux decline: The same amount of biomass was found for all spacer thicknesses after the same run time at the same feed flow, while the flux reduction decreased with thicker spacer.
- The flux decline caused by biomass accumulation can be reduced by using a thicker spacer.
- Spatial distribution of the biofilm differs with feed spacer thickness.

Our findings are in agreement with reported data for reverse osmosis cross-flow systems: thicker spacers reduce impact of biofouling on performance. This result clearly contradicts observations obtained with particulate and colloidal fouling in forward osmosis.

Numerical Study of Biofouling in Forward Osmosis

Abstract

This study evaluates with numerical simulations supported by experimental data the impact of biofouling on membrane performance in a cross-flow forward osmosis (FO) system. The two-dimensional numerical model couples liquid flow with solute transport in the FO feed and draw channels, in the FO membrane support layer and in the biofilm developed on one or both sides of the membrane. The developed model was tested against experimental measurements at various osmotic pressure differences and in batch operation without and with the presence of biofilm on the membrane active layer. Numerical studies explored the effect of biofilm properties (thickness, hydraulic permeability and porosity), biofilm membrane surface coverage, and biofilm location on salt external concentration polarization and on the permeation flux. The numerical simulations revealed that (i) when biofouling occurs, external concentration polarization became important, (ii) the biofilm hydraulic permeability and membrane surface coverage have the highest impact on water flux, and (iii) the biofilm formed in the draw channel impacts the process performance more than when formed in the feed channel. The proposed mathematical model helps to understand the impact of biofouling in FO membrane systems and to develop possible strategies to reduce and control biofouling.

Published as:

Szilárd S. Bucs, Rodrigo Valladares Linares, Johannes S. Vrouvenvelder, Cristian Picioreanu (2016) Impact of spacer thickness on biofouling in forward osmosis. *Water Research* **106**: 86 – 97.

INTRODUCTION

Forward osmosis (FO) is a membrane technology in rapid development, based on the difference in osmotic pressure between two liquids separated by a semi-permeable membrane, with a range of possible water treatment applications. Compared to other membrane filtration processes like reverse osmosis or nanofiltration, in FO almost no external hydraulic pressure is required for the process (Mulder, 1996). The driving force in FO is the osmotic pressure difference, such that water is extracted from the low osmotic pressure solution, also referred to as feed water, into the high osmotic pressure draw solution. Forward osmosis (FO) can play a bridging role in the integration of upstream and downstream water treatment processes, and could reduce energy consumption of the entire desalination or water recovery and reuse processes (Valladares Linares et al., 2014b). One of the main advantages of FO compared to conventional membrane processes for desalination and wastewater recovery (i.e. nanofiltration, NF, and reverse osmosis, RO) is the limited amount of external energy required to extract water from the feed solution (Valladares Linares et al., 2014b).

Use of FO for water reclamation was demonstrated in applications like oil/gas wastewater (Hickenbottom et al., 2013), landfill wastewater treatment and water recycling in space missions (Cath et al., 2005; Holloway et al., 2007). Bench scale tests demonstrated the potential of FO in municipal wastewater recovery combined with seawater desalination processes (Valladares Linares et al., 2013; Werner et al., 2013). Other studies evaluated the possibility of using FO systems as a pre-treatments in membrane desalination technologies for low-pressure desalination processes while simultaneously recovering water from a recycled feed solution (Achilli et al., 2014; Boo et al., 2013; Hoover et al., 2011). For desalination applications of FO, there are two possible approaches, *direct* and *indirect* desalination. In a *direct* FO desalination processes fresh water is directly extracted from seawater or brackish water by using the high salinity water as feed solution and an osmotic reagent as draw solution. An additional process is required for fresh water recovery from the diluted draw solution (Li et al., 2013; McCutcheon et al., 2005). A full-scale plant commissioned in 2012 is demonstrating the benefits and the viability of *direct* FO desalination (Modern Water Inc., 2012). In *indirect* FO desalination, the high salinity water is used as draw solution and an impaired water such as

secondary wastewater effluent is used as of feed solution (Valladares Linares et al., 2013). The attractiveness of *indirect* FO desalination beside the low-cost draw solution (seawater or brackish water) relies on the diluted draw solution which can be used as feed water in a subsequent desalination process like reverse osmosis, thus reducing the cost of the entire desalination process (Yangali-Quintanilla et al., 2011).

However, as in other membrane filtration processes, FO also has the potential of membrane fouling. In certain FO operation conditions, the membrane can suffer from fouling on one side or on both sides. During *indirect* FO desalination when both the feed (secondary wastewater effluent) and the draw (seawater) solutions have fouling potential, deposition of unwanted material on the membrane surface can occur. Similar to other membrane filtration processes (e.g. reverse osmosis), accumulation and growth of microorganisms on the membrane surface is highly possible, leading to biofouling (Shannon et al., 2008; Vrouwenvelder et al., 2008b). Only a few studies investigated the impact of biofouling on FO systems (Valladares Linares et al., 2014a; Yoon et al., 2013; Zou et al., 2013). Yoon et al., (2013) showed that the occurrence of biofouling in FO is less severe regarding flux decline when comparing to reverse osmosis. Zou et al., (2013) and Valladares Linares et al., (2014) investigated the impact of different spacer geometries in a cross-flow system on biofouling. Both studies showed an increase in water flux with the spacer inserted in the flow channel. Also noted was that the impact of the same amount of biomass on flux decline was lower when using a thicker spacer (Valladares Linares et al., 2014a). However, none of the FO membrane fouling studies investigated the impact of biofouling on both sides of the membrane simultaneously.

An important particularity of FO membrane filtration compared to other membrane systems such as reverse osmosis and/or ultrafiltration is a different occurrence of concentration polarization (CP). In FO systems three kinds of CP are distinguished: concentrative and dilutive external concentration polarization (ECP) and internal concentration polarization (ICP). The concentrative ECP corresponds to that observed in reverse osmosis systems. Unlike in RO systems, the dilutive ECP occurs in the draw solution side of the membrane due to the permeate flux and ICP takes place in the membrane porous support layer. It was shown that both external concentration polarization effects reduce the

process driving force (i.e., the osmotic pressure difference), however their impact on water flux is minor. The most important and process- limiting concentration polarization was found to be the internal concentration polarization (McCutcheon and Elimelech, 2006). Consequently, the difference in driving force and its impact on the filtration processes prevent the direct transplantation of research results from different membrane systems, for example from NF and RO to FO.

The novelty of is work consists in the evaluation of biofouling effects on membrane performance in a cross-flow FO system with numerical simulations, also supported by experimental studies. The numerical model was used to study the impact of (i) biofilm properties (thickness, hydraulic permeability, and porosity), biofilm membrane surface coverage, and biofilm location (feed channel, draw channel and both) on FO membrane performance, and (ii) biofouling on external concentration polarization in different FO operation conditions.

MATERIALS AND METHODS

Experimental setup

A lab-scale FO membrane system was used for the experimental evaluation of permeation fluxes without and with biofilm development on the membranes. Two peristaltic pumps (Cole-Parmer) circulated in closed loop the feed and draw solutions at similar cross-flow velocities (8.6 cm s^{-1}). The pumps were connected to two reservoirs with the same volume (1.25 L), one for the feed solution and one for the draw solution. Each reservoir was placed on a digital scale (Mettler Toledo) connected to a computer. The water flux through the membrane was calculated from the change in weight of the reservoirs. All experiments were performed at 20℃.

Cellulose triacetate (HTI, Scottsdale, AZ) forward osmosis membrane with a thickness of ~50 μm was used for the experiments. In all cases, the membrane active layer faced the feed solution while the support layer was in contact with the draw solution. This configuration was shown to be the most effective to prevent membrane fouling (Mi and Elimelech, 2008; Wang et al., 2010).

The membrane was placed into a custom-made flow cell from poly(methyl methacrylate) (PMMA), with an active membrane area of 20 cm^2. The flow cell

was designed to allow operation without and with the presence of spacer in the feed and draw channels. The feed and draw channels height were the same and could fit 46 mil (1,168 mm) thick spacers. For the studies with spacer, a 46 mil spacer produced by Hydration Technology Innovation (HTI, Scottsdale, AZ) was used on both sides of the membrane. A more detailed description of the flow cell can be found in previous studies (Li et al., 2012).

For flux measurements at various osmotic pressure differences sodium chloride (NaCl) solutions were prepared. The feed solution salt concentration was kept constant at 0.58 $kg \cdot m^{-3}$ while the draw solution concentration was varied from 5.8 $kg \cdot m^{-3}$ to 78.8 $kg \cdot m^{-3}$.

The biofouling experiments were run in a repeated batch mode. Each batch cycle was interrupted after 20 h of operation and the feed and draw solutions were replaced by fresh solutions (salt concentrations of 2 $kg \cdot m^{-3}$ in feed and 40 $kg \cdot m^{-3}$ in draw), then the next cycle was started. To ensure biofilm formation in the feed channel, a municipal secondary effluent (Al-Ruwais wastewater treatment plant, Saudi Arabia) was used as feed solution for the first 20 h. The effluent characteristics were: chemical oxygen demand (COD) 25 $mg \cdot L^{-1}$, total organic carbon (TOC) 4.84 $mg \cdot L^{-1}$, pH 7.1, conductivity 2.33 $mS \cdot cm^{-1}$, osmotic pressure 0.38 bar, total suspended solids (TSS) 2.25 $mg \cdot L^{-1}$ and volatile suspended solids (VSS) 2.15 $mg \cdot L^{-1}$. The adenosine triphosphate (ATP) concentration of the effluent was 215 $pg \cdot mL^{-1}$, which corresponds to a bacterial cell concentration of approx. 10^7 $cells \cdot mL^{-1}$. For the subsequent five FO filtration cycles, the feed solution was a synthetic municipal wastewater as described in (Valladares Linares et al., 2014a, 2013), initially with 360 mg $COD \cdot L^{-1}$, 115 mg $TOC \cdot L^{-1}$ and pH 5.66. All the chemicals were purchased from Sigma-Aldrich (Munich, Germany) and had a purity grade higher than 99.5%. All solutions were prepared with deionized (DI) ultra-pure water (Valladares Linares et al., 2014a, 2013).

Model description

A two-dimensional mathematical model was developed to investigate numerically the impact of biofouling on the performance of forward osmosis processes. The model includes liquid flow coupled with the mass transport of the solute (salt) through the feed and draw channels, through the asymmetric permeable membrane, and through a biofilm present on the FO membrane.

Model geometry

Without biofilm, the model geometry included three domains: feed and draw channels separated by a membrane support layer (Figure 8-1a), while the thin membrane active layer was assimilated with a boundary in this model.

The flow channel length (L_X) was chosen tenfold smaller than the length of the flow cell used for the experimental studies.

Table 8.1: Model parameters and experimental conditions

Parameter	Symbol	Value	Unit	Source
Model geometry				
channel length	L_X	10	mm	chosen
channel height	L_Y	1.17	mm	46 mil Filmtech™ spacer
membrane thickness	L_S	50	µm	Valladares Linares et al., 2014
spacer fibre thickness	d_M	0.58	mm	Valladares Linares et al., 2014
spacer mesh size	L_M	4.1	mm	Valladares Linares et al., 2014
Experimental conditions				
average inlet flow velocity	u_{in}	8.6	$cm \cdot s^{-1}$	Valladares Linares et al., 2014
feed salt concentration inlet or initial (biofouling case)	$C_{F,0}$	2	$kg \cdot m^{-3}$	Valladares Linares et al., 2014
draw salt concentration inlet or initial (biofouling case)	$C_{D,0}$	40	$kg \cdot m^{-3}$	Valladares Linares et al., 2014
initial solution volume in feed reservoir	$V_{F,0}$	1.25	L	Valladares Linares et al., 2014
initial solution volume in draw reservoir	$V_{D,0}$	1.25	L	Valladares Linares et al., 2014
membrane area	A_M	20	cm^2	Valladares Linares et al., 2014
temperature	T	293	K	Valladares Linares et al., 2014
Water and solute properties				
feed water density	ρ_F	999	$kg \cdot m^{-3}$	Craittenden et al., 2012
draw solution density	ρ_D	1020	$kg \cdot m^{-3}$	McCutcheon and Elimelech, 2006
water viscosity	η	10^{-3}	Pa·s	Crittenden et al., 2012
salt diffusion coefficient in water	D_W	1.33×10^{-9}	$m^2 \cdot s^{-1}$	McCutcheon et al. 2006
salt diffusion coefficient in support layer	D_S	0.18×10^{-9}	$m^2 \cdot s^{-1}$	Calculated as L_S/K_S
Membrane properties				
water permeability	A	0.57	$L \cdot m^{-2} \cdot h^{-1} \cdot bar$	Phillip et al. 2010
solute permeability	B	0.33	$L \cdot m^{-2} \cdot h^{-1}$	Phillip et al. 2010
membrane structural parameter	S	360	µm	McCutcheon et al. 2006
salt resistivity of support layer	K_S	2.7×10^5	$s \cdot m^{-1}$	McCutcheon et al. 2006
water permeability of support layer	K_{WS}	2×10^{-15}	m^2	Dreszer et al., 2013
support layer porosity	ε_S	0.3	-	Calculated as $\tau \cdot L_S / S$ (chosen tortuosity τ=2)
Biofilm properties				
Porosity	ε_B	0.5	-	Radu et al., 2010
Permeability	K_B	10^{-17}	m^2	Dreszer et al., 2013
salt diffusion coefficient in biofilm	D_B	0.66×10^{-9}	$m^2 \cdot s^{-1}$	Calculated as $\varepsilon_B \cdot D_W$
biomass specific growth rate	μ	0.81	d^{-1}	fitted with 46 mil experimental data from Valladares Linares et al., 2014
initial biofilm thickness	$L_{B,0}$	5	µm	Chosen
maximum biofilm thickness	$L_{B,E}$	150	µm	Valladares Linares et al., 2014
biofilm thickness	L_B	150	µm	Valladares Linares et al., 2014

This length was small enough to allow performing computationally efficient numerical simulations, while maintaining a size representative for the FO system (i.e., including several spacer fibres).

The heights of the two flow channels (L_Y) and membrane support layer thickness (L_S) were those used in the experimental studies. When the biofilm was present, it constituted a fourth planar domain with thickness L_B. Although not completely realistic, the feed and draw channel spacer fibres were circular and arranged in a zig-zag configuration mimicking a two-dimensional axial slice in a three-dimensional flow channel (Figure 8-1b). The diameter (d_M) and distance between the spacer fibres (L_M) corresponded with the 46 mil spacer geometry used for the experimental studies (Table 8.1).

Fluid flow

The flow in the feed and draw channels was calculated from steady-state laminar Navier-Stokes equations 8-1:

$$\rho(\mathbf{u}\cdot\nabla)\mathbf{u} + \nabla p = \nabla\cdot(\eta\nabla\mathbf{u})$$
$$\nabla\cdot\mathbf{u} = 0 \qquad 8\text{-}1$$

where u = (u_x, u_y) is the vector of local liquid velocity, p is the pressure, ρ and η are the density and dynamic viscosity of the solution at 293 K, respectively.

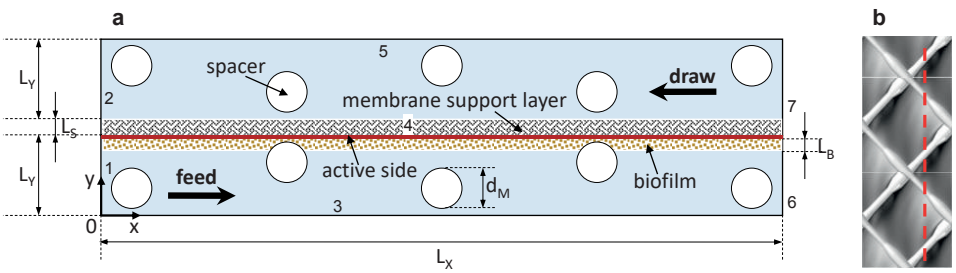

Figure 8-1: (a) Illustration of the forward osmosis (FO) model geometry. The model space is divided to three domains: feed and draw channels (blue colour, with bold arrows indicating the flow directions) and membrane support layer (woven grey). The membrane active layer (red line) is facing the feed channel side and it represents a boundary. When present, the biofilm (yellow dotted zone) constitutes a fourth domain. Symbols are explained in Table 8.1. Numbers represent the different boundaries of the computational domains, as explained in Table 8.2. (b) Spacer fibres are arranged in such a way to mimic an imaginary 2D plane along the red dashed line in a 3D flow channel.

The steady-state laminar flow assumption is justified considering the low Re number used in the experiments (Re ≈ 80, calculated according to Schock and Miquel, 1987), as shown in Bucs et al., (2015).

The membrane support layer and biofilm domains were treated as porous media and Brinkman flow was assumed according to equation 8-2:

$$\frac{\eta}{K}\mathbf{u} + \nabla p = \frac{\eta}{\varepsilon}\nabla^2\mathbf{u}$$
$$\nabla \cdot \mathbf{u} = 0 \qquad 8\text{-}2$$

where K and ε are the permeability and porosity of membrane support layer (K_{WS} and ε_S) and biofilm (K_B and ε_B).

The boundary conditions used are listed in Table 8.2. Fully developed laminar flow profiles with average velocity u_{in} were imposed at the feed and draw channel inlets, while the pressure was set to zero at the outlet boundaries. No-slip conditions were applied to the spacer surface and to the bottom and top boundaries of the feed and draw channels, respectively. Flow continuity was assumed between the support layer or biofilm surface and the draw or feed channels. A flux of water J_W was imposed on the membrane active layer, proportional with the local osmotic pressure difference ($\Delta\pi$) and the permeability for water (A) (eq.(3) (Sagiv et al., 2014):

$$J_W = A(\pi_{draw} - \pi_{feed}) = A \cdot \Delta\pi \qquad 8\text{-}3$$

The osmotic pressures in the draw and feed solution (π_{draw} and π_{feed}) were calculated from Van't Hoff eq.(4) (Mulder, 1996, p. 283):

$$\pi = 2C \cdot R \cdot T \qquad 8\text{-}4$$

function of local salt concentrations C_{draw} and C_{feed} at the membrane surface, universal gas constant R and temperature T (Table 8.2).

Salt transport

Sodium chloride was assumed the only soluble compound relevant for this model, transported by convection and diffusion in both of the flow channels (equation 8-5).

$$D\nabla^2 C - \mathbf{u}\nabla C = 0 \qquad 8\text{-}5$$

where D is the diffusion coefficient and C is the local salt concentration. The salt diffusion coefficient was considered equal in the feed and draw solutions (D_W), whereas lower values were taken in the membrane support layer (D_S) and in the biofilm (D_B) domains (Table 8.1).

Table 8.2: Boundary conditions for the FO model geometry presented in Figure 8-1a.

boundary no.	feed side		draw side	
	fluid flow	salt transport	fluid flow	salt transport
1	$u_x = 6u_{in}(1 - y/L_y)y/L_y$ $u_y = 0$	$C = C_F$	-	-
2	-	-	$p = 0$	$-\mathbf{n}\cdot D_W\nabla C = 0$
3 and spacer	$\mathbf{u} = 0$	$-\mathbf{n}\cdot D_W\nabla C = 0$	-	-
4	$u_x = 0$ $u_y = -J_W$	$-\mathbf{n}\cdot\mathbf{J} = J_S$	$u_x = 0$ $u_y = J_W$	$-\mathbf{n}\cdot\mathbf{J} = -J_S$
5 and spacer	-	-	$\mathbf{u} = 0$	$-\mathbf{n}\cdot D_W\nabla C = 0$
6	$p = 0$	$-\mathbf{n}\cdot D_W\nabla C = 0$	-	-
7	-	-	$u_x = -6u_{in}(1 - y/L_y)y/L_y$ $u_y = 0$	$C = C_D$

In the inlet, the solutions contained salt with concentrations C_F (feed channel) and C_D (draw channel). Typical no-diffusion conditions applied at the outlet boundaries for both channels, while the spacer surface, bottom and top boundaries were impermeable walls. In FO processes, draw solute leaks through the membrane into the feed side, as described by (equation 8-6, (Sagiv et al., 2014):

$$J_S = B(C_{draw} - C_{feed}) \qquad 8\text{-}6$$

where B is the membrane permeability for salt, and C_{draw} and C_{feed} are the local salt concentrations in the draw and feed channels, respectively. The flux of salt is in opposite direction to the water flux.

Biofilm development

To study the impact of biofilms formed on the membrane on the FO process performance, three cases were investigated: (i) a continuous planar biofilm with thickness increasing in time (thus roughly simulating biofilm growth); (ii) a continuous planar layer with thickness constant in time; and (iii) a patchy biofilm formed by microbial colonies of various size, but constant in time. In the first two cases, the biofilm of uniform thickness covered the whole membrane area, while in the third case the patchy biofilm covered only 50% of the membrane, but had the same biofilm volume as in the second case. By assuming, for simplicity, unlimited biomass growth at constant specific rate μ and constant biomass concentration in the biofilm, the increase in biofilm thickness L_B in case (i) is represented by equation 8-7:

$$L_B = L_{B0} \exp(\mu t) \qquad 8\text{-}7$$

In all cases, the biofilm was represented as a computational domain and flow continuity was applied at the moving biofilm-liquid interface (Figure 8-1).

Water and solute transport in biofilms are functions of the biofilm properties and morphology. According to Darcy's law, permeation flux through the biofilm, J_W, is function of the pressure drop over the biofilm, fluid viscosity, biofilm permeability and thickness (equation 8-8) (Dreszer et al., 2013):

$$J_W = \frac{K_B}{\eta \cdot L_B} \Delta p \qquad 8\text{-}8$$

This means that also the hydraulic resistance, R_B defined by equation 8-9, is time dependent because the biofilm thickness can change in time:

$$R_B = \frac{L_B}{K_B} \qquad 8\text{-}9$$

Model solution

The two-dimensional liquid flow and salt transport were solved in COMSOL Multiphysics (v5.1, Comsol Inc., Burlington, MA), on a triangular finite-element mesh with a maximum size of 5 μm, using a stationary solver. In case of biofilm growth, a moving mesh procedure was applied for the time-dependent biofilm-liquid interface, while the liquid flow and salt transport were also solved in time.

Simulation of batch operation

To simulate the batch process, the model was extended to include the feed solution concentration and draw solution dilution in time, together with the change in feed and draw solution volumes, V_F and V_D (equation 8-10 – 8-13):

$$\frac{dV_F}{dt} = -J_W \cdot A_M \; ; \qquad \frac{dC_F}{dt} = \left(J_W C_F + J_S\right) \cdot \frac{A_M}{V_F} \qquad \text{8-10, 8-11}$$

$$\frac{dV_D}{dt} = J_W \cdot A_M \; ; \qquad \frac{dC_D}{dt} = -\left(J_W C_D + J_S\right) \cdot \frac{A_M}{V_D} \qquad \text{8-12, 8-13}$$

where C_F and C_D are the salt concentrations of feed and draw solutions, and A_M is the membrane area. The initial values are listed in Table 8.1.

RESULTS AND DISCUSSION

The aim of this study was to evaluate the impact of biofilms on the performance of FO processes. Although concentration polarization is considered in the developed model, a detailed study of its impact on process performance here is out of scope. First, a two-dimensional model was developed for the FO without biofilm presence and the results were compared with experimental data at different osmotic pressures and in a batch operation. Second, the model was extended to include biofilm development in the feed channel and compared with experimental results. Third, the calibrated model was used to investigate the biofilm impact on concentration polarization, and the effects of biofilm properties (i.e. thickness, roughness, porosity, and permeability) on the performance of an FO process. Finally, the influence of biofilm location (i.e., in draw channel, in feed channel or in both) was evaluated.

Evaluation of the forward osmosis model

To evaluate the proposed numerical model, simulations were compared with experimental measurements. In total three sets of flux measurements were performed: (i) at different osmotic pressures, (ii) in batch operation to record the flux decline due to solution dilution in time and (iii) with biofilm growth under batch operation.

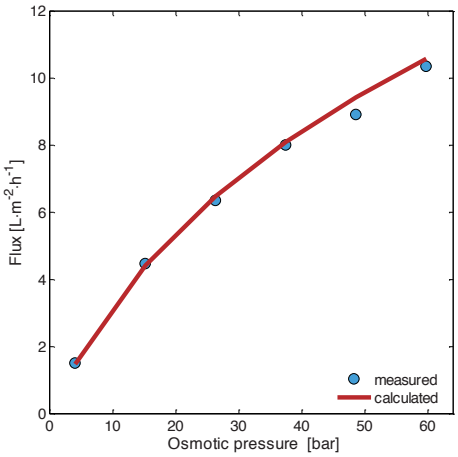

Figure 8-2: Measured (blue circles) and calculated (red line) water flux at different osmotic pressure differences, without the presence of spacer or biofilms. Model parameters used are presented in Table 8.1.

Water flux increase with increasing osmotic pressure

Water flux was experimentally measured at various salt concentrations in the feed and draw solutions. For these experimental measurements, no spacer was used in the flow cell and the conditions were set to minimize the possibility of biofilm formation. Consequently, no spacer and no biofilm were considered in this model version.

The feed solution salt concentration (NaCl) was kept at 0.58 kg·m^{-3} for all the experimental measurements and the concentration in the draw solution was varied from 5.8 kg·m^{-3} up to 78.8 kg·m^{-3} in steps of 14.6 kg·m^{-3}. The experimental setup was operated in batch mode, one hour for each salt concentration, and the average flux in that hour was calculated.

Membrane parameters for the numerical simulations, such as, membrane water permeability (A= 0.44 L·m^{-2}·h^{-1}·bar), membrane solute permeability (B= 0.26 L·m^{-2}·h^{-1}) were taken from Phillip et al., 2010. The salt diffusion coefficient in the support layer (D_S), support layer water, and solute permeability (K_{WS}, K_S), were also taken from literature (Dreszer et al., 2013; McCutcheon and Elimelech, 2006)(Table 8.1). To evaluate the model and the applied parameters, the flux was calculated at the same solute concentrations in the feed and draw solutions as used in the experiments. Comparing the calculated and measured flux increase with increasing osmotic pressure confirmed that, in

this case, the model describes the process accurately without further parameter fitting (Figure 8-2).

Flux decline in batch experiments

In a batch FO process, the water flux decreases in time because the draw solution gets diluted, while the feed solution becomes more concentrated in salt. To further test the model in dynamic conditions, the flux decline in a batch process was first experimentally measured. The batch experiment was performed by recirculating 1.25 L of feed and draw solutions through the flow channels with spacers for a period of 1200 minutes (20 h).

For the whole batch period, the model predicts a linear flux decline similar to the experimental results (Figure 8-3a). As described by the model (equation 8-8 – 8-11), the flux decline depends on the experimental conditions and membrane properties. For these studies, the 20 cm^2 membrane coupons were cut out from a larger sheet membrane, showing differences in permeability. For FO membranes, a relatively high standard deviation (>30 %) in membrane properties is possible, as shown by Phillip et al. (2010). While the experimental conditions were set, the values for membrane properties in the numerical model had to be adjusted to describe the measurements (values from Table 8.1). In this way, membrane water permeability and the membrane solute permeability were increased by 30 percent in the numerical model compared with the values used in the previous osmotic pressure simulations. By increasing the membrane water permeability, A, not only that a higher flux is achieved, but the draw solution is also diluted faster, which results in a more rapid flux decline (Figure 8-3a). Higher membrane solute permeability, B, also increases the dilution rate of the draw solution, but we found that the water flux decline is more sensitive to the membrane water permeability.

These results were further used to provide consistent initial values and calibrated membrane parameter values for the FO simulations with biofilm.

Flux decline in repeated batch studies with biofilm formation

Repeated batch experiments were performed under conditions favourable for biofilm development in the feed channel (with spacers). For the draw channel, conditions were kept to avoid biofilm development (i.e., no inoculation and no substrate). Flux through the membrane, as a performance parameter for the FO process, was monitored during the experimental period.

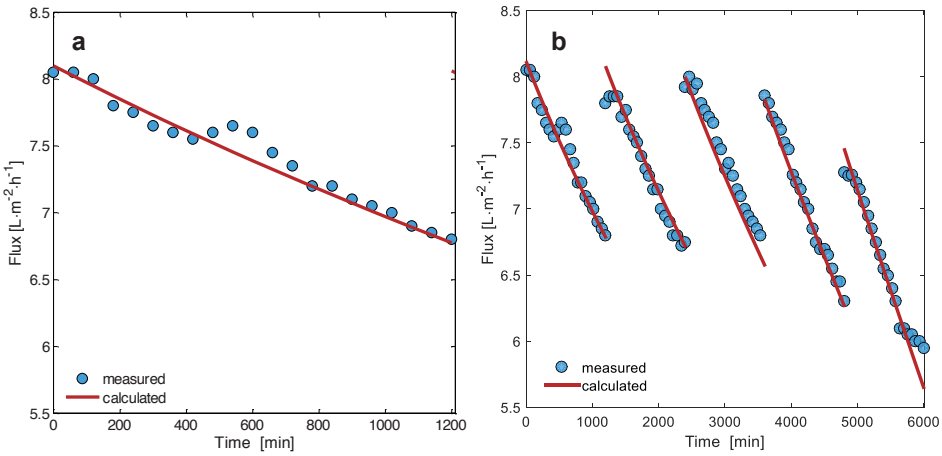

Figure 8-3: (a) Measured (blue circles) and calculated (red line) water flux decline over time due to the dilution of draw solution in batch operation, with spacers but without biofilms. (b) Combined impact of dilution and biofilm formation on flux in forward osmosis system operated in repeated batch mode, measured (blue circles) and model (red lines).

In each cycle, the water flux declined not only because of dilution of the draw solution but also due to biofilm formation. After each cycle (1200 min) the solutions were replaced by fresh solutions, but the biofilm built up in each cycle remained and increasingly affected the flux (Figure 8-3b). As the biomass accumulated in the system, the rate of the flux decline within one cycle increased (i.e. steeper flux-time slopes). The faster water flux decline for the later cycles can be explained by the increased resistance of the developed biofilm (Valladares Linares et al., 2015).

Biofilm properties (such as thickness, permeability, porosity and growth rate) may vary as the biofilm develops. Simulations of the repeated batch experiment were run with simple exponential biofilm growth in the feed channel. This ideal scenario for biofilm growth is probably not realistic for long-term biofilm development, but it proves to be representative for the initial phase of biofilm formation when the nutrients are still in excess (Vrouwenvelder et al., 2009a).

In the numerical model the biomass growth rate (μ) and the initial biofilm thickness ($L_{B,0}$) were set such that the maximum biofilm thickness ($L_{B,E}$) reached at the end of the five cycles was 150 μm, similarly to the thickness measured by Valladares-Linares et al. (2014). To keep the model simple the biofilm porosity (ε_B) was kept constant, while the water permeability of the biofilm (K_B) had to be decreased with the biofilm age. However, for a real

biofilm these parameters (thickness, porosity and water permeability) are changing simultaneously with the biofilm age. For the first two cycles, K_B=10^{-16} m^2, while for last three cycles a smaller value of 10^{-17} m^2 was used in the model to represent the flux measurements (Dreszer et al., 2013; Martin et al., 2014).

In these conditions, the comparison of measured flux decline with the model results shows that the model can describe well the impact of biofilms on the FO process performance (Figure 8-3b).

Biofilm effect on FO performance

The biofilm impact on concentration polarization and the effects of biofilm properties and biofilm location on the performance of an FO process were further evaluated with the calibrated model only, no experimental studies were performed.

Impact of biofilm on water flux and concentration polarization

The effect of spacer presence on water flux was first investigated in a clean FO system. With spacers on both sides of the membrane, a small flux variation was observed along the membrane (± 0.15 $L \cdot m^{-2} \cdot h^{-1}$), while without spacer the flux increased continuously towards the end of the flow channel because of the counter flow operation (Figure 8-4a, blue lines). The average water flux was only one percent higher with spacer than without.

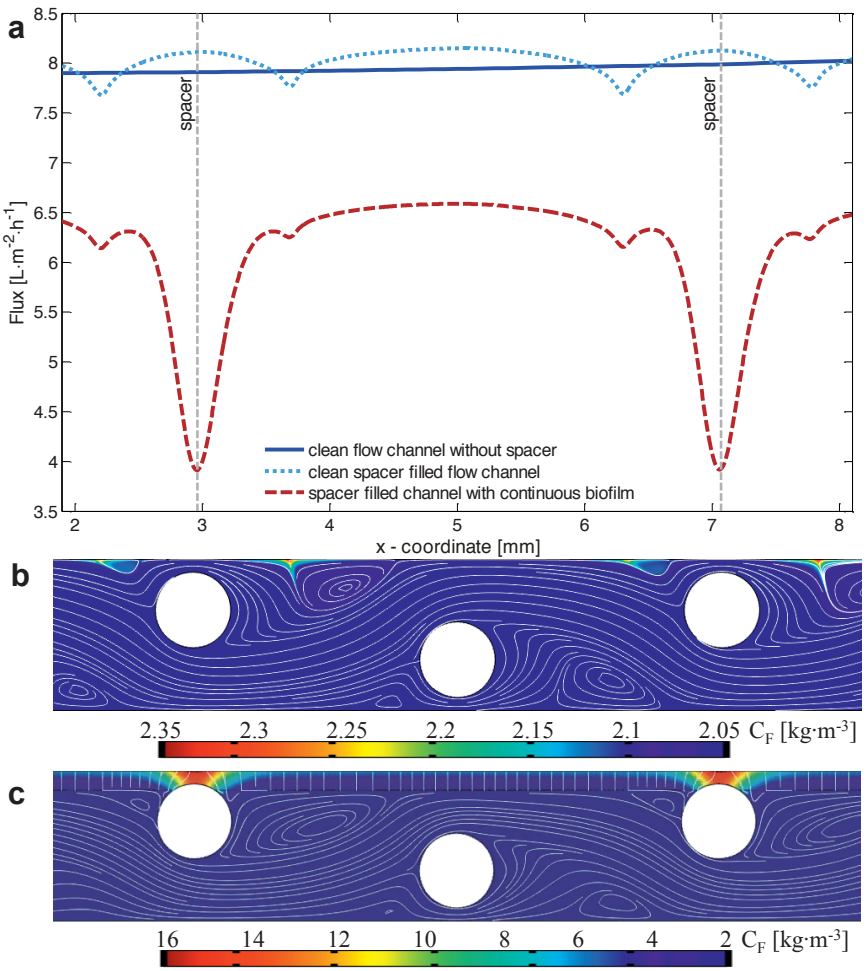

Figure 8-4: (a) Calculated water flux along the membrane: without spacer (continuous blue line), with spacer (dotted blue line) and with spacer and biofilm (dashed red line). The vertical dashed grey lines indicate the locations of the spacer fibres close to the membrane surface. (b) Salt concentration field in clean feed channel. (c) Salt concentration field with uniform thickness biofilm on the feed side of the membrane (top figure). The colours in (b) and (c) represent the solute concentration, the white streamlines indicate the water flow (from left to right). The biofilm leads to large concentration polarization and sharp water flux decrease close to the spacer fibres.

Visualization of the 2-D solute concentration distribution confirms that the presence of spacer has a small influence on the concentration polarization: the maximum solute concentration at the membrane was 2.35 kg m^{-3} (in isolated spots only) compared with an inlet concentration of 2 kg m^{-3} (Figure 8-4b). The role of the spacers is to keep the membrane sheets apart and, by enhancing fluid mixing, to reduce concentration polarization at the membrane surface.

While in reverse osmosis feed spacers are needed to reduce concentration polarization close to the membrane surface (Radu et al., 2010; Subramani et al., 2006), it is known that in FO processes the concentration polarization at the membrane surface (external concentration polarization, ECP) does not significantly affect the water flux (Qin et al., 2010; Tan and Ng, 2008).

The water flux limiting factor in FO processes is the internal concentration polarization (ICP) within the membrane support layer (Gray et al., 2006; McCutcheon and Elimelech, 2006). However, the water flux considerably decreased (~20 percent) when a continuous biofilm on the feed side of the membrane was included in the model. Although the water flux profile along the membrane is similar to the flux profile without biofilm, a sharp flux decrease at the spacer fibres close to the membrane was observed (Figure 8-4a, dashed red line). The sharp flux decrease, corresponding to high ECP, is the result of the 150 μm (L_B) thick biofilm that completely fills up the space between the membrane and spacer fibres close to the membrane (Figure 8-4c).

As shown in Figure 8-5, the presence of spacer and the ECP became important in the presence of biofilms. The osmotic pressure difference (the driving force of the FO process) decreased with 18 percent (an effective $\Delta\pi$=11.7 bar, compared with 14.3 bar) in the case when the spacer fibres are far from the membrane (Figure 8-5a) and with 50 percent (an effective $\Delta\pi$=7.2 bar, compared with 14.2 bar) when the fibres are close to the membrane and, thus, in contact with the biofilm (Figure 8-5b). The biofilm leads to increased ECP because it drastically limits the convective transport and creates a diffusion-dominated mass transfer layer. This is also reflected in the almost linear concentration profiles in the biofilm and support layer (Figure 8-5). At higher water fluxes, the increased contribution of convection may lead to nonlinear concentration profiles in the support layer, as reported in earlier studies (Su and Chung, 2011; Suh and Lee, 2013).

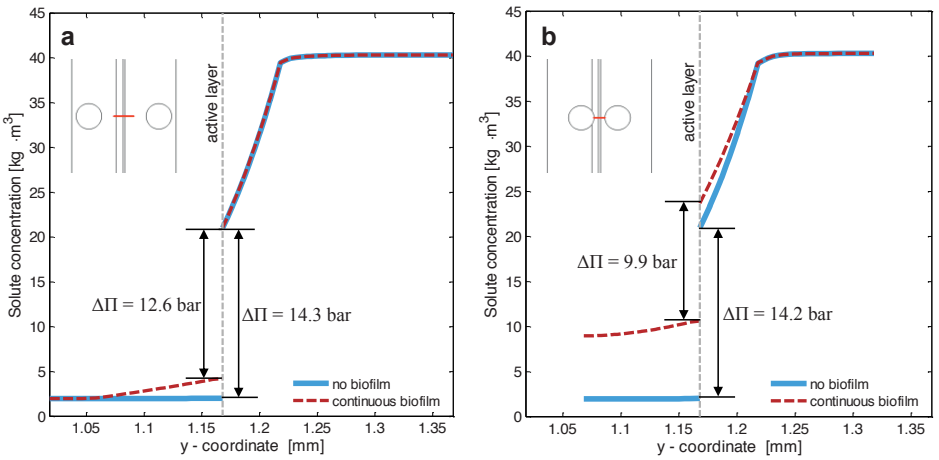

Figure 8-5: Salt concentration profiles in the feed channel, membrane support layer and draw channel next to the membrane, without (continuous blue line) and with (dashed red line) a continuous and uniform biofilm layer. (a) Profiles at a location where the spacer fibres are far from the membrane. (b) Profiles at a position where the spacer fibres are close to the membrane. When the biofilm joins the spacer fibres with the membrane (b), the external concentration polarization is highly increased.

In the lab-scale as well as in a full-scale FO system the spacer is in full contact with the membrane surface at several locations. In these locations, the membrane is "shaded", and no water permeation is possible. Areas next to the spacer fibres close to the membrane are favourable locations for biofilm formation (Araújo et al., 2012a; Baker et al., 1995; Vrouwenvelder et al., 2009a). Furthermore, ECP increases in the biofilm presence and, in the case of a thick and dense biofilm, may even become the limiting factor for the water flux. Similar effects were reported for reverse osmosis systems (Chong et al., 2008a; Radu et al., 2010).

Effect of biofilm properties

As the biofilm develops on the membrane surface, it becomes part of the separation process. Water and solute transport in biofilms are functions of the biofilm hydraulic permeability K_B and porosity ε_B. To simulate the impact of biofilms on the FO processes performance, several biofilm parameters had to be defined. However, experimentally measured biofilm hydraulic resistance or permeability values are scarce in the literature (Dreszer et al., 2013; Martin et al., 2014; McDonogh et al., 1994). The reported values for biofilm hydraulic permeability vary between 10^{-15}-10^{-18} m^2 and most of these were measured for biofilms developed in reverse osmosis or microfiltration systems.

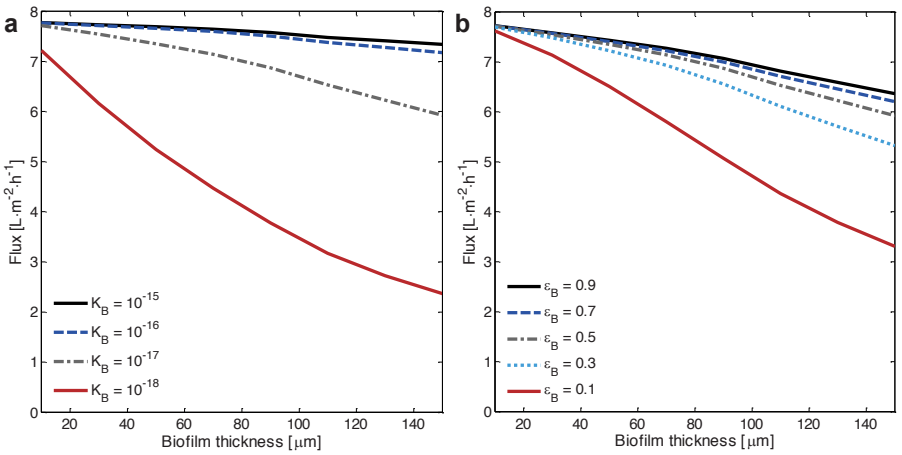

Figure 8-6: Flux decline at different biofilm thickness on the membrane feed side, calculated with spacers in the flow channels. (a) Effect of different biofilm permeability (K_B, in m^2). (b) Effect of different biofilm porosities (ε_B).

To evaluate how the hydraulic permeability influences the permeate production in an FO process, parametric sensitivity simulations were performed with increasing biofilm thickness at various biofilm hydraulic permeability (Figure 8-6a).

Results showed significant flux decline even for a relatively thin biofilm (L_B = 5 μm) when the biofilm hydraulic permeability was K_B=10^{-18} m^2 (Figure 8-6a, continuous red line). However, a compact biofilm with such a low permeability is unlikely to form in FO systems due to the relatively low water flux and pressure. On the other hand, high hydraulic permeability values such as 10^{-15} and 10^{-16} m^2 had an insignificant impact on flux even with thick (>100 μm) biofilms. Therefore, for the simulations with biofilm development compared with the experimental data, previously presented, the K_B was set to 10^{-16} m^2 for thin biofilm (first two cycles) and changed to 10^{-17} m^2 as the biofilm got thicker. For the rest of the simulations, the hydraulic permeability was kept constant at 10^{-17} m^2, in line with values reported by Martin et al. (2014).

Beside hydraulic permeability, the biofilm porosity also affects the permeation flux. Porosity can be defined as the volume fraction of the water phase in the biofilm. In general, as a result of spatial distributions of microbial species, biotic and abiotic components, porosity (along with other biofilm parameters) changes with biofilm age and thickness (Zhang and Bishop, 1994). The impact

on flux of different biofilm porosities was evaluated (Figure 8-6b). Limited information can be found in the literature about biofilm porosity, with values generally varying from 0.2 to 0.9 (Lewandowski, 2000; Picioreanu et al., 2009; Radu et al., 2010; Zhang and Bishop, 1994). Simulations with various porosity and biofilm thickness showed that porosity significantly affects the flux only below values of 0.5, which are usually obtained under fast flow conditions with high erosion and detachment rates. In addition, biofilm maturation can also lead to dense cell layers especially in the deeper part of the biofilm, by this decreasing the biofilm porosity. Moreover, another effect of biofilm porosity is related to the decrease of effective salt diffusion coefficient with decreasing porosity, which leads to enhanced concentration polarization and thus less water flux.

The aim of these simulations was to understand how each parameter individually affects the water flux. Nevertheless, all three biofilm parameters (permeability, porosity and thickness) are linked and, in real biofilm systems, all change simultaneously in time. It was shown that in FO (where no applied hydraulic pressure is present) the biofilms tend to grow thicker and more porous and patchy, therefore with less hydraulic resistance (Kwan et al., 2015). This is contrary to what was observed for biofilms formed under applied hydraulic pressure in RO systems (Kwan et al., 2015; Xie et al., 2015). Clearly, measurements obtained in FO conditions are needed to reveal how the biofilm parameters change in time and to supply the numerical models with realistic parameter values.

Biofilm roughness and membrane surface coverage

In general, an average biofilm thickness is reported in the literature, with no or little information regarding the biofilm distribution along the membrane, due to the difficulty to evaluate the local biofilm thickness under operating conditions. Measurements with dyes colouring the liquid phase in a flow channel (e.g., rhodamine) can give a rough estimate of the average biofilm thickness (Prest et al., 2012; Staal et al., 2011). With other imaging techniques such as optical coherence tomography (OCT) and confocal laser scanning microscopy (CLSM) the local biofilm thickness can be accurately measured but only on small areas (Dreszer et al., 2013; Valladares Linares et al., 2015; West et al., 2015).

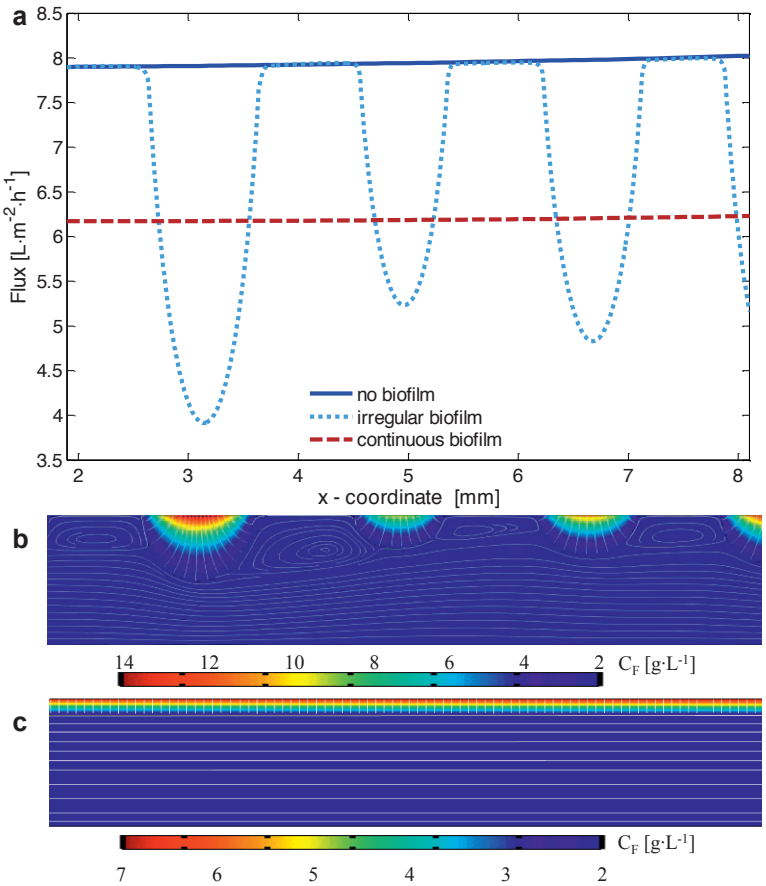

Figure 8-7: (a) Calculated water flux along the membrane: without biofilms (continuous blue line), with patchy biofilm (dotted blue line) and with continuous uniform biofilm (dashed red line), on the membrane active side. The average water flux obtained was: 7.9 $L \cdot m^{-2} \cdot h^{-1}$ (no biofilm), 6.4 $L \cdot m^{-2} \cdot h^{-1}$ (patchy biofilm) and 6 $L \cdot m^{-2} \cdot h^{-1}$ (continuous biofilm). (b) Salt concentration field in the patchy biofilm case. (c) Salt concentration field with uniform thickness biofilm. The colours represent the solute concentration, the white streamlines indicate the water flow (from left to right).

Therefore, to evaluate the impact of membrane coverage with biofilm on the FO flux, numerical simulations were performed with the same amount of biofilm in the feed channel (i.e., same biovolume or average thickness) but with different membrane coverage (i.e., different biofilm roughness and membrane coverage).

Two biofilm types were evaluated with the numerical model. A continuous, constant thickness biofilm covering the whole membrane surface, and a patchy,

irregular biofilm covering only 50 percent of the total membrane area. Figure 8-7a shows the flux profile along the membrane without biofilm and with irregular and continuous biofilm layers. Relative to the flux obtained in the clean channel, the continuous biofilm yielded 20 percent flux decrease. In the case of the patchy biofilm, the flux decrease depends on the local biofilm thickness. Maximum flux is obtained on the membrane areas not covered by biomass, whereas the flux strongly declines under the biomass colonies which lead to more concentration polarization. The biofilm enhanced concentration polarization (BECP) was also observed in the RO process, both experimentally and explained by numerical simulations (Chong et al., 2008a; Herzberg and Elimelech, 2007a; A. I. Radu et al., 2012; Radu et al., 2010). The average water flux over the whole membrane area was with seven percent lower for the continuous foulant layer than for the patchy biofilm (6 $L \cdot m^{-2} \cdot h^{-1}$ compared with 6.4 $L \cdot m^{-2} \cdot h^{-1}$). This effect has been observed also in ultrafiltration (UF) by Martin et al, 2014. Their study concluded that the fouling layer resistance depends not only on the thickness or volume of the fouling layer, but also on its spatial distribution. Namely, for two spatial distributions with the same mean thickness, it was found that the more heterogeneous distribution will have the higher permeate flux (Martin et al., 2014). Our results confirm that the membrane surface coverage by biofilm is indeed an important parameter to be measured and reported, besides the overall biofilm volume or thickness. However, for FO membranes the impact of biofilm resistance is less pronounced than in UF because the membrane resistance in FO is the dominant one, while UF membranes have a lower hydraulic resistance than the biofilm. Typically microfiltration (MF) and UF membranes resistance are between 10^{11} m^{-1} to 10^{13} m^{-1}, while nanofiltration (NF), RO are 10^{-14} m^{-1} to 10^{-15} m^{-1} (Dreszer et al., 2013), compared with the biofilm resistance in this study which was between 10^{-16} and 10^{-17} m^{-1}.

Impact of biofilm location on flux

During indirect water desalination, high salinity water is used as draw solution and impaired-quality water source such as wastewater effluent or urban storm water runoff is used as feed solution (Valladares Linares et al., 2014b). Seawater and brackish water have a high potential as draw solutions in indirect FO processes. In such a case, fouling can occur on both feed and draw sides of the membrane.

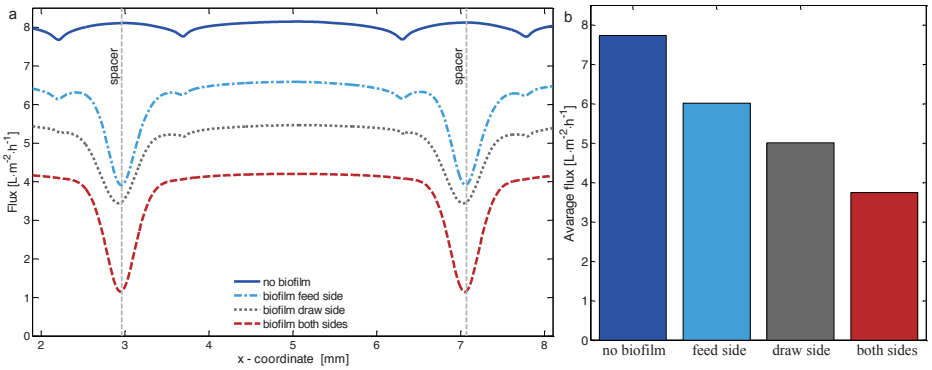

Figure 8-8: Impact of monolayer biofilm location on the water flux, with spacers in the flow channels. (a) Calculated flux along the membrane. (b) Average flux over the whole membrane surface. The four considered scenarios were: no biofilm (continuous blue line), biofilm only on the feed side (blue dotted line), biofilm only at the draw side (grey dash-dot line) and biofilm on both sides (red dashed line) of the membrane. Biofilm presence on the draw side of the membrane leads to higher flux decline than the same amount of biomass was present on the feed side.

To evaluate the impact of fouling on the different membrane sides, simulations were run with continuous biofilm layers (i) only on the feed side, (ii) only on the draw side and (iii) on both sides of the membrane. In general fouling develops faster on the membrane support layer as it was shown by Mi and Elimelech (2008) and Wang et al., (2010). In our study, the membrane support layer is in contact with the draw solution. However, in this model case the biofilm development was not considered: only the impact on membrane performance of the same amount of biomass on the different membrane sides was evaluated (a constant biofilm thickness of 150 µm).A lower water flux resulted when the biofilm was only on the draw side of the membrane, compared with the biofilm on the feed side (6.5 $L \cdot m^{-2} \cdot h^{-1}$ vs. 5.9 $L \cdot m^{-2} \cdot h^{-1}$, respectively, Figure 8-8). This is caused by the higher ECP in the draw channel when a biofilm is present compared with the feed channel (Figure 8-9). Since the draw solution has a significantly higher solute concentration compared to the feed solution, the impact of dilutive ECP in the presence of biofilm is higher. As expected, the highest flux decline was obtained when biofilms of 150 µm thickness were present on both sides of the membrane (Figure 8-8).

Based on the simulation results it can be concluded that fouling on the draw side of the membrane has a higher impact on the FO process performance than on the feed side.

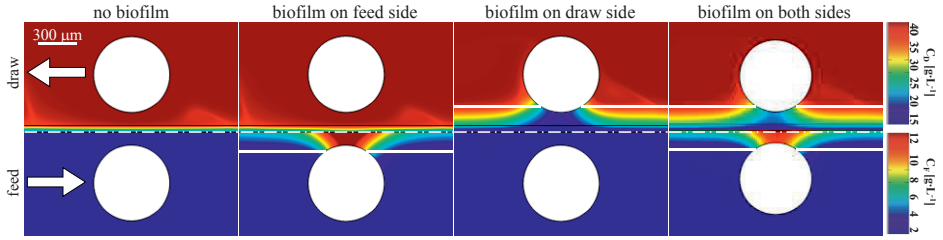

Figure 8-9: Calculated salt concentration fields without biofilm and with biofilm on the feed, draw and on both sides of the membrane. The white circles are the spacer fibres in the flow channels, the continuous white line represents the biofilm surface and the white dash-dot line is the membrane active layer. The largest external concentration polarization is induced by the biofilm presence on the draw side of the membrane. Note the different colour scales for salt concentration in feed (2-12 kg m^{-3}) and in draw solution (15-40 kg m^{-3}).

Foulant deposition on the membrane draw side is possible in indirect desalination with FO when seawater or brackish water is used as draw solution (Valladares Linares et al., 2014b). Since the experiments in FO systems mainly focused on fouling accumulation on the membrane feed side (Mi and Elimelech, 2010; Valladares Linares et al., 2014a, 2014b; Wang et al., 2010), experimental studies are needed to further investigate the impact of biofilm formation in the draw side of the FO membrane.

CONCLUSIONS

The experimental and computational evaluation of biofilm formation in forward osmosis (FO) processes led to the following conclusions:

- Two-dimensional numerical simulations combining fluid flow with salt transport describe well the experimental FO flux measurements at (i) various osmotic pressure differences and (ii) in batch operation with and without biofilm on the membrane active layer.
- The presence of a biofilm on the membrane significantly affects the external concentration polarization and can become the limiting factor for water permeation in FO systems.
- Unlike in RO systems, the same amount of biomass leads to more water flux decline when the biofilm develops on the draw side of the FO membrane compared to the biofilm formed on the feed side, due to higher concentration polarization induced by foulant layer in the draw channel.
- Not only biofilm properties such as hydraulic permeability and mean thickness, but also the biofilm porosity and spatial heterogeneity must be considered when evaluating biofouling effects on the performance

of membrane-based separation systems. Since FO biofilms tend to grow thicker, and more porous than in RO, measurements obtained in FO conditions are needed to reveal how the biofilm parameters change in time and to supply the numerical models with realistic parameter values.

٩

Outlook

GENERAL CONCLUSIONS

This thesis explored different phenomena and factors contributing to biofouling of spiral-wound membrane processes. In order to accurately evaluate the hydrodynamics and nutrient load effects on the foulant accumulation, new experimental devices and methods had to be developed. Furthermore, two- and three-dimensional computational models were build, which coupled hydrodynamics, mass transport and reaction of solutes (salts and microbial nutrients) and biofilm growth.

New experimental devices. First, an automatic control system for obtaining constant flow through membrane fouling simulators was developed and tested (*Chapter 2*). Compared with the manual flow control system (up to ~ 9% variations in flow rate), much lower flow variations were observed for the automatic system (<1% deviations from the set point value). Further, it was shown that fluctuations of feed water flow rate have a direct effect on the pressure drop and biofilm development. Therefore, sensitive water flow monitoring is essential for an accurate evaluation of the impact of fouling accumulation on membrane performance parameters. Second, a miniaturized fully transparent flow cell embedding feed spacer was designed and made out of glass slides to enable particle image velocimetry (PIV) measurements (*Chapter 3*). With this method the two-dimensional velocity flow field could be visualized at different channel heights, thanks to the narrow focal depth of the used lens, therefore enabling the spatial water flow characterization.

Computational models. In parallel with the experimental determination of the flow field in spacer-filled channels, a computational fluid dynamic (CFD) model was developed (*Chapter 3*). Because of the feed spacer presence, the CFD simulations had to be performed in a complex three-dimensional computational domain. The feed spacer geometry was represented in the model with a high accuracy, by taking into account the irregularity of the fibre shape (i.e., necking regions, thick and thin fibres, etc.). Both experimental and numerical results confirmed the existence of laminar steady flow until approximately 0.15 $m \cdot s^{-1}$ and the onset of unsteady flow above this linear flow velocity. The importance of considering accurate feed spacer geometry (versus regular cylinders) was demonstrated (*Chapter 3* and *Chapter 6*). Measurements confirmed that the developed model results matched the measured flow

accurately and could be used for describing and understanding fouling in membrane systems. The model was extended with mass transport of solutes and used to study biofouling effects on the pressure drop in the feed channel (*Chapter 6*) and, for the first time in literature, to describe the biofilm impact on the flux and salt transport in forward osmosis membrane systems (*Chapter 8*).

Impact of biofouling. Using the newly developed experimental setup and numerical models several possible factors affecting biofouling in spiral wound membrane feed channels were evaluated: (i) feed stream nutrient load; (ii) linear flow velocity; (iii) permeate flux; (iv) shear rate by continuous air sparging; (v) feed spacer geometry (shape, thickness); (vi) biofilm location (membrane or spacer in flow channels; feed or draw side in forward osmosis); (vii) membrane and feed spacer surface properties (coatings).

The effect of *nutrient load* on biofouling under various operating conditions was systematically investigated. It was found that the nutrient load is the main factor determining the amount of biofilm accumulated in the feed channels (*Chapter 4*). Namely, an increase in the nutrient load leads to more biomass accumulation in the feed channel. However, the degree in which the biofilm reduces the system performance is influenced by the membrane system operating conditions: the *linear flow velocity* and the *permeate flux*. With an increasing flow velocity and/or permeate flux, for the same amount of biomass, the membrane process performance showed a greater decline. Therefore, to delay the biofilm formation a lower feed flow rate (i.e. linear flow velocity and shear) is recommended, which results as well in a lower impact of biofouling on process performance.

Results of this thesis emphasise the key importance of feed spacers on the biomass accumulation and performance of nanofiltration, reverse and forward osmosis membrane modules (*Chapter 4*, *Chapter 6* and *Chapter 7*). Numerical modelling results revealed that the location where the biofilm forms leads to considerable differences in the feed channel pressure drop. Biofilm on the *spacer filaments* causes a higher feed channel pressure drop than when developed on the membrane surface. This is due to a sharp reduction of *channel porosity* by the biofilm formed on the feed spacer. Feed channel porosity has been shown to have a higher impact on pressure drop increase than spacer thickness only. Moreover, not only the feed spacer thickness but also the

spacer *fibre geometry* is important, because this has a stronger effect on the flow channel porosity. The relative feed channel pressure drop increase due to biomass accumulation, is much higher at smaller channel porosities. Although feed thinner spacers allow higher packing densities of the spiral-wound module (more efficiency without fouling), (Schwinge et al., 2004b), at the same feed flow rate, thicker spacers would promote a lower pressure drop increase when overgrown with biomass (higher efficiency when fouling is present). In forward osmosis the decline in permeate flux can also be reduced by using a thicker spacer.

Numerical simulations on forward osmosis revealed also that external *concentration polarization* is greatly affected by the presence of biofilms (*Chapter 8*). External concentration polarization can therefore become the limiting factor for water permeation in forward osmosis systems. Interestingly, unlike in reserve osmosis systems, the same amount of biomass leads to a stronger water flux decline when the biofilm develops on the draw side of the forward osmosis membrane compared to the biofilm formed on the feed side. Computer simulations indicate that the foulant layer in the draw channel is able to induce a higher external concentration polarization. Since forward osmosis biofilms tend to grow thicker and more porous than reverse osmosis biofilms, this points to the need to acquire more data in forward osmosis conditions in order to determine how the *biofilm parameters* (porosity, hydraulic permeability, thickness) change in time.

Coating (e.g., with amphiphilic copolymers) has been frequently proposed for surface properties modification of membranes, to avoid or reduce membrane fouling in reverse osmosis systems. To evaluate the influence of the coating on biofilm formation, only long-term experiments (weeks with biofilm accumulation) were found suitable. Experiments presented in this thesis showed that coating can delay fouling and that the biofilm composition changed when formed on coated surfaces (*Chapter 5*). Moreover, the applied coating was resistant to membrane cleaning, property not reported by other studies.

In conclusion, all the experiments showed that in spite of various ways to reduce biofouling in spiral-wound membrane systems, its occurrence cannot be avoided but only delayed.

FUTURE DIRECTIONS

Mechanics of biofilm growth and detachment
Experimental and modelling results obtained in this thesis showed that the same amount of biofilm impacted differently the membrane process performance (feed channel pressure drop and flux). It was hypothesized that different biofilm location (membrane and spacer) and biofilm geometrical properties (porosity, thickness and roughness), mechanical characteristics (rigidity, viscoelasticity, density) and hydraulic measures (permeability) would all contribute to the alteration of the process performance. Therefore, future studies should be oriented at: (i) the biofilm structural characterization; (ii) understanding the extent in which each biofilm property affects the membrane separation process performance, (iii) developing methods to engineer biofilm properties so that biofouling would have only a low or delayed impact on the filtration process and to be easily removable.

Biofilm imaging. Most direct biofilm characterization can be obtained by microscopy methods. Scanning electron microscopy (SEM) usually changes the biofilm structure and is it "off-line", therefore other imaging methods must be employed (*Chapter 5* and *Chapter 7*). Confocal laser scanning microscopy (CLSM) can be on-line or off-line and could maintain the biofilm structure, however the sample must be fluorescent (either auto-fluorescent or stained – which may influence the biofilm behaviour and structure). In addition, the observed area with CLSM is rather small for this application (*Chapter 5* and *Chapter 7*). Computed Tomography (CT) can acquire three-dimensional images of the biofilm surface attached to support materials with highly complex geometry, but contrast agents must be added (Haaksman et al., 2017).

Recent progress in the three-dimensional *in-situ* non-destructive biofilm imaging has been achieved by Magnetic Resonance Imaging (MRI) (Graf von der Schulenburg et al., 2008) and Optical Coherence Tomography (OCT) (Blauert et al., 2015). Optical coherence tomography can investigate biofilm formation *in-situ* and without staining.

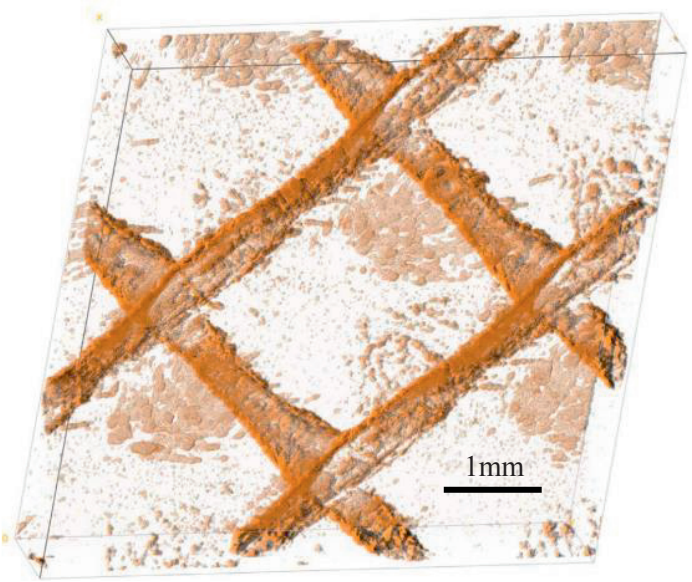

Figure 9-1: Three-dimensional OCT image with biomass (brown colour), feed spacer, membrane and cover glass. Figure adapted from: Fortunato et al. (2017).

It has been used to examine biofouling in membrane filtration systems to evaluated the suitability of OCT to study the biofilm development, and performance parameters change (e.g., feed channel pressure drop, flux) using different types of membranes (RO, UF, MF) (Derlon et al., 2013; Dreszer et al., 2014b; Fortunato et al., 2017a, 2017b).

Biofilm mechanical properties (elasticity modulus and Poisson ratio) can also be estimated from real-time cross sectional OCT scans of biofilms (Blauert et al., 2015).

The main advantages of the OCT technique are: (i) it enables three-dimensional observation and quantification of the biofilm over a representatively large area (millimetres); (ii) it is totally non-invasive, requires no staining and can be performed during the operation of a lab-scale membrane setup and biofilm formation can be observed in time (Figure 9-1). An example of recent study using OCT clearly showing specific and reproducible locations of biofilm growth in a spacer-filled channel with permeation (resented in Figure 9-1).

Biofilm mechanical characterization. Biofilm mechanical and hydraulic properties should be evaluated in relation to operating conditions and with membrane system performance decline. Three-dimensional biofilm scans can

be numerically processed in order to extract structural (morphology) parameters such as: biovolume, biofilm thickness and roughness, porosity (Fortunato et al., 2017a). Importantly, hardly accessible mechanical properties can be evaluated with the time-dependent OCT scans, which is a clear advantage of this technique.

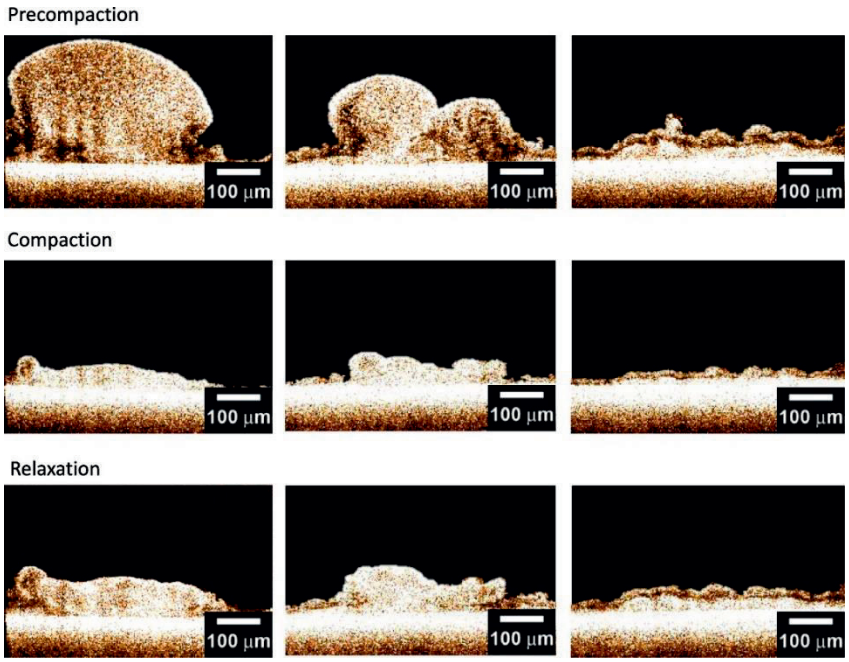

Figure 9-2: Optical coherence tomography the biofilm at different locations in the flow channel: (top) initially; (middle) compacted by flux increase; (bottom) relaxed to the initial permeate flux. Figure from: Valladares Linares et al. (2016).

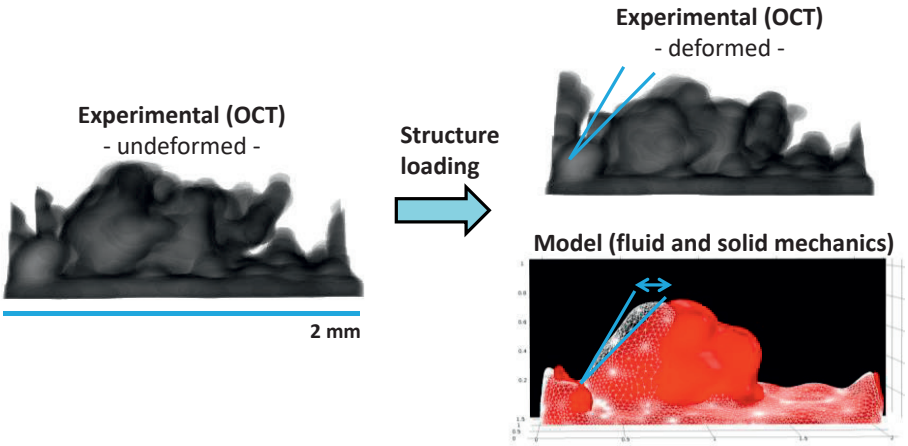

Figure 9-3: Determination of the elastic modulus by using deformed and undeformed biofilm geometry from optical coherence tomography in a fluid-structure interaction numerical model. Figure courtesy of C. Picioreanu.

For example, biofilm rigidity, viscoelasticity and density should be measured, as these strongly correlate with biofilm detachment and therefore with cleanability of the membrane system. Biofilm response under operational changes can be immediately observed, such as compaction with increased water flux (as shown in Figure 9-2).

In this way, the behaviour of biofilms formed in different membrane filtration processes (i.e., reversed osmosis versus forward osmosis) can be evaluated.

Furthermore, the determined biofilm properties can provide input values in numerical models, while models will be used to increase the understanding and to predict biofouling effects on membrane process performance. Base on the three-dimensional OCT scans biofilm properties can be individually evaluated in computational models, which is an advantage because decoupling effects is mostly not possible experimentally (Figure 9-3).

Membrane cleaning methods. Evaluations of new cleaning strategies for biofilm removal are still scarcely reported. By understanding how the biofilm forms and reacts to operation conditions, one could propose more effective cleaning methods. With advanced imaging techniques like optical coherence tomography the immediate impact of various physical and chemical agents could be assessed. Examples of physical cleaning methods include: variation in shear by pulsating flow (Radu et al., 2012) or air sparging (Cornelissen et al.,

2007), back-washing and osmotic shock (Mi and Elimelech, 2010). Chemical cleaning is widely used in industrial applications, however, to what extend is the biofilm removed and the mechanisms of biofilm removal are less known.

Biofouling mitigation strategies

Surface modification. Understanding the early stages of biofilm formation could lead to the development of "antifouling" coatings for membrane and spacer surfaces (*Chapter 5*). Until now, no reported coating could prevent biofilm formation on long term. However, in most of the reports the cleanability of the membrane was not evaluated after the biofilm formed over the coated surface. Therefore, focus could change from biofouling prevention only, to prevention and biofilm removal.

New spacer designs. Based on results obtained in this thesis (e.g., *Chapter 6* and *Chapter 7*), the spacer geometry plays an important role on biofilm formation and, most probably, also on the efficient biofilm removal from the membrane system.

A possible optimization loop leading to the design of better spacers is suggested in Figure 9-4. Several commercial feed spacers can be screened for their hydrodynamics, mass transport and fouling properties (*Chapter 6*). An accurate geometry can be obtained by X-ray computed tomography of a selected spacer (CT scanning step (Haaksman et al., 2017)). This geometry is imported in a computer aided design (CAD) package and a virtual three-dimensional (3D) spacer model will be generated. This virtual model is furthermore altered so that a redesigned spacer geometry will be proposed, according to pre-existing knowledge on how different spacer elements contribute to membrane performance. The new spacer design is first evaluated numerically for hydrodynamics and mass transfer properties (CFD models, (Haaksman et al., 2017)). Based on the numerical simulations, the spacer geometry is further improved. Once the simulations indicate a superior spacer, a prototype will be manufactured by three-dimensional printing (Siddiqui et al., 2016). The prototype is further evaluated in lab-scale experimental setups (e.g., in membrane fouling simulators) for hydrodynamics (pressure drop and permeation), mass transfer (concentration polarization) and fouling behaviour (biofouling, scaling) and associated cleanability.

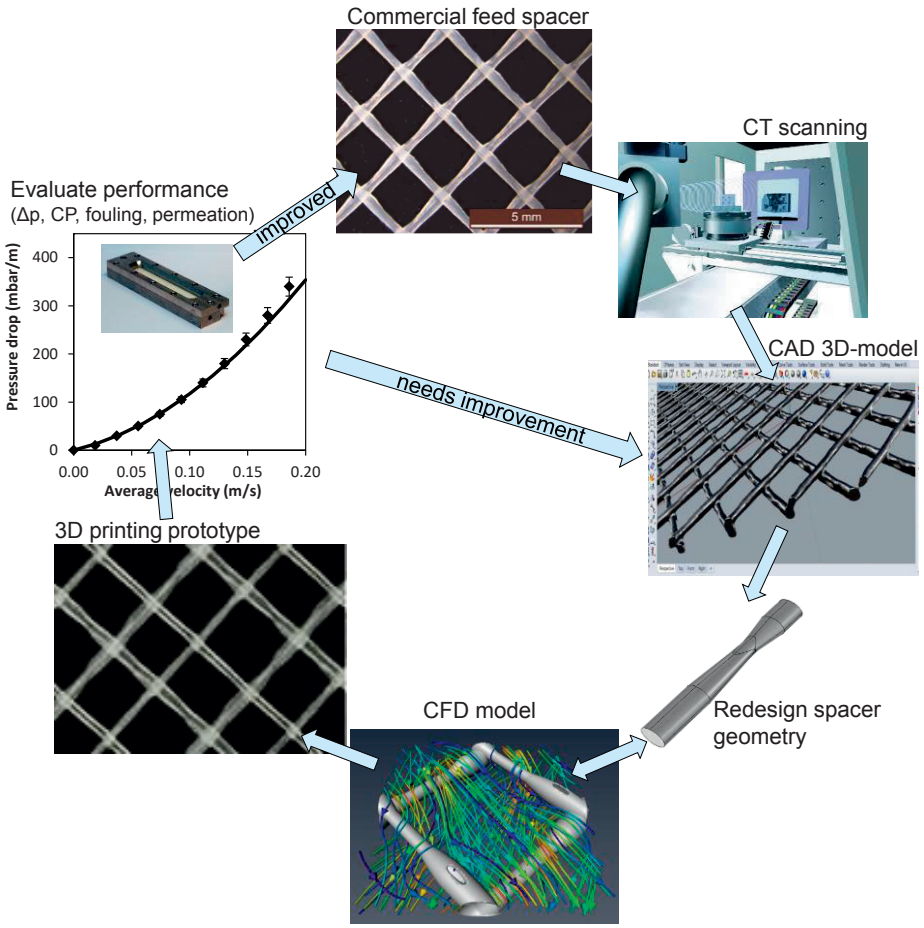

Figure 9-4: Proposed steps in the design of improved spacers for membrane filtration systems.

If the lab-scale tests indicate a successful spacer design, this can be transferred to pilot scale and eventually it could be commercialized. If the tests reveal that the spacer need improvement, a new virtual design should be proposed and the testing cycle continues (Figure 9-4).

Numerical evaluation. For an accurate assessment of the virtual design, progress in the numerical modelling has to be achieved in several areas. The computational fluid dynamics would need to include, beside the laminar steady flow (*Chapter 6* and *Chapter 8*) also the unsteady and time-dependent flows. As it was shown in this thesis (*Chapter 3*) at velocities used in practice the flow begins to develop unsteady behaviour. Especially in fouling conditions the flow channel porosity changes which may lead to onset of flow instability.

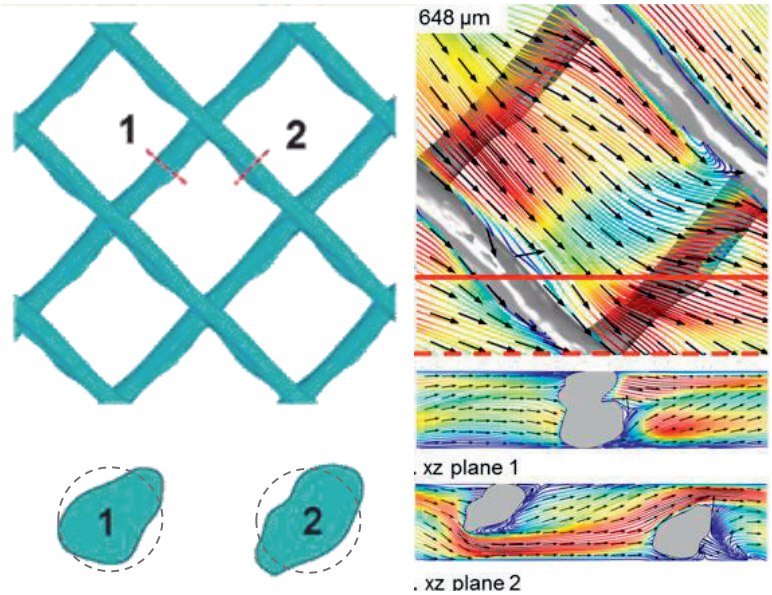

Figure 9-5: Top view and cross sections of a spacer geometry scanned by X-ray computed tomography (CT) together with simulated water flow. Figure adapted from Haaksman et al. (2017). The dashed-line circles represent cross-sections as they would appear from top-view microscopic observation.

This requires the use of computational fluid dynamics methods which can represent both steady and unsteady flows, such as direct numerical simulations (DNS) (Fortunato et al., 2017b; Koutsou et al., 2007). Another important aspect of the numerical simulations which has to be considered is the representativeness of the modelled spacer geometry.

As the spacer fibres in practise do not have a perfectly circular cross-section and their diameter is variable along the fibres (Haaksman et al., 2017), the simplified spacer geometries (used as well in this thesis) may not be sufficient to characterize the hydraulic impact of the virtual spacer (Figure 9-5). Therefore, spacers geometries derived from X-ray computed tomography scans should be used in numerical simulations.

CONCLUSIONS

1. Controlling biofouling and biofilm formation requires better understanding of biofilm development under representative hydraulic conditions for practise.

2. Novel imaging and analytical methods allows to study biofilm formation on-line in-situ and are able to deliver information on the biofilm morphology and mechanical properties.
3. Understanding biofilms mechanics, novel control and engineering strategies can be developed to mitigate biofouling in spiral wound membrane systems.

References

Achilli, A., Prante, J.L., Hancock, N.T., Maxwell, E.B., Childress, A.E., 2014. Experimental results from RO-PRO: A next generation system for low-energy desalination. Environ. Sci. Technol. 48, 6437–6443. doi:10.1021/es405556s

Adout, A., Kang, S., Asatekin, A., Mayes, A.M., Elimelech, M., 2010. Ultrafiltration membranes incorporating amphiphilic comb copolymer additives prevent irreversible adhesion of bacteria. Environ. Sci. Technol. 44, 2406–11. doi:10.1021/es902908g

Ahmad, A.L., Lau, K.K., Abu Bakar, M.Z., 2005. Impact of different spacer filament geometries on concentration polarization control in narrow membrane channel. J. Memb. Sci. 262, 138–152. doi:10.1016/j.memsci.2005.06.056

Al Ashhab, A., Gillor, O., Herzberg, M., 2014. Biofouling of reverse-osmosis membranes under different shear rates during tertiary wastewater desalination: Microbial community composition. Water Res. 67, 86–95. doi:10.1016/j.watres.2014.09.007

Amadei, C.A., Yang, R., Chiesa, M., Gleason, K.K., Santos, S., 2014. Revealing Amphiphilic Nanodomains of Anti-Biofouling Polymer Coatings. ACS Appl. Mater. Interfaces 6, 4705–4712. doi:10.1021/am405159f

An, G., Lin, J., Li, J., Jian, X., 2011. In situ monitoring of membrane fouling in spiral-wound RO modules by UTDR with a sound intensity modeling. Desalin. Water Treat. 32, 226–233. doi:10.5004/dwt.2011.2704

Antony, A., Low, J.H., Gray, S., Childress, A.E., Le-Clech, P., Leslie, G., 2011. Scale formation and control in high pressure membrane water treatment systems: A review. J. Memb. Sci. 383, 1–16. doi:10.1016/j.memsci.2011.08.054

Araújo, P.A., Kruithof, J.C., Van Loosdrecht, M.C.M., Vrouwenvelder, J.S., 2012a. The potential of standard and modified feed spacers for biofouling control. J. Memb. Sci. 403–404, 58–70. doi:10.1016/j.memsci.2012.02.015

Araújo, P.A., Miller, D.J., Correia, P.B., van Loosdrecht, M.C.M., Kruithof, J.C., Freeman, B.D., Paul, D.R., Vrouwenvelder, J.S., 2012b. Impact of feed spacer and membrane modification by hydrophilic, bactericidal and biocidal coating on biofouling control. Desalination 295, 1–10. doi:10.1016/j.desal.2012.02.026

Asatekin, A., Olivetti, E.A., Mayes, A.M., 2009. Fouling resistant, high flux nanofiltration membranes from polyacrylonitrile-graft-poly(ethylene oxide). J. Memb. Sci. 332, 6–12. doi:10.1016/j.memsci.2009.01.029

ASTM, 1993. ASTM Standards on Material and Environmental Microbiology.

Baker, J., Stephenson, T., Dard, S., Cote, P., 1995. Characterisation of fouling of nanofiltration membranes used to treat surface waters. Environ. Technol. 16, 977–985. doi:10.1080/09593331608616335

Baker, J.S., Dudley, L.Y., 1998. Biofouling in membrane systems — A review. Desalination 118, 81–89. doi:10.1016/S0011-9164(98)00091-5

Bakke, R., Kommedal, R., Kalvenes, S., 2001. Quantification of biofilm accumulation by an optical approach. J. Microbiol. Methods 44, 13–26. doi:10.1016/S0167-

7012(00)00236-0

Bartels, C., Hirose, M., Fujioka, H., 2008. Performance advancement in the spiral wound RO/NF element design. Desalination 221, 207–214. doi:10.1016/j.desal.2007.01.077

Baxamusa, S.H., Gleason, K.K., 2009. journal of membrane. Adv. Funct. Mater. 19, 3489–3496. doi:10.1002/adfm.200900943

Ben-Sasson, M., Zodrow, K.R., Genggeng, Q., Kang, Y., Giannelis, E.P., Elimelech, M., 2014. Surface functionalization of thin-film composite membranes with copper nanoparticles for antimicrobial surface properties. Environ. Sci. Technol. 48, 384–393. doi:10.1021/es404232s

Bereschenko, L.A., Prummel, H., Euverink, G.J.W., Stams, A.J.M., van Loosdrecht, M.C.M., 2011. Effect of conventional chemical treatment on the microbial population in a biofouling layer of reverse osmosis systems. Water Res. 45, 405–416. doi:10.1016/j.watres.2010.07.058

Bertheas, U., Majamaa, K., Arzu, A., Pahnke, R., 2009. Use of DBNPA to control biofouling in RO systems. Desalin. Water Treat. 3, 175–178. doi:10.5004/dwt.2009.457

Beun, J.J., Van Loosdrecht, M.C.M., Heijnen, J.J., 2002. Aerobic granulation in a sequencing batch airlift reactor. Water Res. 36, 702–712. doi:10.1016/S0043-1354(01)00250-0

Beyenal, H., Donovan, C., Lewandowski, Z., Harkin, G., 2004. Three-dimensional biofilm structure quantification. J. Microbiol. Methods 59, 395–413. doi:10.1016/j.mimet.2004.08.003

Beyer, F., Rietman, B.M., Zwijnenburg, A., van den Brink, P., Vrouwenvelder, J.S., Jarzembowska, M., Laurinonyte, J., Stams, A.J.M., Plugge, C.M., 2014. Long-term performance and fouling analysis of full-scale direct nanofiltration (NF) installations treating anoxic groundwater. J. Memb. Sci. 468, 339–348. doi:10.1016/j.memsci.2014.06.004

Blanco, A., Torres, E., Fuente, E., Negro, C., 2011. New Tool To Monitor Biofilm Growth in Industrial Process Waters. Ind. Eng. Chem. Res. A-H. doi:dx.doi.org/10.1021/ie101422m

Blauert, F., Horn, H., Wagner, M., 2015. Time-resolved biofilm deformation measurements using optical coherence tomography. Biotechnol. Bioeng. 112, 1893–1905. doi:10.1002/bit.25590

Boo, C., Elimelech, M., Hong, S., 2013. Fouling control in a forward osmosis process integrating seawater desalination and wastewater reclamation. J. Memb. Sci. 444, 148–156. doi:10.1016/j.memsci.2013.05.004

Boorsma, M.J.J., Dost, S., Klinkhamer, S., Schippers, J.C.C., 2011. Monitoring and controlling biofouling in an integrated membrane system. Desalin. Water Treat. 31, 347–353. doi:10.5004/dwt.2011.2352

Brzozowska, A.M., Spruijt, E., de Keizer, A., Cohen Stuart, M.A., Norde, W., 2011.

On the stability of the polymer brushes formed by adsorption of ionomer complexes on hydrophilic and hydrophobic surfaces. J. Colloid Interface Sci. 353, 380–91. doi:10.1016/j.jcis.2010.09.074

Bucs, S.S., Farhat, N., Siddiqui, A., Valladares Linares, R., Radu, A., Kruithof, J.C., Vrouwenvelder, J.S., 2015. Development of a setup to enable stable and accurate flow conditions for membrane biofouling studies. Desalin. Water Treat. 1–9. doi:10.1080/19443994.2015.1057037

Bucs, S.S., Linares, R.V., Marston, J.O., Radu, A.I., Vrouwenvelder, J.S., Picioreanu, C., 2015. Experimental and numerical characterization of the water flow in spacer-filled channels of spiral-wound membranes. Water Res. 87, 299–310. doi:10.1016/j.watres.2015.09.036

Bucs, S.S., Radu, A.I., Lavric, V., Vrouwenvelder, J.S., Picioreanu, C., 2014a. Effect of different commercial feed spacers on biofouling of reverse osmosis membrane systems: A numerical study. Desalination 343, 26–37. doi:10.1016/j.desal.2013.11.007

Bucs, S.S., Valladares Linares, R., van Loosdrecht, M.C.M., Kruithof, J.C., Vrouwenvelder, J.S., 2014b. Impact of organic nutrient load on biomass accumulation, feed channel pressure drop increase and permeate flux decline in membrane systems. Water Res. 67, 227–42. doi:10.1016/j.watres.2014.09.005

Butt, F.H., Rahman, F., Baduruthamal, U., 1997. Hollow fine fiber vs. spiral-wound RO desalination membranes Part 1: Pilot plant evaluation. Desalination 109, 67–82. doi:10.1016/S0011-9164(97)00053-2

Carnahan, R.P., Bolin, L., Suratt, W., 1995. Biofouling of PVD-1 reverse osmosis elements in the water treatment plant of the City of Dunedin, Florida. Desalination 102, 235–244. doi:10.1016/0011-9164(95)00059-B

Casey, T.A., Sakakibara, J., Thoroddsen, S.T., 2013. Scanning tomographic particle image velocimetry applied to a turbulent jet. Phys. Fluids 25, 25102. doi:10.1063/1.4790640

Cath, T.Y., Adams, D., Childress, A.E., 2005. Membrane contactor processes for wastewater reclamation in space: II. Combined direct osmosis, osmotic distillation, and membrane distillation for treatment of metabolic wastewater. J. Memb. Sci. 257, 111–119. doi:10.1016/j.memsci.2004.07.039

Chekli, L., Phuntsho, S., Shon, H.K., Vigneswaran, S., Kandasamy, J., Chanan, A., 2012. A review of draw solutes in forward osmosis process and their use in modern applications. Desalin. Water Treat. 43, 167–184. doi:10.1080/19443994.2012.672168

Chen, M.-Y., Lee, D.-J., Yang, Z., Peng, X.F., Lai, J.Y., 2006. Fluorecent Staining for Study of Extracellular Polymeric Substances in Membrane Biofouling Layers. Environ. Sci. Technol. 40, 6642–6646. doi:10.1021/es0612955

Chong, T.H., Wong, F., Fane, A., 2008a. The effect of imposed flux on biofouling in reverse osmosis: Role of concentration polarisation and biofilm enhanced osmotic pressure phenomena. J. Memb. Sci. 325, 840–850.

doi:10.1016/j.memsci.2008.09.011

Chong, T.H., Wong, F.S., Fane, A.G., 2008b. Implications of critical flux and cake enhanced osmotic pressure (CEOP) on colloidal fouling in reverse osmosis: Experimental observations. J. Memb. Sci. 314, 101–111. doi:10.1016/j.memsci.2008.01.030

Cloete, T.E., Maluleke, M.R., 2005. The use of the Rotoscope as an online, real-time, non-destructive biofilm monitor. Water Sci. Technol. 52, 211–216.

Cornelissen, E., Vrouwenvelder, J.S., Heijman, S., Viallefont, X., Vanderkooij, D., Wessels, L.P., 2007. Periodic air/water cleaning for control of biofouling in spiral wound membrane elements. J. Memb. Sci. 287, 94–101. doi:10.1016/j.memsci.2006.10.023

Creber, S.A., Pintelon, T.R., Graf von der Schulenburg, D.A.W., Vrouwenvelder, J.S., van Loosdrecht, M.C.M., Johns, M.L., 2010a. Magnetic resonance imaging and 3D simulation studies of biofilm accumulation and cleaning on reverse osmosis membranes. Food Bioprod. Process. 88, 401–408. doi:10.1016/j.fbp.2010.08.010

Creber, S.A., Vrouwenvelder, J.S., van Loosdrecht, M.C.M., Johns, M.L., 2010b. Chemical cleaning of biofouling in reverse osmosis membranes evaluated using magnetic resonance imaging. J. Memb. Sci. 362, 202–210. doi:10.1016/j.memsci.2010.06.052

Crittenden, O.C., Rhodes Trussell, R., Hand, D.W., Howe, K.G., Tchobanoglous, G., 2012. MWH's Water Treatment: Principles and Design, Third edit. ed. John Wiley & Sons, Inc. doi:10.1002/9781118131473

Da Costa, A.R., Fane, A.G., Wiley, D.E., 1994. Spacer characterization and pressure drop modelling in spacer-filled channels for ultrafiltration. J. Memb. Sci. 87, 79–98. doi:10.1016/0376-7388(93)E0076-P

Derlon, N., Koch, N., Eugster, B., Posch, T., Pernthaler, J., Pronk, W., Morgenroth, E., 2013. Activity of metazoa governs biofilm structure formation and enhances permeate flux during Gravity-Driven Membrane (GDM) filtration. Water Res. 47, 2085–2095. doi:10.1016/j.watres.2013.01.033

Dickson, J.M., Whitacker, G., DeLeeuw, J., Spencer, J., 1994. Dilute single and mixed solute systems in a spiral wound reverse osmosis module. Part II. Experimental data and application of the model. Desalination 99, 1–18. doi:10.1016/0011-9164(94)00116-2

Donlan, R.M., Piede, J.A., Heyes, C.D., Sanii, L., Murga, R., Edmonds, P., El-Sayed, I., El-Sayed, M.A., 2004. Model system for growing and quantifying Streptococcus pneumoniae biofilms in situ and in real time. Appl. Environ. Microbiol. 70, 4980–4988. doi:10.1128/AEM.70.8.4980-4988.2004

DOW, 2014. DOW FILMTEC™ Membranes, Cleaning Procedures for DOW FILMTEC FT30 Elements.

Dreszer, C., Flemming, H.-C., Wexler, A.D., Zwijnenburg, A., Kruithof, J.C., Vrouwenvelder, J.S., 2014a. Development and testing of a transparent membrane biofouling monitor. Desalin. Water Treat. 52, 1807–1819.

doi:10.1080/19443994.2013.874708

Dreszer, C., Vrouwenvelder, J.S., Paulitsch-Fuchs, A.H., Zwijnenburg, A., Kruithof, J.C., Flemming, H.C., 2013. Hydraulic resistance of biofilms. J. Memb. Sci. 429, 436–447. doi:10.1016/j.memsci.2012.11.030

Dreszer, C., Wexler, A.D.D., Drusová, S., Overdijk, T., Zwijnenburg, A., Flemming, H.-C.H.-C., Kruithof, J.C.C., Vrouwenvelder, J.S.J.S., 2014b. In-situ biofilm characterization in membrane systems using Optical Coherence Tomography: formation, structure, detachment and impact of flux change. Water Res. 67, 243–54. doi:10.1016/j.watres.2014.09.006

Duddridge, J.E., Kent, C.A., Laws, J.F., 1982. Effect of Surface Shear Stress on the Attachment of\rPseudomonas fluorescens to Stainless Steel under\rDefined Flow Conditions. Biotechnol. Bioeng. 24, 153–164.

Elsinga, G.E.E., Scarano, F., Wieneke, B., Oudheusden, B.W. van W. van, 2005. Tomographic particle image velocimetry, in: 6th International Symposium on Particle Image Velocimetry. Pasadena, pp. 933–947.

Fimbres-Weihs, G.A., Wiley, D.E., 2010. Review of 3D CFD modeling of flow and mass transfer in narrow spacer-filled channels in membrane modules. Chem. Eng. Process. Process Intensif. 49, 759–781. doi:10.1016/j.cep.2010.01.007

Fimbres-Weihs, G.A., Wiley, D.E., Fletcher, D.F., 2006. Unsteady Flows with Mass Transfer in Narrow Zigzag Spacer-Filled Channels: A Numerical Study. Ind. Eng. Chem. Res. 45, 6594–6603. doi:10.1021/ie0602431

Fimbres-Weihs, G.A., Wiley, D.E.E., 2007. Numerical study of mass transfer in three-dimensional spacer-filled narrow channels with steady flow. J. Memb. Sci. 306, 228–243. doi:10.1016/j.memsci.2007.08.043

Flemming, H.-C., 2002. Biofouling in water systems--cases, causes and countermeasures. Appl. Microbiol. Biotechnol. 59, 629–40. doi:10.1007/s00253-002-1066-9

Flemming, H.-C., 1997. Reverse osmosis membrane biofouling. Exp. Therm. Fluid Sci. 14, 382–391. doi:10.1016/S0894-1777(96)00140-9

Flemming, H.-C., Schaule, G., Griebe, T., Schmitt, J., Tamachkiarowa, A., 1997. Biofouling—the Achilles heel of membrane processes. Desalination 113, 215–225. doi:10.1016/S0011-9164(97)00132-X

Flemming, H.-C., Wingender, J., 2010. The biofilm matrix. Nat Rev Micro 8, 623–633.

Flemming, H.C., 2003. Role and levels of real-time monitoring for successful anti-fouling strategies - An overview, in: Water Science and Technology. pp. 1–8.

Fortunato, L., Bucs, S., Linares, R.V., Cali, C., Vrouwenvelder, J.S., Leiknes, T., 2017a. Spatially-resolved in-situ quantification of biofouling using optical coherence tomography (OCT) and 3D image analysis in a spacer filled channel. J. Memb. Sci. 524, 673–681. doi:10.1016/j.memsci.2016.11.052

Fortunato, L., Qamar, A., Wang, Y., Jeong, S., Leiknes, T., 2017b. In-situ assessment of biofilm formation in submerged membrane system using optical coherence

tomography and computational fluid dynamics. J. Memb. Sci. 521, 84–94. doi:10.1016/j.memsci.2016.09.004

Gao, Y., Haavisto, S., Tang, C.Y., Salmela, J., Li, W., 2013. Characterization of fluid dynamics in spacer-filled channels for membrane filtration using Doppler optical coherence tomography. J. Memb. Sci. 448, 198–208. doi:10.1016/j.memsci.2013.08.011

GE Water, 2009. Utilization of Chemical Treatments to Maintain and Restore Membrane Performance.

Geraldes, V., Semião, V., de Pinho, M.N., 2002. The effect of the ladder-type spacers configuration in NF spiral-wound modules on the concentration boundary layers disruption. Desalination 146, 187–194. doi:10.1016/S0011-9164(02)00467-8

Geraldes, V., Semião, V., Norberta Pinho, M., 2003. Hydrodynamics and concentration polarization in NF/RO spiral-wound modules with ladder-type spacers. Desalination 157, 395–402. doi:10.1016/S0011-9164(03)00422-3

Gimmelshtein, M., Semiat, R., 2005. Investigation of flow next to membrane walls. J. Memb. Sci. 264, 137–150. doi:10.1016/j.memsci.2005.04.033

Graf von der Schulenburg, D.A., Pintelon, T.R.R., Picioreanu, C., Van Loosdrecht, M.C.M., Johns, M.L., 2009. Three-dimensional simulations of biofilm growth in porous media. AIChE J. 55, 494–504. doi:10.1002/aic.11674

Graf von der Schulenburg, D.A., Vrouwenvelder, J.S., Creber, S.A., van Loosdrecht, M.C.M., Johns, M.L., 2008. Nuclear magnetic resonance microscopy studies of membrane biofouling. J. Memb. Sci. 323, 37–44. doi:10.1016/j.memsci.2008.06.012

Gray, G.T., McCutcheon, J.R., Elimelech, M., 2006. Internal concentration polarization in forward osmosis: role of membrane orientation. Desalination 197, 1–8. doi:10.1016/j.desal.2006.02.003

Greenlee, L.F., Lawler, D.F., Freeman, B.D., Marrot, B., Moulin, P., 2009. Reverse osmosis desalination: Water sources, technology, and today's challenges. Water Res. 43, 2317–2348. doi:10.1016/j.watres.2009.03.010

Guillen, G., Hoek, E.M. V, 2009. Modeling the impacts of feed spacer geometry on reverse osmosis and nanofiltration processes. Chem. Eng. J. 149, 221–231. doi:10.1016/j.cej.2008.10.030

Haaksman, V.A., Siddiqui, A., Schellenberg, C., Kidwell, J., Vrouwenvelder, J.S., Picioreanu, C., 2017. Characterization of feed channel spacer performance using geometries obtained by X-ray computed tomography. J. Memb. Sci. 522, 124–139. doi:10.1016/j.memsci.2016.09.005

Habimana, O., Semião, A.J.C., Casey, E., 2014. The role of cell-surface interactions in bacterial initial adhesion and consequent biofilm formation on nanofiltration/reverse osmosis membranes. J. Memb. Sci. 454, 82–96. doi:10.1016/j.memsci.2013.11.043

Herzberg, M., Elimelech, M., 2007a. Biofouling of reverse osmosis membranes: Role

of biofilm-enhanced osmotic pressure. J. Memb. Sci. 295, 11–20. doi:10.1016/j.memsci.2007.02.024

Herzberg, M., Elimelech, M., 2007b. Physiology and genetic traits of reverse osmosis membrane biofilms: a case study with Pseudomonas aeruginosa. ISME J 2, 180–194.

Hickenbottom, K.L., Hancock, N.T., Hutchings, N.R., Appleton, E.W., Beaudry, E.G., Xu, P., Cath, T.Y., 2013. Forward osmosis treatment of drilling mud and fracturing wastewater from oil and gas operations. Desalination 312, 60–66. doi:10.1016/j.desal.2012.05.037

Hobbie, J.E., Daley, R.J., Jasper, S., 1977. Use of nuclepore filters for counting bacteria by fluorescence microscopy. Appl. Environ. Microbiol. 33, 1225–1228.

Holloway, R.W., Childress, A.E., Dennett, K.E., Cath, T.Y., 2007. Forward osmosis for concentration of anaerobic digester centrate. Water Res. 41, 4005–14. doi:10.1016/j.watres.2007.05.054

Hoover, L.A., Phillip, W.A., Tiraferri, A., Yip, N.Y., Elimelech, M., 2011. Forward with osmosis: Emerging applications for greater sustainability. Environ. Sci. Technol. 45, 9824–9830. doi:10.1021/es202576h

Hunter, J.D., 2007. MatplotlibL A 2D graphics environment. Comput. Sci. Eng. 9, 90–95.

Hydranautics, 2001. Troubleshooting Your RO – Hydranautics.

Kang, G., Cao, Y., 2012. Development of antifouling reverse osmosis membranes for water treatment: A review. Water Res. 46, 584–600. doi:10.1016/j.watres.2011.11.041

Kang, S., Choi, H., 2005. Effect of surface hydrophobicity on the adhesion of S. cerevisiae onto modified surfaces by poly(styrene-ran-sulfonic acid) random copolymers. Colloids Surfaces B Biointerfaces 46, 70–77. doi:10.1016/j.colsurfb.2005.08.017

Khan, M.T., Busch, M., Molina, V.G., Emwas, A.H., Aubry, C., Croue, J.P., 2014. How different is the composition of the fouling layer of wastewater reuse and seawater desalination RO membranes? Water Res. 59, 271–282. doi:10.1016/j.watres.2014.04.020

Kim, I.C., Lee, K.H., 2006. Dyeing process wastewater treatment using fouling resistant nanofiltration and reverse osmosis membranes. Desalination 192, 246–251. doi:10.1016/j.desal.2005.05.030

Koutsou, C.P., Karabelas, a. J., 2010. Towards optimization of spacer geometrical characteristics for spiral wound membrane modules. Desalin. Water Treat. 18, 139–150. doi:10.5004/dwt.2010.1382

Koutsou, C.P., Yiantsios, S.G., Karabelas, A.J., 2009. A numerical and experimental study of mass transfer in spacer-filled channels: Effects of spacer geometrical characteristics and Schmidt number. J. Memb. Sci. 326, 234–251. doi:10.1016/j.memsci.2008.10.007

Koutsou, C.P.P., Yiantsios, S.G.G., Karabelas, A.J.J., 2007. Direct numerical simulation of flow in spacer-filled channels: Effect of spacer geometrical characteristics. J. Memb. Sci. 291, 53–69. doi:10.1016/j.memsci.2006.12.032

Krebs, C.J., 1999. Ecological Methodology, 2nd ed. Benjamin/Cummings.

Kwan, S.E., Bar-Zeev, E., Elimelech, M., 2015. Biofouling in forward osmosis and reverse osmosis: Measurements and mechanisms. J. Memb. Sci. 493, 703–708. doi:10.1016/j.memsci.2015.07.027

Kwok, W.K., Picioreanu, C., Ong, S.L., Van Loosdrecht, M.C.M., Ng, W.J., Heijnen, J.J., 1998. Influence of biomass production and detachment forces on biofilm structures in a biofilm airlift suspension reactor. Biotechnol. Bioeng. 58, 400–407. doi:10.1002/(SICI)1097-0290(19980520)58:4<400::AID-BIT7>3.0.CO;2-N

Lattemann, S., Kennedy, M.D., Schippers, J.C., Amy, G., 2010. Chapter 2 Global Desalination Situation. Sustain. Sci. Eng. doi:10.1016/S1871-2711(09)00202-5

Lehtola, M.J., Juhna, T., Miettinen, I.T., Vartiainen, T., Martikainen, P.J., 2004. Formation of biofilms in drinking water distribution networks, a case study in two cities in Finland and Latvia. J. Ind. Microbiol. Biotechnol. 31, 489–494. doi:10.1007/s10295-004-0173-2

Lewandowski, Z., 2000. Notes on biofilm porosity. Water Res. 34, 2620–2624. doi:10.1016/S0043-1354(00)00186-X

Li, D., Zhang, X., Simon, G.P., Wang, H., 2013. Forward osmosis desalination using polymer hydrogels as a draw agent: Influence of draw agent, feed solution and membrane on process performance. Water Res. 47, 209–215. doi:10.1016/j.watres.2012.09.049

Li, F., Meindersma, W., de Haan, A.B., Reith, T., 2002. Optimization of commercial net spacers in spiral wound membrane modules. J. Memb. Sci. 208, 289–302. doi:10.1016/S0376-7388(02)00307-1

Li, Z.Y., Yangali-Quintanilla, V., Valladares-Linares, R., Li, Q., Zhan, T., Amy, G., 2012. Flux patterns and membrane fouling propensity during desalination of seawater by forward osmosis. Water Res. 46, 195–204. doi:10.1016/j.watres.2011.10.051

Liu, J., Liu, Z., Xu, X., Liu, F., 2015. Saw-tooth spacer for membrane filtration: Hydrodynamic investigation by PIV and filtration experiment validation. Chem. Eng. Process. Process Intensif. 91, 23–34. doi:10.1016/j.cep.2015.03.013

Louie, J.S., Pinnau, I., Ciobanu, I., Ishida, K.P., Ng, A., Reinhard, M., 2006. Effects of polyether–polyamide block copolymer coating on performance and fouling of reverse osmosis membranes. J. Memb. Sci. 280, 762–770. doi:10.1016/j.memsci.2006.02.041

Louie, J.S., Pinnau, I., Reinhard, M., 2011. Effects of surface coating process conditions on the water permeation and salt rejection properties of composite polyamide reverse osmosis membranes. J. Memb. Sci. 367, 249–255. doi:10.1016/j.memsci.2010.10.067

Madaeni, S.S., Ghaemi, N., 2007. Characterization of self-cleaning RO membranes coated with TiO2 particles under UV irradiation. J. Memb. Sci. 303, 221–233. doi:10.1016/j.memsci.2007.07.017

Majamaa, K., Aerts, P.E.M., Groot, C., Paping, L.L.M.J., van den Broek, W., van Agtmaal, S., 2010. Industrial water reuse with integrated membrane system increases the sustainability of the chemical manufacturing. Desalin. Water Treat. 18, 17–23. doi:10.5004/dwt.2010.1284

Majamaa, K., Johnson, J.E., Aerts, P.E.M., 2009. Improved reverse osmosis element construction reducing differential pressure in high fouling conditions, in: Proceedings IDA World Congress. Dubai.

Majamaa, K., Johnson, J.E., Bertheas, U., 2012. Three steps to control biofouling in reverse osmosis systems. Desalin. Water Treat. 42, 107–116. doi:10.5004/dwt.2012.2466

Majamaa, K., Lehtinen, M., Pilipenko, P., 2009. Comparision of cellulose acetate and nanofi ltration membranes for color removal from a norwegian lake. Desalin. Water Treat. 9, 9–14. doi:10.5004/dwt.2009.746

Malek, A., Hawlader, M.N.A., Ho, J.C., 1996. Design and economics of RO seawater desalination. Desalination 105, 245–261. doi:10.1016/0011-9164(96)00081-1

Manz, B., Volke, F., Goll, D., Horn, H., 2003. Measuring Local Flow Velocities and Biofilm Structure in Biofilm Systems With Magnetic Resonance Imaging (MRI). Biotechnol. Bioeng. 84, 424–432. doi:10.1002/bit.10782

Margalit, E., Leshansky, A., Freger, V., 2013. Modeling and analysis of hydrodynamic and physico-chemical effects in bacterial deposition on surfaces. Biofouling 29, 977–989. doi:10.1080/08927014.2013.823483

Martin, K.J., Bolster, D., Derlon, N., Morgenroth, E., Nerenberg, R., 2014. Effect of fouling layer spatial distribution on permeate flux: A theoretical and experimental study. J. Memb. Sci. 471, 130–137. doi:10.1016/j.memsci.2014.07.045

Matin, A., Khan, Z., Gleason, K.K., Khaled, M., Zaidi, S.M.J., Khalil, A., Moni, P., Yang, R., 2014a. Surface-modified reverse osmosis membranes applying a copolymer film to reduce adhesion of bacteria as a strategy for biofouling control. Sep. Purif. Technol. 124, 117–123. doi:10.1016/j.seppur.2013.12.032

Matin, A., Khan, Z., Zaidi, S.M.J., Boyce, M.C., 2011a. Biofouling in reverse osmosis membranes for seawater desalination: Phenomena and prevention. Desalination 281, 1–16. doi:10.1016/j.desal.2011.06.063

Matin, A., Ozaydin-Ince, G., Khan, Z., Zaidi, S.M.J., Gleason, K., Eggenspiler, D., 2011b. Random copolymer films as potential antifouling coatings for reverse osmosis membranes. Desalin. Water Treat. 34, 100–105. doi:10.5004/dwt.2011.2804

Matin, A., Shafi, H.Z., Khan, Z., Khaled, M., Yang, R., Gleason, K., Rehman, F., 2014b. Surface modification of seawater desalination reverse osmosis membranes: Characterization studies & performance evaluation. Desalination

343, 128–139. doi:10.1016/j.desal.2013.10.023

McCutcheon, J.R., Elimelech, M., 2006. Influence of concentrative and dilutive internal concentration polarization on flux behavior in forward osmosis. J. Memb. Sci. 284, 237–247. doi:10.1016/j.memsci.2006.07.049

McCutcheon, J.R., McGinnis, R.L., Elimelech, M., 2005. A novel ammonia-carbon dioxide forward (direct) osmosis desalination process. Desalination 174, 1–11. doi:10.1016/j.desal.2004.11.002

McDonogh, R., Schaule, G., Flemming, H.-C., 1994. The permeability of biofouling layers on membranes. J. Memb. Sci. 87, 199–217. doi:10.1016/0376-7388(93)E0149-E

Melo, L.F., Bott, T.R., 1997. Biofouling in water systems. Exp. Therm. Fluid Sci. 14, 375–381. doi:10.1016/S0894-1777(96)00139-2

Mi, B., Elimelech, M., 2010. Organic fouling of forward osmosis membranes: Fouling reversibility and cleaning without chemical reagents. J. Memb. Sci. 348, 337–345. doi:10.1016/j.memsci.2009.11.021

Mi, B., Elimelech, M., 2008. Chemical and physical aspects of organic fouling of forward osmosis membranes. J. Memb. Sci. 320, 292–302. doi:10.1016/j.memsci.2008.04.036

Miettinen, I.T., Vartiainen, T., Martikainen, P.J., 1997. Phosphorus and bacterial growth in drinking water. Appl. Environ. Microbiol. 63, 3242–3245.

Miller, D.J., Araújo, P.A., Correia, P.B., Ramsey, M.M., Kruithof, J.C., van Loosdrecht, M.C.M., Freeman, B.D., Paul, D.R., Whiteley, M., Vrouwenvelder, J.S., 2012. Short-term adhesion and long-term biofouling testing of polydopamine and poly(ethylene glycol) surface modifications of membranes and feed spacers for biofouling control. Water Res. 46, 3737–53. doi:10.1016/j.watres.2012.03.058

Mo, H., Ng, H.Y., 2010. An experimental study on the effect of spacer on concentration polarization in a long channel reverse osmosis membrane cell. Water Sci. Technol. 61, 2035–2041.

Modern Water Inc., 2012. Modern Water commissions Al Najdah FO plant. Membr. Technol. doi:10.1016/S0958-2118(12)70202-1

Monod, J., 1941. Growth of bacterial populations in function of concentration of a hydrocarbon diet. C. R. Hebd. Seances Acad. Sci 771–773.

Mulder, M., 1996. Basic Principles of Membrane Technology, Second. ed, Journal of Membrane Science. Springer Netherlands. doi:10.1007/978-94-009-1766-8

Nguyen, T., Roddick, F.A., Fan, L., 2012. Biofouling of water treatment membranes: a review of the underlying causes, monitoring techniques and control measures. Membranes (Basel). 2, 804–40. doi:10.3390/membranes2040804

O'Toole, G., Kaplan, H.B., Kolter, R., 2000. Biofilm formation as microbial development. Annu. Rev. Microbiol. 54, 49–79. doi:10.1146/annurev.micro.54.1.49

Palmer, R.J., White, D.C., 1997. Developmental biology of biofilms: implications for treatment and control. Trends Microbiol. 5, 435–440. doi:10.1016/S0966-842X(97)01142-6

Pang, C.M., Hong, P., Guo, H., Liu, W.T., 2005. Biofilm formation characteristics of bacterial isolates retrieved from a reverse osmosis membrane. Env. Sci Technol 39, 7541–7550. doi:10.1021/es050170h

Pankratz, T., 2012. Water Desalination Report. Desalination 48, 1–4.

Paris, T., Skali-Lami, S., Block, J.-C., 2007. Effect of wall shear rate on biofilm deposition and grazing in drinking water flow chambers. Biotechnol. Bioeng. 97, 1550–1561. doi:10.1002/bit.21321

Park, J.Y., Acar, M.H., Akthakul, A., Kuhlman, W., Mayes, A.M., 2006. Polysulfone-graft-poly(ethylene glycol) graft copolymers for surface modification of polysulfone membranes. Biomaterials 27, 856–65. doi:10.1016/j.biomaterials.2005.07.010

Peña, N., Gallego, S., del Vigo, F., Chesters, S.P., 2012. Evaluating impact of fouling on reverse osmosis membranes performance. Desalin. Water Treat. 3994, 1–11. doi:10.1080/19443994.2012.699509

Pereira, M.O., Kuehn, M., Wuertz, S., Neu, T., Melo, L.F., 2002. Effect of flow regime on the architecture of a Pseudomonas fluorescens biofilm. Biotechnol. Bioeng. 78, 164–171. doi:10.1002/bit.10189

Peyton, B.M., 1996. Effects of shear stress and substrate loading rate on Pseudomonas aeruginosa biofilm thickness and density. Water Res. 30, 29–36. doi:10.1016/0043-1354(95)00110-7

Phillip, W.A., Yong, J.S., Elimelech, M., 2010. Reverse draw solute permeation in forward osmosis: Modeling and experiments. Environ. Sci. Technol. 44, 5170–5176. doi:10.1021/es100901n

Picioreanu, C., Van Loosdrecht, M.C.M., Heijnen, J.J., 2000. Effect of diffusive and convective substrate transport on biofilm structure formation: A two-dimensional modeling study. Biotechnol. Bioeng. 69, 504–515. doi:10.1002/1097-0290(20000905)69:5<504::AID-BIT5>3.0.CO;2-S

Picioreanu, C., Van Loosdrecht, M.C.M., Heijnen, J.J., 1998a. Mathematical modeling of biofilm structure with a hybrid differential- discrete cellular automaton approach. Biotechnol. Bioeng. 58, 101–116. doi:10.1002/(SICI)1097-0290(19980405)58:1<101::AID-BIT11>3.0.CO;2-M

Picioreanu, C., Van Loosdrecht, M.C.M., Heijnen, J.J., 1998b. A new combined differential-discrete cellular automaton approach for biofilm modeling: Application for growth in gel beads. Biotechnol. Bioeng. 57, 718–731. doi:10.1002/(SICI)1097-0290(19980320)57:6<718::AID-BIT9>3.0.CO;2-O

Picioreanu, C., Vrouwenvelder, J.S., van Loosdrecht, M.C.M., 2009. Three-dimensional modeling of biofouling and fluid dynamics in feed spacer channels of membrane devices. J. Memb. Sci. 345, 340–354. doi:10.1016/j.memsci.2009.09.024

Prest, E.I., Staal, M., Kühl, M., van Loosdrecht, M.C.M., Vrouwenvelder, J.S., 2012. Quantitative measurement and visualization of biofilm O2 consumption rates in membrane filtration systems. J. Memb. Sci. 392–393, 66–75. doi:10.1016/j.memsci.2011.12.003

Qin, J.J., Chen, S., Maung, H.O., Kekre, K.A., Cornelissen, E.R., Ruiken, C.J., 2010. Experimental studies and modeling on concentration polarization in forward osmosis. Water Sci. Technol. 61, 2897–904. doi:10.2166/wst.2010.078

Quirynen, M., Bollen, C.M., 1995. The influence of surface roughness and surface-free energy on supra- and subgingival plaque formation in man. A review of the literature. J. Clin. Periodontol. 22, 1–14. doi:10.1111/j.1600-051X.1995.tb01765.x

Radu, A.I., van Steen, M.S.H., Vrouwenvelder, J.S., van Loosdrecht, M.C.M., Picioreanu, C., 2014. Spacer geometry and particle deposition in spiral wound membrane feed channels. Water Res. 64, 160–176. doi:10.1016/j.watres.2014.06.040

Radu, A.I., Vrouwenvelder, J.S., van Loosdrecht, M.C.M., Picioreanu, C., 2012. REMOVED: Modeling Biofouling, Scaling and Combined Fouling in Reverse Osmosis Membrane Devices. Procedia Eng. 44, 341–342. doi:http://dx.doi.org/10.1016/j.proeng.2012.08.409

Radu, A.I., Vrouwenvelder, J.S., van Loosdrecht, M.C.M., Picioreanu, C., 2011. Biofouling in membrane devices treating water with different salinities: a modeling study. Desalin. Water Treat. 34, 284–289. doi:10.5004/dwt.2011.2803

Radu, A.I., Vrouwenvelder, J.S., van Loosdrecht, M.C.M., Picioreanu, C., 2010. Modeling the effect of biofilm formation on reverse osmosis performance: Flux, feed channel pressure drop and solute passage. J. Memb. Sci. 365, 1–15. doi:10.1016/j.memsci.2010.07.036

Radu, A.I.I., Vrouwenvelder, J.S., van Loosdrecht, M.C.M.C.M., Picioreanu, C., 2012. Effect of flow velocity, substrate concentration and hydraulic cleaning on biofouling of reverse osmosis feed channels. Chem. Eng. J. 188, 30–39. doi:10.1016/j.cej.2012.01.133

Ridgeway, H.F., Foundation, A.R., 2003. Biological Fouling of Separation Membranes Used in Water Treatment Applications. AWWA Research Foundation.

Ridgway, H.F., Kelly, A., Justice, C., Olson, B.H., 1983. Microbial fouling of reverse-osmosis membranes used in advanced wastewater treatment technology: Chemical, bacteriological, and ultrastructural analyses. Appl. Environ. Microbiol. 45, 1066–1084.

Ronen, A., Lerman, S., Ramon, G.Z., Dosoretz, C.G., 2015. Experimental characterization and numerical simulation of the anti-biofuling activity of nanosilver-modified feed spacers in membrane filtration. J. Memb. Sci. 475, 320–329. doi:10.1016/j.memsci.2014.10.042

Rukapan, W., Khananthai, B., Chiemchaisri, C., Chiemchaisri, W., Srisukphun, T., 2012. Short- and long-term fouling characteristics of reverse osmosis membrane

at full scale leachate treatment plant. Water Sci. Technol. 65, 127–134. doi:10.2166/wst.2011.844

Sablani, S.., Goosen, M.F.., Al-Belushi, R., Wilf, M., 2001. Concentration polarization in ultrafiltration and reverse osmosis: a critical review. Desalination 141, 269–289. doi:10.1016/S0011-9164(01)85005-0

Sablani, S.S., Goosen, M.F.A., Al-Belushi, R., Gerardos, V., 2002. Influence of spacer thickness on permeate flux in spiral-wound seawater reverse osmosis systems. Desalination 146, 225–230. doi:10.1016/S0011-9164(02)00477-0

Saeed, A., Vuthaluru, R., Yang, Y., Vuthaluru, H.B., 2012. Effect of feed spacer arrangement on flow dynamics through spacer filled membranes. Desalination 285, 163–169. doi:10.1016/j.desal.2011.09.050

Sagiv, A., Zhu, A., Christofides, P.D., Cohen, Y., Semiat, R., 2014. Analysis of forward osmosis desalination via two-dimensional FEM model. J. Memb. Sci. 464, 161–172. doi:10.1016/j.memsci.2014.04.001

Sagle, A.C., Van Wagner, E.M., Ju, H., McCloskey, B.D., Freeman, B.D., Sharma, M.M., 2009. PEG-coated reverse osmosis membranes: Desalination properties and fouling resistance. J. Memb. Sci. 340, 92–108. doi:10.1016/j.memsci.2009.05.013

Salvador Cob, S., Beaupin, C., Hofs, B., Nederlof, M.M., Harmsen, D.J.H., Cornelissen, E.R., Zwijnenburg, A., Genceli Güner, F.E., Witkamp, G.J., 2012. Silica and silicate precipitation as limiting factors in high-recovery reverse osmosis operations. J. Memb. Sci. 423–424, 1–10. doi:10.1016/j.memsci.2012.07.016

Schneider, R., Ferreira, L., Binder, P., Bejarano, E., Goes, K., Slongo, E., Machafo, C., Rosa, G., 2005. Dynamics of organic carbon and of bacterial populations in a conventional pretreatment train of a reverse osmosis unit experiencing severe biofouling. J. Memb. Sci. 266, 18–29. doi:10.1016/j.memsci.2005.05.006

Schock, G., Miquel, A., 1987. Mass transfer and pressure loss in spiral wound modules. Desalination 64, 339–352. doi:10.1016/0011-9164(87)90107-X

Schwinge, J., Neal, P.R., Wiley, D.E., Fletcher, D.F., Fane, A.G., 2004a. Spiral wound modules and spacers. J. Memb. Sci. 242, 129–153. doi:10.1016/j.memsci.2003.09.031

Schwinge, J., Neal, P.R., Wiley, D.E., Fletcher, D.F., Fane, A.G., 2004b. Spiral wound modules and spacers: Review and analysis. J. Memb. Sci. doi:10.1016/j.memsci.2003.09.031

Schwinge, J., Wiley, D.E., Fletcher, D.F., 2002. Simulation of the Flow around Spacer Filaments between Channel Walls. 2. Mass-transfer Enhancement,. ndustrial Eng. Chem. Res. 41, 4879–4888. doi:10.1021/ie011015o

Shakaib, M., Hasani, S.M.F., Mahmood, M., 2007. Study on the effects of spacer geometry in membrane feed channels using three-dimensional computational flow modeling. J. Memb. Sci. 297, 74–89. doi:10.1016/j.memsci.2007.03.010

Shannon, M. a, Bohn, P.W., Elimelech, M., Georgiadis, J.G., Mariñas, B.J., Mayes, A.M., 2008. Science and technology for water purification in the coming decades. Nature 452, 301–310. doi:10.1038/nature06599

Siddiqui, A., Farhat, N., Bucs, S.S., Linares, R.V., Picioreanu, C., Kruithof, J.C., Van Loosdrecht, M.C.M., Kidwell, J., Vrouwenvelder, J.S., 2016. Development and characterization of 3D-printed feed spacers for spiral wound membrane systems. Water Res. 91, 55–67. doi:10.1016/j.watres.2015.12.052

Sim, L.N., Wang, Z.J., Gu, J., Coster, H.G.L., Fane, A.G., 2013. Detection of reverse osmosis membrane fouling with silica, bovine serum albumin and their mixture using in-situ electrical impedance spectroscopy. J. Memb. Sci. 443, 45–53. doi:10.1016/j.memsci.2013.04.047

Staal, M., Prest, E.I., Vrouwenvelder, J.S., Rickelt, L.F., K??hl, M., Kühl, M., 2011. A simple optode based method for imaging O 2 distribution and dynamics in tap water biofilms. Water Res. 45, 5027–5037. doi:http://dx.doi.org/10.1016/j.watres.2011.07.007

Stewart, P.S., Franklin, M.J., 2008. Physiological heterogeneity in biofilms. Nat Rev Micro 6, 199–210.

Stoodley, P., Dodds, I., Boyle, J.D., Lappin-Scott, H.M., 1998. Influence of hydrodynamics and nutrients on biofilm structure. J. Appl. Microbiol. 85 Suppl 1, 19S–28S. doi:10.1111/j.1365-2672.1998.tb05279.x

Su, J., Chung, T.-S., 2011. Sublayer structure and reflection coefficient and their effects on concentration polarization and membrane performance in FO processes. J. Memb. Sci. 376, 214–224. doi:10.1016/j.memsci.2011.04.031

Subramani, A., Hoek, E.M. V, 2008. Direct observation of initial microbial deposition onto reverse osmosis and nanofiltration membranes. J. Memb. Sci. 319, 111–125. doi:10.1016/j.memsci.2008.03.025

Subramani, A., Kim, S., Hoek, E., 2006. Pressure, flow, and concentration profiles in open and spacer-filled membrane channels. J. Memb. Sci. 277, 7–17. doi:10.1016/j.memsci.2005.10.021

Suh, C., Lee, S., 2013. Modeling reverse draw solute flux in forward osmosis with external concentration polarization in both sides of the draw and feed solution. J. Memb. Sci. 427, 365–374. doi:10.1016/j.memsci.2012.08.033

Suidan, M.T., Rittmann, B.E., Traegner, U.K., 1987. Criteria establishing biofilm-kinetic types. Water Res. 21, 491–498. doi:10.1016/0043-1354(87)90198-9

Sun, C., Leiknes, T., 2012. Two-stage biofilm-MBR for nitrogen removal and enhanced membrane performance. Water Sci. Technol. 66, 588–593. doi:10.2166/wst.2012.211

Tan, C.H., Ng, H.Y., 2008. Modeling of external and internal concentration polarization effect on flux behaviour of forward osmosis. Water Sci. Technol. Water Supply 8, 533. doi:10.2166/ws.2008.116

Tang, C.Y., Chong, T.H., Fane, A.G., 2011. Colloidal interactions and fouling of NF

and RO membranes: a review. Adv. Colloid Interface Sci. 164, 126–43. doi:10.1016/j.cis.2010.10.007

Tang, C.Y., Kwon, Y.-N., Leckie, J.O., 2009. Effect of membrane chemistry and coating layer on physiochemical properties of thin film composite polyamide RO and NF membranes. Desalination 242, 168–182. doi:10.1016/j.desal.2008.04.004

Tasaka, K., Katsura, T., Iwahori, H., Kamiyama, Y., 1994. Analysis of RO elements operated at more than 80 plants in Japan. Desalination 96, 259–272. doi:10.1016/0011-9164(94)85177-8

Tijhuis, L., Hijman, B., Van Loosdrecht, M.C.M., Heijnen, J.J., 1996. Influence of detachment, substrate loading and reactor scale on the formation of biofilms in airlift reactors. Appl. Microbiol. Biotechnol. 45, 7–17. doi:10.1007/s002530050641

Tran, T., Bolto, B., Gray, S., Hoang, M., Ostarcevic, E., 2007. An autopsy study of a fouled reverse osmosis membrane element used in a brackish water treatment plant. Water Res. 41, 3915–3923. doi:10.1016/j.watres.2007.06.008

Valladares Linares, R., Bucs, S.S., Li, Z., AbuGhdeeb, M., Amy, G., Vrouwenvelder, J.S., 2014a. Impact of spacer thickness on biofouling in forward osmosis. Water Res. 57, 223–33. doi:10.1016/j.watres.2014.03.046

Valladares Linares, R., Li, Z., Abu-Ghdaib, M., Wei, C.H., Amy, G., Vrouwenvelder, J.S., 2013. Water harvesting from municipal wastewater via osmotic gradient: An evaluation of process performance. J. Memb. Sci. 447, 50–56. doi:10.1016/j.memsci.2013.07.018

Valladares Linares, R., Li, Z., Sarp, S., Bucs, S.S., Amy, G., Vrouwenvelder, J.S., 2014b. Forward osmosis niches in seawater desalination and wastewater reuse. Water Res. 66, 122–39. doi:10.1016/j.watres.2014.08.021

Valladares Linares, R., Wexler, A.D., Bucs, S.S., Dreszer, C., Zwijnenburg, A., Flemming, H.-C., Kruithof, J.C., Vrouwenvelder, J.S., 2015. Compaction and relaxation of biofilms. Desalin. Water Treat. 1–13. doi:10.1080/19443994.2015.1057036

van Loosdrecht, M.C.M., Bereschenko, L., Radu, A., Kruithof, J.C., Picioreanu, C., Johns, M.L., Vrouwenvelder, J.S., 2012. New approaches to characterizing and understanding biofouling of spiral wound membrane systems. Water Sci. Technol. 66, 88–94. doi:10.2166/wst.2012.096

Van Loosdrecht, M.C.M., Eikelboom, D., Gjaltema, A., Mulder, A., Tijhuis, L., Heijnen, J.J., 1995. Biofilm structures. Water Sci. Technol. 32, 35–43. doi:10.1016/0273-1223(96)00005-4

Van Paassen, J.A.M., Kruithof, J.C., Bakker, S.M., Kegel, F.S., 1998. Integrated multi-objective membrane systems for surface water treatment: pre-treatment of nanofiltration by riverbank filtration and conventional ground water treatment. Desalination 118, 239–248. doi:10.1016/S0011-9164(98)00137-4

Venault, A., Liu, Y.H., Wu, J.R., Yang, H.S., Chang, Y., Lai, J.Y., Aimar, P., 2014. Low-biofouling membranes prepared by liquid-induced phase separation of the

PVDF/polystyrene-b-poly (ethylene glycol) methacrylate blend. J. Memb. Sci. 450, 340–350. doi:10.1016/j.memsci.2013.09.004

Villacorte, L.O., Kennedy, M.D., Amy, G.L., Schippers, J.C., 2009. The fate of Transparent Exopolymer Particles (TEP) in integrated membrane systems: Removal through pre-treatment processes and deposition on reverse osmosis membranes. Water Res. 43, 5039–5052. doi:10.1016/j.watres.2009.08.030

Vrouwenvelder, J.S., Bakker, S.M., Cauchard, M., Le Grand, R., Apacandie, M., Idrissi, M., Lagrave, S., Wessels, L.P., van Paassen, J.A.M., Kruithof, J.C., van Loosdrecht, M.C.M., 2007a. The membrane fouling simulator: A suitable tool for prediction and characterisation of membrane fouling, in: Water Science and Technology. pp. 197–205. doi:10.2166/wst.2007.259

Vrouwenvelder, J.S., Bakker, S.M., Wessels, L.P., van Paassen, J.A.M., 2007b. The Membrane Fouling Simulator as a new tool for biofouling control of spiral-wound membranes. Desalination 204, 170–174. doi:10.1016/j.desal.2006.04.028

Vrouwenvelder, J.S., Beyer, F., Dahmani, K., Hasan, N., Galjaard, G., Kruithof, J.C., Van Loosdrecht, M.C.M., 2010a. Phosphate limitation to control biofouling. Water Res. 44, 3454–66. doi:10.1016/j.watres.2010.03.026

Vrouwenvelder, J.S., Buiter, J., Riviere, M., van der Meer, W.G.J., van Loosdrecht, M.C.M., Kruithof, J.C., 2010b. Impact of flow regime on pressure drop increase and biomass accumulation and morphology in membrane systems. Water Res. 44, 689–702. doi:10.1016/j.watres.2009.09.054

Vrouwenvelder, J.S., Graf von der Schulenburg, D.A.A., Kruithof, J.C.C., Johns, M.L.L., van Loosdrecht, M.C.M.C.M., 2009a. Biofouling of spiral-wound nanofiltration and reverse osmosis membranes: a feed spacer problem. Water Res. 43, 583–94. doi:10.1016/j.watres.2008.11.019

Vrouwenvelder, J.S., Hinrichs, C., Sun, A.R., Royer, F., van Paassen, J.A.M., Bakker, S.M., van der Meer, W.G.J., Kruithof, J.C., van Loosdrecht, M.C.M., 2008a. Monitoring and control of biofouling in nanofiltration and reverse osmosis membranes. Water Sci. Technol. Water Supply 8, 449–458.

Vrouwenvelder, J.S., Hinrichs, C., Van der Meer, W.G.J., Van Loosdrecht, M.C.M., Kruithof, J.C., 2009b. Pressure drop increase by biofilm accumulation in spiral wound RO and NF membrane systems: role of substrate concentration, flow velocity, substrate load and flow direction. Biofouling 25, 543–555. doi:10.1080/08927010902972225

Vrouwenvelder, J.S., Manolarakis, S.A., van der Hoek, J.P., van Paassen, J.A.M., van der Meer, W.G.J., van Agtmaal, J.M.C., Prummel, H.D.M., Kruithof, J.C., van Loosdrecht, M.C.M., 2008b. Quantitative biofouling diagnosis in full scale nanofiltration and reverse osmosis installations. Water Res. 42, 4856–4868. doi:10.1016/j.watres.2008.09.002

Vrouwenvelder, J.S., Manolarakis, S. a., Veenendaal, H.R., van der Kooij, D., 2000. Biofouling potential of chemicals used for scale control in RO and NF membranes. Desalination 132, 1–10. doi:10.1016/S0011-9164(00)00129-6

Vrouwenvelder, J.S., Picioreanu, C., Kruithof, J.C.C., van Loosdrecht, M.C.M.C.M., 2010c. Biofouling in spiral wound membrane systems: Three-dimensional CFD model based evaluation of experimental data. J. Memb. Sci. 346, 71–85. doi:10.1016/j.memsci.2009.09.025

Vrouwenvelder, J.S., Van Der Kooij, D., 2001. Diagnosis, prediction and prevention of biofouling of NF and RO membranes. Desalination 139, 65–71. doi:10.1016/S0011-9164(01)00295-8

Vrouwenvelder, J.S., van Loosdrecht, M.C.M., Kruithof, J.C., 2011a. Early warning of biofouling in spiral wound nanofiltration and reverse osmosis membranes. Desalination 265, 206–212. doi:10.1016/j.desal.2010.07.053

Vrouwenvelder, J.S., Van Loosdrecht, M.C.M., Kruithof, J.C., 2011b. A novel scenario for biofouling control of spiral wound membrane systems. Water Res. 45, 3890–8. doi:10.1016/j.watres.2011.04.046

Vrouwenvelder, J.S., van Paassen, J.A.M., Kruithof, J.C., van Loosdrecht, M.C.M., 2009c. Sensitive pressure drop measurements of individual lead membrane elements for accurate early biofouling detection. J. Memb. Sci. 338, 92–99. doi:10.1016/j.memsci.2009.04.016

Vrouwenvelder, J.S., van Paassen, J.A.M., van Agtmaal, J.M.C., van Loosdrecht, M.C.M., Kruithof, J.C., 2009d. A critical flux to avoid biofouling of spiral wound nanofiltration and reverse osmosis membranes: Fact or fiction? J. Memb. Sci. 326, 36–44. doi:10.1016/j.memsci.2008.09.029

Vrouwenvelder, J.S., van Paassen, J.A.M., Wessels, L.P., van Dam, A.F., Bakker, S.M., Vanpassen, J., Wessels, L.P., Vandam, A., Bakker, S.M., 2006. The Membrane Fouling Simulator: A practical tool for fouling prediction and control. J. Memb. Sci. 281, 316–324. doi:10.1016/j.memsci.2006.03.046

Wagner, M., Manz, B., Volke, F., Neu, T.R., Horn, H., 2010. Online assessment of biofilm development, sloughing and forced detachment in tube reactor by means of magnetic resonance microscopy. Biotechnol. Bioeng. 107, 172–181. doi:10.1002/bit.22784

Wang, C., Such, G.K., Widjaya, A., Lomas, H., Stevens, G., Caruso, F., Kentish, S.E., 2012. Click poly(ethylene glycol) multilayers on RO membranes: Fouling reduction and membrane characterization. J. Memb. Sci. 409–410, 9–15. doi:10.1016/j.memsci.2012.02.049

Wang, Y., Wicaksana, F., Tang, C.Y., Fane, A.G., 2010. Direct microscopic observation of forward osmosis membrane fouling. Environ. Sci. Technol. 44, 7102–7109. doi:10.1128/JVI.01705-10

Wanner, O., Eberl, H., Morgenroth, E., Noguera, D., Picioreanu, C., Rittmann, B., van Loosdrecht, M.C.M., Wanner, O., 2006. Mathematical modeling of biofilms, Scientific and technical report series.

Wanner, O., Gujer, W., 1986. A multispecies biofilm model. Biotechnol. Bioeng. 28, 314–328. doi:10.1002/bit.260280304

Wasche, S., Horn, H., Hempel, D.C., 2002. Influence of growth conditions on biofilm

development and mass transfer at the bulk/biofilm interface. Water Res. 36, 4775–4784. doi:10.1016/S0043-1354(02)00215-4

Werner, C.M., Logan, B.E., Saikaly, P.E., Amy, G.L., 2013. Wastewater treatment, energy recovery and desalination using a forward osmosis membrane in an air-cathode microbial osmotic fuel cell. J. Memb. Sci. 428, 116–122. doi:10.1016/j.memsci.2012.10.031

West, S., Wagner, M., Engelke, C., Horn, H., 2015. Optical coherence tomography for the in situ three-dimensional visualization and quantification of feed spacer channel fouling in reverse osmosis membrane modules. J. Memb. Sci. 498, 345–352. doi:10.1016/j.memsci.2015.09.047

Wijeyekoon, S., Mino, T., Satoh, H., Matsuo, T., 2004. Effects of substrate loading rate on biofilm structure. Water Res. 38, 2479–2488. doi:10.1016/j.watres.2004.03.005

Willems, P., Deen, N.G., Kemperman, A.J.B., Lammertink, R.G.H., Wessling, M., van Sint Annaland, M., Kuipers, J.A.M., van der Meer, W.G.J., 2010. Use of Particle Imaging Velocimetry to measure liquid velocity profiles in liquid and liquid/gas flows through spacer filled channels. J. Memb. Sci. 362, 143–153. doi:10.1016/j.memsci.2010.06.029

Wolfaardt, G.M., Lawrence, J.R., Robarts, R.D., Caldwell, S.J., Caldwell, D.E., 1994. Multicellular organization in a degradative biofilm community. Appl. Environ. Microbiol. 60, 434–446.

Xie, M., Lee, J., Nghiem, L.D., Elimelech, M., 2015. Role of pressure in organic fouling in forward osmosis and reverse osmosis. J. Memb. Sci. 493, 748–754. doi:10.1016/j.memsci.2015.07.033

Xu, P., Bellona, C., Drewes, J.E., 2010. Fouling of nanofiltration and reverse osmosis membranes during municipal wastewater reclamation: Membrane autopsy results from pilot-scale investigations. J. Memb. Sci. 353, 111–121. doi:10.1016/j.memsci.2010.02.037

Yang, H.-L., Lin, J.C.-T., Huang, C., 2009. Application of nanosilver surface modification to RO membrane and spacer for mitigating biofouling in seawater desalination. Water Res. 43, 3777–86. doi:10.1016/j.watres.2009.06.002

Yang, R., Goktekin, E., Wang, M., Gleason, K.K., 2014. Molecular fouling resistance of zwitterionic and amphiphilic initiated chemically vapor-deposited (iCVD) thin films. J. Biomater. Sci. Polym. Ed. 25, 1687–1702. doi:10.1080/09205063.2014.951245

Yangali-Quintanilla, V., Li, Z., Valladares, R., Li, Q., Amy, G., 2011. Indirect desalination of Red Sea water with forward osmosis and low pressure reverse osmosis for water reuse. Desalination 280, 160–166. doi:10.1016/j.desal.2011.06.066

Yi, Z., Zhu, L.-P., Xu, Y.-Y., Zhao, Y.-F., Ma, X.-T., Zhu, B.-K., 2010. Polysulfone-based amphiphilic polymer for hydrophilicity and fouling-resistant modification of polyethersulfone membranes. J. Memb. Sci. 365, 25–33.

doi:10.1016/j.memsci.2010.08.001

Yiantsios, S.G., Karabelas, A.J., 2003. Deposition of micron-sized particles on flat surfaces: effects of hydrodynamic and physicochemical conditions on particle attachment efficiency. Chem. Eng. Sci. 58, 3105–3113. doi:10.1016/S0009-2509(03)00169-6

Ying, W., Gitis, V., Lee, J., Herzberg, M., 2013. Effects of shear rate on biofouling of reverse osmosis membrane during tertiary wastewater desalination. J. Memb. Sci. 427, 390–398. doi:10.1016/j.memsci.2012.09.054

Yoon, H., Baek, Y., Yu, J., Yoon, J., 2013. Biofouling occurrence process and its control in the forward osmosis. Desalination 325, 30–36. doi:10.1016/j.desal.2013.06.018

Zhang, C., Liang, Z., Hu, Z., 2014. Bacterial response to a continuous long-term exposure of silver nanoparticles at sub-ppm silver concentrations in a membrane bioreactor activated sludge system. Water Res. 50, 350–358. doi:10.1016/j.watres.2013.10.047

Zhang, T.C., Bishop, P.L., 1994. Density, porosity, and pore structure of biofilms. Water Res. 28, 2267–2277. doi:10.1016/0043-1354(94)90042-6

Zhang, W., Sileika, T.S., Chen, C., Liu, Y., Lee, J., Packman, A.I., 2011. A novel planar flow cell for studies of biofilm heterogeneity and flow-biofilm interactions. Biotechnol. Bioeng. 108, 2571–2582. doi:10.1002/bit.23234

Zhao, Y.-H., Zhu, B.-K., Kong, L., Xu, Y.-Y., 2007. Improving Hydrophilicity and Protein Resistance of Poly(vinylidene fluoride) Membranes by Blending with Amphiphilic Hyperbranched-Star Polymer. Langmuir 23, 5779–5786. doi:10.1021/la070139o

Zhao, Y.F., Zhu, L.P., Yi, Z., Zhu, B.K., Xu, Y.Y., 2013. Improving the hydrophilicity and fouling-resistance of polysulfone ultrafiltration membranes via surface zwitterionicalization mediated by polysulfone-based triblock copolymer additive. J. Memb. Sci. 440, 40–47. doi:10.1016/j.memsci.2013.03.064

Zinn, M.S., Kirkegaard, R.D., Palmer, R.J., White, D.C., 1999. Laminar flow chamber for continuous monitoring of biofilm formation and succession. Methods Enzymol., Methods in Enzymology 310, 224–232. doi:10.1016/S0076-6879(99)10020-X

Zou, S., Wang, Y.N., Wicaksana, F., Aung, T., Wong, P.C.Y., Fane, A.G., Tang, C.Y., 2013. Direct microscopic observation of forward osmosis membrane fouling by microalgae: Critical flux and the role of operational conditions. J. Memb. Sci. 436, 174–185. doi:10.1016/j.memsci.2013.02.030

List of publications

JOURNAL ARTICLES (● mark chapters of this thesis)

Szabolcs Szilveszter, Botond Ráduly, Szilárd S. Bucs, Beáta Ábrahám, Szabolcs Lányi, Dan Niculae Robescu (2012) Activated sludge floc characterization by confocal laser scanning microscopy. *Environmental Engineering and Management Journal* **11**: 669-674.

● Szilárd S. Bucs, Andrea I. Radu, Vasile Lavric, Johannes S. Vrouwenvelder, Cristian Picioreanu (2014) Effect of different commercial feed spacers on biofouling of reverse osmosis membrane systems: a numerical study, *Desalination*, **343**: 26-37. *Chapter 6 in this Thesis.*

● Szilárd S. Bucs, Rodrigo Valladares Linares, Mark C.M. van Loosdrecht, Joop C. Kruithof, Johannes S. Vrouwenvelder (2014) Impact of organic nutrient load on biomass accumulation, feed channel pressure drop increase and permeate flux decline in membrane systems. *Water Research* **67**: 227–42. *Chapter 4 in this Thesis.*

● Rodrigo Valladares Linares, Szilárd S. Bucs, Zhenyu Li, Muhannad Abu-Ghdeeb, Gary Amy, Johannes S. Vrouwenvelder (2014) Impact of spacer thickness on biofouling in forward osmosis. *Water Research* **57**: 223 – 233. *Chapter 7 in this Thesis.*

Rodrigo Valladares Linares, Zhenyu Li, Sarper Sarp, Szilárd S. Bucs, Gary Amy, Johannes S. Vrouwenvelder (2014) Forward osmosis niches in seawater desalination and wastewater reuse. *Water Research* **66**: 122-139.

● Szilárd S. Bucs, Nadia Farhat, Amber Siddiqui, Rodrigo Valladares Linares, Andrea I. Radu, Joop C. Kruithof, Johannes S. Vrouwenvelder (2015) Development of a setup to enable stable and accurate flow conditions for membrane biofouling studies. *Desalination and Water Treatment*, **57 (28)**: 12831-12901. *Chapter 2 in this Thesis.*

● Szilárd S. Bucs, Rodrigo Valladares Linares, Jeremy O. Marston, Andrea I. Radu, Johannes S. Vrouwenvelder, Cristian Picioreanu (2015) Experimental and numerical characterization of the water flow in spacer-filled channels of spiral-wound membranes. *Water Research* **87**: 299–310. *Chapter 3 in this Thesis.*

Nadia Farhat, Marc Staal, Amber Siddiqui, Sergey M. Borisov, Szilárd S. Bucs, Johannes S. Vrouwenvelder (2015) Early non-destructive biofouling detection and spatial distribution: Application of oxygen sensing optodes. *Water Research* **83**: **10-20.**

Zhenyu Li, Rodrigo Valladares Linares, Szilárd S. Bucs, Cyril Aubry, Noreddine Ghaffour, Johannes S. Vrouwenvelder, Gary Amy (2015) Calcium carbonate scaling in seawater desalination by ammonia–carbon dioxide forward osmosis: Mechanism and implications. *Journal of Membrane Science* **458**: 36-43.

- Szilárd S. Bucs, Rodrigo Valladares Linares, Johannes S. Vrouvenvelder, Cristian Picioreanu (2016) Impact of spacer thickness on biofouling in forward osmosis. *Water Research* **106**: 86 – 97. *Chapter 8 in this Thesis.*

Nadia Farhat, Johannes S. Vrouwenvelder, Mark C. M. van Loosdrecht, Szilárd S. Bucs, Marc Staal (2016) Effect of water temperature on biofouling development in reverse osmosis membrane systems. *Water Research* **103**: 149-159.

Rodrigo Valladares Linares, Adam D. Wexler, Szilárd S. Bucs, Claudia Dreszer, Arie Zwijnenburg, Hans-Curt Flemming, Joop C. Kruithof, Johannes S. Vrouwenvelder (2016) Compaction and relaxation of biofilms. *Desalination and Water Treatment* **57**: 12902-12914.

Amber Siddiqui, Nadia Farhat, Szilárd S. Bucs, Rodrigo Valladares Linares, Cristian Picioreanu, Joop C. Kruithof, Mark C. M. van Loosdrecht, James Kidwell, Johannes S. Vrouwenvelder (2016) Development and characterization of 3D-printed feed spacers for spiral wound membrane systems. *Water Research* **91**: 55-67.

Nadia Farhat, Marc Staal, Szilárd S. Bucs, Mark C.M. van Loosdrecht, Johannes S. Vrouwenvelder (2016) Spatial heterogeneity of biofouling under different cross-flow velocities in reverse osmosis membrane systems. *Journal of Membrane Science* **520**: 964-971.

Rodrigo Valladares Linares, Luca Fortunato, Nadia Farhat, Szilárd S. Bucs, Marc Staal, Einar O. Fridjonsson, Mike L. Johns, Johannes S. Vrouwenvelder, TorOve Leiknes (2016) Mini-review: novel non-destructive in situ biofilm characterization techniques in membrane systems. *Desalination and Water Treatment* **57**: 48-49.

- Szilárd S. Bucs, Rodrigo Valladares Linares, Nadia Farhat, Asif Matin, Zafarullah Khan, Mark C.M. van Loosdrecht, Rong Yang, Minghui Wang, Karen K. Gleason, Joop C. Kruithof, Johannes S. Vrouwenvelder (2017) Coating of reverse osmosis membranes with amphiphilic copolymers for biofouling control. *Desalination and Water Treatment* **68**: 1-11. *Chapter 5 in this Thesis.*

Amber Siddiqui, Ingrid Pinel, Emmanuelle I. Prest, Szilárd S. Bucs, Mark C.M. van Loosdrecht, Joop C. Kruithof, Johannes S. Vrouwenvelder (2017) Application of DBNPA dosage for biofouling control in spiral wound membrane systems. *Desalination and Water Treatment.* In press.

Amber Siddiqui, Stefan Lehmann, Szilárd S. Bucs, Marion Fresquet, Laurie Fel, Emmanuelle I. E. C. Prest, Julien Ogier, Carsten Schellenberg, Mark C.M. van Loosdrecht, Joop C. Kruithof, Johannes S. Vrouwenvelder (2017) Predicting the impact of feed spacer modification on biofouling by hydraulic characterization and biofouling studies in membrane fouling simulators. *Water Research* **110**: 281-287.

Luca Fortunato, Szilárd S. Bucs, Rodrigo Valladares Linares, Corrado Cali, Johannes S. Vrouwenvelder, TorOve Leiknes (2017) Spatially-resolved in-situ quantification of biofouling using optical coherence tomography (OCT) and 3D image analysis in a spacer filled channel. *Journal of Membrane Science* **524**: 673-681.

PATENTS

Szilárd S. Bucs, Marc Staal, Sacco te Lintel Hekker, Johannes S. Vrouwenvelder, Non-intrusive in-line analytical sensor that allows detection and differentiation of different types of fouling by the use of non-intrusive spectral analysis of the fouling material in combination with pressure drop measurements. Submitted application WO 2016092371 A1.

CONFERENCES (only oral presentations by Sz. Bucs)

1st International Conference on Desalination using Membrane Technology, 7-10 April, 2013, Sitges– Spain. Szilárd S. Bucs, Andrea I. Radu, Cristian Picioreanu, Mark C. M. van Loosdrecht, Johannes S. Vrouwenvelder. Numerical study of preferential biomass attachment and spacer geometry effects on biofouling of reverse osmosis membrane systems.

The 7th IWA Specialised Membrane Technology Conference and Exhibition for Water and Wastewater Treatment and Reuse August 25 - 29, 2013, Toronto, Canada. Szilárd S. Bucs, Andrea I. Radu, Cristian Picioreanu, Mark C. M. van Loosdrecht, Johannes S. Vrouwenvelder. Impact of feed spacer geometry and biomass localization on performance of spiral wound reverse osmosis membrane systems.

Desalination for the Environment: Clean Water and Energy Grand Resort Hotel, Limassol, Cyprus, 11–15 May 2014. Szilárd S. Bucs, Rodrigo Valladares Linares, Jeremy O. Marston, Andrea I. Radu, Johannes S. Vrouwenvelder, Cristian Picioreanu. Flow characterization in spiral wound membrane systems by particle image velocimetry and numerical modeling.

4th IWA Conference on Membrane Technology. Ho Chi Minh City, Vietnam, 2 – 6 December 2014. Szilárd Bucs, Rodrigo Valladares Linares, Jeremy Marston, Andrea Radu, Johannes Vrouwenvelder, Cristian Picioreanu. “Impact of feed spacer on hydrodynamics in spiral wound membrane modules, an experimental and numerical study”.

Desalination for the Environment: Clean Water and Energy, 22 – 26 May 2016, Rome, Italy. “Membrane biofouling: impact of organic substrate load”. Szilárd Bucs, Rodrigo Valladares Linares, Mark van Loosdrecht, Joop C. Kruithof, Johannes S. Vrouwenvelder.

IWA World Water Congress & Exhibition 2016, Brisbane, Australia. “The Importance Of Flow Behaviour In Spiral Wound Membrane Systems”. Szilárd Bucs, Rodrigo Valladares Linares, Cristian Picioreanu, Johannes S. Vrouwenvelder.

The 9th International Desalination Workshop, November 13-16, 2016, Abu Dhabi, United Arab Emirates. “Biofouling of forward osmosis membranes” Szilárd Bucs, Cristian Picioreanu, Hans Vrouwenvelder.

International Conference on Membranes in Drinking and Industrial Water Production 6–8 February 2017, Leeuwarden, The Netherlands. “Spatially-resolved in-situ quantification of biofilms using optical coherence tomography in a spacer filled membrane systems” Szilárd Bucs, Luca Fortunato, Rodrigo Valladares Linares, Johannes S. Vrouwenvelder.

Acknowledgements

Firstly, I would like to express my sincere gratitude to my advisor promotors Johannes Vrouwenvelder and Cristian Picioreanu for the continuous support of my Ph.D study and related research, for their patience, motivation, and immense knowledge. Their guidance and stimulation motivated and helped me in all the time of my research and writing of this thesis. I could not have imagined having better advisors and mentor for my Ph.D study.

Besides my advisors, I would like to thank for Mark C.M. van Loosdrecht and Joop C. Kruithof for their insightful comments and encouragement.

My deepest appreciation to my colleague Andrea Radu an enthusiastic and hard working person, her contribution to my professional formation are invaluable. My sincere thanks also goes to my friend and colleague Rodrigo Valladares Linares, for the motivating discussions, creativity and dedication and for all the fun we have had in the last four years.

I am indebted to my colleagues who supported me in Water Desalination and Reuse Centre at King Abdullah University of Science and Technology (Saudi Arabia). Their experience, advice and support contributed significantly to my progress. I would like to acknowledge Nadia Farhat and Marc Staal for the stimulating discussions.

I would like to thank to every person from Delft University of Technology who were involved in my doctoral education.

Last but not the least, I would like to thank my family who made it possible for me to study through their support and motivation: to my mom Mária, my father József and my sister Erika for supporting me spiritually throughout my Ph.D study and my life in general.